Controlled crystallization of calcium carbonate under langmuir monolayers

Rajam, S.

Award date:
1990

Awarding institution:
University of Bath

CONTROLLED CRYSTALLIZATION OF CALCIUM CARBONATE UNDER LANGMUIR MONOLAYERS

THESIS SUBMITTED FOR THE DEGREE OF DOCTOR OF PHILOSOPHY IN CHEMISTRY

BY

S. RAJAM

1990

SCHOOL OF CHEMISTRY

UNIVERSITY OF BATH

ProQuest LLC
789 East Eisenhower Parkway
P.O. Box 1346
Ann Arbor, MI 48106-1346

CONTROLLED CRYSTALLIZATION OF CALCIUM CARBONATE UNDER LANGMUIR MONOLAYERS.

SUBMITTED BY S. RAJAM

FOR THE DEGREE OF DOCTOR OF PHILOSOPHY
OF THE UNIVERSITY OF BATH
1990.

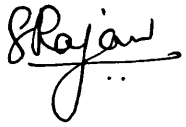

SUMMARY

The work reported in this thesis has been involved in developing a model system to biomineralization with a view to identifying mechanisms involved in the use of organised organic surfaces in the controlled nucleation of inorganic solids. In the present system, Langmuir monolayers have been used as two-dimensional templates for calcium carbonate nucleation from supersaturated calcium bicarbonate solution.

$CaCO_3$ crystals grown by inorganic methods in the absence of monolayers gave non-specific rhombohedral calcite crystals, whereas crystal growth under stearate and octadecylamine monolayers was well controlled and highly specific. The crystals were morphologically distinct and crystallographically oriented with respect to the monolayer surface. Under stearate monolayers the $(\bar{1}1.0)$ face of calcite crystals or (00.1) face of vaterite crystals were formed depending on the supersaturation of the bicarbonate solution, whereas under amine monolayers two different orientations (00.1) and (11.0) and morphological forms of vaterite were formed irrespective of supersaturation changes.

A controlling mechanism for structural selectivity, and preferred orientation has been explained in terms of electrostatic charge accumulation, stereochemical correlation and structural correspondence. Structural analyses of crystals were carried out by X-ray diffraction and IR spectrophotometry, morphological analysis was

done by optical and scanning electron microscopy, and elemental analysis was carried out by EDXA and atomic absorption spectophotometry.

Whereas charged monolayers effectively control the crystallization of $CaCO_3$, octadecanol, a neutral monolayer inhibits crystal nucleation. Cholesterol a neutral bulky steroid molecule did not have any effect on crystallization. The packing density of monolayers is also important for oriented crystallization and isostearic acid, having an inter-headgroup spacing incommensurate with the crystal lattice of calcite, did not induce oriented nucleation. The effect of competitive ion binding on the oriented nucleation of $CaCO_3$ crystals under charged monolayers was studied by increasing the ionic strength of the solution with sodium and lithium. The number of oriented calcite crystals was significantly reduced at [Ca]:[M] = 1:20.

An additional interesting observation resulting from this study was the formation of well developed basal (00.1) faces of calcite in the presence of lithium. Similar studies with sodium could not bring about this morphological change and this indicates that lithium, due to its small ionic radius, stabilizes the high energy crystal face by incorporation into surface interstitial sites.

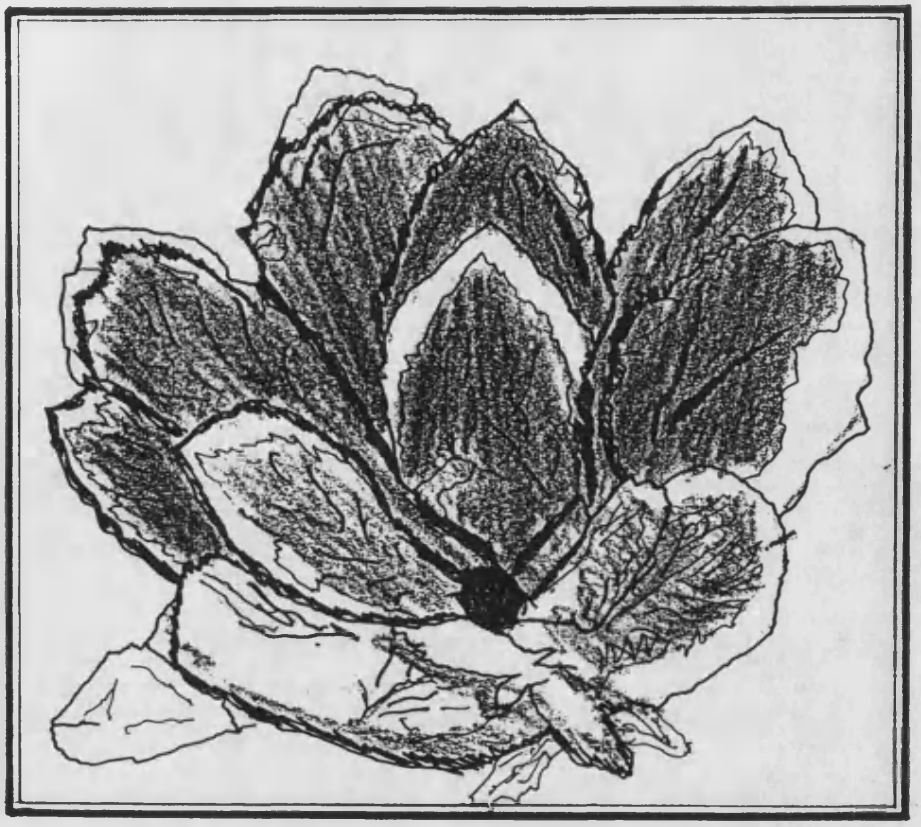

THIS PIECE OF WORK IS
DEDICATED TO MY DAUGHTERS, RAMA AND LATHA.

ACKNOWLEDGEMENTS

I greatly appreciate and thank Dr. S.Mann for his valuable guidance throughout the period of this work. I also thank Dr. B.R.Heywood, for her constant advice and for her collaboration with the work. I would like to express my thanks to Dr. R.J.Davey and Prof. J.D.Birchall of ICI, Runcorn for their valuable suggestions.

My thanks are due to Mr. J.M.Didymus and Mr.J.B.A.Walker for their valuable help in the laboratory.

Thanks are also due to Dr. G.Love, Mrs. K.Powell and Mr. H.Perrott of the Electron Optics Group for their assistance with the scanning electron microscopy.

I also thank Dr. N.H.C.Sparks, Mrs. V.J.Wade, Mr. R. Stevens, Mr. N.Reeves and Miss F.Meldrum and all my other colleagues of the Chemistry Department and friends for their help and encouragement.

My thanks are due to Mr. B.Chapman and Mr. A.Carver for their assistance in the X-Ray diffraction analysis.

I thank SERC and ICI plc for the financial support for this course.

Last but not least, I kindly acknowledge and thank my husband Reddy, my children Rama and Latha and my dear friend Anne, for their help and tolerance during the period of my work.

CONTENTS

CHAPTER II

CHAPTER III

CONTROLLED CRYSTALLIZATION OF CALCIUM CARBONATE CRYSTALS UNDER STEARIC ACID MONOLAYERS

CHAPTER IV

$CaCO_3$ CRYSTALLIZATION UNDER AMINE MONOLAYERS

CHAPTER V

INFLUENCE OF MODIFIED MONOLAYERS IN CONTROLLING THE CRYSTALLIZATION OF $CaCO_3$

CHAPTER VI

INFLUENCE OF CATIONS ON ORIENTED CRYSTALLIZATION OF CALCIUM CARBONATE UNDER CHARGED MONOLAYERS

CHAPTER VII

CHAPTER I

INTRODUCTION

1.1 OBJECTIVES:

A fundamental concept in the process of biomineralization deals with the molecular recognition of inorganic materials at organised organic macromolecular substances. Currently, much is known about the microstructural and the chemical features of designed materials, but the understanding of the molecular processes taking place during synthesis remains at a very elementary stage of development.

The objective of this Thesis is to understand the principles and mechanisms by which an organised organic matrix can mediate the crystallization of an inorganic material, using concepts derived from a knowledge of biomineralization, and to simulate these biologically controlled mineralization processes *in vitro*. This knowledge in turn can be used to develop a model system to biomineralization.

The main work concerns the crystallization of calcium carbonate under compressed organised organic monolayers (octadecanoic acid, octadecylamine, octadecanol and cholesterol) formed at air/water interfaces. The crystal structure, morphology, orientation and nucleation density of the crystals formed were studied. The effects of polarity and packing density of the monolayers, and the ionic concentration of the solution were also investigated.

This chapter provides an overview of the main aspects covered by my work reported in this thesis; Viz, (a) the mechanisms involved in biomineralization, (b) formation of stable Langmuir monolayers and (c) $CaCO_3$ crystal chemistry involving the polymorphic description and

details.

1.2 BIOMINERALIZATION AND BIOMINERALS:

Biomineralization is a diverse, widespread and common phenomenon that refers to the processes by which organisms form minerals. Organisms are capable of forming a diverse array of minerals. These biogenic minerals commonly have attributes which distinguish them from their inorganic counterparts. Furthermore, organisms are capable of controlling even the trace elements and isotopic compositions of the minerals they form so that these are out of equilibrium with the environment.

Crystals thus formed in biological systems are often of uniform size, have oriented crystallographic axes, and adopt sizes and shapes quite different from those found in their non-biological counterparts. Another difference between biologically and inorganically formed minerals involves their geochemical properties as well. All these factors indicate that biogenic crystals are formed under well controlled conditions.

Biogenic minerals have been widely distributed in the biosphere and contribute significantly to sedimentary environments. So far, 66 minerals have been reported [1] that are formed in biological systems. The most abundant and conspicuous biominerals being the phosphate and carbonate salts of calcium that are found in conjunction with organic polymers such as collagen and chitin, that give structural support

to bones and shells. Salts of barium, strontium, silicon and iron are also common. Opal emerges as the second most extensively formed biogenic mineral. Ferrihydrite and related ferric oxide minerals rank third and magnetite (Fe_3O_4), first discovered as a biomineralization product in chiton teeth [2], and now known to be synthesised by magnetotactic bacteria [3,4], honey bees [5], and homing pigeons may well prove to be widespread [6].

$CaCO_3$ mineral can precipitate as calcite, aragonite and vaterite or amorphous calcium carbonate. All occur in specific ways in nature and sometimes the three main forms are found in the same mineralized product. Calcite is the main mineral component in coccoliths [7], mammalian otoconia [8] and most egg shells [9] and mollusc shells. Foliated calcite forms the bulk of the shells of the living oysters *(ostreacea)* and window-pane jingle shells *(anomiacea)*. The calcium carbonate of mollusc shells occurs as calcite in some species, as aragonite in others, and in certain species deposit calcite in one portion of the shell and aragonite in another portion of the same shell. Aragonite is also widespread being the common main mineral component in corals, fish otoliths [8], amphibian otoconia [8] and turtle egg shells [10]. It is found in pearls, bivalves and gastropod shells. The nacreous layer in the gastropodes *(Gibbula, Calliostoma, Trochus and Haliotis)* in the bivalves is composed of the aragonite tablets [11]. Vaterite, the metastable polymorph of crystalline calcium carbonate is precipitated in nature by a variety of organisms, both normally and under pathological conditions [12-18]. It has been found in the egg shells of gastropods belonging to the genus

ampullana. It is also located in fish species (*Acipencer sturio* - a sturgeon and *Gadus monnhera* - a cord) [14-18]. Lowenstam also reported about the sessile benthic marine animal, the tunicate (*Herdmania momus*) and on its mineralization of vaterite. Further he commented on its possible evolutionary and sedimentary implications [19]. Vaterite and amorphous calcium carbonate have also been identified in the leucocytes or calcium cells of the mantle and reproductive tissues of certain snails [20]. Vaterite also occurs in the gastropod *Panacea paludosa* in the golgi apparatus of the mantle epithelial cells; in the foot; in the regulating muscle activity; in the albumin capsule gland of the female and in the egg capsules [21]. All three anhydrous crystalline modifications have been identified in gallstones [22,23].

1.3 FUNCTIONS OF BIOMINERALS:

According to a recent review, the majority of biogenic minerals which are often calcium containing, mostly hydrated, and may be mono-crystalline, polycrystalline or amorphous are shown to be of different functional value to the organism [24]. The functions of biominerals are as protective devices (outer shells), structural supports (bones), aids to attack (teeth and horns) as various kinds of sensors (magnetic or gravitational) or as concentrated deposits of required elements, wastes or poisons. Many unicellular organisms build cytoskeletons by depositing hydrated silica, a form of amorphous glass; in protozoa and algae this inorganic polymer is often sculpted into exquisite rods, perforated discs and reticular frameworks that are species-specific and have long been used

as diagnostic characteristics in systematic biology. Minerals are also put to special uses, for example, as magnetic sensors in magnetotactic bacteria (Fe_3O_4), gravity balance devices ($CaCO_3$, $CaSO_4$, $BaSO_4$), deterrence against predators (SiO_2, $CaCO_3$), iron storage and mobilization (Fe_2O_3. nH_2O in the protein ferritin), love darts in snails ($CaCO_3$) and eye lenses ($CaCO_3$) in fossilized trilobites. The hard parts formed by these minerals are living structures which may undergo active demineralization and remodelling in response to environmental and biological stress. Bone, for example, provides an essential store of calcium in vertebrates and calcium oxalate is a calcium source in plants.

1.4 CONTROLLED MINERALIZATION:

The precision of replication of biominerals in terms of structure, morphology and distribution in each species suggests that there are highly specific mechanisms of controlled crystal growth formation and spatial organization within the biological system. The minerals are formed by normal cellular processes to form organised structures in cells ranging from bacteria, algae and protozoa to osteoblasts of bone. The minerals may be in membrane-bound vesicles within cells, in the mucilaginous layers of cell walls in bacteria or impregnated in biopolymers in extracellular space. There are numerous examples of control in biomineralization being effected by vesicle walls. Two such examples of relatively well studied processes are the coccolithophoridae [25] and sea urchin skeletons [26] where single crystals of calcite are formed inside a vesicle [27,28]. In all these

examples, the common mode of crystal formation in the tissues is through the initial formation of a structural framework. The regulation of crystallization in these cells is partly accomplished by an array of matrix macromolecules, many of which are synthesised by specific cells for this purpose. A subset of the matrix macromolecules is closely associated with the mineral phase and hence is thought to regulate crystal growth by some mechanisms as yet unknown. The widespread use of a preconstructed organic framework in which the minerals grow is in itself an indication of the existence of a common approach towards biomineralization. Mineralized tissues are usually formed by the initial elaboration of a structural organic framework composed of a complex heterogeneous mixture of macromolecules such as proteins and polysaccharides into which ions of mineral phase permeate and crystallise.

The minerals formed in the biological system are well defined and often have beautiful morphologies (Figs. 1.1.A & 1.1.B).. Foliated calcite, one of the rarest of the 328 morphological forms of the mineral, calcite, has been reported by several workers [29-32]. Lowenstam [21] has shown that the calcitic prismatic layer of the bivalve *(Mytilus californianus)* is an example of organic matrix-mediated biomineralization process. Several detailed examples have been illustrated by Watabe [33] showing the crystalline characteristics of calcareous structures, the sites of their formation, nucleation and growth of minerals, the organic matrix and other factors controlling the crystalline patterns concentrating mainly on calcium carbonate.

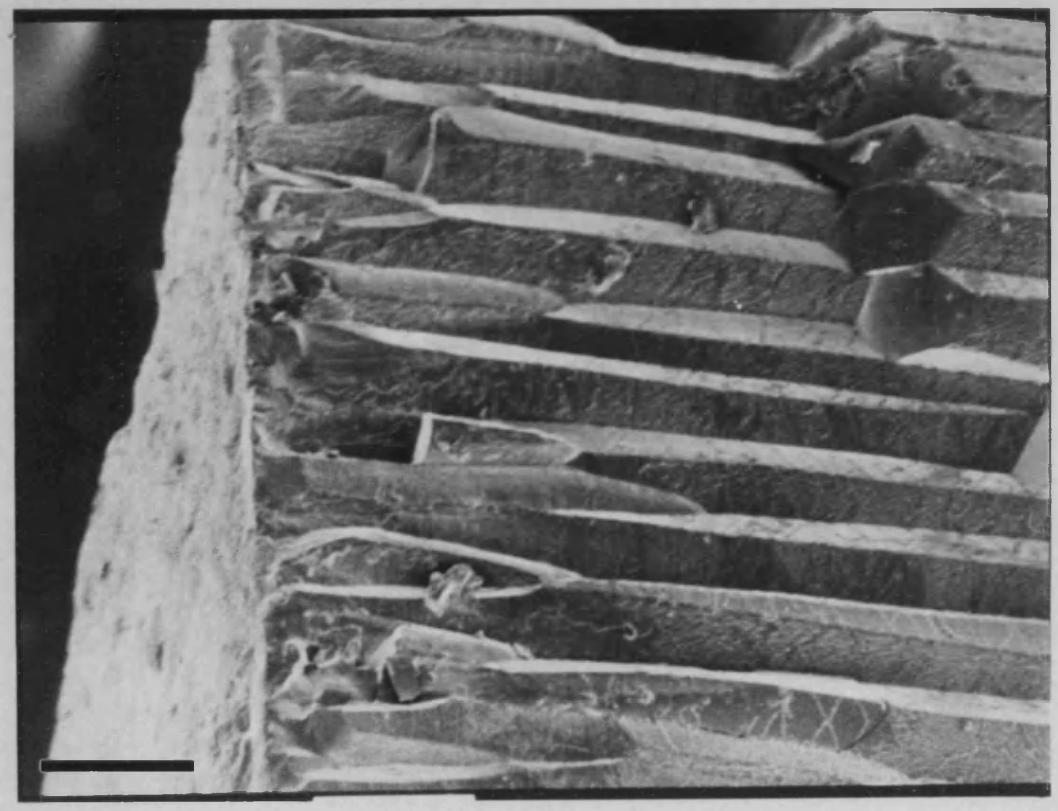

FIG. 1.1: (A) SEM MICROGRAPH SHOWING THE ORIENTATION OF PRISMATIC CALCITE IN MOLLUSC SHELL (Scale bar = 50 μm)

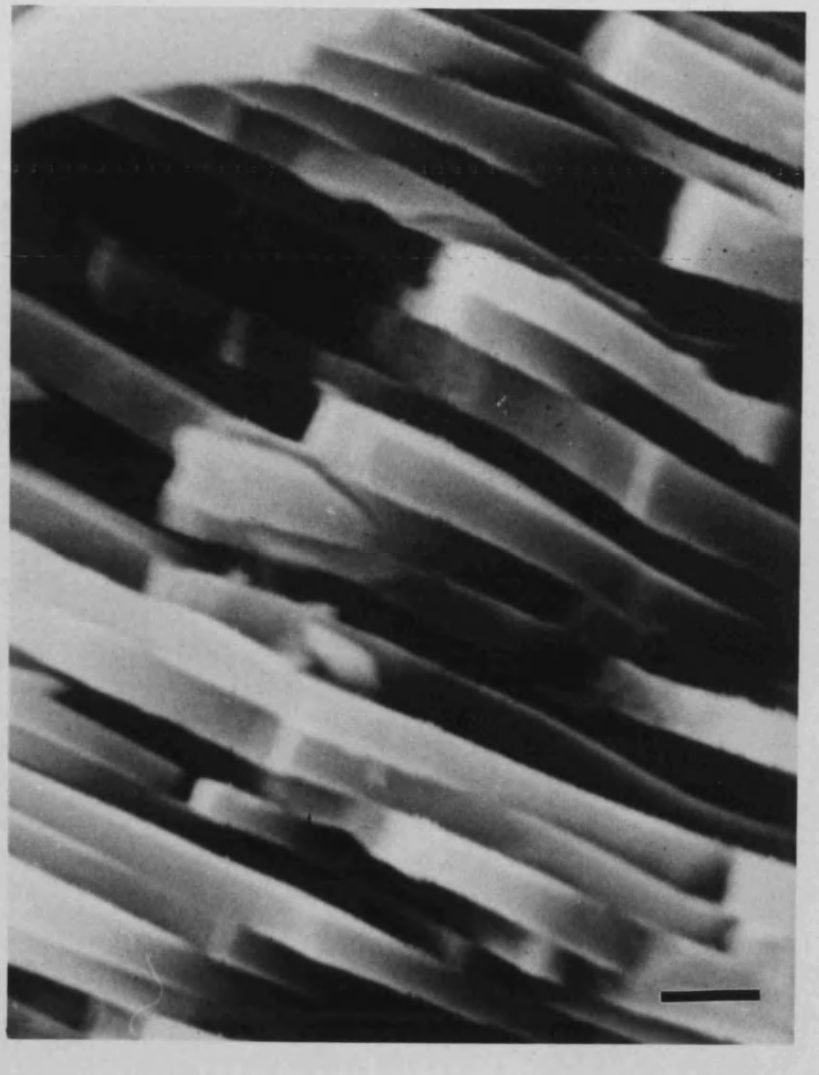

FIG. 1.1: (B) SEM MICROGRAPH SHOWING THE ORIENTATION OF ARAGONITE CRYSTALS IN NACREOUS LAYER IN MOLLUSC SHELL (Scale bar = 1 μm)

The processes of biomineralization can in principle be easily divided into two classes; one in which control is exercised in some way over mineralization and other in which it is not. In practice the differentiation is not that simple as all organisms do exercise some control at one level or another even if it simply involves, for example, removing from the shell some undesirable metabolic end product or ion that combines with another ion in the external medium and precipitates. To differentiate between processes that are not specifically designed for mineralization, but do in fact result in mineral being formed, and processes in which a specific task is set up for the purpose of mineralization, Lowenstam [21] coined the phrase "biologically-induced mineralization" for the former situation. The latter is more aptly referred to as "biologically-controlled mineralization", a term proposed by Mann [34].

(i) **BIOLOGICALLY-INDUCED MINERALIZATION:** This process generally occurs in the open environment and not in a space particularly delineated for this purpose. No specialised cellular or macromolecular involvement is set up to induce mineralization. The minerals themselves if they are crystalline, have habits that are the same or are very similar to, those formed by their inorganic counter parts; they have a wide range of sizes and are usually random aggregates. One particularly characteristic feature of this induced mineralization is that the type of mineral formed is a function of the environmental conditions in which the organism lives during the mineral formation. The same organism in different environments can form different minerals [35]. This process appears to be the

predominant process among the monera and fungi, and it occurs fairly frequently in the protoctists. Some examples of biologically induced mineralization in animals are the calcite cryatals formed in the axial skeleton of the pennatulid sea fan [35], and the weddelite $CaC_2O_4.(2+x)H_2O$ and brushite $CaHPO_4.2H_2O$ crystals that form the layers of biologically controlled deposits of calcite in the mandible or beak of nautilus [36].

(ii) **BIOLOGICALLY-CONTROLLED MINERALIZATION:** Much of the work in biomineralization is formally aimed at understanding the controlled processes that are involved in mineralization in biology which differentiates this process from the inorganic world. However, it is already apparent that many biological systems can combine different control processes and end up with a unique final product. Therefore, it is necessary to identify and understand various processes that are involved in producing the final mineralization product.

One of the most important features of the biologically controlled mineralization is that the site at which mineral forms is first sealed off from the environment by a barrier through which ions can not freely diffuse. This particular controlled mineralization termed as "space delineation", is a fundamental part of the mechanism that cells use to control mineralization [37,38]. The lipid bilayers are the most common means of space delineation. Occasionally water insoluble macromolecules (proteins and/or polysaccharides) that polymerize to form impervious sheets were also used as materials for space delineation. In ferritin protein, a highly specialised form of space delineation takes place. The iron in some

ferritins is deposited as para-crystalline ferrihydrite, whereas in others (eg. certain types of bacteria) it is an iron phosphate mineral. The use of a protein shell to create the space for mineral deposition appears to be unique. In some other organisms the barriers used for space delineation also participate in mineral formation itself. For example, some of the lipids in the vesicle membranes are acidic and may also contain membrane proteins that participate directly in controlling aspects of mineralization [39].

There is a growing body of information on the structure, composition and synthesis of macromolecules [40]. But the key and the exciting question is to identify the molecular processes that produce minerals of precise form with uniform particle size, novel crystal morphology and specific crytallographic orientation.

1.5 NATURE OF ORGANIC MOLECULES:

The organic matrix, a phrase coined by Le Gros Clark for bone [41] is now widely used in a variety of contexts. We refer here to the organic matrix as a continuous sheet like structure that sub-divides the mineralization space. The fact that organic matrix-like macromolecules are extracted out of a mineral phase does not necessarily imply that they exist as continuous membranes, as they could also be dispersed monomers or discontinuous aggregates. The latter situation has been proposed for echinoderm skeletons by Berman et al [42]. Thus many biominerals, unlike their inorganic counterparts, are composite materials often consisting of mineral sub-units ordered within an organic matrix. These matrix

macromolecules are probably not associated with all biologically formed minerals but, in general, mineralization processes that are controlled in some way by the organism tend to have associated macromolecules. There is no doubt that these macromolecules fulfil important functions both during the formation of the mineral and in their contribution to the biomechanical properties of the matured product.

The organic components are generally proteins (collagen, dentin, elastin and conchiolin), polysaccharides (β-chitin), proteoglycans and lipids. Two different classes of proteins have been extracted from biominerals [43]. One fraction is composed of aspartic acid rich proteins possibly associated with small amounts of polysaccharide and the second fraction contains serine rich proteins that are associated with large amounts of polysaccharides. Generally this organic matrix or phase is a minor constituent of the biomineral. However, its contribution by weight varies rather widely, for example in mollusc shells, generally from 0.01% to 5% [44,45]. In recent studies Weiner [46] and Swift et al [47] suggested that sea urchin test skeletal plates contain functional proteins specific to the biomineral. But in some organisms, like scallop shell the ridges of their shells are composed of greater than 30% matrix by weight, but the rest of the shell has much less matrix [48]. This suggests apart from controlling mineralization, the matrix is also involved in mechanical aspects of biomineral structure [49]. Furthermore, some organic molecules associated with mineral may be incorporated more or less incidentally during mineral growth. For example osteonectin, thought earlier to be a

bone specific protein has been identified in several non-mineralizing tissues [50] and calmodulin, a ubiquitous regulatory protein has been extracted from gill concretions of fresh water mussels [51]. In such cases, these proteins may be involved in cellular regulation associated with the mineral growth. Some polyanionic polymers which seem to be nearly universal in their distribution in calcified biominerals do fulfil the role of matrix during mineral formation [52,53]. These polymers are usually proteins containing negatively charged side groups that are intimately involved in mineralization.

The organic matrix in a broad sense can be classified into soluble and insoluble components. In most recent studies, the matrix has been isolated by dissolution of powdered biomineral at near neutral pH with relatively high concentrations of EDTA. The whole matrix extract was then fractionated into EDTA soluble and insoluble components by centrifugation. For molluscan systems the soluble matrix is enriched in the anion protein and the insoluble matrix is more hydrophobic in nature [54,55] and possibly contains other components such as chitin [56,57]. These soluble matrices often have covalently bound polysaccharides and are acidic, being rich in carboxylate groups and sometimes sulphate. The insoluble macromolecules are referred to as framework macromolecules. All the tissues contain acidic glycoproteins and/or proteoglycans. One possible exception in which they may be absent is the calcareous alga *(Halimeda)* [58-60], which forms its aragonitic crystals under poorly controlled conditions [40]. However, various skeletal hard parts are formed under

relatively well controlled conditions and acidic macromolecules are found to be present in them. This observation strongly supports the notion that these acidic macromolecules fulfil important functions in biomineralization. The fact that they are highly charged in itself implies that these are actively involved in regulating mineral formation. Furthermore, in the few cases in which their locations in the tissue are known, they are closely associated with the mineral. The distribution of major framework macromolecules between phyla presents an entirely different picture as compared to the acidic macromolecules. The framework macromolecular types vary considerably from tissue to tissue and a number of mineralized hard parts from various organisms do not appear to have any framework macromolecules at all. The diversity of framework macromolecular types and the fact that they are present in small amounts or are absent suggest their major function is not in biomineralization per se, but in contributing to the mechanical properties of the products.

1.6 CONTROLLED CRYSTALLIZATION OF THE MINERALS AND THE INFLUENCE OF THE ORGANIC MATRIX:

In many mineralization processes, particularly those occurring in most skeletal hard parts, the space set up by cells and/or polymerized macromolecules is further sub-divided prior to mineralization by an assemblage of organic matrix macromolecules. The influence of these macromolecules is important in the regulation of formation and growth of the mineral. The role of organic macromolecules in initiating the

nucleation of the inorganic solids and regulating the growth of the mineral is influenced partly by the matrix components, and partly by chemical control [24]. It is in this area of biological mechanisms of nucleation and growth control that significant new concepts have been developed and the analysis of these ideas in simplified physico-chemical systems should provide information about the regulation of nucleation in biomineralization. The processes controlling biomineralization are shown in Fig. 1.2 schematically.

The organic macromolecules are found to be organised at sites of biomineralization where they are often involved in controlling mineral nucleation and growth. In single cell organisms, the control is effected by setting up spatial boundaries, within which local supersaturation levels are developed by selective ion transport in the isolated cellular compartments. For example, diatoms form shells of amorphous silica and the shape of the mineral formed is controlled by the structure of the membranes building up the spatial boundaries. This indicates that mineral morphology can be controlled by the membrane bound compartments of biological systems. Apart from this, there is a further correlation between the organic macromolecules and the crystal properties of the mineral formed in multi-cellular organisms. For example, calcium phosphate is mineralized within the fibrils of collagen as sub-micrometre sized plates. In turkey tendon, the $\underline{c}$ axis lies parallel to the plane of the plates as well as to the collagen fibre axis, and the $\underline{a}^*$ axis lies perpendicular to the plane of the plate [61,62]. Similar observations were

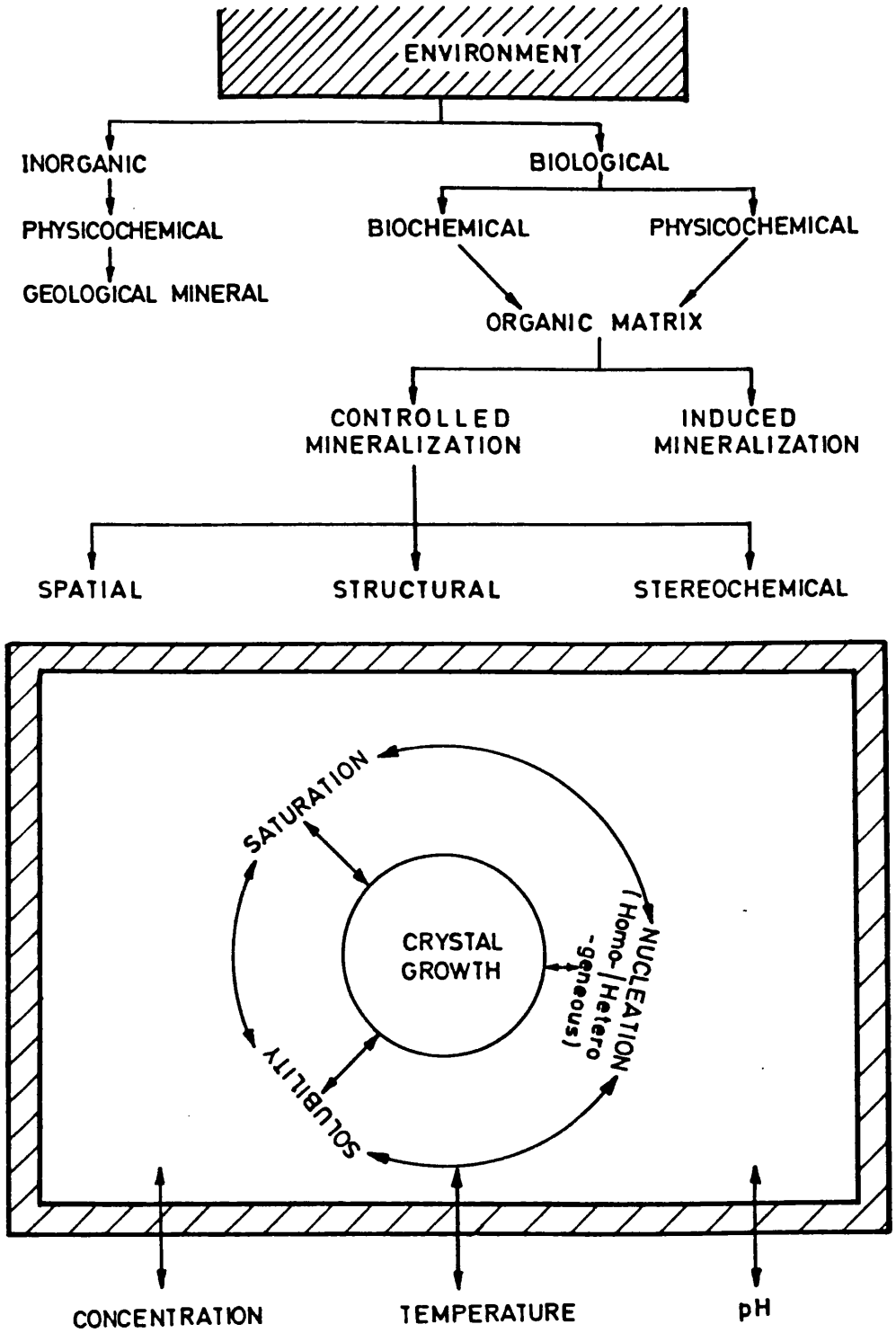

FIG. 1.2: SCHEMATIC REPRESENTATION OF THE PROCESSES INVOLVED IN MINERALIZATION INDICATING THE ROLE OF ORGANIC MATRIX IN BIOLOGICAL SYSTEMS.

also made in the nacreous inner layer of some mollusc shells. In this layer, protein-polysaccharide macromolecules control the formation of aragonite within the matrices such that the c axes of each aragonite crystal lies perpendicular to the plane of the organic template [63,64]. Thus these matrix materials, apart from their functional value to the mechanical properties of the biomineral, are involved in molecular interactions which impart specific crystallographic properties to the mineral formed. In different mollusc shells, aragonite crystals develop in different modes of formations, for example, as a brick wall or "stack of coins" arrangement with the c axis of each crystal always perpendicular to the organic template [63,64]. A similar organisation of the organic macromolecules in specific orientations is also present in avian egg shells where the protein molecules become the origin of nucleation, and oriented calcite forms along the crystallographic c axis of the mineral.

The orientation of the mineral nuclei at the organic matrix is controlled by the molecular processes involved at the organic surface. The localised oriented structure, various chemical processes and the topography of these macromolecules seem to be the primary factors in controlling the mineralization of calcium phosphate in mature bone [65-69]. When the collagen fibres obtained from decalcification of the bone and the modified collagen fibres were used in *in vitro* crystallization of calcium phosphate, the modified collagen could not nucleate the mineral in the same way as the decalcified collagen fibres could [69]. However, more detailed studies are required to elucidate the exact mechanisms of mineral formation

under the effective control of the organic matrix. Recent ideas developed in this area show that the hydrophobic part of the organic matrix can act as an insoluble component to build up a framework, but the hydrophilic part of the organic molecules is involved directly in regulating mineralization.

The nature of organic molecules involved in mineralization is generally complex and composed of various components. These components vary from species to species, and in different regions, within the same species [70,71]. In the study of mollusc shells, one primary factor identified was that the various EDTA soluble components obtained in various species were similar [72] and correlated with the ultrastructure of the mineral formed, but EDTA insoluble components were variable in composition and structure. This implies that the organisation of the matrix molecules precedes the nucleation of aragonite crystals. Thus the nature of organisation of acidic and hydrophobic macromolecules (eg. as anti-parallel β-pleated sheet polypeptide chains and β-chitin) [73, 74] proves to be responsible for the mechanical and structural properties observed in shells.

Having shown that the organic macromolecules are specifically involved in regulating mineralization, the processes encountered can be classified into several sections. The foremost mechanism involves the formation of a molecular cage with particular orientation of the macromolecules. These molecules control the supersaturation/ionic concentration and differentiate the internal region from the environment. Hence the physico-chemical conditions are effected differently within the molecular compartment when compared to the

surroundings. Similarly, the organic substrates can create a charge density at specific locations, where organic macromolecules induce the cation binding and thereby induce nucleation of the mineral. The initial charge accumulation and the ionic binding sites prior to nucleation have been studied and a primary mechanism by which matrix initiates, regulates and controls mineral growth through adsorption to crystal nuclei or growing crystals has been proposed [75-78].

^{31}P nmr spectroscopic studies of calcium binding to phosphorylated serine residues of dentine phospho-protein in the presence of calcium phosphate have been reported [79]. These studies show that the charge accumulation and weak ion binding become important factors in controlling mineralization. Furthermore, this effect is enhanced by the specific size of the nucleation zone at which the nucleation occurs. The mineralization of hydroxyapatite in bone, rather than amorphous calcium phosphate or brushite ($CaHPO_4.2H_2O$) proceeds in a highly oriented manner, with the $\underline{c}$ axis running parallel to the collagen fibre axis. This indicates that the collagen-matrix accumulates calcium and phosphate ions [80] generating specific regions for the oriented nucleation of the crystalline phase.

The physico-chemical control effected by the organic macromolecules alone cannot explain all the oriented mineralization processes. There are other correlations such as structural matching and stereochemical relations between the organic matrix and the mineral formed. The epitaxial relation or the structural matching has been reported in only

a few biominerals. For example in mollusc shell, many species show that both the c and b axes of the anti-parallel β-pleated sheet of the matrix and the mineralized aragonite crystal lattice are oriented with structural matching at the interface. This correspondence is identified throughout in each matrix plane, but the alignment of the ab plane of the β-pleated sheet changes, and results in differences in crystal orientations, each crystal having its c axis perpendicular to the matrix surface, but with the a and b axes aligned parallel to the matrix surface in different orientations (Fig.1.1 A,B,C). A suitable mechanism has been proposed for the crystallochemical relation observed between the mineral and the matrix in various species of mollusc shells [63,73,74], (Fig.1.2 A,B,C). Calcium binding to the aspartic acid residues of the matrix corresponds to the configuration of the ab plane of aragonite with the matrix periodic structure showing a close structural match along the a axis, whereas along the b axis, there is no structural correspondence [81]. These examples clearly indicate that the formation of regiospecific sites by charge accumulation and weak ion binding, and the development of the configuration of the matrix that could structurally match with incipient crystal lattice, are possible mechanisms in the controlled mineralization in biology.

However, more detailed analysis of the process of biomineralization indicates that the above mentioned charge accumulation and structural correspondence alone cannot explain the preferred formation with the orientation along c axis of calcite in certain locations and aragonite crystals in different locations since both structures have similar

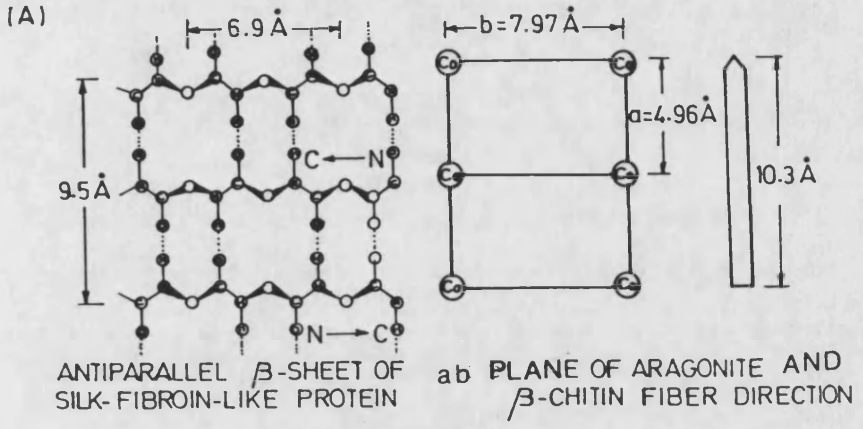

FIG. 1.1: (C)

(Reproduced with permission from Weiner, S., and Traub, W.,) Figure from "On Biomineralization " edited by Lowenstam, H.A. and Weiner, S., Oxford university Press, (1989) New York, Oxford.

Ca-Ca distances, on specific crystal faces. Hence the preferred formation of one over the other requires some other relationship between the organic matrix and the mineral formed. Essentially, the stereochemical correspondence between the matrix molecules and the (001) face of calcite and aragonite, determines the mineral to be formed. In calcite and aragonite, (001) faces comprise carbonate anions that are oriented in stereochemically different manner located between adjacent calcium layers running perpendicular to the c axis. If the matrix molecules can induce a binding configuration of cations that mimic a specific layer of a crystal face with the correct stereochemical motif, then nucleation may be energetically favoured along one preferred crystallographic direction.

The importance of stereochemical correspondence has been confirmed experimentally in some *in vitro* systems [91]. These studies showed that the morphology of calcium dicarboxylate salts, synthesised in the presence of aspartic acid-rich proteins were stereochemically related. A similar effect was observed for calcite crystals nucleated on stereochemically-related faces of proteins adsorbed onto a rigid substrate. The attachment of aspartic acid-rich proteins on the (001) face of the crystal, revealed by the immunofluorescence staining of the crystals, showed that the organisation of the carboxylate components attached to the β-pleated sheet surface could be stereochemically correlated to the carbonates of the crystal face.

Charge accmulation, epitaxial correspondence and stereochemical correlation between the matrix and the mineral formed have

been reported individually for various minerals. But there is a possibility that the combined effect of these factors is also responsible for the oriented nucleation of the crystals. Evidence for this combined effect, arises from some recent *in vitro* experiments, where polyaspartate adsorbed onto polystyrene films in the ß-sheet conformation, did not induce oriented $CaCO_3$ nucleation unless the film was sulphonated. Similarly sulphonated polystyrene films without the adsorbed polyaspartate substrates gave only very few oriented crystals. This study showed clearly that the combined effect of charge accumulation, structural matching and stereochemical correspondence was responsible for oriented nucleation [83].

1.7 MODEL SYSTEM TO BIOMINERALIZATION:

The importance of an organic matrix in biomineralization and its influence on the structure, morphology and orientation of the mineral formed had been demonstrated experimentally *in vitro*. The widely used approach for studying the functions of these acidic organic macromolecules is to examine in various ways their effect on crystal nucleation and growth *in vitro* systems. The kinetics of crystal growth have been measured in the presence of different matrix macromolecules under a variety of conditions [84-87]. Combinations of matrix components have been used to detect a collaborative effect [88] and the ability of the demineralized matrix to induce crystal nucleation has been recently identified [89,90]. The manner in which acidic matrix macromolecules interact with different structural surfaces of various crystals have been examined. With an objective to understand the principles that govern the

interactions and to gain insight into the mechanisms by which these matrix constituents regulate crystal growth *in vivo*, Addadi and Weiner [91] have attempted to build a model system to biomineralization. They have adapted a similar method reported on mechanistic studies of the effect of "tailor-made" low molecular weight additives on the growth of organic crystals [92,93]. These studies showed that stereoselective adsorption of an additive onto a specific crystal face results in a drastic decrease in its growth rate relative to that of unaffected faces. Since the crystal morphology is determined by the relative growth rate of the slowest growing faces, the interaction of the additive affects the overall morphology. Analysis of morphological changes is therefore a means of pin-pointing the specific crystal faces that adsorb the additive (thus increasing in relative area) and thereby studying the nature of the interactions between the additive and the growing crystal.

Addadi and Weiner [91] used different matrix macromolecules extracted from mollusc shells as the additives and the crystals of various calcium dicarboxylates as well as calcite as the substrates. They have examined two classes of matrix macromolecules, the aspartic acid-rich proteins and serine-rich protein - polysaccharide complexes that are present in mineralised tissues from widely varying phyla [72] which could perform different and possibly cooperative roles in crystal growth *in vivo*. They have shown that aspartic acid-rich proteins after binding calcium, are capable of actively inducing, regulating, and inhibiting crystal growth *in vitro*. However, serine-rich proteins-polysaccharide complexes, under their

in vitro conditions, gave no noticeable effect on the growing crystals. Also it has been emphasised that the combined factors of charge density, ion spacing and structural effect may in part contribute to the interactions, but they alone cannot account for the observed specificity [91].

1.8 BIOMIMETIC SYSTEMS:

Landau et al [94] developed a biomimetic system and used it to investigate the precipitation of α-glycine and sodium chloride under well organised two dimensional macromolecular layer which showed that structural requirements are necessary for oriented crystallization. For sodium chloride, monolayers of positive, negative and zwitterionic charge induced crystal nucleation from faces of the type {100}, {110} and {111}, the latter two faces not being naturally occurring. In a stereochemical approach aimed at the understanding of crystal nucleation on a molecular level the oriented crystallization of glycine at air - solution interface covered with monolayers of resolved α-amino acids has been studied [95] in detail. Three different monolayers with different packing motifs of the polar head groups were used. These results implied that the packing of the polar headgroups determined the nucleation rate and the degree of orientation of the attached growing crystals. Landau et al [96] reported of their achievement of growing oriented crystals of the α-form of glycine under chiral two dimensional films of α-amino acids, by virtue of a structural match between the monolayers and the *ac* surface layer of the

attached growing glycine crystals. Such monolayers of α-amino acid of R-configuration containing long hydrocarbon chains, induce glycine to crystallize with its (010) face attached to the monolayer and by symmetry the corresponding S-amino acid monolayers induce attachment of the (0-10) face of glycine. It was also shown that the replacement of the fluorocarbon chain induced analogous crystallizations, but, with only a partial degree of orientation, whereas monolayers of a resolved amino acid bearing a cholesteroyl moiety did not promote crystallization of glycine. Monolayers of R- and S- amino acids induce attachment of both (010) and (0-10) faces of glycine. Thus they have clearly demonstrated that when α-amino acids are immobilized and the polar amino acid headgroups assume a structure similar or identical to that of one of the layers at a given face of α-glycine, they promote oriented nucleation both at the air/water and solid/water interfaces from these faces. So the oriented crystallisation is controlled, partly by the stereochemical recognition between the mineral and the two dimensional organic moiety, and partly by the packing arrangements of the compressed organic monolayers.

1.9 LANGMUIR FILMS, THEIR PREPARATON, STRUCTURE AND PROPERTIES:

Monolayers have been known considerably longer than have micelles or vesicles. Benjamin Franklin and Lord Rayleigh have investigated these monolayers towards the end of the last century [97]. Techniques for monolayer handling, developed by Pockels [98], were

standardised in the 1930's [99-103] and improved in the 1970's [104-108]. Since Langmuir and Blodgett's pioneering work in this area after whom these films have been named, hundreds of materials were studied in the form of mono-/multi-molecular films on water surfaces, under normal ambient conditions of temperature and pressure. These studies generally fall into two categories. The first and by far the most extensively studied consists of simple, non-polymeric substances which are substantially insoluble, but whose molecules have sufficient attraction for the subphase to permit them to spread and disperse at the surface. The second class consists of a wide range of polymeric materials, including certain proteins as well as synthetic polymers which are positively adsorbed at the liquid/gas interface. Further, long chain carboxylic acids, alcohols, oximes, ketones, amines, ammonium salts, sulphates and sulphonates have been used most frequently as monolayer forming substances [97]. Monolayers formed from phospholipids [109], porphyrins [110], chlorophyll [111], polypeptides [112] and polymers [113-115] have also been investigated.

Most of these monolayer forming substances are amphiphatic molecules containing alkyl chains of twelve or more carbon atoms. The polar headgroups of these surfactants are attracted to and/or in contact with water, the subphase, while their hydrocarbon tails protrude above it. When a solution of film forming molecules in any of the water immiscible solvents which are chemically inert and volatile such as chloroform, hexane, benzene, toluene, cyclohexane, ethyl ether, dimethylformamide and dimethyl sulfoxide is placed on a water surface, the solution spreads rapidly to

cover the available area. As the solvent evaporates a monolayer is formed as dictated by the amphiphilic nature of film forming molecule. Among the solvents however, toluene and chloroform were found to be heavy and exhibited a slow evaporation rate, while petroleum ether was light and evaporated faster. The fast evaporation of petroleum ether was found to result in agglomerates in the dispersed monolayer. Hence while using more volatile solvents like petroleum ether, low concentrated solutions were preferred. But with chloroform, concentration was not so critical [97]. However, when a coherent film is formed the individual molecules have two distinct regions; a hydrophilic headgroup which is easily soluble in water and a long/bulky hydrocarbon chain, which provides a hydrophobic or oleophilic tail. Fig. 1.3 shows an idealised and a somewhat more realistic monolayer.

(i) Thermodynamics of monolayer formation: Water has the unique combination of properties on its surface that makes the aqueous phase by far the most favoured subphase for Langmuir film formation. The nature of the interactions between the water surface and insoluble monolayer are quite significant and had been studied in detail [97]. The surface of a liquid always has excess free energy; this is due to the difference in environment between surface molecules and those in the bulk. In particular hydrogen bonding forces in water tend to set up loosely defined networks that will inevitably be modified near the surface. The themodynamics of liquid surfaces and the interactions of materials have been reviewed by Gaines [97]. The surface tension ((γ) of a plane interface is given

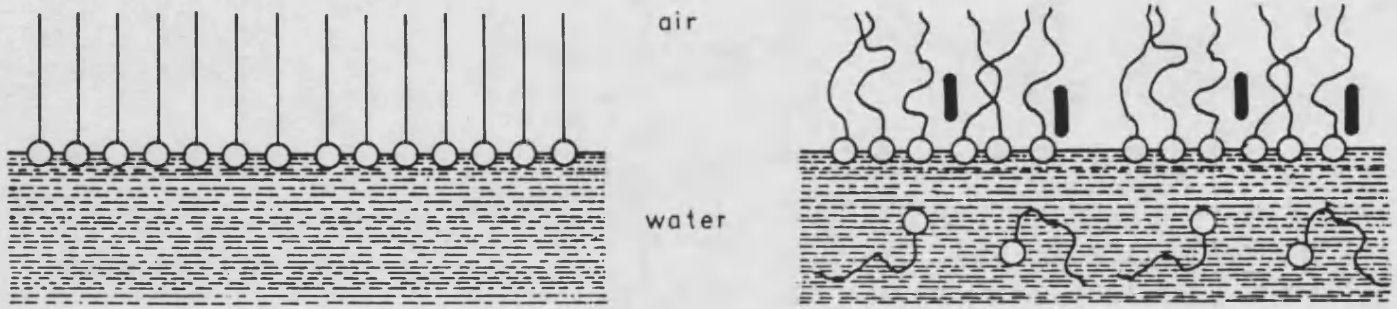

FIG. 1.3: DIAGRAM SHOWING AN IDEALIZED AND SOMEWHAT MORE REALISTIC MONOLAYER FORMATION

by the partial differential,

$$\gamma = (\delta G / \delta A)_{P,T,n_i}$$

where G is the Gibbs free energy of the system, A is the surface area and temperature (T), pressure (P) and composition (n_i) are held constant. The surface tension of water is 73 mN m^{-1} (dynes cm^{-1}) at 293 k and at atmospheric pressure. This is an exceptionally high value compared to most other liquids and goes some way towards water's pre-eminence as a subphase. When a classic monolayer forming material such as stearic acid is spread on the water-air interface, the solution spreads rapidly to cover the available area, their interactions are small, as the distance between the molecules is large, and this can be regarded as forming a two dimensional gas. Under these conditions the surface monolayer has relatively little effect on the water's surface tension. When the barrier system is used to reduce the area of the surface available to the monolayer, the molecules exert a repulsive effect on each other. This two dimensional analogue of a pressure is referred to as surface pressure (Π). For a plane surface at equilibrium the relationship, $\Pi = \gamma - \gamma_o$, holds good, where γ is the surface tension in the absence of the monolayer, γ_o is the value when the monolayer is present. It follows that the maximum possible surface pressure for a monolayer on a water surface at 293 K is 73 mN m^{-1}, but normally encountered values are much lower [97].

(ii) <u>Surface pressure-area isotherms</u>: The single most important indicator of the monolayer properties of a material is given by a plot of surface pressure as a function of area of water surface available to each

molecule. This is carried out at constant temperature and is accordingly known as a surface pressure/area isotherm, and is often abbreviated to 'isotherm'. Equilibrium values could be measured on a point to point basis, but it is more commonly recorded as a pseudo-equilibrium isotherm by compressing the film at a constant rate while continuously monitoring the surface pressure. Depending on the material being investigated repeated compressions and expansions are used necessarily to achieve a reproducible trace. A number of distinct regions have been identified on examining the isotherm and studied in detail [97-112]. When the surface area is reduced from its initial high value there is a gradual onset of surface pressure until an approximately horizontal region is reached. In the horizontal region the hydrophobic chains which were originally distributed near the water surface, are being lifted away. The surface pressure at which this occurs is usually very small (< 1 mN m^{-1}) [97] because of the weakness of interaction between water and the tail-groups. After this unresolved part of the isotherm there follows a second abrupt transition to a steeply sloping linear region, where the compressibility 'c' defined by the equation,

$C = -1/A\ (\delta A/\delta \Pi)_{T,P,n_i}$, is approximately constant.

At surface areas over 20 A^2/molecule there is an abrupt increase of slope. This is clearly due to a phase change and represents a transition to an ordered solid-like arrangement of the two-dimensional array of molecules. The compressibility in this region is also constant, but is lower by about a factor of 10. If this second linear portion of the isotherm is extrapolated to zero surface pressure the intercept gives the area per

molecule of the film that would be expected for the hypothetical state of an uncompressed close-packed layer. The interpretation of the Π-A behaviour of monolayers (gaseous, liquid, solid) in uncondensed, partially condensed and fully condensed films conventionally followed a two dimensional kinetic analysis corresponding to the three-dimensional ideal gas theory and ignored the subphase liquid. This approach simply assumes [116] that the molecules of the film move about with average kinetic energy of 1/2 kT (k is the Boltzman constant, 1.3805×10^{-16} mN m^{-1} deg^{-1} $molecule^{-1}$) for each degree of freedom. The two dimensions in the plane of the surface lead to a kinetic energy of kT which is assumed to produce the surface pressure, and this leads to an ideal two dimensional gas equation

$$\Pi A = kT$$

If Π is in mN m^{-1} and A is $Å^2$/molecule, their product should be 411.7 at 298 K. If this ideal gas equation were obeyed the surface pressure would be expected to be about 1 mN m^{-1} at 400 $Å^2$/molecule about 0.5 mN m^{-1} at 800 $Å^2$/molecule and about 0.1 mN m^{-1} at about 4000 $Å^2$/molecule. The kinetic analysis of monolayer reveals that the ideal gas behaviour, which ignores the subphase liquid molecules is obviously open to considerable criticism. A fundamentally more satisfactory way to treat extremely dilute insoluble layers, is the thermodynamic consideration of an osmotic equilibrium, in which one component, the monolayer substance, is constrained to remain in the surface while the other (the subphase liquid) is equilibrated throughout the system. The surface pressure observed is then the result of the lowering of the chemical potential of the subphase

molecules in the surface layer due to their dilution by film forming molecules. The film pressure γ is equated to the difference in the chemical potential of the subphase liquid between the surface and the bulk. When the usual infinite dilution approximations for both bulk and surface are introduced, equation $\Pi A = kT$ again results. The experimental realisation of this behaviour however, is more difficult. Deviations from ideal gas behaviour were shown by plotting ΠA against Π or A. Various attempts have been made to allow for such imperfect gas behaviour. It is possible to believe that the molecules in gaseous monolayers lie nearly flat. On the basis of evidence it is suggested that the average configuration in a gaseous monolayer is more nearly flat than vertically extended. At the opposite extreme are the condensed films, in which the molecules are arranged in nearly their closest possible packing. Condensed monolayers of the long chain fatty acids, alcohols and glycerides were the substances studied by Langmuir in his work on insoluble monolayers [117]. In those films, he has shown that the molecules stand upright with their terminal polar groups in water and their long chains closely packed. The pressure-area plots were nearly straight and very steep indicating low compressibility in the condensed layers. This reflects the presence of strong chain-chain interactions which hold the molecules in their closest-packed arrangement, with little dependence on the surface pressure. In condensed films of homologous series of long chain compounds, the Π - A diagrams show little variation with chain length, the area occupied by a molecule being substantially independent of the number of carbon atoms in

the saturated chain. For a single long chain, the area is about 20Å²/molecule, almost the same as the cross-sectional area in the bulk crystal determined by X-ray measurements [118]. Electron diffraction studies on monolayers transferred to solids confirm that the chains are oriented nearly vertically with respect to the surface. For more complex molecules, the area in a condensed film is generally quite close to that found for the appropriate projection of molecular model. Cholesterol, for example occupies about 40 Å²/molecule in its condensed film, and this is very nearly the cross-section of a model of the cholesterol ring system. This fact provides important confirmatory evidence for the revision of the structure of sterols [97].

Phase transitions of phospholipid monolayers have been analysed in terms of their surface pressure-area isotherms, and surface area-temperature isobars [119,120]. From the data available the presence of four different phases could be seen. Below 15°C, two different crystalline phases were reported and above 26°C, two fluid phases were shown. Between 15 and 26°C, the surface pressure-area isotherms have shown an ideal gas-liquid-solid monolayer formation. Ionization of monolayers have been studied by Davies and Rideal [121]. Many monolayer forming materials contain functional groups that ionize under acidic and basic conditions. The extent of ionization depends on the surface pH (pH_s) which is related to the bulk pH (pH_b) by $pH_s = pH_b + e\psi/2.3kT$ where, ψ is the interfacial potential. Change of surface pressure due to ionization is given by, $\Delta\Pi = \Pi - \Pi_o = -\epsilon d\psi$, where π and π_o are surface pressures of

the ionized and non-ionized monolayers, and ϵ is the surface charge density. Ionic monolayers contain bound and free counterions that, like those in micelles, set up an electrical double layer. However, electrical double layer theories are incomplete for monolayers and detailed experiments are scarce. Counterion effects on monolayer surface area-pressure isotherm are similar to those on micelles. The order of interaction for the following monolayers has been studied [122]. For $RCOO^-$ monolayers, the order follows as : $Li^+ > Na^+ > K^+ > Me_4N^+ > Et_4N^+$. For RSO_4^- monolayers, the order follows as : $Cs^+ = Rb^+ > K^+ > Na^+ > Li^+$. For $R\text{-}N\text{-}(CH_3)_3^+$ monolayers, the order follows as: $SCN^- > I^- > NO_3^- > Br^- > Cl^- > F^-$. For $R\text{-}NH(CH_3)_2^+$ and RNH_3^+ monolayers, the order follows as: $Br^- > Cl^-$.

The surface viscosity of the monolayers related to molecular association have also been studied. The multi-valent ions have great effects on the viscosity and solubility of monolayers [123]. The surface viscosities of monomolecular films of 14, 16,18 carbon chain aliphatic alcohols amines, acids and amides were measured as functions of film pressure, substrate pH and the rate of flow of the film [124]. The ionization of monolayers can be caused even by trace impurities in the substrate apart from pH [125]. However for stearic acid monolayers despite increasing ionization the condensed nature of the film was reported to be unchanged up to pH 9 [82]. The surface area, the resistance to evaporation and the surface viscosity were measured for substances such as esters, acids and alcohols, as a function of surface pressure [126]. The monolayer permeability to gases and the differences between bulk and monolayer

processes were discussed in terms of properties such as partition at interfaces and density fluctuations at equilibrium [127]. The monolayer properties of stearic acid have been examined upon sub-solutions of pH 2-11 and reported [128] that at pH 9, there were marked changes in the electrical characteristics and cohesion of the monolayer. The pronounced effect of Ca^{2+} and Mg^{2+} on the monolayers was used to estimate the dissociation constants of complexes of these metals with various sequestering agents. The infra red techniques were used [129] to determine the effect of pH on the composition of stearic acid films on substrates containing dilute solutions of lead, copper, calcium, barium, sodium and quaternary ammonium salts, and reported that the pH region at which interaction of salts with the film occurs is characteristic for a particular salt and is highly sensitive to changes in pH. The frequency and the shape of the carboxylate absorption band, and the effect of hydration and pH on band characteristics suggest that beryllium and barium ions form both calcium-type complexes and more ionic barium-type complexes [130].

The unique characterization by infrared reflection-absorption spectroscopy in the deduction of order-disorder tranformations accompanying interactions of a highly oriented monolayer with physical or chemical external agents is also demonstrated [131]. The orientation and bonding of L-B monolayers of stearic acid and its deuterated analogue deposited on polycrystalline gold and native-oxide aluminium films were also determined by infra red reflectance-absorption spectroscopy [132]. Bagg et al [133] have studied specifically the effect of Ca^{2+} ions

containing sodium phosphate, sodium bicarbonate or ammonium chloride as a buffer on stearic acid monolayers. Surface potentials (ΔV) of monomolecular films of n-long chain alcohols (n=16, 18, 20 and 22) were measured using the ionizing electrode method [134] and interpretations were given in terms of molecular interaction and orientation of various films at different pressures. Apart from pure organic substances, some acid salts such as copper stearate, nickel stearate and zinc stearate were also studied as monolayers [135]. Stearic acid monomolecular films on calcium chloride sub-solutions were characterized at a surface pressure of 31 mN m^{-1} over the pH range 2-9 by film area, surface potential, surface viscosity, monolayer uniformity and stability measurements [136]. The surface film primarily consisted of unionized stearic acid molecules in the pH range 2 - 4.2, and then behaved as a mixture of stearic acid and calcium distearate molecules with increasing sub-solution pH. However, upon exceeding pH 6.4, a structural rearrangement occurred as the ionized molecule began to associate into calcium stearate surface micelles. The close packed monolayer, although uniform below pH 8 was shown to become non-uniform at higher pH values. When the stearic acid monolayers are compressed to solid phase, a slow collapse process occurs as crystallites, intermediate multilayer structures and bulk phase material gradually form [137]. At smaller surface areas the phenomenon of collapse occurs and the compressibility approaches infinity. The onset of collapse depends greatly on such factors as the nature of the film and the rate at which the film is being compressed. In this type of collapse it is believed that molecular

layers are riding on top of each other and disordered multilayers are formed [97].

However, the shape of the isotherm depends greatly on temperature and a number of different phase transitions were reported to be observed when the temperature varied [115]. A wide investigation of a range of homologues of stearic acid has shown that a reduction in chain length can be to some extent, traded for an increase in temperature. The collapse pressures and collapse rates of nine different surfactant monolayers including stearic acid and octadecanol have been studied in detail [138]. The surface pressure-area curves of mixed monolayers of cholesterol with n-long chain fatty acids were analysed at various compositions and temperatures, and reported that the area occupied by the monolayer of fatty acid is somewhat smaller by the addition of cholesterol [139]. Barnes [140] has shown that the apparent evaporation of water depends on the monolayer permeation and is thus related to the resistance of a monolayer to the evaporation of water on which it is spread. The appearance of hysteresis was observed for cholesterol monolayers and was correlated for the permanent loss of molecules from the monolayer occurring during compression which was proved to be dependent logarithmically on the compression rate [141]. The effect of pH on the stability study of stearic acid and octadecanol films on water at various pH by measuring the area of the film under a constant pressure was also examined [142].

Some new optical and x-ray techniques have been developed and applied to surface studies [143]. Among these techniques the x-ray

reflectivity has been previously used to determine the density profile at a liquid-vapour mercury interface [144] as well as the surface roughness of water. However the new prospect on the properties of Langmuir monolayers has been opened up when Bosio et al [145] studied the roughness of films on water subphase using x-ray reflectivity. Later the feasibility of the technique as a non-invasive structural probe for liquid surfaces has been demonstrated by studying the structure of an insoluble monolayer spread on an aqueous subphase containing caesium chloride, cadmium chloride and lanthanum chloride. The pH dependence of the amount of bound cadmium has been used to show that a pk_a value of 5.35 ± 0.05 describes the conversion from acid to cadmium soap [146].

The formation of surface films of amphiphilic polymers at the air-water interface, the transfer of these surface films to solid substrates by means of Langmuir-Blodgett technique, and the structure of the transferred films have been investigated using proton n.m.r spectroscopic methods which revealed that the transferred films maintained the oriented structure of the monolayers at the interface [147]. The polymerization leading to substantial structural changes and the kinetic changes were studied using u.v spectroscopy, small angle x-ray scattering and scanning electron microscopy [148]. The first determination of structure for classical monolayer systems (fatty acid and alcohol) on the surface of water, based on the observation of first and second order diffraction peaks, that showed a distorted hexagonal structure with orthorhombic cell dimensions, were reported by Bohanon et al [149]. In situ microscopic analysis leading to structural inferences have been studied by

x-ray diffraction studies of organic monolayers on the surface of water [150]. Along with normal conventional methods, controlling the micro structure of monomolecular layers has been reviewed on the range of lateral structures which have been deduced using the newly developed techniques of fluorescence microscopy and x-ray scattering [151]. The packing arrangement of a floating monolayer of palmitoyl-(R)-lysine at the air-water interface by grazing incidence x-ray diffraction and reflection measurements were determined [152]. Monolayers of the lipid arachidic acid (C_{20}) and of the phospholipid dimyristoylphosphatidic acid have been studied by x-ray reflection and diffraction techniques [153]. The structure of the monolayer of heneicosanol on water in the region of near close packing was studied by grazing incidence in-plane x-ray diffraction and that had revealed a kink, signalling a phase transition in the monolayer [154].

The dependence of the properties of monolayer on the subphase solution temperature was studied in detail [97]. By decreasing the temperature, the condensation of the molecular layers was found to be made easier as the thermal stability is enhanced. However, it was shown that by lowering the temperature, the viscosity of the monolayer increases, thus making the monolayer brittle. High temperatures in contrast cause the films to expand and ultimately result in thermal forces overcoming the rather weak vander Waal's binding forces which hold the molecules together.

Among the many applications of mono- and multi-layers, the thickness gauge was one of the very few devices to result from the intense

interest during the 1920's and the 1930's. Today a number of other possible applications for thin films have presented themselves. One promising application for LB-films concerns their use as fine-line lithographic resist materials in the fabrication of very large scale integrated circuits. Research is also being conducted into the possibility of incorporating LB-films into electronic devices. One relatively simple application is the thin film gas detector. The electrical conductivity of the phthalocyanines, for example, has been shown to alter in the presence of certain oxidising ambients. LB-film materials have also been put to use as semi-conductors [155,156]. LB-films as adsorbed on amphiphiles on solids for catalysis, enzyme activity on solids and metal implants (thrombosis and blood compatibility) are some of the recent applications. Recently, scientists have used monomolecular films as organised organic matrices for the oriented crystallization of glycine and sodium chloride. The structure of these monolayers could be correlated with the crystal faces formed underneath them [94-96].

1.10 CRYSTAL STRUCTURES OF CALCIUM CARBONATE:

Calcium carbonate occurs in nature in five crystalline forms. Three anhydrous forms of calcium carbonate, calcite, aragonite and vaterite, two hydrated crystalline phases, monohydrate and hexahydrate and amorphous calcium carbonate are all known in biological systems (see section 1.2). Dolomite, $CaMg(CO_3)_2$ is a widely distributed geological mineral. On the

basis of limited evidence, huntite, $Mg_3Ca(CO_3)_4$ may also be present in the mineralizing front during the formation of enamel. In view of the ubiquitous presence of sodium ion in biological systems, it is conceivable that the sodium calcium carbonates, shortite, $Na_2Ca_2(CO_3)_3$, pirssonite, $CaNa_2(CO_3)_2.2H_2O$ or gaylussite, $CaNa_2(CO_3)_2.5H_2O$ may participate in biological mineralization at least in a transitory form. Two further forms, calcite II and calcite III are stable at high pressures. Calcite and vaterite have hexagonal space groups (R3c, $P6_3mmc$), aragonite is orthorhombic (Pmcn) and the hexahydrate is psuedodohexagonal. The plane of the carbonate ions lies perpendicular to the hexagonal or psuedohexagonal axis in calcite and aragonite, and parallel to a similar axis in vaterite and hexahydrate.

(i) **CALCITE**: The structure of calcite mimics that of the cubic close packed structure of sodium chloride by compression along the triad axis with calcium and carbonate ions replacing respectively sodium and chloride ions. The compression along the triad axis gives a rhombohedral cell to calcite such that the three rhomb edges meeting at the triad axis make an angle of 101°55' with each other instead of 90°. This cell is not the unit cell as successive CO_3 triangles point in opposite directions, hence the primitive cell contains two $CaCO_3$ (Fig. 1.4A). The triangular CO_3^{2-} groups occur half way between Ca^{2+} layers and each oxygen has two calcium nearest neighbours (Fig. 1.4B). The distance between calcium layers is 2.86 Å and the distance between calcium ions in the same layer is 4.99Å. Each Ca^{2+} ion

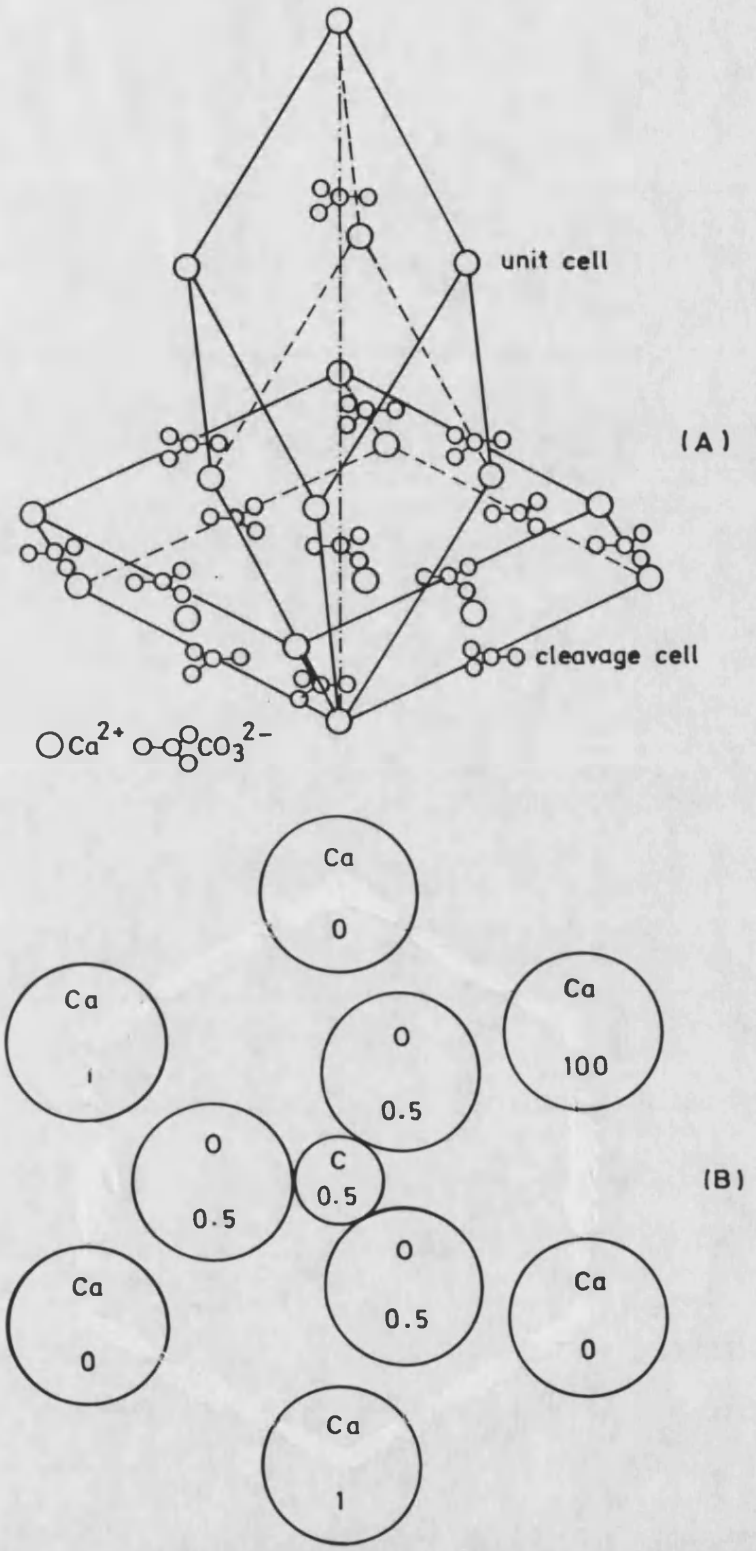

FIG. 1.4: (A) CALCITE RHOMBOHEDRAL UNIT CELL AND CLEAVAGE RHOMBOHEDRAL CELL SHOWING THE POSITION OF CALCIUM AND CARBONATE IN THE CRYSTAL STRUCTURE and (B) THE POSITION OF CARBONATE GROUPS IN CALCITE.

is coordinated by six oxygen atoms. The Ca-O distance is 2.38 Å and C-O is 1.3 Å.

In modern crystallographic usage the symmetry of the calcite unit cell as well as of the whole structure is summarised by the spacegroup $R3c\text{-}D_{3d}$. This latter was assigned by Schiebold [157] and by Wyckoff [158] in their examinations of the structure. Calcite has local point of symmetry of the group 32. The hexagonal unit cell which is rhombohedrally centred has cell contents $6CaCO_3$. The cell parameters are: a: 4.9896 Å, c:17.0610 Å. The positions in the unit cell are:

Ca in 6(b): 0 0 0

C in 6(a): 0 0 1/4

O in 18(c): x 0 1/4 where x=0.2568.

When dealing with rhombohedral calcite, one might use either rhombohedral or hexagonal axial systems. The primary advantage of the hexagonal axial system lies in the disposition of the axes relative to one another. The three a-axes, of equal length, intersect at angles of 120° with respect to one another and lie perpendicular to the c axis. Since the line connecting the apices of the rhombohedron is the three fold axis, all lattice points in a rhombohedron are well described using a hexagonal axial system. Owing to the presence of fourth axis (a_3) used in the hexagonal axial system, four-symbol Miller-Bravais indices (h,k,i,l) are used, where h+k+i=0. This arrangement makes it relatively easy to visualise geometric aspects of the crystal structure, especially planar features at distinct levels along the c axis. In calcite the heights of hexagonal cells are same as for the acute rhombohedral cells, although they contain $6CaCO_3$ and is triply primitive.

Modern descriptions of calcite crystals are given almost exclusively in terms of hexagonal cell. Much of the older literature uses a rhombohedral description, which may be based on either the true unit cell or the morphologic cell (also called a cleavage cell).

The basic configuration of the carbonate group is found to be remarkably uniform in calcite. In its general form the carbonate group resembles an equilateral triangle with oxygen atoms at the corners and a carbon atom at the centre. Lippmann [159] in his recent structural data for CO_3 groups showed that the mean value for the O-C-O angle to be 120° in agreement with the ideal value. He found that the mean C-O bond length to be 1.284 Å which is in good agreement with the ideal value of 1.30 Å. For oxygen atoms in CO_3^{2-} the bond length is 2.22 Å. Based on the uniformity of bond lengths and angles, it is reasonable to assume that the CO_3 group is a fairly rigid structural unit with strong covalency in character. In general the C-O bond will be considerably stronger than the Ca-O bond strength. In calcite the C-O bond strength is four times that of the Ca-O bond. The cleavage plane {10.4} is the one that breaks the least number of Ca-O bonds and no C-O bonds. This explains the normal existence of the rhombohedral {10.4} form of calcite [160].

In calcite structure, the layers of calcium atoms alternate with carbonate layers along the $\underline{c}$ axis. CO_3 groups have like orientation in the same layer, but the reversed orientation in the successive layers. Thus the translation along $\underline{c}$ direction to similar layers is doubled in comparison with analogous translation in the NaCl. Perhaps a better

description of the structure is provided if the position of the oxygen atoms are referred to a pattern of hexagonal close packing. While only approximate, this analogy does show the orientational relationship among carbonate groups in successive layers. Within a given layer of hexagonally-packed oxygens, carbon atoms are introduced such that oxygen coordinates with only one carbon resulting in a hexagonal distribution of C in that layer. Calcium atoms then fill those octahedral interstices (between oxygen layers) that avoid coordination with two oxygens of the same CO_3 group since that O-O distance would be very short. Carbon atoms in successive oxygen layers are distributed so as to avoid superposition over either calcium or carbon atoms in adjacent cation and CO_3 layers. This ensures calcium is then coordinated to 6 oxygens, each belonging to different carbonate groups. The unit translation along the direction of stacking is equivalent to the height of the carbonate layers. In reality the oxygens are not closest packed, and in fact the ideal hexagonal pattern is attained owing to the fore-shortening of the O-O distance (2.22Å) within the carbonate groups. In calcite, the shortest O-O distances between different carbonate groups are 3.19Å across CO_3 planes and 3.26Å within the plane, both considerably larger than twice the effective ionic radius of oxygen (2.72 Å).

(ii) **ARAGONITE**: The second most stable form of calcium carbonate, aragonite is related to the nickel arsenide structure by compression along the hexad axis, again because of the planar CO_3^{2-} ions. The arrangement of carbonate in aragonite is shown in Fig. 1.5(A). All CO_3^{2-} groups which lie

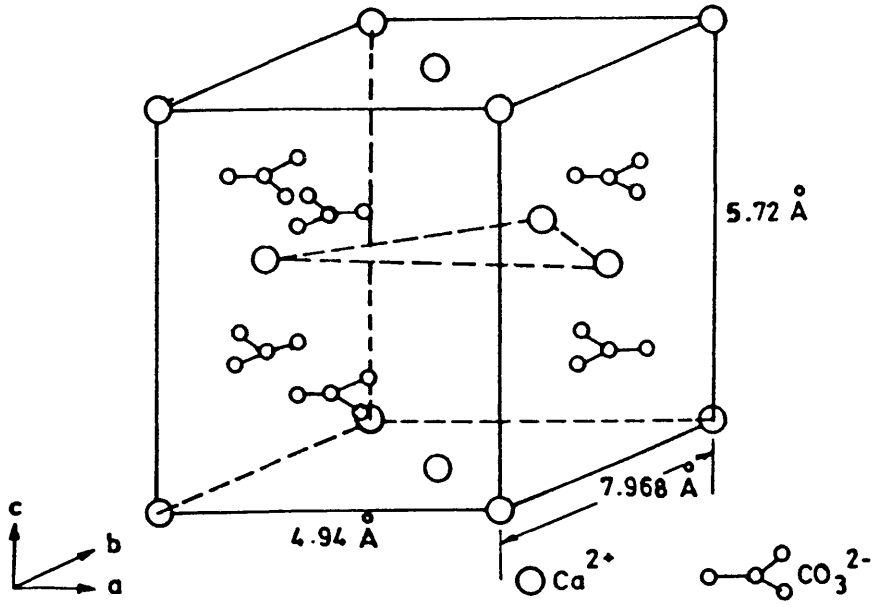

FIG. 1.5: (A) ARAGONITE UNIT CELL STRUCTURE.

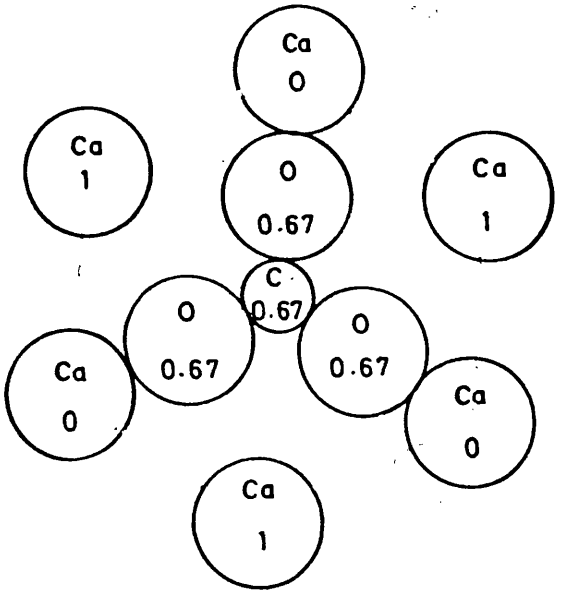

FIG. 1.5: (B) THE ARRANGEMENT OF CALCIUM AND CARBONATE IN ARAGONITE. ALL CABONATE GROUPS LIE IN A ROW PARALLEL TO THE C AXIS.

in a row parallel to the a axis are similarly oriented, but groups which lie in a row parallel to the (110) plane point alternate ways and/or displaced up and down in the direction of the c axis show that although the Ca^{2+} ions are in a hexagonal array, the overall symmetry is orthorhombic (Fig. 1.5B). The unit cell contains four $CaCO_3$. The distance between Ca_{2+} layers is again 2.86 Å.

In calcite, the Ca atoms in a layer lie at the corners of an equilateral triangle of side 4.96 Å, whereas in aragonite one side of the corresponding triangles is 4.94 Å and the other two are 4.66 Å. The Ca-O distance is greater than in calcite, and each Ca^{2+} ion is coordinated by 9 oxygen atoms, but the C-O distance is the same. The space group is Pmcn (D_{2H}).

(iii) **VATERITE:** The metastable form of calcium carbonate, vaterite has a nickel arsenide-related structure, but retains hexagonal symmetry with Ca^{2+} ions in a primitive hexagonal lattice and CO_3^{2-} in an extended hexagonal close-packed structure in the c direction such that the carbonate groups are parallel (or nearly parallel) to the c axis (Fig. 1.6A). X-ray diffraction has been used to determine the dimensions of the pseudo cell which is at 30° to the true cell, hence for the psuedo cell a'= 4.13 ± 0.01 Å, c'= 8.49 ± 0.02 Å and the true cell dimensions are $a = a'\sqrt{3}$ = 7.16 Å, C = 2c' =16.98 Å. In the pseudo cell, the calcium atoms form a trigonal prism, with a C atom at the centre of the prism oriented such that each O atom is equidistant from the two nearest Ca atoms (Fig. 1.6B). Hence, Ca^{2+} is coordinated by 6 oxygen atoms at 2.4 Å and by 2 oxygen atoms at 2.9 Å, and

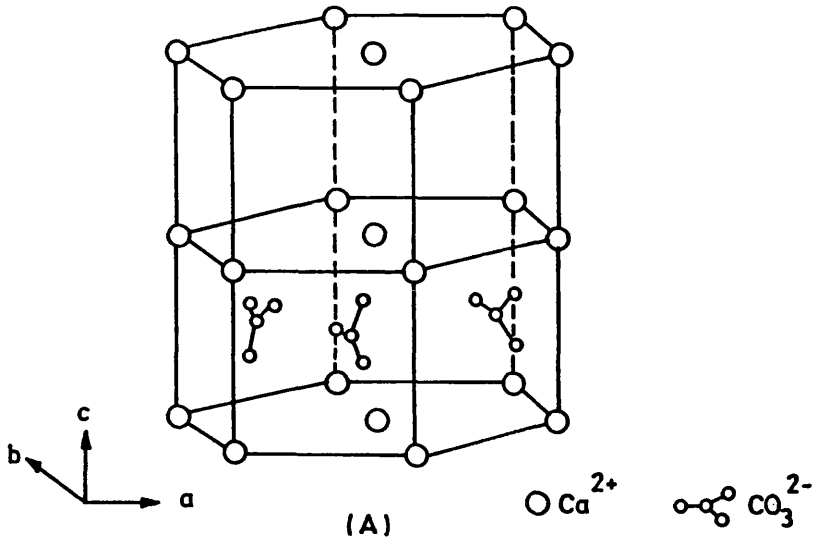

FIG. 1.6: (A) VATERITE UNIT CELL STRUCTURE.

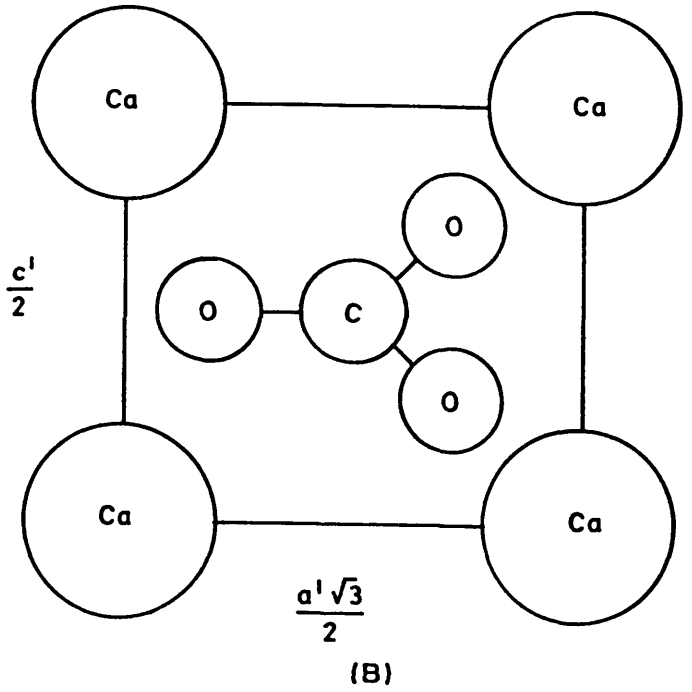

FIG. 1.6: (B) THE ARRANGEMENT OF CARBONATE AND CALCIUM IN VATERITE UNIT CELL.

can be considered to be 8 coordinate. The C-O bond distance is 1.26 Å which is shorter than in aragonite and calcite. The distance between the Ca atoms within a layer is 4.13Å and the distance between the calcium layers is 4.25Å.

The differences in structure result in thermodynamic differences between these three forms. The vaterite structure is susceptible to stacking faults, whereas aragonite is highly ordered. However, calcite has the highest (most negative) free energy of formation, under standard conditions resulting in the order of thermodynamic stabilities: calcite > aragonite > vaterite, and therefore vaterite is the most soluble and calcite the least soluble phase at standard conditions of temperature and pressure. This fact is shown by the solubility products of these three phases represented in the form of log k_{SP} at 25°: Vaterite: -7.60, aragonite: -8.22 and calcite:-8.42 [161,162]. The refractive indices for vaterite have been quoted as ω=1.550 and γ=1.600. The differences in packing lead to the different densities (ρ): aragonite: 2.95, calcite: 2.71 and vaterite: 2.54.

1.11 CRYSTALLIZATION OF CALCIUM CARBONATE BY INORGANIC METHODS:

The crystallization of the sparingly soluble calcium carbonate from aqueous supersaturated solution involves ions or molecules in solution which must break away from their bonding with water and bond together to form a separate solid phase. There are two general categories of crystal nucleus formation, homogeneous and heterogeneous. In the former

the constituent ions in solution come together randomly to form the solid nucleus. In the heterogeneous case the nucleation takes place through the intervention of a substrate phase which may be a dissolved species or a solid suspended in the precipitating solution. In most synthetic systems, one can assume that nucleation is partially heterogeneous since solutions generally contain some impurity particles which can act as heterogeneous nucleators. Kinetic factors are involved in determining the nature of crystal nucleus and of the growing phase. The kinetic factors had been studied by using a highly reproducible seeded growth technique and under certain conditions secondary nucleations induced on the surface of the seed crystals was also analysed. In calcium carbonate crystallization systems, the temperature, supersaturation, surface concentration, pH, ionic strength and the presence of foreign ions are found to be important in determining the nature of the phase that grows in solution. In the nucleation of solid phases from solution the situation is complicated by simultaneous nucleation and growth phenomena taking place all the time.

Nuclei are presumably formed in the first place by chance collisions of several units, and the probability that these units could be present simultaneously in small volume would depend upon both concentration and temperature. Increasing supersaturation therefore promotes the formation of the crystal nuclei and hence speed up the rate of growth, whereas an increasing temperature will tend to disrupt crystal nuclei by thermal motion, with a reduction in the rate of nucleation and a corresponding reduction in growth rate. However the situation is often

complicated when other factors are involved.

Crystallization of calcium carbonate has been the subject studies of several groups for a long time. The kinetics of crystal growth of calcium carbonate was studied using a reproducible growth technique [163,164]. Kitano [165] employing a spontaneous precipitation technique had studied the system in various aspects including the temperature, pH and the influence of various organic and inorganic ions. Friedman et al [166] have stressed the importance of organic substances and pH during carbonate formation reactions. Watabe [167] had mentioned the importance of inorganic ions in the formation of calcium carbonate in biological systems. The influence of magnesium, strontium and sulfate ions on the morphology and polymorphic, and chemical composition of the precipitate was also examined [168]. The spontaneous precipitation of calcium carbonate leading to homogeneous and heterogeneous nucleation of calcite, vaterite or aragonite, and the proportion of each polymorph depending on temperature was studied by using millimolar concentrations of $CaCl_2$ and $NaHCO_3$ solutions [169]. Lippmann [170] had shown that in the absence of seed crystals and of bivalent cations other than Ca^{2+}, the calcium carbonate polymorph precipitation is most clearly determined by nucleation. The polymorph formed at ordinary temperature is calcite, especially in slow precipitations and this is in harmony with thermodynamic stability, whereas the formation of aragonite at or above 30°C is not. From about half way towards 100°C the additional polymorph, vaterite becomes more and more important. Vaterite may also nucleate and grow at ordinary temperature

under suitable conditions. These changes in the polymorphic precipitation have been characterised by Lippmann and was explained in terms of the ratios of CO_3^{2-}/Ca^{2+} in solution, and correlated with the more open structure of vaterite. Vaterite is capable of forming at ordinary temperature not only in certain organisms but also in laboratory precipitates. Vaterite precipitates instead of the most stable polymorph, calcite, from solutions containing ample CO_3^{2-} [171] or from a solution of 1M $CaCl_2$ and 2M NH_3 through which CO_2 gas is passed [172]. The precipitation of calcium carbonate from aqueous solutions at supersaturations sufficient for spontaneous precipitation, but low enough to enable highly reproducible results was carried out with respect to induction period and rates of precipitation. The threshold for the onset of calcium carbonate precipitation at pH 8.6 has been established and the induction periods and rates of precipitation were both found to be strongly dependent on supersaturation [173]. The inhibition of calcite crystallization by inorganic phosphate has been examined and shown to be dependent upon the initial degree of supersaturation of the aqueous solution [174]. The dissolution / precipitation kinetics have been studied [175] using a rotating disc technique, and several kinetic equations were proposed for the mechanism. Ogino et al [176] recently have published a careful investigation of calcium carbonate precipitation processes in supersaturated solutions. They have identified an amorphous calcium carbonate, that has a solubility product of approximately 10^{-6} (mole per litre)^2, which forms during rapid precipitation from supersaturated solutions and subsequently transforms to a mixture of crystalline polymorphs within minutes.

Specifically, this amorphous calcium carbonate transforms either to the unstable polymorphs of vaterite (at low temperatures) and aragonite at high temperatures or to calcite; both vaterite and aragonite polymorphs transform to calcite through a dissolution-reprecipitation mechanism. The growth of calcite crystals formed the rate determining step in the dissolution-reprecipitation process. The crystallization of calcium carbonate on polymeric substrates such as sulfonated polystyrene and polystyrene divinylbenzene was studied [177] and found to give calcium carbonate monohydrate polymorph which slowly changes into the thermodynamically stable calcite.

The inhibition of calcium carbonate crystallization by proteins, polypeptides and other polymers were under study for a long time. Recently it has been reported [178] that polyaspartate molecule of 40 residues could be an optimum sized polymer molecule for the inhibition of crystal nucleation.

The physico-chemical aspects of calcium carbonate precipitation from aqueous solutions of calcium bicarbonate as a result of out-gassing carbon dioxide has been shown by Khayat and Garside [179], which has led to a method of determining the supersaturation of solutions, including the gaseous components.

CHAPTER II

METHODS AND MATERIALS

2. EXPERIMENTAL METHODS:

2.1 LANGMUIR MONOLAYERS:

The experimental methods and the techniques were carefully chosen to suit the crystal growth studies and to make a suitable model for biomineralization. A Langmuir "mini trough" (Fig. 2.1) supplied by Joyce-Loebl was used to prepare two dimensional monomolecular films. It was connected to a pH meter and a X-Y/Y-T chart recorder. The monolayer was always enclosed in a constant perimeter barrier which could be moved so that the area could be altered. The chart recorder was used for recording pressure-area isotherms. The pH meter was used to measure the pH of the solution in the trough and was connected to the chart recorder to enable the pH to be measured and plotted as necessary. It was critical to clean the trough, barrier belt and the rollers thoroughly and to calibrate the recorder and the pH meter before each experiment.

2.1.1 CALIBRATION PROCEDURE: There are three parameters to be calibrated prior to film formation in the Langmuir trough:

(i) **Calibration of surface area**: In the calibration of the surface area, it was necessary to calibrate the chart recorder with the maximum and the minimum areas contained within the constant perimeter barrier. The maximum area was 550 cm^2 and the minimum area 100 cm^2 and hence the area within the barrier was 450 cm^2. This area was calibrated between

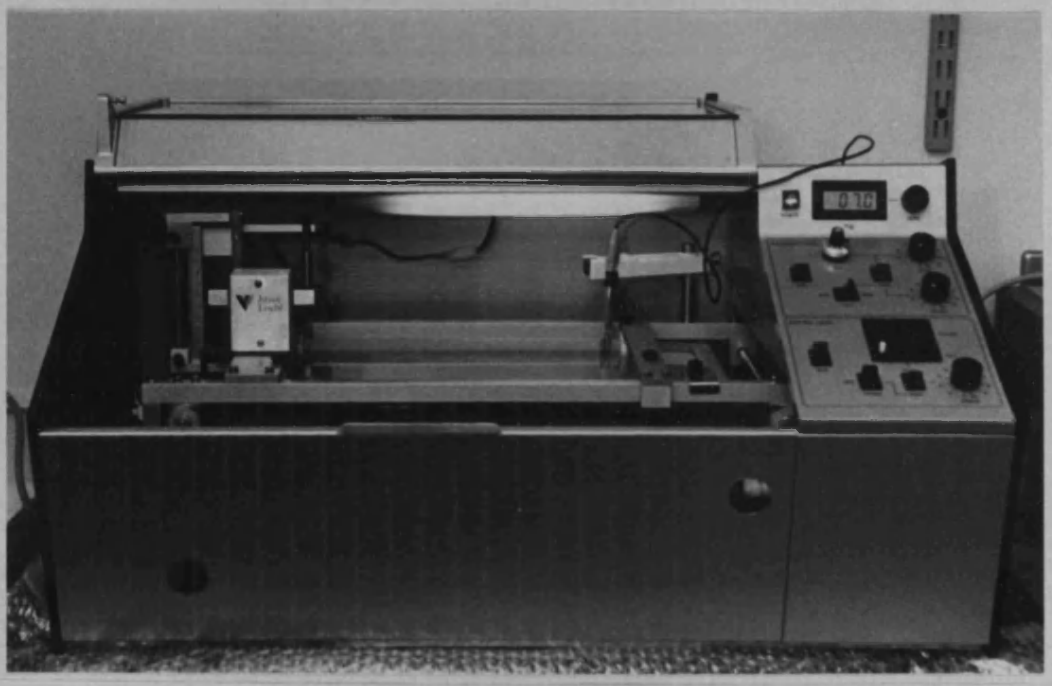

FIG. 2.1: LANGMUIR "MINI TROUGH" USED FOR FILM FORMATION AND CRYSTAL GROWTH

0 and 300 mm on the x-axis, however this could be altered depending on the experiment.

(ii) Calibration of surface pressure: The surface pressure had to be calibrated before each isotherm. A sensitive microbalance with sensor in the liquid surface monitored the differential surface tension. This Whilhelmy plate technique of monitoring pressure was very reliable and enabled the surface pressure to be measured accurately over a wide range. The barrier drive was linked to a microbalance by an electronic feed-back system. The working area, therefore could be compressed until the molecules formed a compact monomolecular film. The Wilhelmy balance was based on a thin plate which was semi-immersed in the subphase and attached to the microbalance vertically above it. Values of weight can thus be related to surface pressure providing the contact angle of the plate with the liquid is zero. Many different materials can be used for the Wilhelmy plate, one of the most effective is filter paper, which was attached to the balance head by a length of a fine wire, that enabled accurate measurements of the extremely small forces involved. It was advisable to ensure that the filter paper strip cross section lay at 90 degrees to the length of the barrier which moved towards it, in order to minimise any interaction with the uniform distribution of the film compression forces. The forces on the plate consist of gravity and surface tension acting downwards and buoyancy due to displaced water upwards. If the plate has negligible thickness and width 1 cm, then $\Delta F = 2\Delta\gamma$, so that the weight measured in milligrams is equal to twice the surface pressure measured in dynes cm^{-1} or $mN\ m^{-1}$.

The microbalance was calibrated and set up for measurements as described below. The manual recommended a strip of filter paper of 1 cm wide and 3 cm length, as the sensor for the Wilhelmy plate balance. However 3 cm was too long for the type of trough supplied (which is optional shallow model) and so pieces around 1.5 cm were used. This did not catch at the bottom of the trough. The paper was hung and the balance zeroed as stated in the manual by using lengths of solder on the left side of the beam. To check the surface purity of the solution the barrier was closed to the minimum area. If the pressure rose high from zero, indicating the presence of impurities on the surface, then the surface was vacuum cleaned again by a glass capillary tube attached to a vacuum pump via a length of rubber tubing. When that had been done, the barrier was reversed to maximum area, the balance zeroed and the surface compressed again at slow speed. This was repeated as necessary, generally 2 to 3 times until the surface was clean. A reading of around 0.5 mg at the minimum area was usually taken to be acceptable. Calibration of the chart recorder using a 100 mg weight was also checked every time. The recorder was calibrated to read 0 mm on the Y1 axis at 0 mg balance reading and 200 mm at 100 mg balance reading. Thus Y1 axis was calibrated to give pressure ranging from zero to 50 mN m^{-1} although other pressure ranges could be established.

(iii) **Calibration of pH meter:** The calibration of pH meter was done using standard buffer solutions at pH 4.0, 7.0 and 9.0 to measure on the Y2 axis which was set up from 0-140 mm to read the pH between 0 to 14.

2.2 PURIFICATION OF WATER:

As the monolayer formation required high purity water, the purification of water was given primary importance throughout. Apparatus cleaning was done using nitric acid, detergent and rinsed with high purity water. Either triple distilled and activated charcoal filtered water or double distilled Purite charcoal column filtered water was used throughout. The pure water gave a pH 6.0 to 6.8.

2.3 PURIFICATION AND ANALYSIS OF CHEMICALS:

Calcium carbonate (AR, BDH) sample was used directly from the bottle. However the purity of the salt, including the polymorphic distribution was checked by X-Ray diffraction. Infrared spectral analysis further confirmed the purity of the sample.

The organic chemicals such as stearic acid, octadecylamine, octadecanol, and cholesterol were obtained in the purest form possible and further purified by recrystallization from chloroform. Their purity was finally checked by microelemental analysis and infrared spectroscopy. Aristar quality solvent chloroform was used to prepare the solutions of monolayer forming materials. Other inorganic chemicals used occasionally such as aluminium chloride, sodium chloride, calcium chloride and lithium chloride (AR, BDH) were taken in the purest form available.

2.4 CLEANING THE TROUGH AND THE GLASSWARE:

The new trough was rinsed well with clean running cold water and decon 90 followed by rinsing with distilled water. Then using 200 ml of AR chloroform it was cleaned and wiped thoroughly. The cleaning with high purity water was repeated twice. Barriers and rollers, when new, were put in a 600 ml beaker added approximately 10 ml of decon 90, soaked for 30 minutes and washed thoroughly with running cold water. They were cleaned ultrasonically for 5 minutes and rinsed with high purity water 3 times and refluxed in isopropyl alcohol vapour for 1 hour. During general use, the barrier and rollers were first cleaned with detergent, then with acid, and chloroform and finally rinsed with high purity water. The glass-ware was cleaned with acid and detergent, and rinsed with high purity water.

2.5 PREPARATION OF MONOMOLECULAR FILMS:

Monomolecular films were formed in the Langmuir trough and surface pressure-area plots were recorded for octadecanoic acid, octadecylamine, octadecanol and cholesterol on pure water, on bivalent cationic solutions, and on calcium bicarbonate solution subphases. The typical method adopted is given below.

The trough was filled with 1.8 l of pure triple distilled water keeping the water level half way up the barrier side. The pH of the solution was measured acccurately. The surface impurities, if any, were removed using a capillary vacuum suction and the surface pressure was

brought down to zero. A solution of stearic acid 10 mg in 10 cm^3 $CHCl_3$ was prepared fresh just before plotting of isotherms to minimise any error in concentration due to loss of chloroform by evaporation. This mass was calculated to give a recommended concentration of around $2.0x10^{-7}$ moles dm^{-3} in the monolayer such that the amount of acid added gave a compressed film midway between the maximum and minimum area of the trough. Stearic acid was applied to the surface using a micrometer syringe which could deliver small quantities of liquids to very accurately known levels up to an accuracy of $2X10^{-4}$ cm^3 or 0.2 µl. Around 60 µl were added accurately each time in order to have a reasonably good area of the monolayer. The drops were added slowly as they required time to disperse. Careful addition also prevented surface bilayer formation. After allowing the chloroform to evaporate with the trough cabinet open, the lid was closed and the balance zeroed. With the manual control mode set at speed 'one' the forward control was engaged and the monolayer slowly compressed at a rate of ≈2 $Å^2$/molecule/minute. The individual plots are given in the relevant chapters. The isotherm was generally complete in ≈10 minutes. It was possible to calculate from the graph the limiting molecular area of the substrate in the monolayer; this is the area occupied by each molecule when the monolayer was in the fully condensed phase. The monolayer was compressed to a point at which the molecular area remained effectively constant for a large change in pressure, thus ensuring the formation of the fully condensed stable monolayer (Fig. 2.2). The pH and the temperature of water was measured accurately each time at the start of the experiment.

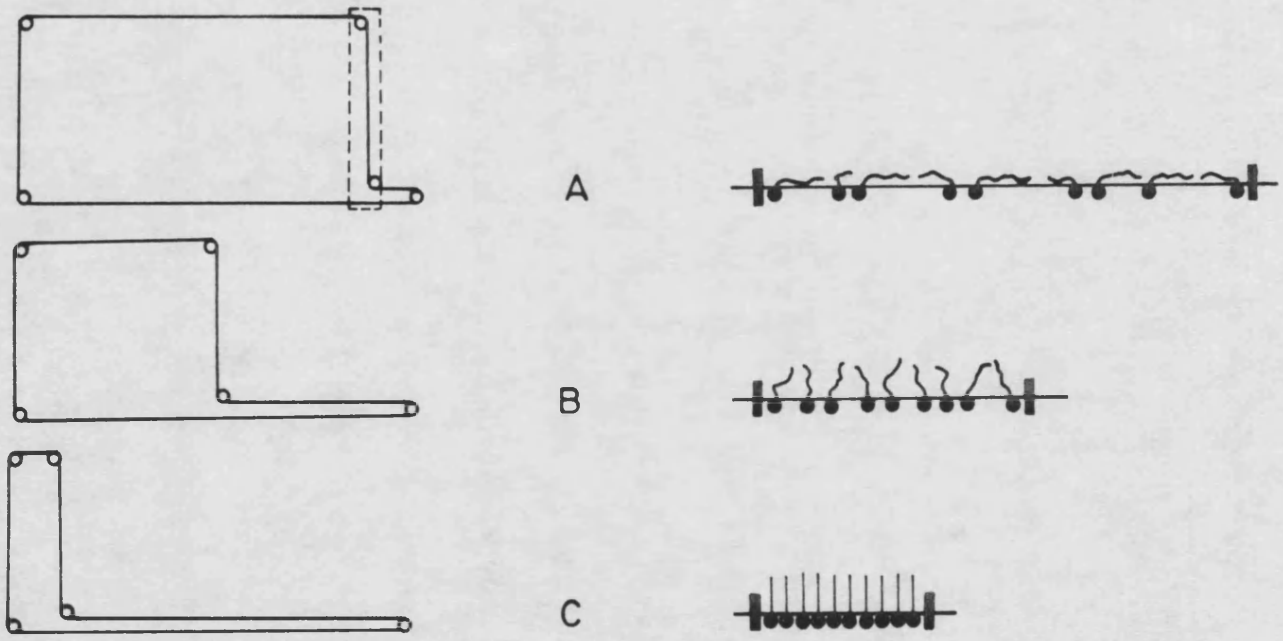

FIG. 2.2: SCHEMATIC DRAWINGS OF FILM COMPRESSION AND THE CORRESPONDING ORIENTATION OF THE MOLECULES IN THE FILM: (A) UNCOMPRESSED LEVEL WITH RANDOM ORIENTATION OF MOLECULES, (B) PARTIALLY COMPRESSED LEVEL WITH SOME ORIENTATION IN THE FILM and (C) FULLY COMPRESSED LEVEL WITH ORIENTED MOLECULES IN THE MONOLAYER.

The initial pH of water varied from experiment to experiment within a range of 5.8 to 6.8. No attempt was made to keep the pH constant for all the experiments as it was important not to have any added ions in the solution. From the limiting molecular area, and from the number of monolayer molecules the area/molecule on various subphase solutions was determined.

To check the surface purity of the subphase and the complete evaporation of the solvent chloroform, a blank run of the isotherm was done by moving the barrier to minimum area on pure water before adding the chloroform and the pressure checked. After adding chloroform on the surface and allowing for 5 minutes to evaporate the isotherm plot was drawn. In both the cases it was expected to give negligible pressure rise in the pressure-area plots.

2.6 CONTROL EXPERIMENTS:

Calcium carbonate has three main crystal forms: calcite, aragonite and vaterite. Many studies have been made of the conditions under which calcium carbonate is formed in various polymorphic forms (see section 1.11). No definite conclusion has yet been reached, however as to the exactness and the significance of the results. In the present system for growing the calcium carbonate crystals the method used by Kitano [180] was followed with slight modifications. Kitano's method involved bubbling of CO_2 gas through a suspension of calcium carbonate to give a bicarbonate solution according to the reaction,

$$CaCO_{3(s)} + CO_{2(g)} + H_2O_{(aq)} \rightleftharpoons Ca^{2+}_{(aq)} + 2HCO_3^-{}_{(aq)} \quad (I)$$

When the solution was left to stand in an open vessel, CO_2 gas would be released by the reverse reaction thus precipitating $CaCO_3$. The advantage of using Kitano's method was that addition of any foreign ions was completely avoided and calcium carbonate was formed from the calcium bicarbonate solution as CO_2 gas escaped. This reaction was used because it is typical for the formation of calcium carbonate by inorganic processes in the hydrosphere. It is one of the "homogeneous precipitation" reactions and no other added ions are present other than calcium, bicarbonate and carbonate ions with hydrogen and hydroxide ions in the mother solution. Therefore the reaction is suitable to study the effect of organic monolayers on the crystallization of calcium carbonate. The factors influencing the precipitation of calcium carbonate from aqueous solution include;

(a) the presence of certain inorganic ions, including hydrogen and hydroxide ions and carbon dioxide in the mother solution

(b) the influence of organic material including enzymes and bacteria

(c) the mechanical conditions

(d) the temperature and

(e) the transformation of the crystal type after the calcium carbonate nuclei had been formed.

The conditions that determine the polymorphic crystallization of calcium carbonate have been discussed by many researchers (see section 1.11) however, many questions still remain unsolved. The temperature of the

mother solution should be considered as one of the most important factors controlling the polymorphic formation.

2.6.1 **EXPERIMENTAL DETAILS:** The initial conditions, based on Kitano's method [165] were as follows:

Ten grams of calcium carbonate (AR, BDH) powder was suspended in 4 litres of triple distilled charcoal filtered water in a plastic container and CO_2 gas was bubbled through at a rate of 0.44 m^3 hr^{-1} for three hours. When CO_2 gas dissolved the equilibrium of the reaction was moved to the right in the equation (1). The purging was then stopped, the solution left to stand for 10 minutes and filtered through a Buchner funnel using Whatman 42 filter paper to remove any undissolved calcium carbonate. Again CO_2 gas was purged for one hour to redissolve any crystal nuclei that may have formed (Fig. 2.3). Thus prepared bicarbonate solution was poured into a plastic tray (24 cm x15 cm) and loosely covered with a glass plate. 1.8 l of the same bicarbonate solution was poured into the trough and the monolayer was spread, and compressed to give a required film formation. It was left undisturbed for t = 16-21 hours, unless early crystals were required for analysis. The schematics of the procedure followed are shown in Fig. 2.4. Crystals collected from the trough and the tray after 16-24 hours were observed by optical microscopy and scanning electron microscopy. Milligrams of the sample collected were analysed by X-ray diffraction analysis. In the later experiments, the following modifications were used.

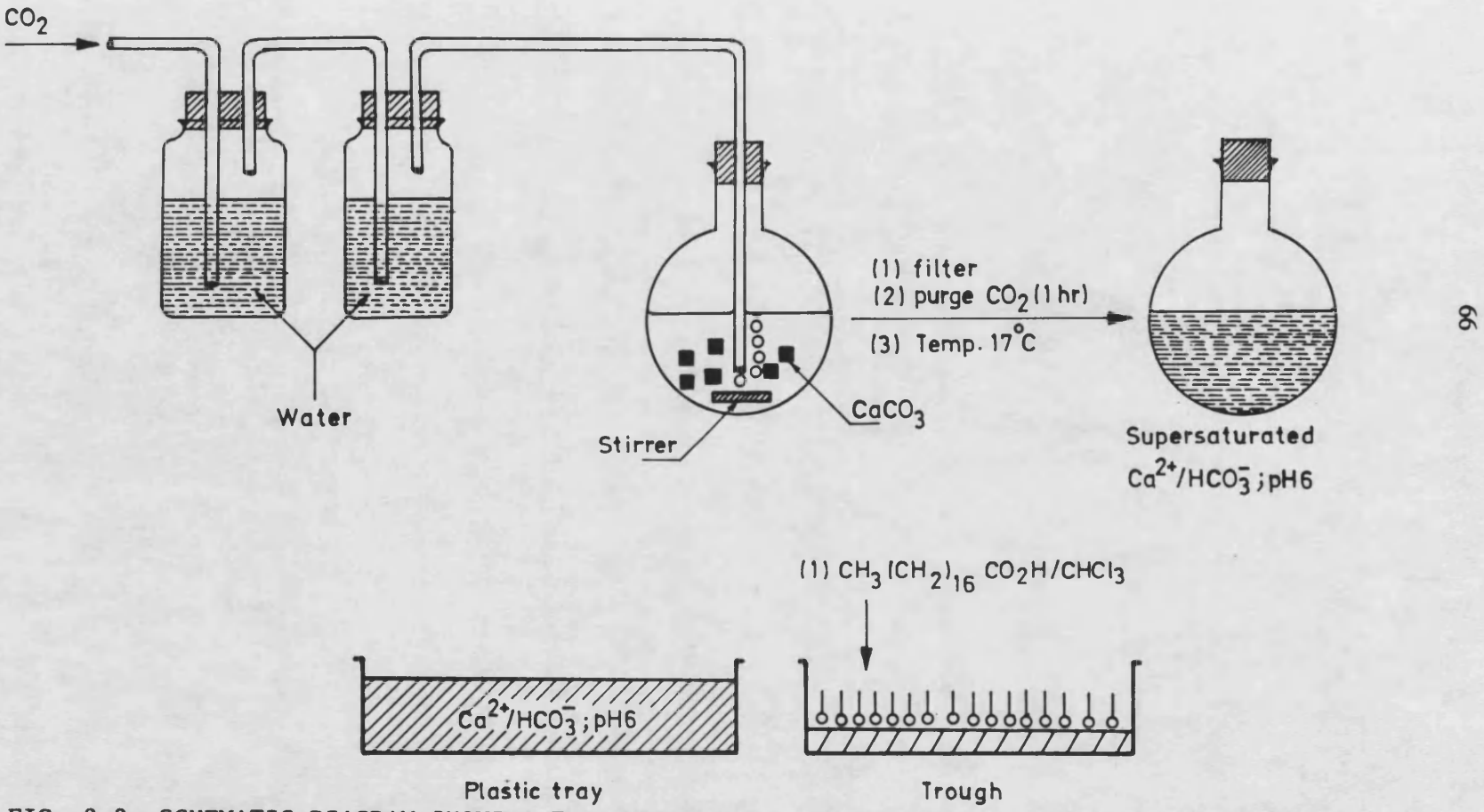

FIG. 2.3: SCHEMATIC DIAGRAM SHOWING THE EXPERIMENTAL CONDITIONS FOR THE PREPARATION OF BICARBONATE SOLUTION.

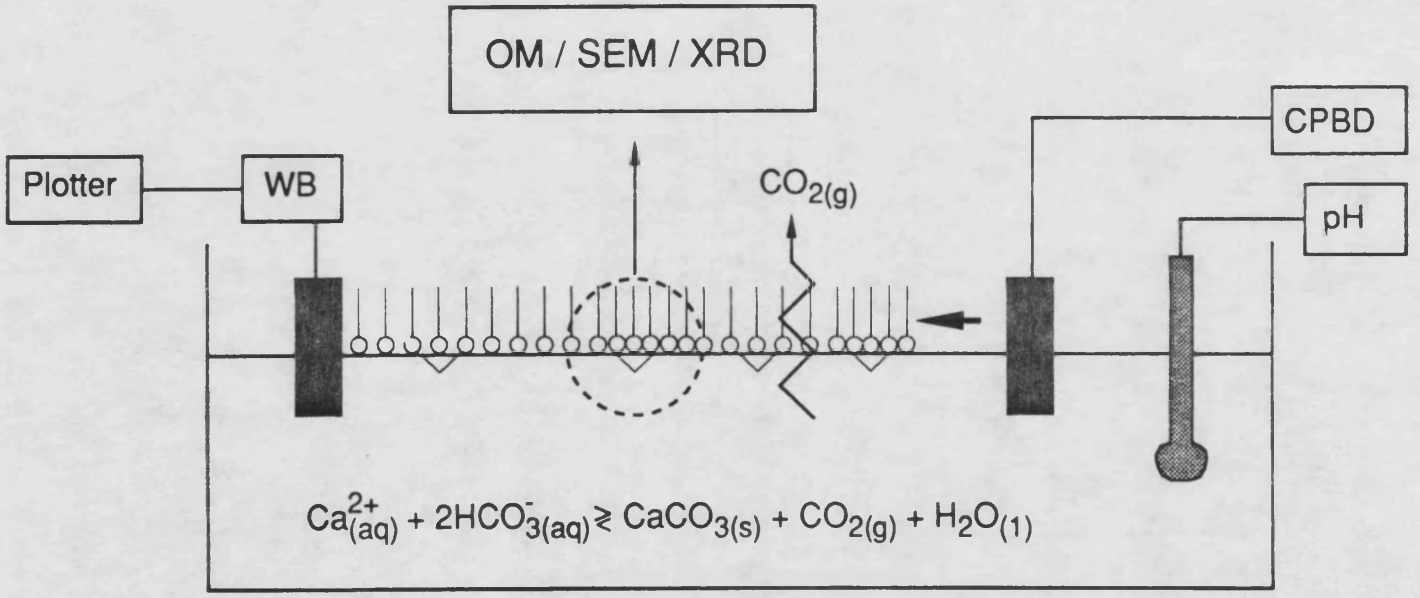

FIG. 2.4: EXPERIMENTAL PROCEDURE FOR THE GROWTH OF CALCIUM CARBONATE CRYSTALS UNDER STEARIC ACID MONOLAYERS.

(OM: Optical microscope; SEM: Scanning Electron Microscope; XRD: X-ray Diffraction; WB: Wilhelmy balance; CPBD: Constant Perimeter Barrier Device).

(a) triple distilled-charcoal filtered water was replaced by double distilled Purite charcoal column filtered water collected in a pyrex glass container.

(b) the CO_2 gas was purged for one hour initially.

(c) instead of overhead mechanical stirrer, magnetic bar stirrer was used.

(d) the CO_2 gas was scrubbed through double distilled Purite filtered water kept in twin Hirsch bottles.

(e) after one hour the undissolved calcium carbonate was filtered and removed and CO_2 gas was purged through the filtrate for 30 minutes.

(f) the prepared supersaturated bicarbonate solution was poured into round glass crystallizing dishes of capacity 500 cm^3. The volume of the bicarbonate solution in the dish was kept as 100 cm^3, and the pH and the temperature of the bicarbonate solution were measured prior to nucleation.

The dishes were loosely covered with clean filter papers and left undisturbed. Clouds of crystals could be observed visually after 2 hours. After 20 hours mature crystals from the surface were picked up on glass slides for optical microscopic observations. The surface crystals were also collected for scanning electron microscopy on stainless steel stubs by gently touching them and removing by surface tension. The remaining crystals were either filtered or picked up on glass slides for XRD analysis. Crystals seen at the bottom of the dish were also collected.

Glass crystallizing dishes were used instead of the trough to enable the direct comparison of the control crystals to the crystals

grown under the monolayers and to allow comparison of the crystals grown under different monolayers at identical conditions. For example, the diameter of the dishes and the volume of the bicarbonate solution taken were kept constant. Hence any change in the structure or morphology of the crystals would be affected by the monolayers only. An identical situation for comparison was not possible in the trough experiments.

The crystals grown under monolayers were collected on the glass slides and the number of crystals were counted. This enabled the nucleation density (numbers/cm^2) to be determined for the monolayer crystals. The detailed determination of the nucleation density of the crystals is described in individual chapters.

2.7 DETERMINATION OF SUPERSATURATION:

The supersaturation of the calcium carbonate solutions can be determined by (a) estimating the concentrations of calcium, carbonate and bicarbonate or (b) by determining the concentration of total calcium calculating other concentrations by known equilibrium constants. In the present work the second method was followed.

The concentration of calcium was determined by EDTA titrimetric method. The sodium salt of EDTA was used for the estimation. Standardisation of EDTA was done using magnesium iodate solution. Standard solutions of calcium chloride were prepared at various concentrations and titrated against EDTA and the calcium amount calculated was checked with the theoretical values. Supersaturated bicarbonate solutions were prepared

as described before (see section 2.6). Thus prepared solutions were used for calcium estimation. 25 ml of the solution was pipetted out into a conical flask and 25 ml of distilled water and 2 ml of 2M hydrochloric acid were added. The solution was boiled for 2 minutes and cooled. 4 ml of (8.0 M) sodium hydroxide solution, six drops of hydroxylamine hydrochloride, six drops of KCN solution and ≈ 30 mg of 2-hydroxy-1-(2-hydroxy-4-sulpho-1-naphthyl- azo)-3-naphthoic acid indicator were added. The solution was then titrated against EDTA solution. The colour changed from red to blue at the end point. The pH of the solution was kept at >12. Using the calcium concentration the supersaturation of the bicarbonate solution was calculated using the computer programme designed by Ali Al Khayat and J. Garside, UMIST, Manchester. [179]

2.8 SAMPLE PREPARATION FOR ANALYSIS:

(i) The crystals were collected by dipping microscopic slides through the surface and lifting them gently without disrupting much of the orientation of crystals. These crystals on the slides were used for optical microscopic analysis.

(ii) For XRD qualitative and quantitative analysis the crystals collected on the slides were finely ground and used.

(iii) For IR spectral analysis the samples were prepared by grinding the crystals from slides and making pellets with KBr.

(iv) For SEM analysis the crystals were either collected on glass cover slips similar to that of glass slides that could give the same view

and orientation of crystals as if being seen from above the surface or using circular stainless steel stubs the crystals were collected by gently touching the surface and lifting them without disrupting the orientation of crystals. This gave a view of the crystals as if being seen from under the surface.

2.9 NUCLEATION DENSITY DETERMINATION:

The number of crystals and hence the number of nuclei formed per unit area of the monolayer was determined in two ways.

(i) It was difficult to observe and count the number of crystals directly from the trough monolayers, so the crystals were carefully picked up by dipping the slide in the trough part of the monolayer and gently lifting the slide to collect a single bed of crystals attached intact on to the slide surface.

(ii) In some experiments, the crystals grown in glass/plastic dishes were viewed *in situ* and the number of crystals per unit area were determined.

2.10 INSTRUMENTAL TECHNIQUES:

Analysis of the crystals grown in the control experiments and under the monolayer were analysed mainly by the following techniques.

(i) **X-RAY DIFFRACTION:** For the preliminary polymorphic analysis of the crystals, X-ray diffraction method was used with the technical help from Mr.B. Chapman and Mr.A. Carver. In this method it was possible to

determine the d-spacings and hence the structure of the crystals. In the present work the instrument used was Philips powder diffractometer Model PW-1130 combined with Debye-Scherrer camera of 11.4592cm diameter and mostly copper K-α radiation (λ=1.5405 A' and occasionally iron K-α radiation (λ = 1.9373 A·) were used. X-ray powder diffraction was carried out as described below. The sample for analysis was usually finely ground, filled in a capillary tube and mounted on a sample holder. The film (Kodak x-ray film) was loaded in the camera and was exposed through holes in the side of the camera to give markers from which the diffraction lines for measurements were obtained. The camera was mounted, the x-ray source was switched on and kept at 40 Kv, the shutter opened and the film was exposed for one and half hours. The film was developed using Kodak developer and fixer. From the measurements made the d- spacings were calculated using Bragg's equation, $n\lambda = 2d \sin\theta$, where λ=1.5418Å (for CuKα); n=1; camera length (r)=11.4592cm; arc length(l) = measured diffraction lines. Therefore $l = 2\pi r x 2\theta/360 = 11.4592 \times \pi\theta = 0.4\theta$. So $\theta = 2.5xl$. Therefore from the Bragg's relation, $1.5418 \times 10^{-10} = 2d \sin(2.5xl)$. Hence $d=0.7709 / \sin(2.5xl)$. These values were then compared with values in the ASTM diffraction files (usually calcite, aragonite and vaterite) to determine the structure of the crystals.

(11) **XRD QUANTITATIVE ANALYSIS**: Quantitative analysis by x-ray diffraction method could give an accurate determination of the amounts of different polymorphic types of crystals present in a sample. The

instrument used in this method was a Philips PW-1710 x-ray diffractometer. Samples were prepared for the analysis by mixing accurately known amounts of crystals under investigation with weighed amounts of corundum (γ-Al_2O_3). This was used as the internal standard. A calibration curve was derived from known samples prior to the estimation of unknown compositions of experimental crystals. Furthermore, this method was used for the analysis of the adsorption of the foreign ions in the crystal lattice. The heights of peaks were measured to determine the intensities of the d-spacings and any displacement of peaks from theoretical positions was noted for any lattice adsorption in the crystals.

(iii) **INFRARED SPECTROPHOTOMETRY:** The IR spectral analysis was carried out using Perkin-Elmer model-1420 infrared spectrometer. The Perkin-Elmer model-1720 FT-IR spectrometer was used where there was need for better resolution of the spectrum. The samples were used in the form of KBr pellets or as KBr mixtures in cells for FT-IR spectrometer.

(iv) **OPTICAL MICROSCOPY:** In order to study the nature of the crystals collected on the glass slides, they were studied by optical microscopy. For most of the preliminary work the zoom stereomicroscope MEIJI EM series model EMZ combined with Olympus OM 10 camera was used. One main advantage of this microscope was that crystals grown in small crystallizing dishes could be studied *in situ*. The magnification range of this microscope was from X14 to X90 (X3.5 to X22.5 for photography).

When more details of the crystals were required, a Carl Zeiss D-7082 model Axiophot compound optical microscope equipped with a parfocalized Panasonic TV camera and video monitor was used. Magnification in this instrument varied from X100 to X500 (X25 to X125 for photography). Using the optical microscope it was possible to study the general orientation of the crystals grown in the system with and without the monolayer. Their size, shape and their nucleation density under the monolayer could also be determined. However due to the lack of the depth of the field the detailed morphological analysis could be done only with scanning electron microscopy.

(v) **SCANNING ELECTRON MICROSCOPY:** The instruments generally used were either a JEOL 35C or JEOL T330 models. The main principle in these instruments is that a beam of electrons is focussed on the surface of a sample that gives the image of the sample from the intensity of the back-scattered electrons (see Appendix). The results appear on the readout device as a visual image of the surface of the sample. The results were similar to those obtained from an optical microscope except that the magnification was considerably greater and the depth of the field was high and hence the resolution was greater. The sample was usually placed on a stage similar to a microscopic stage. The stage was generally accurately moved while the sample was observed through the microscope until the sampling site was located. Movement was stopped at the chosen site and the electron beam was discharged. The energy of the electron beam was

determined by the change in potential between the cathode and the anode. Typical potential used in the present work varied from 5 KeV to 20 KeV. The large number of electrons that strike the sample could cause an accumulation of charge which must be disseminated. In the present system as the crystals were loosely attached to the sample holders (stubs) and so the charging problems were high. However samples coated with gold/platinum for a longer period facilitated the dispersal of the charge. Details of sample collection and the coating time which varied from sample to sample were explained in the individual chapters.

CHAPTER III

CONTROLLED CRYSTALLIZATION OF CALCIUM CARBONATE CRYSTALS UNDER STEARIC ACID MONOLAYERS

3.1 INTRODUCTION:

A fundamental concept in the study of biomineralization and biogenic minerals involves in part the regulatory processes by complex organic materials, during the formation of minerals. These organic macromolecules are made by the organisms with a precise structure, to induce controlled crystallization with a specific structural and stereochemical selectivity of the mineral formed (see chapter I, section 1.6).

A number of different experimental strategies have been developed to elucidate the mechanisms of controlled crystallization at an organised organic template. One approach has been to isolate the matrix constituents from mineralized tissues and examine the growth of calcium salts in the presence of these moieties [91,94,181]. These studies indicate that the stereochemical conformation of both the sulphate residues and β-sheet carboxylates of acidic matrix macromolecules exert a significant influence upon the oriented nucleation and growth of the mineral phase [83]. Although this work has offered new insights into the importance of stereospecificity in controlled crystallization, details of the interfacial structure *in vivo* are lost during the isolation procedures. Thus the exact mode of operation of the proteins could not be determineed. To avoid this, organised monomolecular films have been used for systematic investigation into the structural requirements for nucleation of chiral organic crystals [95,96]. Using a similar method, Landau et al [94] demonstrated that the formation of two dimensional Langmuir monolayers with known headgroup

spacings and polarity, induces the orientated crystallization of NaCl and amino acids from supersaturated solutions.

In this thesis, I have developed this method of using compressed two dimensional surfactant films as organised templates for crystal formation. The aim has been to investigate the influence of headgroup charge and stereochemistry, and packing density of acid monolayers as well as solution conditions on the structure and the orientation of crystals nucleated under the organic surface. This chapter describes the formation of calcium carbonate crystals from various supersaturated calcium bicarbonate solutions in the presence of compressed, partially compressed and uncompressed monolayers of stearic acid.

Stearic acid forms a very stable monomolecular film. Fig.3.1 shows the molecular structure of stearic acid [$CH_3(CH_2)_{16}COOH$] and Fig. 3.2 shows a space-filling model of the acid molecule. Stearic acid at room temperature and pressure exists in the solid form (m.p.69.8°C). It is insoluble in water and freely soluble in organic solvents such as chloroform, n-hexane and ether. Among these organic solvents chloroform was used as a solvent for preparing stearic acid solutions. Many studies on these films have been reported. The surface area per molecule has been given as just over 20Å^2 for stearic acid monolayers. This value is close to that occupied by stearic acid molecules in single crystals and interpretation of a compact film as a two dimensional solid was confirmed by x-ray measurements [118]. The dependence of the stability of this monolayer on the hydrophobic chain length and the hydrophobic/hydrophilic

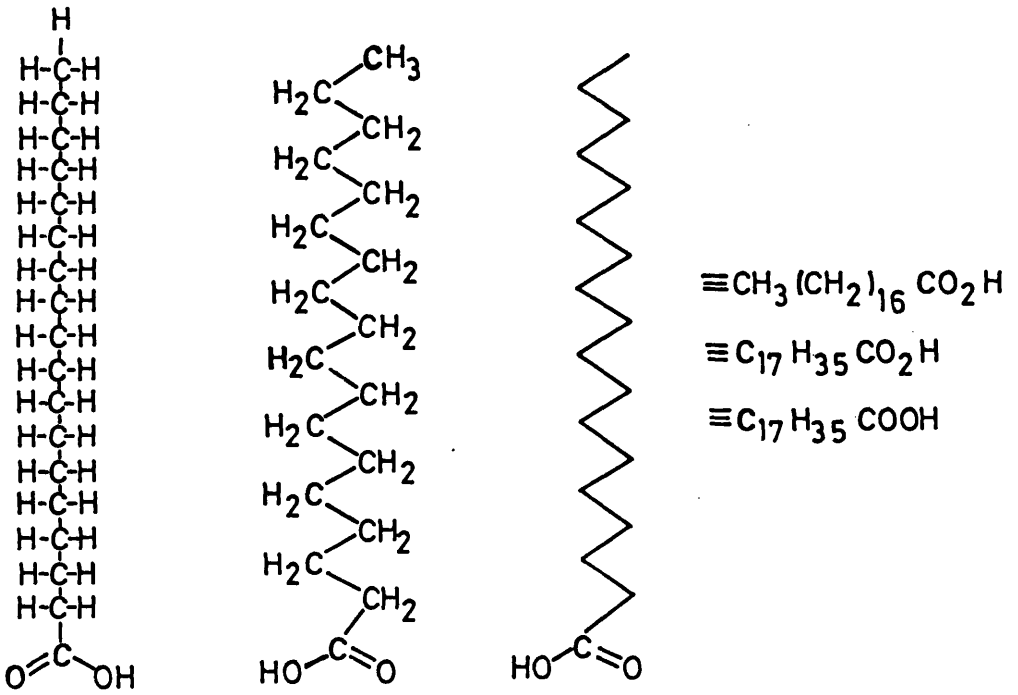

FIG. 3.1: STRUCTURE OF STEARIC ACID MOLECULE.

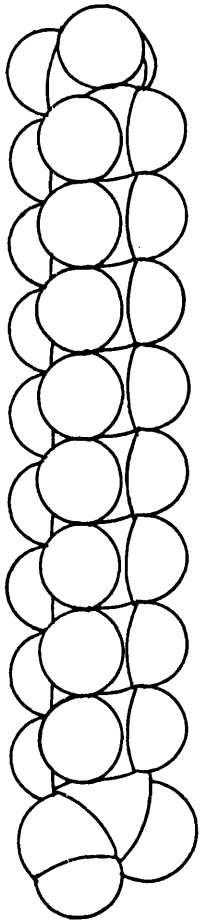

FIG. 3.2: COMPUTER DRAWN STRUCTURE OF STEARIC ACID MOLECULE

balance has been examined [97], and stearic acid was reported to lose <0.001% per minute of the molecules in solution subphase. Ionization of stearic acid at various pH has been reported [182]. When the subphase had been acidified with a mineral acid to pH 4.0, its ionization was completely suppressed so that it behaves as a neutral molecule. At higher pH, ionization occurs to form hydrogen ions in the subphase and carboxylate ions in the monolayer. Although pure water has a pH of 7.0, carbon dioxide from the atmosphere dissolves in the subphase and slightly acidifies it to Ca. pH 5.8. The value expected for the pK_a of stearic acid in solution is 4.8, but on the water surface it is shifted to 5.6, although the situation is further complicated in the presence of metal cations in the aqueous phase. In calcium chloride solutions the pK_a of the acid is around 6.0 [182]. When the pH is greater than 7.0 and when singly charged ions (Na^+ or K^+) are present, the solubility of the acid increases and micelles were reported to be formed. When the cations are doubly charged, the monolayer is stable at air/water interface [97]. The surface pressure-area curves have been studied for stearic acid on Cd^{2+}, Cu^{2+}, Ca^{2+}, Ba^{2+}, Pb^{2+}, Sr^{2+}, Fe^{3+} and Al^{3+} [130,136,142]. The incorporation of these ions in the film accounts for small change in surface area per molecule. Divalent cations cause electroneutrality in the film and di- and tri-valent ions give extremely rigid films with a high shear modulus [183]. The extent of incorporation of ions into the film depending on pH and the nature of incorporated ions has been studied by Newman [135].

Electron diffraction of monolayers transferred to solids show that the molecules are oriented vertically with respect to the surface. Recent development in this area led to the study of these molecules in the floating Langmuir monolayer films using x-ray reflectivity, x-ray scattering and neutron scattering techniques, and infrared spectral analysis. Bohanon et al [183] have reported on the determination of structures for the fatty acid and alcohol monolayer systems on the surface of water, based on the observations of first- and second-order x-ray diffraction peaks and showed that the fatty acid monolayers assume in the highest-pressure phase, a distorted hexagonal structure with orthorhombic cell dimensions a = 7.5 Å and b = 5.0 Å, in the fully condensed films.

3.2 EXPERIMENTAL:

Stearic acid >99% pure (AR,BDH) was used throughout. The acid was further purified by recrystallizing in chloroform (Aristar). Recrystallized acid was carefully dried in air and the purity determined by elemental analysis and by infrared spectral analysis.

Microelemental analysis was done and the percentage of individual elements were compared with theoretical values.
Infrared spectral analysis was obtained and the characteristic peaks were observed for stearic acid.

3.2.1 SURFACE PRESSURE-AREA ISOTHERMS OF STEARIC ACID:

As an important preliminary step to study the calcium carbonate crystals under stearic acid monolayers in the Langmuir trough, the surface-area isotherms of stearic acid were plotted under pure water and Ca^{2+}-containing solution subphases (for detailed procedure see chapter II, section 2.5). Surface pressure-area plots were also obtained on cadmium chloride solutions for comparision. However the anionic nature and the pH of the solution were different for the two solutions.

The pH and the temperature of the solution were measured acccurately prior to the plotting of each isotherm. The mass was calculated to give a recommended concentration of around $2.0x10^{-7}$ moles dm^{-3} in the monolayer. Around 60 µl were added accurately each time in order to have a reasonably good area of the monolayer. From the limiting molecular area and from the number of acid molecules, the area/molecule on pure water subphase was calculated. A blank run of the isotherm with solvent chloroform was done on pure water. Hysteresis was checked for acid monolayers for the loss of any acid molecules during compression and the track of the isotherm was retraced. Surface pressure-area isotherms were recorded as before for stearic acid monolayers compressed on cadmium chloride solution subphases at a concentration of $2.5x10^{-3}$ moles dm^{-3} and at a pH of 5.3.

Isotherm plots of stearic acid were recorded from calcium chloride solution at a pH of 5.5 and temperature 302 K. Surface pressure-area curves were also plotted on calcium bicarbonate solution subphases.

The pH of the bicarbonate solutions were between 5.8-6.0 and the temperature was 290±1 K (preparation of calcium bicarbonate solution has been given in detail in chapter II, section 2.6).

3.2.2 CRYSTAL GROWTH STUDIES UNDER STEARIC ACID MONOLAYERS:

Monolayer films were formed at various compression levels on $Ca(HCO_3)_2$ solution subphases. The $CaCO_3$ crystals nucleated and grown under the acid films were studied by x-ray diffraction, IR spectral analysis, and optical and scanning electron microscopy. Crystals grown under similar conditions in the absence of monolayers were also collected and studied for detailed comparison.

Crystallization experiments were carried out under compressed monolayers with various compression levels at surface pressures of 45 mN m^{-1} (solid phase), 20 mN m^{-1} (liquid phase) and 1 mN m^{-1} (gas phase) in the Langmuir trough. Crystals were collected from the monolayer subphase interface at various time intervals (45 minutes - 21 hours) after compression for structural and morphological analyses (for detailed sample collection see chapter II, section 2.8).

Bulk sample for x-ray diffraction and IR spectral analyses were obtained by sweeping the surface with the barrier, and collecting the aggregated crystals on glass slides. Crystals for optical microscopy were viewed *in situ* or on glass slides dipped through the compressed films. The nature of the orientation of the crystals grown at the monolayer-subphase interface was determined by scanning electron microscopy.

The crystallization experiments were also done in thoroughly cleaned glass crystallization dishes. Compressed acid films were formed by adding known amounts of acid surfactant to form a solid phase film on the vacuum cleaned subphase surface. Using this method, a systematic dilution of the solutions were made using the same bicarbonate solution, and the influence of changes in the supersaturation was studied. On successive dilution of the stock supersaturated solution (total = 9 mM) to give total Ca concentrations of approximately 4.5, 2.25 and 1.13 mM were made in the glass dishes and the monolayers were spread on the surface, and the dishes were loosely covered with filter paper lids. Crystals collected from these experiments were studied in detail for changes in structure, morphology, orientation, size and nucleation density of the crystals, formed under the monolayer.

A simple method was designed to grow the crystals in small plastic petri dishes so that the number of crystals formed under the monolayer could be counted in situ from the dishes directly under the optical microscope. Care was taken to reproduce the experiment as much as possible. However, certain factors such as adding the monolayer molecules and condensing them slowly to give a coherent monolayer was not possible as the monolayer could not be compressed in the petri dishes and the number of molecules required to form the solid/liquid phase monolayers were added at one time. Apart from this the monolayer area/volume of the solution with a 'deep well' position under the monolayer could not be maintained the same way as in the trough experiments. However experience

showed that good monolayer could be formed in petri dishes/glass crystallizing dishes and the crystal nucleation and growth of calcium carbonate could be reproducible in theee dishes. The striking difference between the trough/plastic dishes and glass crystallizing dishes was that carbon dioxide bubbles adhered to the bottom surface in the trough and in the plastic dishes whereas bubble formation did not occur in the glass dishes because of the difference in surface texture and hydrophilic nature of the substrates. Apart from this, the time gap from stopping the purging of CO_2 and laying the monolayer was at least 20 minutes in the trough experiments whereas it was, on maximum, 5 minutes in the crystallizing dish experiments.

Size measurements of the mature and early crystals were done using optical and scanning electron micrographs. Nucleation densities were determined as an average of several experimental samples. Crystals were collected on glass slides and counted in the areas selected at random using the optical microscope equipped with a video monitor. The number of crystals counted were >1500. The morphological and crystallographical orientations were determined from SEM micrographs.

3.3 RESULTS:

(1) **PURITY OF STEARIC ACID:** The purity of acid determined from the microelemental analysis is shown below.

Stearic acid ($C_{18}H_{36}O_2$)	%C	%H	%O
Calculated value	75.93	12.82	11.25
Experimental value	75.90	12.72	11.38

The FT-IR spectra of stearic acid is shown in Fig. 3.3. The C-H stretching frequency of the aliphatic methyl and methylene groups were observed at 2950, 2930 and 2850 cm^{-1} respectively. Absorption bands of terminal methyl group at 2950 cm^{-1} due to the asymmetric stretching mode and a symmetric mode at 2850 cm^{-1} were observed. Peaks at 1460 and 1380 cm^{-1} indicated the presence of a terminal methyl group attached to a carbon exhibiting in-plane bending motions. The methylene groups (> 4) in a linear aliphatic chain gave the absorption peak at 720 cm^{-1} due to the weak rocking motion. The carbonyl peak gave a strong band at 1700 cm^{-1}. The carboxyl group showed bands arising from their super position of C=O, C-O, C-OH and O-H vibrations. Of four characteristic bands, three of these (overlapped with aliphatic C-H stretching frequency, 1300, 2700 and 940 cm^{-1}) were associated with vibrations of the carboxyl O-H group.

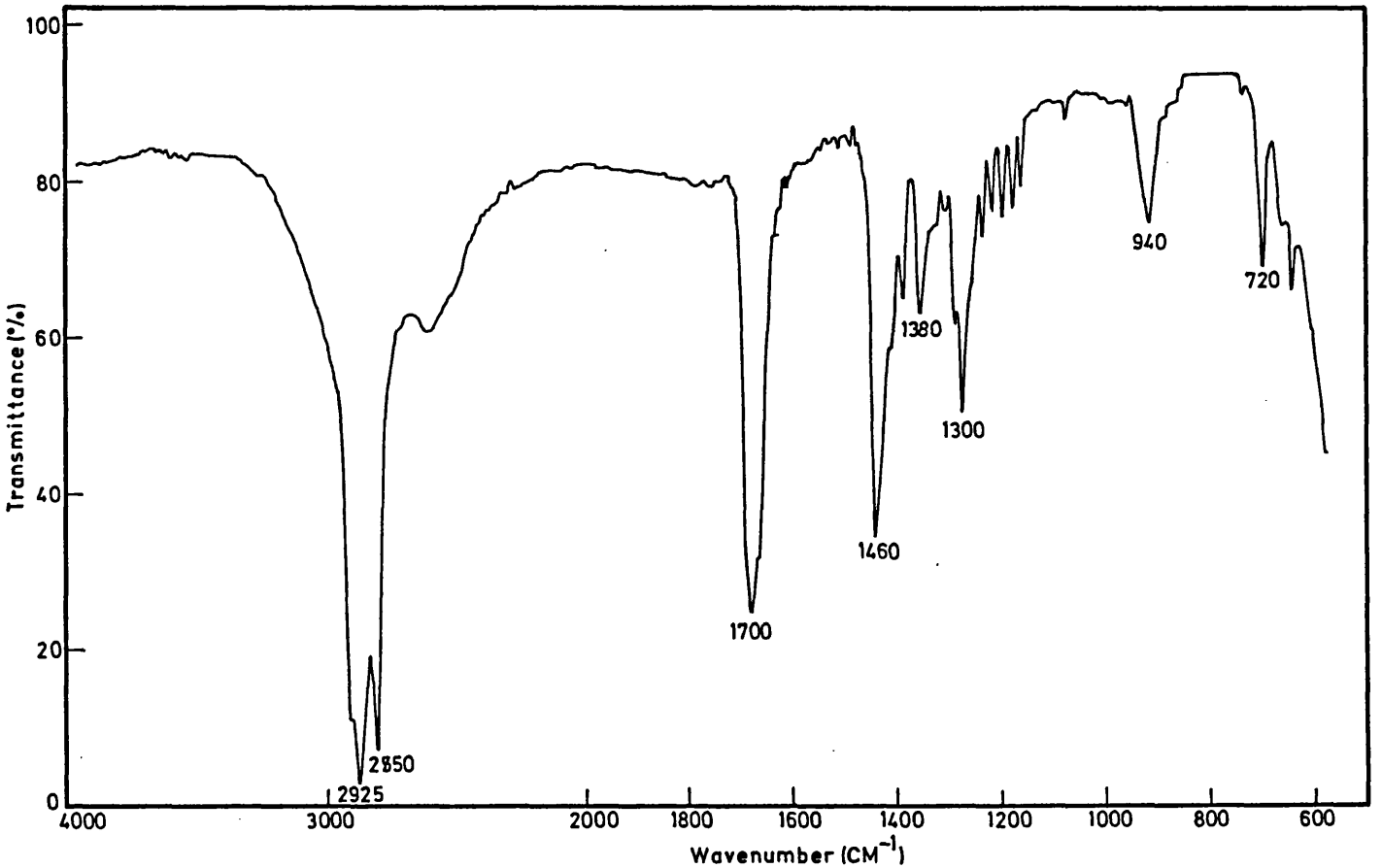

FIG. 3.3: INFRARED SPECTRUM OF PURE STEARIC ACID.

(i) SURFACE PRESSURE-AREA ISOTHERMS OF STEARIC ACID: The compression isotherms on water without the monolayer showed no pressure rise and indicated the absence of surface-active impurities (Fig. 3.4). When pure chloroform was spread on the surface and the isotherm plotted, a completely flat isotherm was obtained showing that the chloroform was pure and rapidly evaporated from the surface (Fig. 3.4). Hence any pressure rise in the isotherms and the nature of the isotherms depended on the nature of the monolayer-forming acid molecules in the experiments described below.

The isotherm of stearic acid on pure water in a typical experiment (Fig. 3.5) gave an area per molecule 21Å^2 although the values varied by ±1Å^2. Thus the data were reproducible within the limited conditions imposed to prevent temperature variations. Within the temperature range used there was no difference in the nature of the isotherms, but the areas increased slightly 0.5 to 1 Å^2 at the lower side of the temperature. The isotherms were not markedly different under the pH conditions used. The nature of the isotherms showed three different regions, (a) gas phase (uncondensed monolayer), (b) liquid phase (partially condensed monolayer) and (c) solid phase (fully condensed monolayer) isotherms representing different arrangements of the molecules. In the gas phase monolayer form there was no pressure rise in the isotherm and the area/molecule was >30 Å^2. In the liquid phase monolayer, the pressure started to rise and the nature of this part of the curve was dependent to some extent on the nature of the subphase solution. On pure water, it

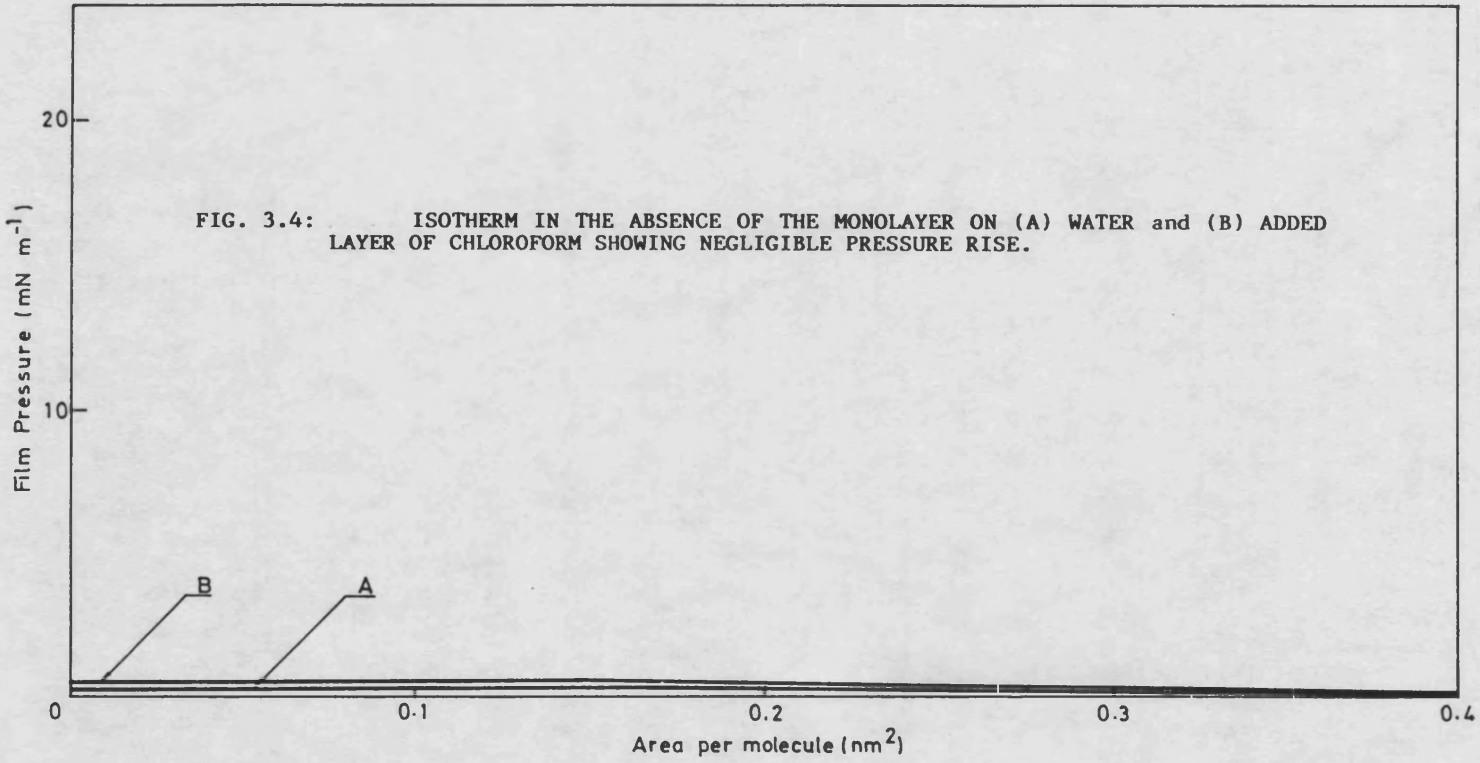

FIG. 3.4: ISOTHERM IN THE ABSENCE OF THE MONOLAYER ON (A) WATER and (B) ADDED LAYER OF CHLOROFORM SHOWING NEGLIGIBLE PRESSURE RISE.

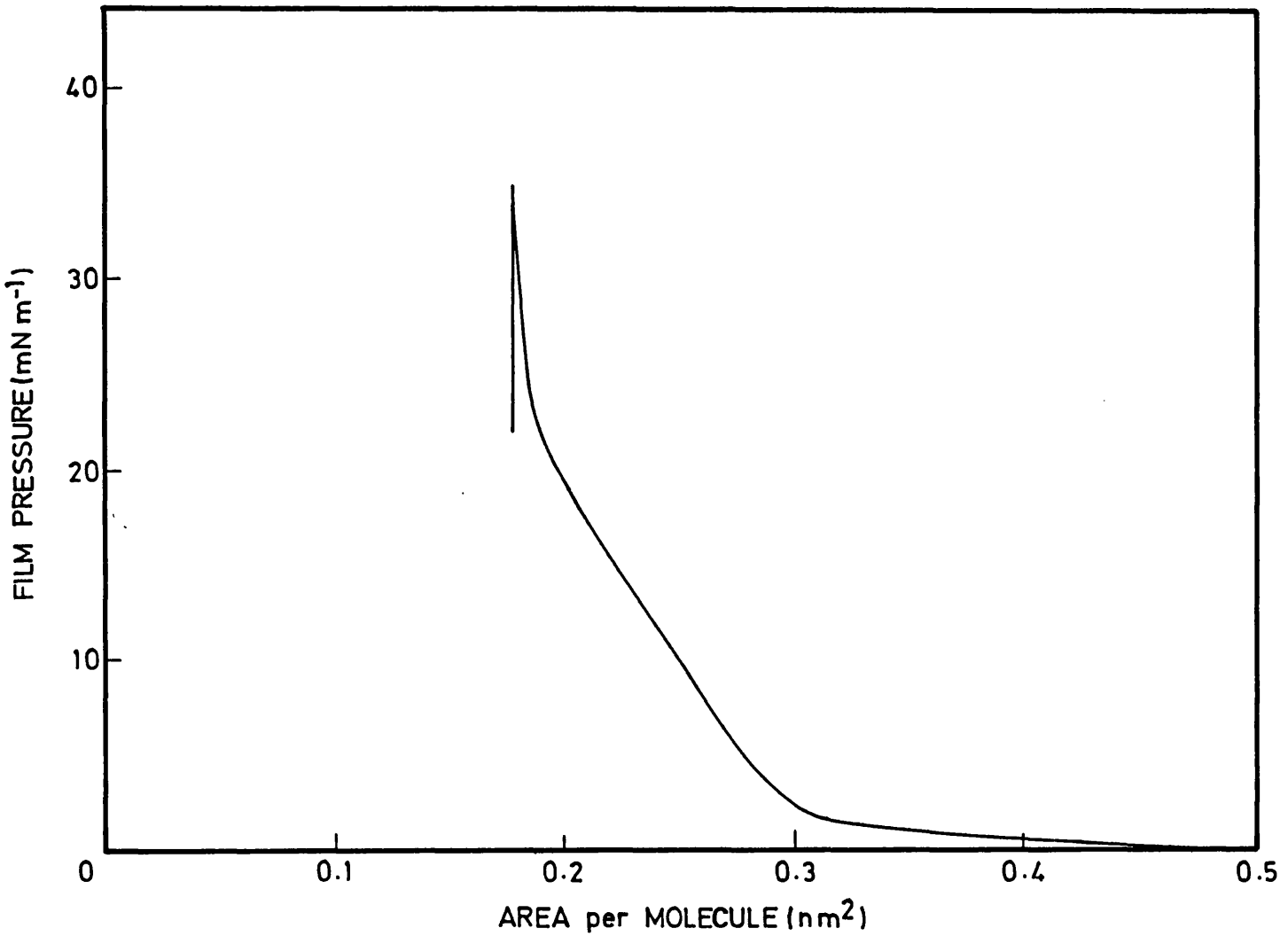

FIG. 3.5: PRESSURE-AREA PLOT OF STEARIC ACID MOLECULES FORMING SOLID PHASE MONOLAYER ON PURE WATER SUBPHASE.

it formed a slightly expanded liquid phase and the pressure increased to around 20 mN m^{-1} at which point a clear transition occurred to form a fully condensed monolayer. At this point there was very little change in the area/molecule but the pressure rose to 40 mN m^{-1}. No hysteresis was noticed on surface pressure-area curves of acid molecular films, i.e. when the isotherm curves were retraced, they followed the same track (Fig. 3.6). The isothermal plot of stearic acid on 2.5 mM concentrations of calcium chloride and cadmium chloride solution subphases looked similiar to pure water isotherm except that instead of having an expanded liquid phase, they were slightly condensed in the liquid phase. The respective limiting area per molecule was 22 $Å^2$ and 21 $Å^2$ (Figs. 3.7B and 3.7A).

The limiting area/molecule of solid films on [Ca] = 10 mM of calcium bicarbonate solutions was 23 ± 1 $Å^2$ and the surface pressure measured was 45 mN m^{-1} (Fig. 3.7C). For partially compressed films the area/molecule ranged from 25-30 $Å^2$ and had surface pressures of 1-10 mN m^{-1}. The uncompressed films were formed around the surface pressure of 1 mN m^{-1} giving an area/molecule of > 30 $Å^2$.

The isotherm plots of stearic acid on bicarbonate solution subphase looked similar to the plots drawn on calcium chloride solution except that they were slightly more condensed in the liquid phase and the transition from liquid to solid phase was clear and sharp. This reflects the much higher [Ca] of these subphases.

From the limiting area/molecule data the head group spacing of the acid molecule in the monolayer was calculated. Assuming a hexagonal

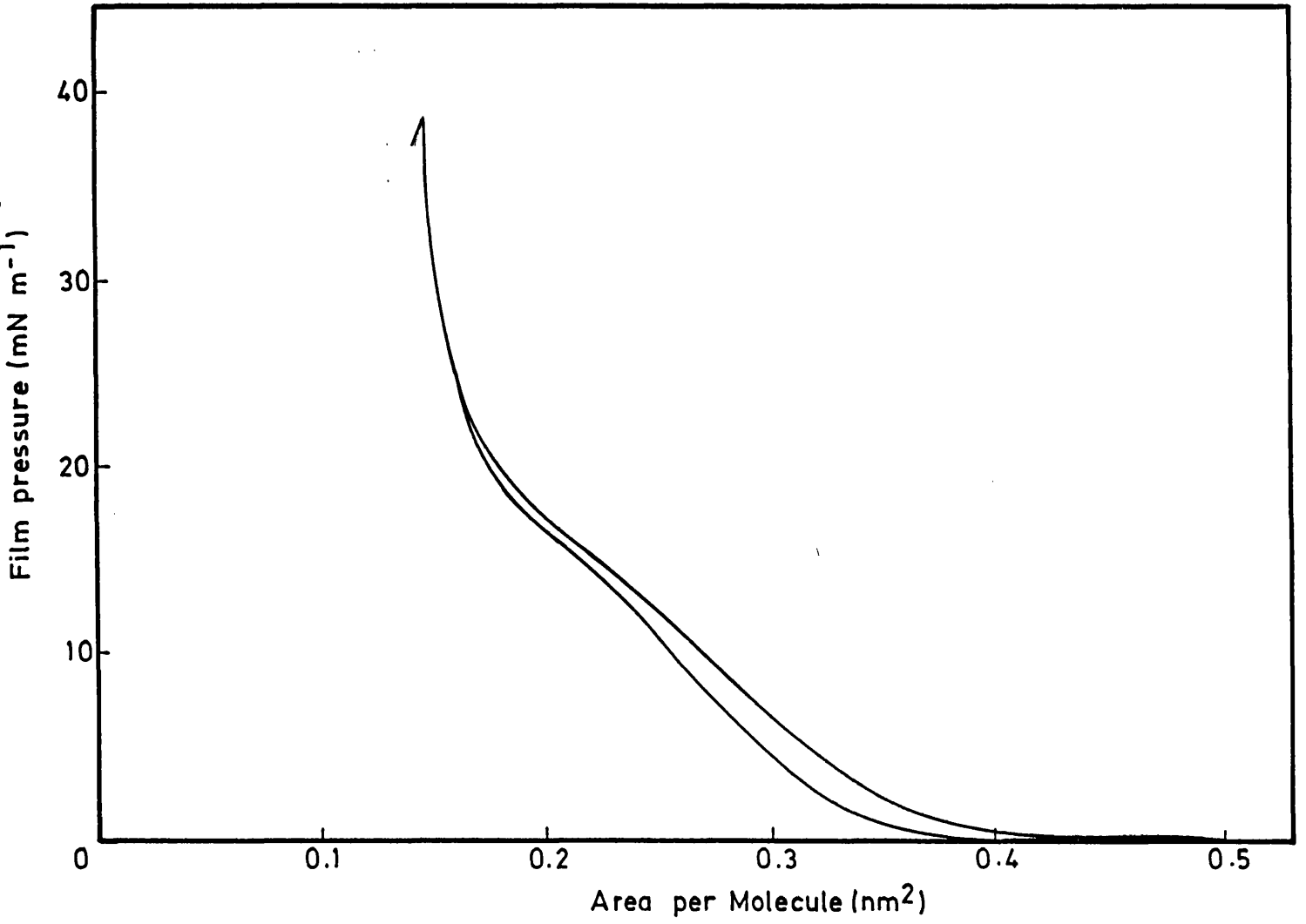

FIG. 3.6: HYSTERESIS CHECKING FOR THE STABILITY OF STEARIC ACID MONOLAYER.

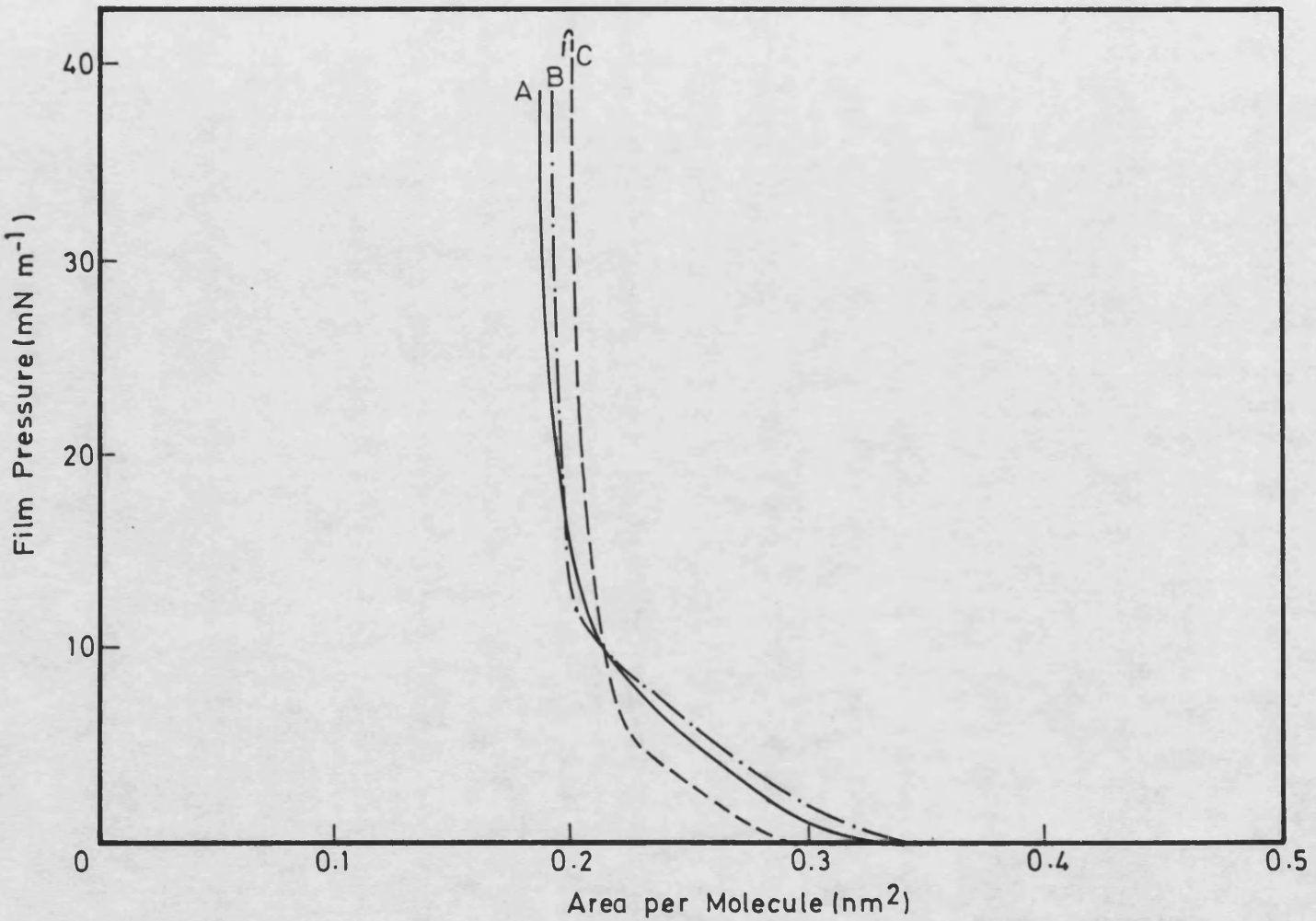

FIG. 3.7: PRESSURE-AREA CURVES OF STEARIC ACID ON (A) CADMIUM CHLORIDE, [Cd]=2.5 mM, (B) CALCIUM CHLORIDE, [Ca]=2.5 mM and (C) CALCIUM BICARBONATE, [Ca]=10 mM SOLUTION SUBPHASES.

structure, the inter-headgroup spacing was calculated as Ca. 5.0 Å for a limiting molecular area of 24 $Å^2$.

3.3.2 CRYSTAL GROWTH EXPERIMENTS:

(i) CRYSTALS GROWN IN THE ABSENCE OF MONOLAYER: The randomly aggregated crystals were observed by eye at the air/water interface after 21 hours. The polymorphic form of the crystals formed in these control experiments were determined by XRD analysis. The main polymorph formed was calcite. Table 3.1 shows the XRD diffraction data for crystals collected in a typical experiment. In a few repeated experiments, one or two lines corresponding to vaterite were also present. However, no aragonite lines could be seen. The presence of vaterite lines were not consistent and in some experiments they could not be observed at all. Quantitative XRD measurement made for one experiment showed that at least 68% of the crystals by weight were calcite (Table 3.2). However, this percentage increased to 100% in various experiments.

Optical microscopic observations (Fig. 3.8) showed that the crystals were mainly rhombohedral calcite crystals. Truncated rhombohedral calcite crystals were also observed particularly when the temperature was less than 290 K. Some more dendritic growth of vaterite crystals was also noticed. Occasionally, needle-like bunches of aragonite were located. When the pH of the solution was >6, the proportion of calcite formed was very high and no vaterite lines were observed in the XRD data.

Table 3.1: XRD data for the crystals grown in the absence of monolayers

d-spacings in Angstroms (Å)		
Experimental	Theoretical	
Control	Calcite	Vaterite
		4.245
3.843	3.852	
		3.577
		3.296
3.030	3.030	
2.831	2.834	
		2.735
2.262	2.284	
		2.219
		2.122
2.079	2.094	
		2.065
1.901	1.907	
1.865	1.872	
		1.857
		1.825
		1.648
1.619	1.604	
1.591	1.582	
		1.544
		1.477
1.468	1.506	
1.437	1.440	
1.417	1.416	
		1.351
1.334	1.336	
		1.331
		1.286
1.175	1.177	
1.141	1.141	

Table 3.2: XRD quantitative analysis of polymorphic composition of $CaCO_3$ crystals

Crystals grown	[Ca] mM	% weight	
		Calcite	Vaterite
Control	9.0	68	24
Control	4.5	82	15
Monolayer	9.0	70	28
Monolayer	4.5	10	90

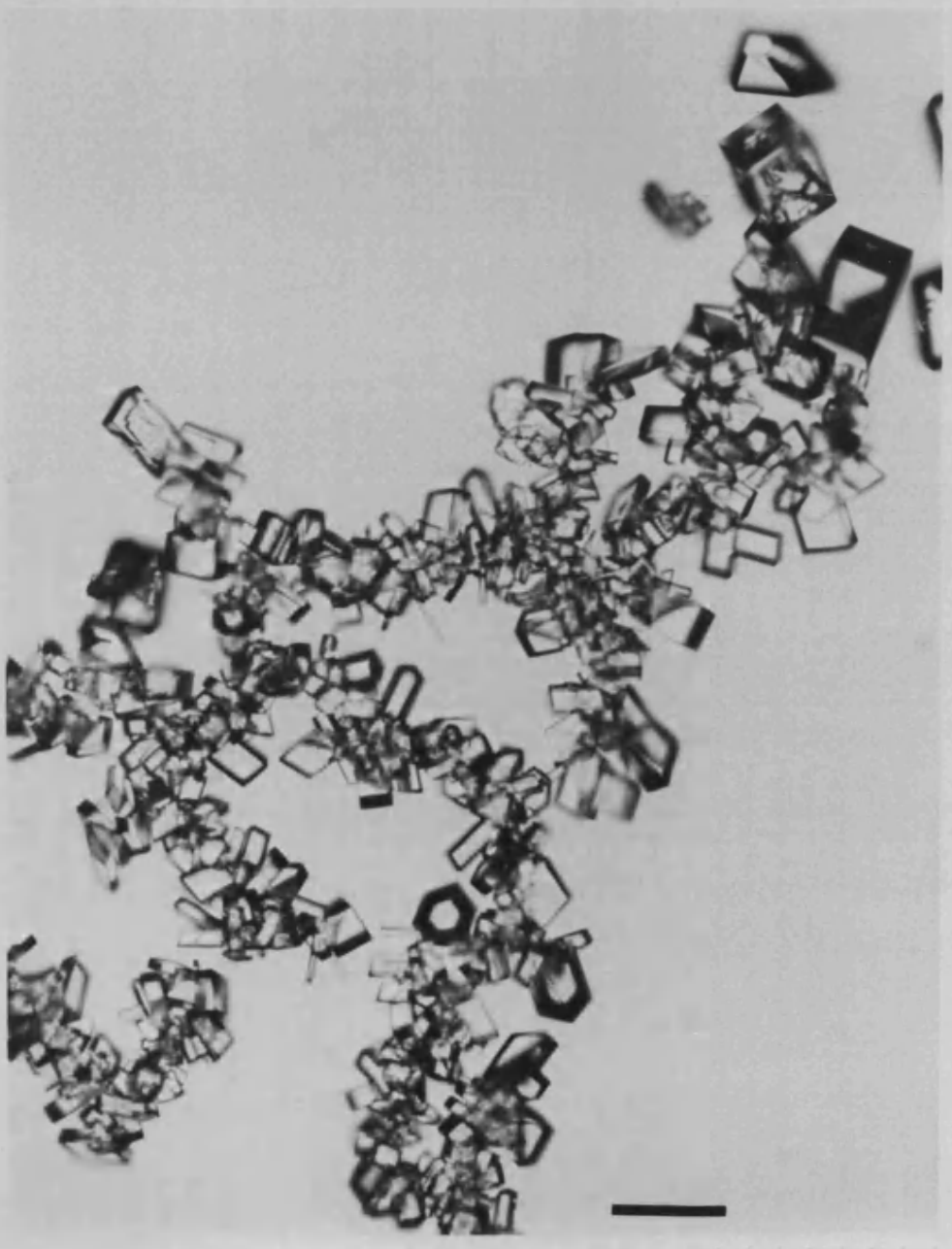

FIG. 3.8: RHOMBOHEDRAL CALCITE CRYSTALS RECORDED FROM OPTICAL MICROSCOPE GROWN FROM SUPERSATURATED BICARBONATE SOLUTIONS IN THE ABSENCE OF STEARIC ACID MONOLAYER. (Scale bar: 50 um).

Scanning electron microscopy showed that the calcite crystals formed at the air/water interface comprised symmetry related {10.4} rhomb faces (Fig. 3.9). The surface of the crystals were smooth and no roughening was observed. Twinning of the crystals was not seen and inter-growths were sometimes observed. The size measurements made from optical and SEM micrographs were heterogeneous (Fig. 3.10). The mean size of the crystals was 30 μm with a standard deviation of 12.5 μm. The nucleation density of the crystals could not be determined because of crystal aggregation.

A minority of crystals were formed at the bottom of the containers. These were small, discrete, smooth and non-oriented calcite rhombs. Sizes of these bottom crystals varied from 5-20 μm. Changing the total [Ca] had no significant influence in the control experiments. On reducing the [Ca] from 9.0 mM to 1.3 mM, the surface crystals remained intergrown and the vaterite minor component was reduced or absent.

Fig. 3.11 gives the FT-IR spectra of the product, calcite. For the planar CO_3 group having trigonal symmetry, there are four expected fundamental modes of vibrations. In calcite, theoretically, it is expected to have three distinct peaks and the peak around 1090 cm^{-1} due to the symmetric stretching should be absent. As expected, there were three characteristic peaks observed in the IR spectra of calcite and the peak at 1090 cm^{-1} was absent which indicated the absence of vaterite. The absorption bands at 708, 868 and 1376 cm^{-1} were due to the planar bending, out of plane bending and anti-symmetric stretching frequencies

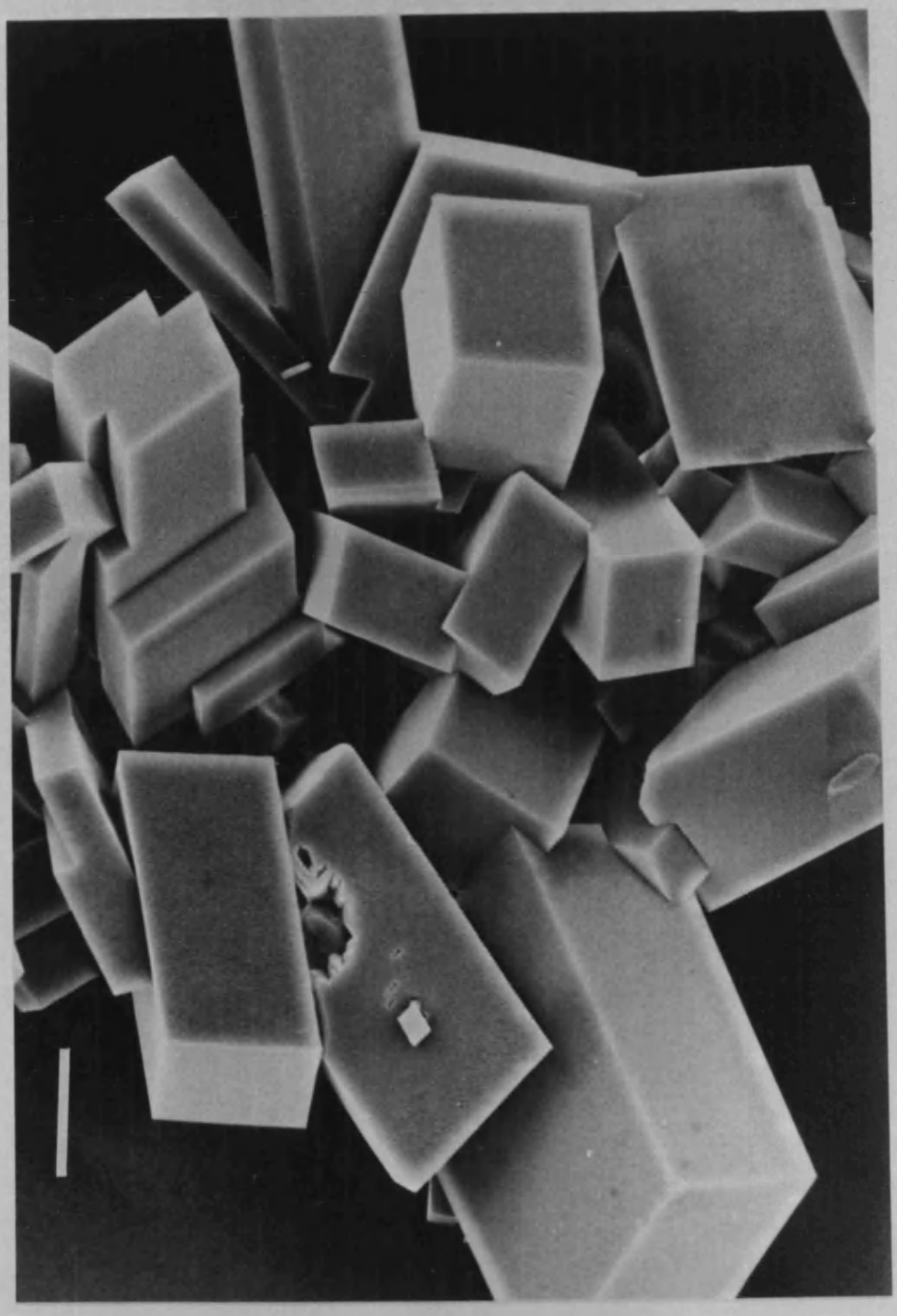

FIG. 3.9: SEM OF RHOMBOHEDRAL CALCITE CRYSTALS GROWN FROM SUPERSATURATED BICARBONATE SOLUTION IN THE ABSENCE OF A STEARIC ACID MONOLAYER (Scale bar = 10 μm)

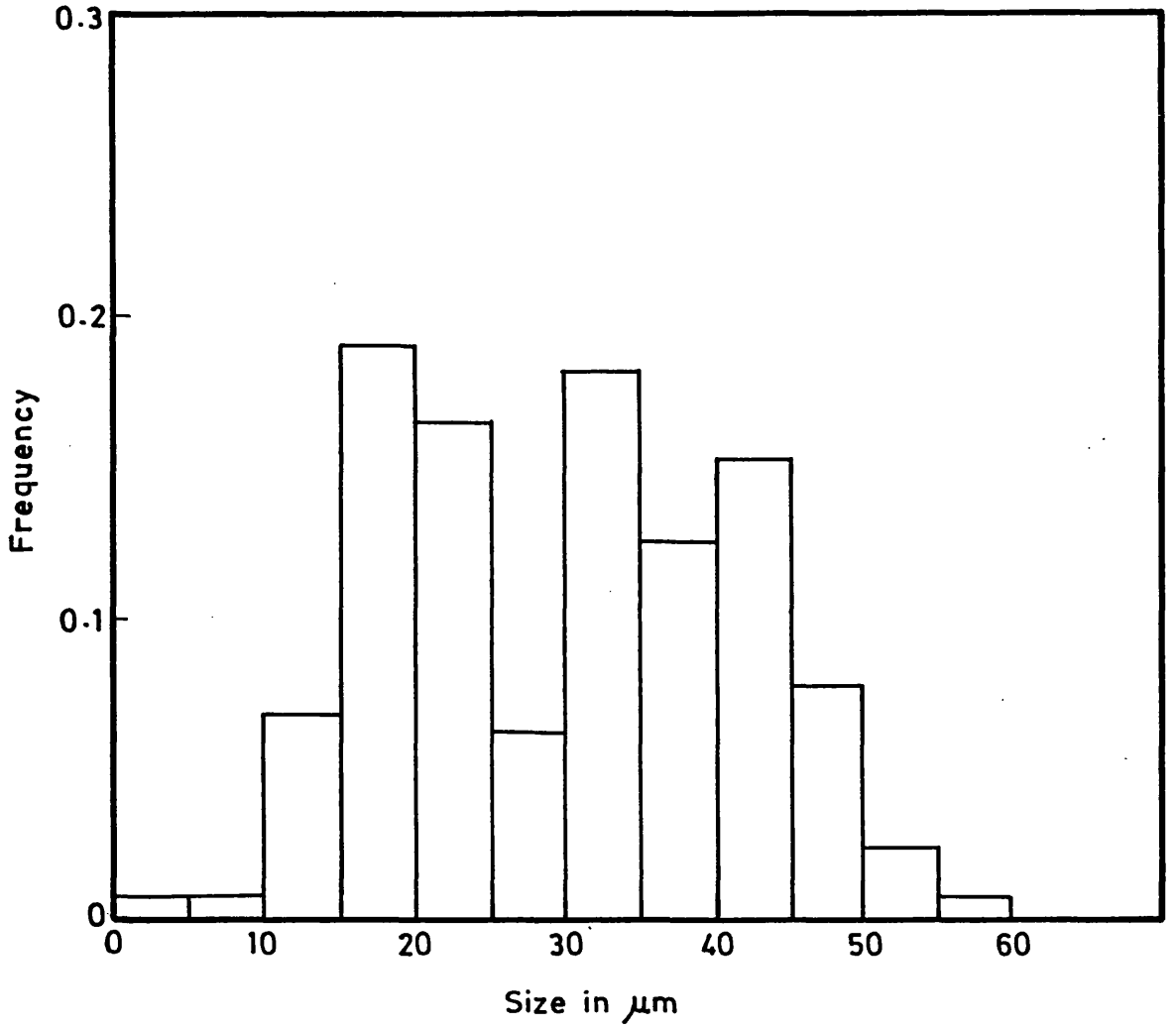

FIG. 3.10: HISTOGRAM SHOWING THE SIZE DISTRIBUTION OF CONTROL CRYSTALS.

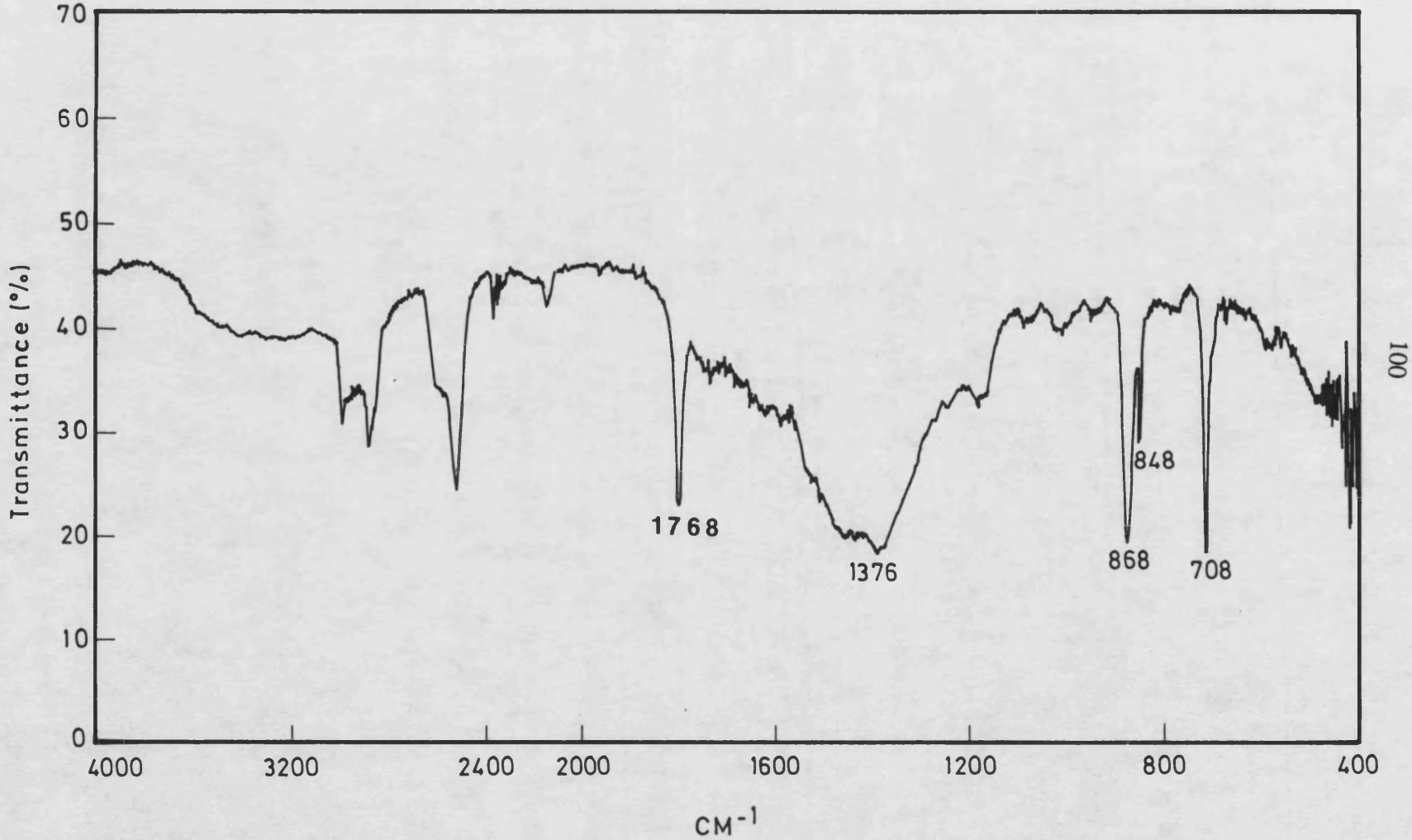

FIG. 3.11: IR SPECTRUM OF CALCITE CRYSTALS GROWN IN THE ABSENCE OF STEARIC ACID MONOLAYER.

respectively. The peaks at 708 and 868 & 848 cm^{-1} were sharp single bands. The absorption band 1376 cm^{-1} was broad and strong, and found to be asymmetrical.

(ii) CRYSTAL GROWTH FROM MONOLAYER EXPERIMENTS AT [Ca] = 4.5 mM: Crystals formed at the air/water interface under acid monolayers at [Ca] = 4.5 mM were almost grown as single bed of crystals and the XRD data as shown in Table 3.3 and Fig. 3.12 gave exclusively vaterite, whereas, the control crystals were mainly calcite. When the [Ca] was increased by increasing the level of carbon dioxide dissolved by changing the flow time or by the flow rate, the crystals obtained were a mixture of calcite and vaterite (Table 3.4). After 16 hours, the monolayer surface appeared visually to be coherent and the crystals were packed intact under the monolayer. Fig. 3.13A shows an optical micrograph of the monolayer system recorded *in situ*. When the collected crystals were observed by optical microscope, uniformly spaced and homogeneously sized floret shaped crystals were noticed. Crystals from the surface were collected in such a way that the florets were oriented as if being viewed from above the monolayer (Fig. 3.13B). The dish crystals exhibited similar orientation and symmetry as trough crystals (Fig. 3.13C). These crystals exhibited hexagonal symmetry with the six fold rotation axis perpendicular to the monolayer surface. On the basis of the crystal symmetry of vaterite (chapter I, section 1.10) this indicated that the crystallographic c axis

Table 3.3: XRD data for the crystals grown under stearic acid monolayers at [Ca] = 4.5 mM

d-spacings in Angstroms (Å)		
Experimental	Theoretical	
Trough	Calcite	Vaterite
4.241		4.245
	3.852	
3.576		3.577
3.290		3.296
	3.030	
	2.834	
2.726		2.735
	2.284	
2.202		2.219
2.112		2.122
	2.094	
2.060		2.065
	1.907	
	1.872	
1.857		1.857
1.820		1.825
1.645		1.648
	1.604	
	1.582	
1.534		1.544
1.471		1.477
	1.506	
	1.440	
	1.416	
1.358		1.351
	1.336	
1.308		1.331
1.283		1.286
	1.177	
	1.141	

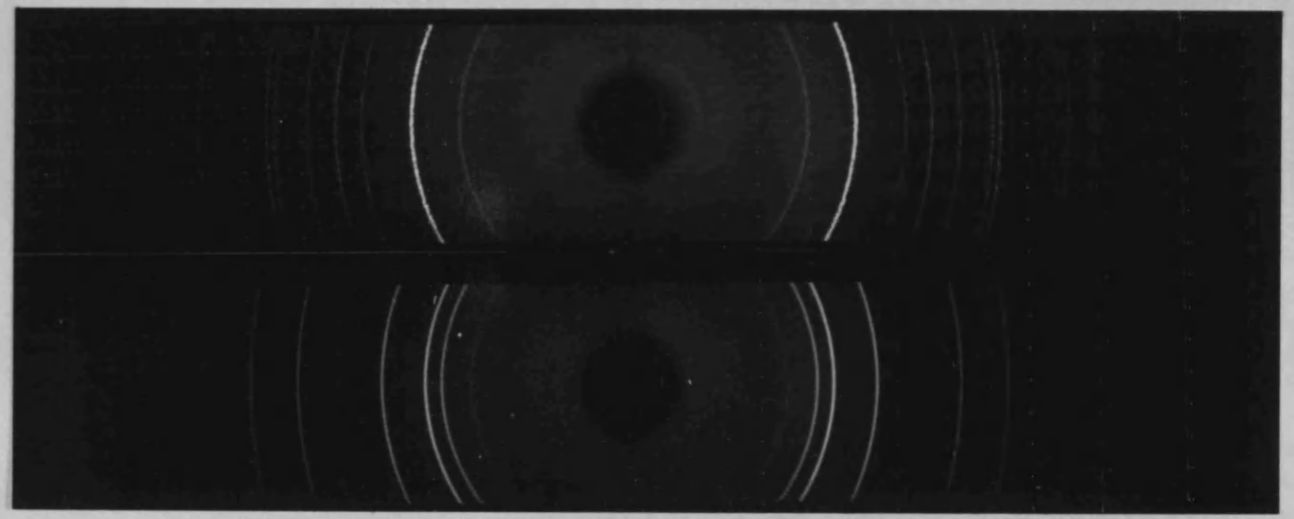

FIG. 3.12: XRD PHOTOGRAPHS OF $CaCO_3$ CRYSTALS: (A) CRYSTALS GROWN IN THE ABSENCE OF A MONOLAYER (B) CRYSTALS GROWN IN THE PRESENCE OF A MONOLAYER AT [Ca] = 4.5 mM

Table 3.4: XRD data of the mature crystals grown under acid monolayer at intermediate concentration of calcium (8.4 mM)

d-spacing (Å)	Calcite	Aragonite	Vaterite
4.240		4.212	4.245
3.818	3.858		
3.565		3.396	3.577
3.287		3.273	3.296
3.037	3.030		
2.724	2.834	2.700	2.735
2.487	2.495	2.481	2.219
2.316			
2.275	2.284	2.328	
2.155			2.122
2.093	2.094	2.106	2.065
1.912	1.907	1.977	1.857
1.869	1.873	1.882	1.825
1.816	1.626	1.814	1.825
1.600	1.604	1.698	1.648
1.524	1.525	1.535	

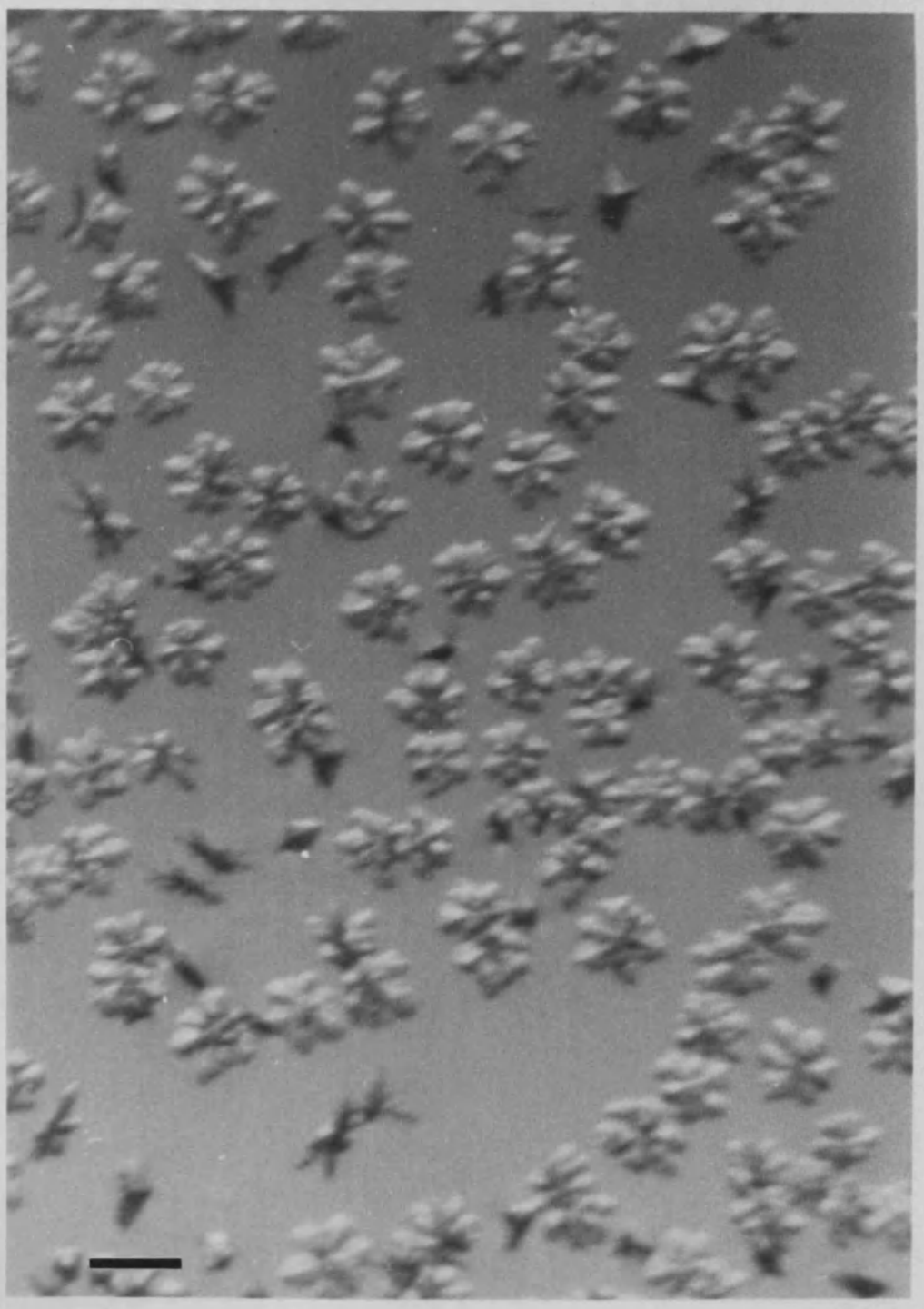

FIG. 3.13: (A) OPTICAL MICROGRAPH OF VATERITE (*IN SITU*) CRYSTALS SHOWING THE ORIENTATIONS OF THE CRYSTALS UNDER THE MONOLAYER FROM PETRI DISH EXPERIMENTS (Scale bar = 100 μm)

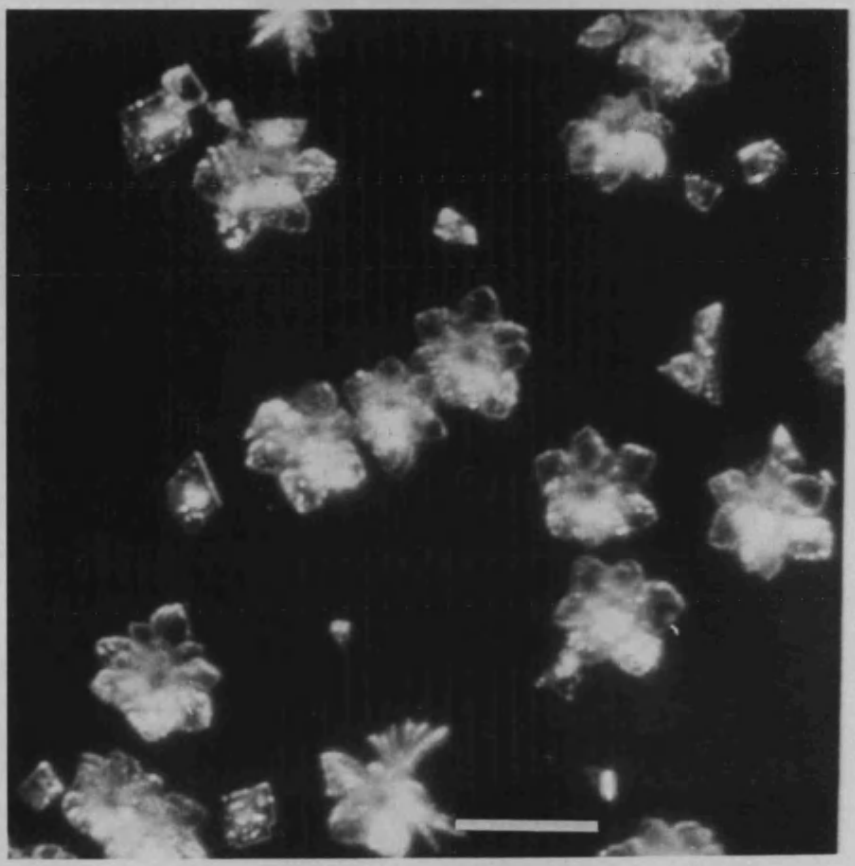

FIG. 3.13: (B) OPTICAL MICROGRAPH OF VATERITE SHOWING THE ORIENTATIONS OF THE CRYSTALS UNDER THE MONOLAYER IN THE TROUGH (VIEW FROM ABOVE MONOLAYER) (Scale bar = 100 μm)

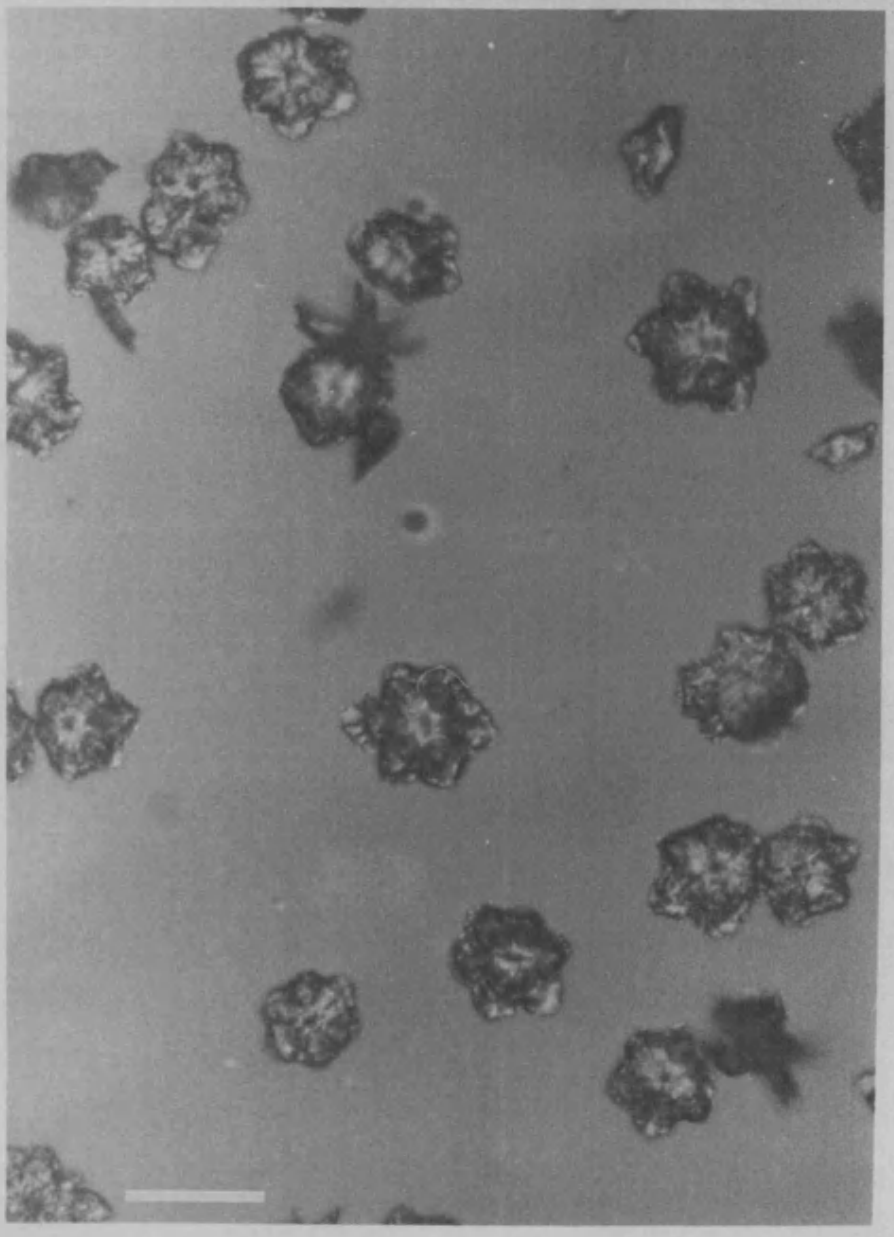

FIG. 3.13: (C) OPTICAL MICROGRAPH SHOWING THE ORIENTATIONS OF THE VATERITE CRYSTALS GROWN UNDER THE MONOLAYER IN THE GLASS CRYSTALLIZATION DISHES AT [Ca] = 4.5 mM (Scale bar = 50 μm)

was aligned perpendicular to the monolayer surface. The size distribution of the crystals (Fig. 3.14) shows the highly homogeneous nature of the crystals when compared with the control experiments (Fig. 3.10). The mean size of the crystals grown in the trough were 80 μm. Vaterite florets from glass dish experiments were slightly smaller and had a mean size of 60 μm. The number of crystals per unit area was, on an average, 6350 per cm^2 (Table 3.5). This number varied slightly under fluctuating supersaturation and room temperature conditions of different experiments.

The mature (16 -21 hours) crystals were studied by scanning electron microscopy. First of all these studies confirmed the observations obtained under optical microscope. Furthermore, it gave a detailed information on the orientation of the crystals and their surface textures. The surface of the vaterite crystals were roughened (Fig. 3.15). The crystals were viewed from two different directions. When they were viewed as if from under the monolayer the central disk appeared to be the point of contact with the monolayer. Further growth of the crystals were away from the monolayer into the solution. When the crystals were viewed as if from above the monolayer, the elevated point of contact of the disk and the hexagonal symmetry of the floret could be clearly seen (Fig. 3.16). The orientation of the hexagonal plates coplanar with the monolayer showed that these plates were aligned with the c (00.1) face parallel to the surface of the monolayer. A high magnification SEM micrograph (Fig. 3.17) clearly shows the hexagonal plates oriented parallel to the plane of the monolayer. However, it was clear that further outgrowths had their c axes inclined to

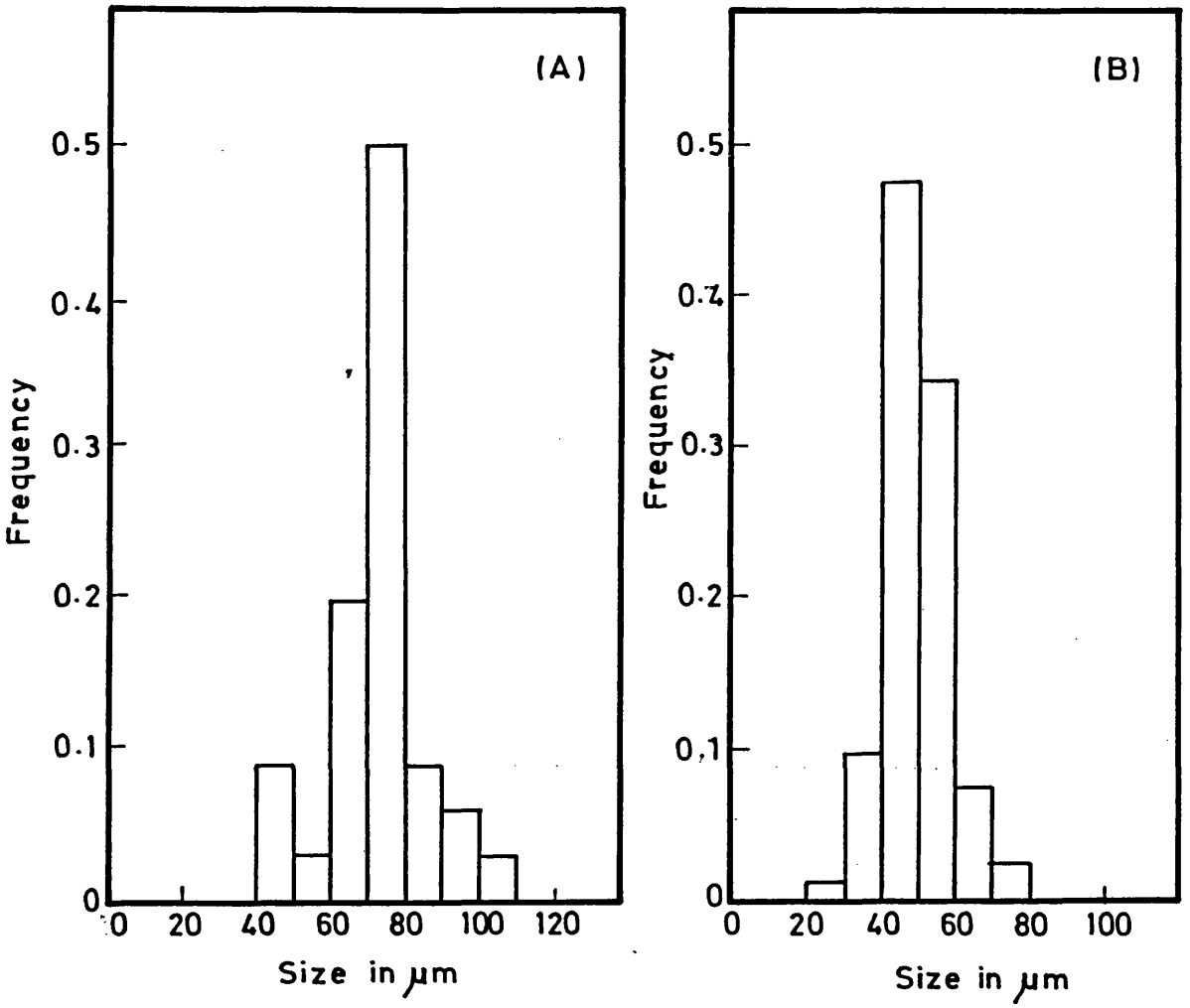

FIG. 3.14: HISTOGRAM OF CRYSTAL SIZE DISTRIBUTION OF VATERITE FLORETS FROM (A) TROUGH and (B) DISH EXPERIMENTS (Measurements made from micrographs).

Table 3.5: Nucleation density showing structural and morphological types of $CaCO_3$ crystals grown under stearic acid monolayers.

[Ca] mM	Monolayer state	Calcite		Non-oriented calcite	Vaterite		Total
		Type I	Type II		Type I	Type II	
9.0	Solid	5025	675	825	325	---	6850
9.0	Liquid	2550	725	1050	325	---	4900
4.5	Solid	500	150	450	4900	350	6350
4.5	Liquid	575	250	825	2700	300	4675
2.3	Solid	300	75	350	1000	---	1725
1.2	Solid	375	175	475	275	---	1300

Nucleation density = Number of crystals/1 cm^2

FIG. 3.15: SEM OF THE VATERITE FLORETS: FRONT VIEW FROM UNDER THE MONOLAYER (Scale bar = 10 μm)

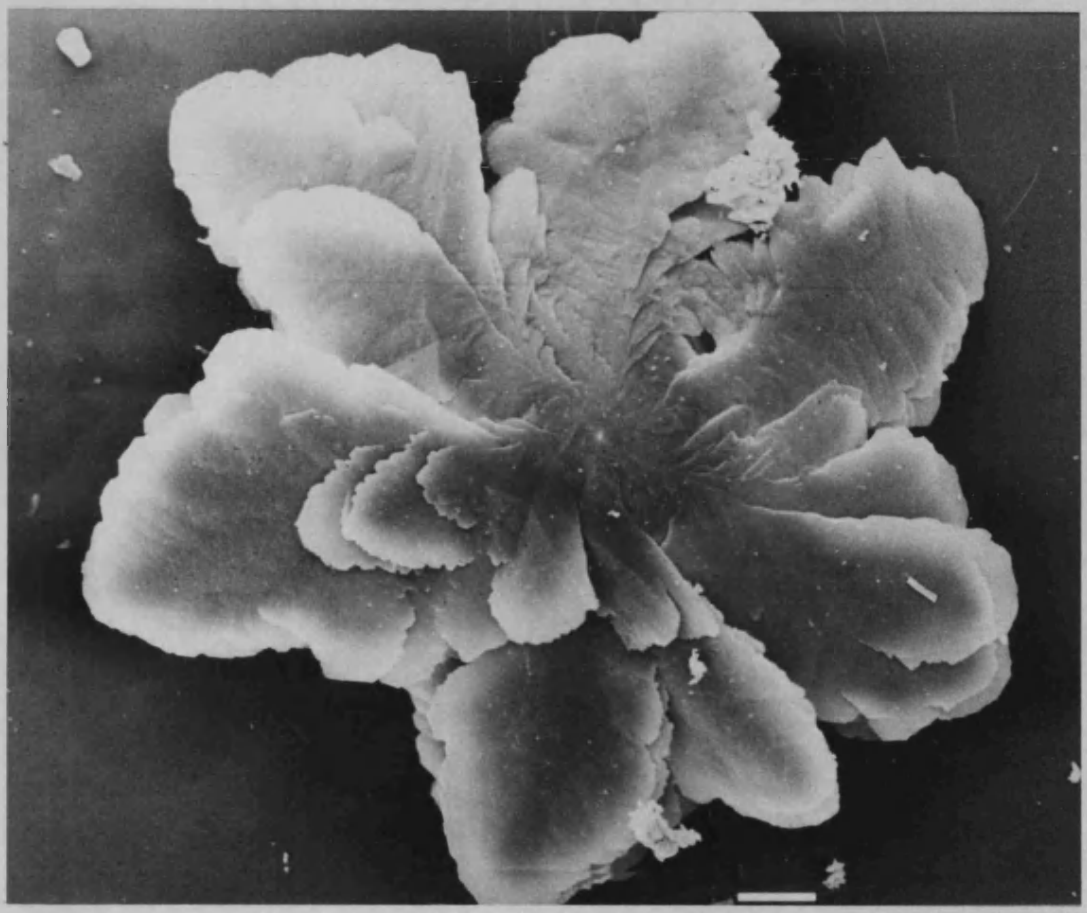

FIG. 3.16: SEM OF THE VATERITE FLORETS: VENTRAL VIEW SEEN FROM ABOVE THE MONOLAYER (Scale bar = 10 μm)

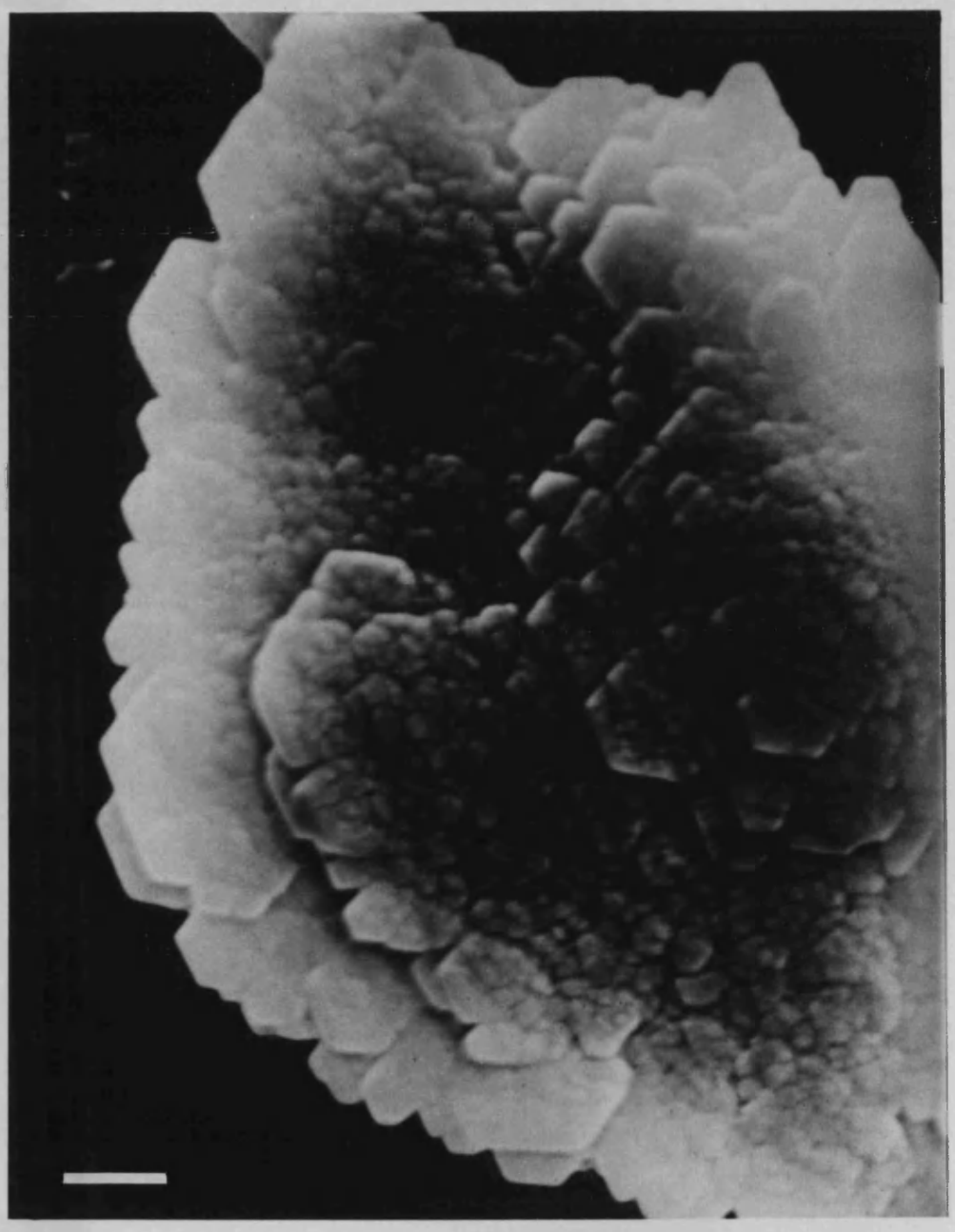

FIG. 3.17: EDGE OF THE FLORET CRYSTALS SHOWING THE HEXAGONAL PLATE FORMATION (Scale bar = 1 μm)

the plane of the monolayer indicating the polycrystalline nature of the mature crystals. The early crystals collected at time 45 minutes were biconvex shaped disks (Fig. 3.18). Crystals viewed from above the monolayer (3.18A) (comparable to the central elevated disk of the mature florets) and from the side (Fig. 3.18B) could be seen in the same images. It is probable that when the early crystals were collected on the stubs, they would have fallen over due to their small sizes.

From SEM analysis, it was determined that the diameter of the early disks were highly homogeneous (Fig. 3.19). At around 45 minutes, prominent outgrowths appeared from the edges of the disks (Fig. 3.18). Growth of the crystals into the solution phase was probably a diffusion controlled process. The prominent outgrowths in the form of hexagonal plates from the edges of the disks resulted in a hat like feature (Fig. 3.18C), showing an elevation in the centre and could be observed in the crystals collected within an hour after compression of the monolayer. These outgrowths increased in size and the mature florets were formed finally from them. The ventral cone like feature in the centre of the disk probably represents the original point of contact to the monolayer. They continued to remain in the same way and was noticed in the mature, 16 hours grown florets. Thick crystals showed the complex hexagonal morphology and roughened surface indicated the faster growth rate. Intergrowth of the crystals was rarely observed.

Leaving the crystals under the monolayer did not change the size of the crystals, but resulted in substantial remodelling of the

FIG. 3.18: SEM OF THE EARLY VATERITE CRYSTALS: (A) TOP VIEW (B) SIDE VIEW AND (C) MATURE DISK GROWN UNDER SOLID PHASE MONOLAYER [t = 45 min] (Scale bar = 10 μm)

FIG. 3.18 (D) SEM OF THE EARLY VATERITE CRYSTALS GROWN UNDER LIQUID PHASE MONOLAYER [t = 20 min] (Scale bar = 5 μm)

vaterite floret morphology. The aged florets were less complex, exhibited a clearer hexagonal symmetry, were generally thicker and showed extensive surface dissolution (ill-defined edges and etch pits). When the crystals were left at the interface for a longer period of 15 days they showed complete dissolution of highly soluble metastable polymorph vaterite, and the formation of non-oriented calcite. Monolayer organisation seemed to have been lost over this length of time.

Among the vaterite florets a further morphological type (type II) was also present in trace amounts. This form was common under octadecylamine monolayers and is described in detail in Chapter IV.

3.3.3. EFFECT OF COMPRESSION CHANGES: Increasing or decreasing the monolayer area within a small range, did not affect the crystal structure and morphology of the oriented vaterite crystals; however, the nucleation density was reduced and the percentage of non-oriented calcite crystals increased (Table 3.5). The sizes of the crystals grown were slightly larger. The data showed that the nucleation density was reduced from 100% to 74%, when the monolayer was changed from solid to liquid phase. However, the numbers of monolayer forming acid molecules when compared from solid to liquid phase were not reduced to the same extent but only reduced by 18% within a definite surface area. Furthermore, the distribution in the disk diameters of the early crystals indicated a slight increase in the homogeneity of the crystal nucleation in the liquid phase monolayer (Fig. 3.19B, and Fig 3.18D). This showed that the nucleation

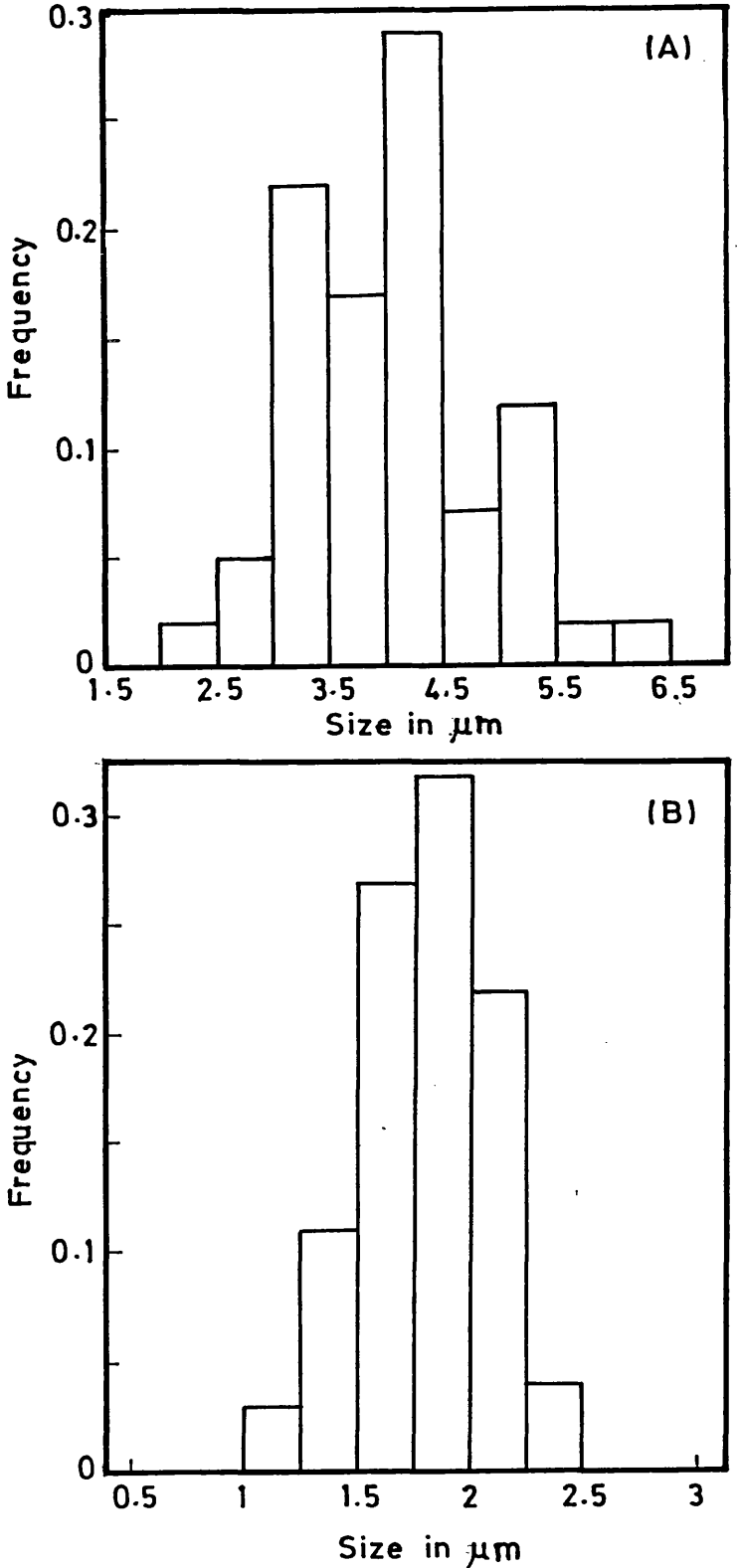

FIG. 3.19: HISTOGRAM SHOWING THE SIZE DISTRIBUTION OF EARLY CRYSTALS COLLECTED UNDER (A) SOLID PHASE (At t=45 min.) and (B) LIQUID PHASE (At t=20 min.) MONOLAYERS.

density was affected by the rigidity of the monolayers, but the structure morphology and orientation remained unaffected.

Crystallization under uncompressed stearic acid monolayers resulted in a mixture of vaterite and calcite crystals. The number of crystals were less in these gas phase monolayers with a high percentage of non-oriented crystals. There were no changes in the alignment and morphology of the oriented crystals grown. The monolayer was not visually coherent and different patches of non-uniform areas of monolayer with different densities of crystals were seen across the surface. This suggests that the surface was condensed in localised regions even in the gas-like state presumably local Ca binding can induce domain formation and some degree of oriented nucleation in these expanded films.

3.3.4 CRYSTAL GROWTH FROM MONOLAYER EXPERIMENTS

AT [Ca] = 9 mM: The change in the supersaturation of the solution had a profound effect on the crystals grown under the monolayer. The measurement of the supersaturation was complicated as it depended on the speciation of bicarbonate and carbonate, pH and dissolved CO_2 concentration. The concentration of calcium in the solution was used as a marker for supersaturation changes.

Crystals grown at an increased concentration of calcium at 9.0 mM gave a striking change in the result. Crystals grown under the monolayer at this high concentration of calcium were mainly calcite of distinct morphology. Qualitative XRD showed the strong lines of calcite

table 3.6) and quantitative XRD data of a typical experiment (calibration curve - Fig. 3.20) gave at least 70% by weight of the crystals as calcite. FT-IR spectral analysis of these crystals also confirmed the structure of calcite (Fig. 3.21.A). At this juncture, it is interesting to observe that the FT-IR data gives some insight into the possible incorporation of the carboxylate groups into the crystal lattice of calcite crystals. Fig. 3.3 shows the IR absorption band for the carboxyl group of stearic acid under normal conditions at 1700 cm^{-1}, whereas IR spectra (Fig. 3.21.B) of stearic acid monolayer detected along with the calcite crystals gave a strong absorption band at 1581 cm^{-1}. The shift in the absorption band for the carboxyl C=O group from 1700 to 1581 cm^{-1}, (characteristic absorption peak for the ionized carboxyl group) indicates the high percentage of the ionization of the carboxyl group under the monolayer. Similar observations using cadmium salt solutions under acid monolayers has been reported recently [192]. Repeated washings did not completely eliminate the stearate molecules from the crystals.

However, the morphology of the calcite crystals was different from the normal rhombohedral calcite crystals. Dish crystals when viewed *in situ* under optical microscopy were found to be highly homogeneous discrete thin plates of rhombohedral calcite. These crystals were collected and viewed under optical microscopy (Fig. 3.22). SEM micrographs showed that these plates had a smooth oriented elevation in the centre (Fig. 3.23). But the basal surface was roughened and the side edges were smooth. This predominant morphological form (type I) exhibited C_{2v}

Table 3.6: XRD data of the mature crystals grown under the monolayer at high concentration of calcium (9.0 mM)

d-spacing (Å)	Calcite	Aragonite	Vaterite
3.850	3.852	4.212	4.245
3.565		3.396	3.577
3.284		3.273	3.296
3.029	3.030		
2.732	2.834	2.700	2.735
2.489	2.495	2.481	2.219
2.285	2.284	2.328	2.122
2.093	2.094	2.106	2.065
1.908	1.907	1.977	1.857
1.889	1.873	1.882	1.825
1.812	1.626	1.814	1.825
1.600	1.604	1.698	1.648

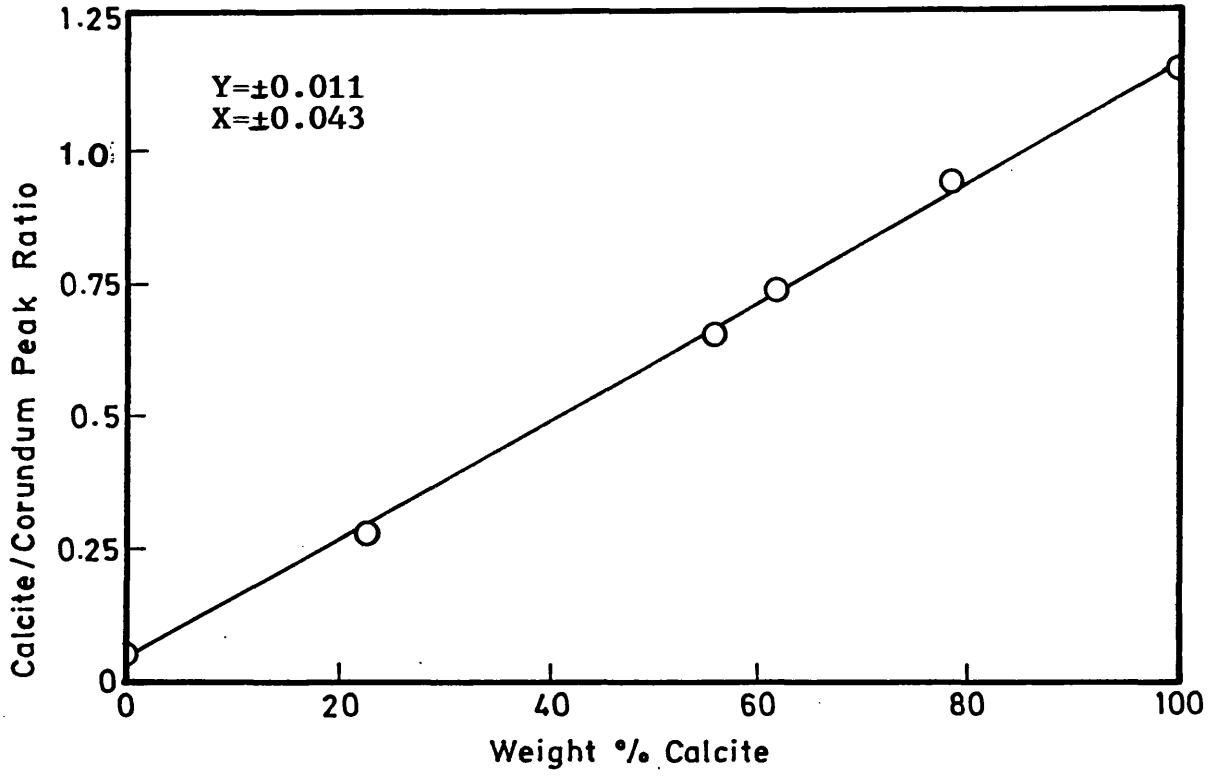

FIG. 3.20: XRD QUANTITATIVE ANALYSIS - CALIBRATION PLOT FOR THE ESTIMATION OF POLYMORPHIC COMPOSITION OF CALCIUM CARBONATE.

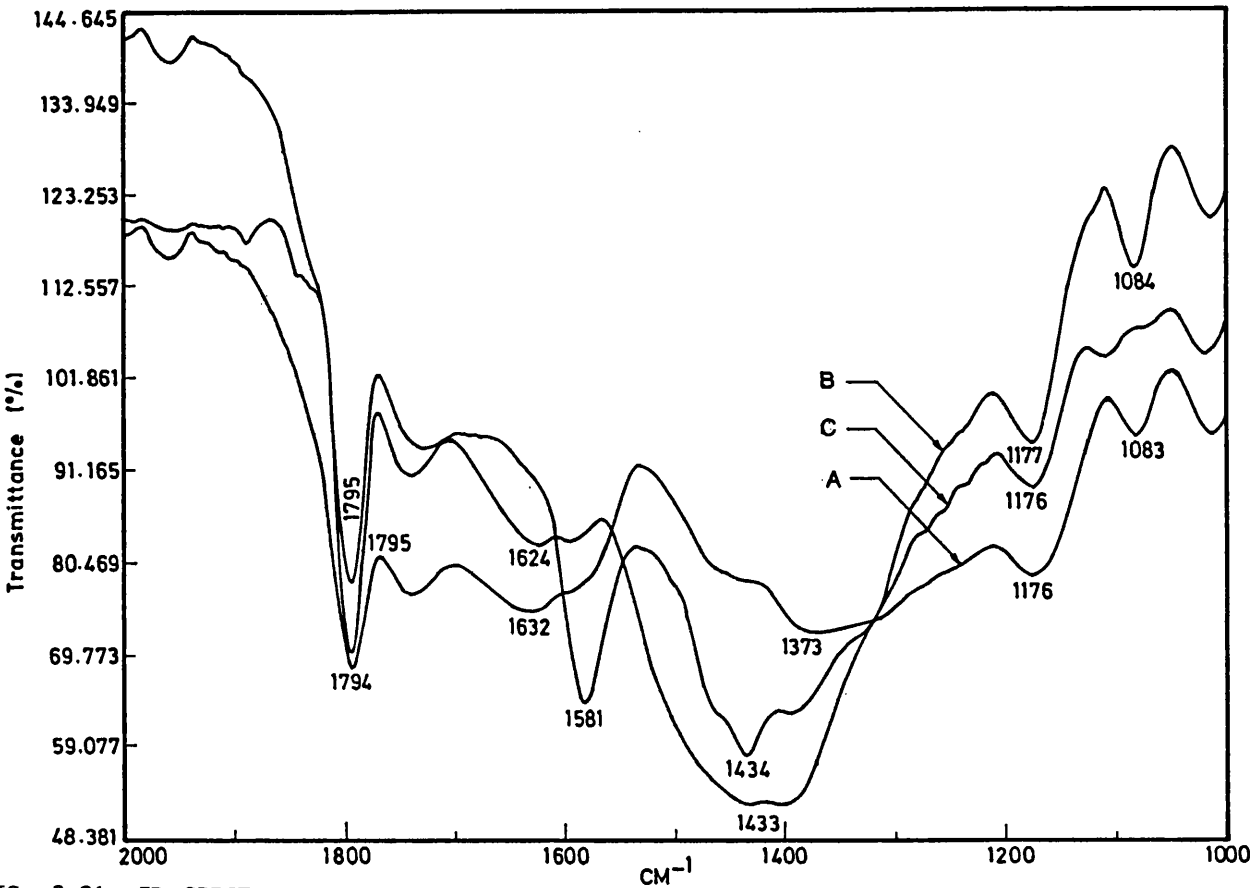

FIG. 3.21: IR SPECTRA OF CALCITE PLATES GROWN UNDER ACID MONOLAYER: (A) SAMPLE PRIOR TO WASHING, (B) AFTER WASHING WITH CHLOROFORM and (C) AFTER SEVERAL WASHINGS.

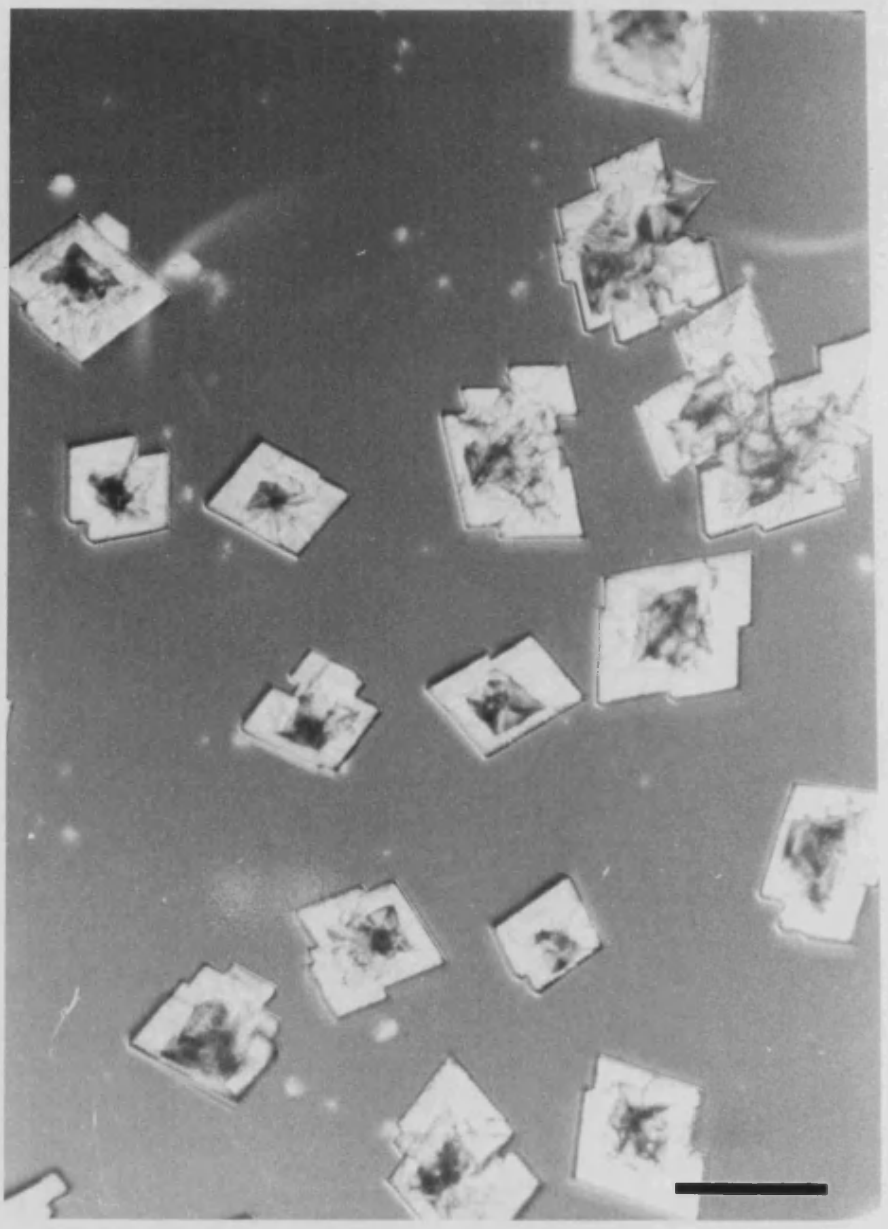

FIG. 3.22: OPTICAL MICROGRAPH OF CALCITE CRYSTALS GROWN UNDER ACID MONOLAYER AT HIGHER CONCENTRATION OF CALCIUM (9 mM) (Scale bar = 50 μm)

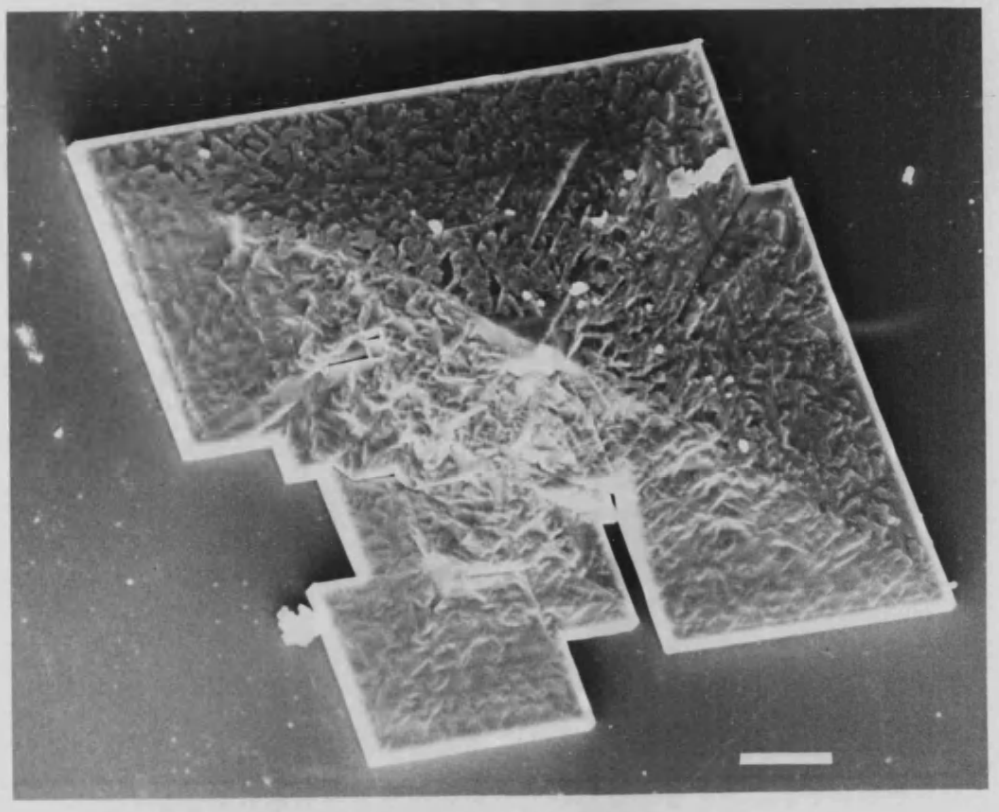

FIG. 3.23: SEM OF ORIENTED CALCITE PLATE (Scale bar = 10 μm)

symmetry with all four edges of the basal (10.4) face being expressed. The crystals had smooth rhombohedral (10.4) side faces and were often wedge-shaped. There were changes in crystal textures at different sides of the long diagonal of the rhombohedral basal plate (Fig. 3.24). The thicker crystal half was well defined and generally had uninterrupted (10.4) edges whilst the thinner side contained fissures and stepped edges. Viewed from below the monolayer, the crystals had smooth rhombohedral (10.4) basal faces (Fig. 3.25). Many crystals contained a central cavity (Fig. 3.26) indicative of diffusion-limited growth probably caused by supersaturation gradients accompanying loss of CO_2 at the air/water interface. The crystallographic direction parallel to the long diagonal of the (10.4) basal face corresponds to the a axis. This axis is perpendicular to [001] direction of the calcite rhombs.

The smooth central elevation of calcite plates comprised three inclined faces, two of which were related by reflection symmetry (Fig. 3.27). The intersection of these two faces formed a ridge which when viewed in projection ran parallel to the $[20.\bar{1}]$ direction. A second ridge, formed by the intersection with the remaining face was aligned parallel to the a axis. The apex of the elevated feature was irregular and no crystallographic faces could be observed. The size measurements showed that the base plates of the crystals were of a narrow particle size distribution with a mean length 60 μm and σ = 10.5 (Fig. 3.28). There were not much differences between the length and width sizes of the crystal (Fig. 3.29). The size of central elevation was around 5 - 10 μm across.

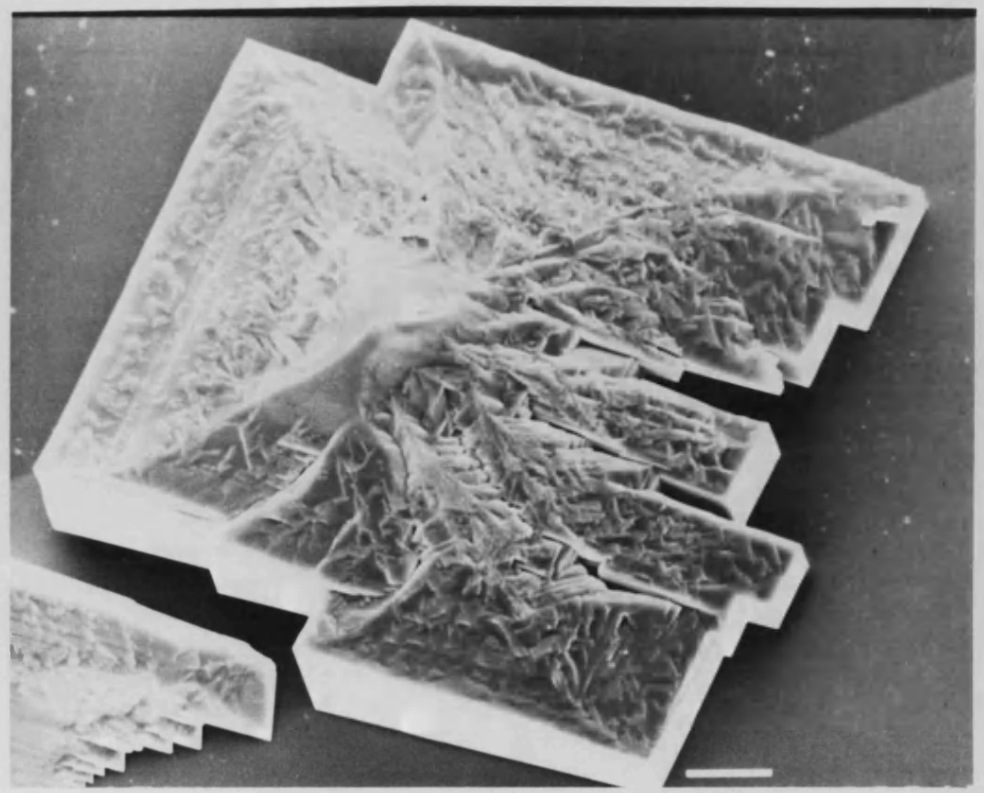

FIG. 3.24: SINGLE FULL PLATE SHOWING THE ROUGHENED SURFACE AND THE WEDGE SHAPE OF THE CRYSTAL (Scale bar = 10 μm)

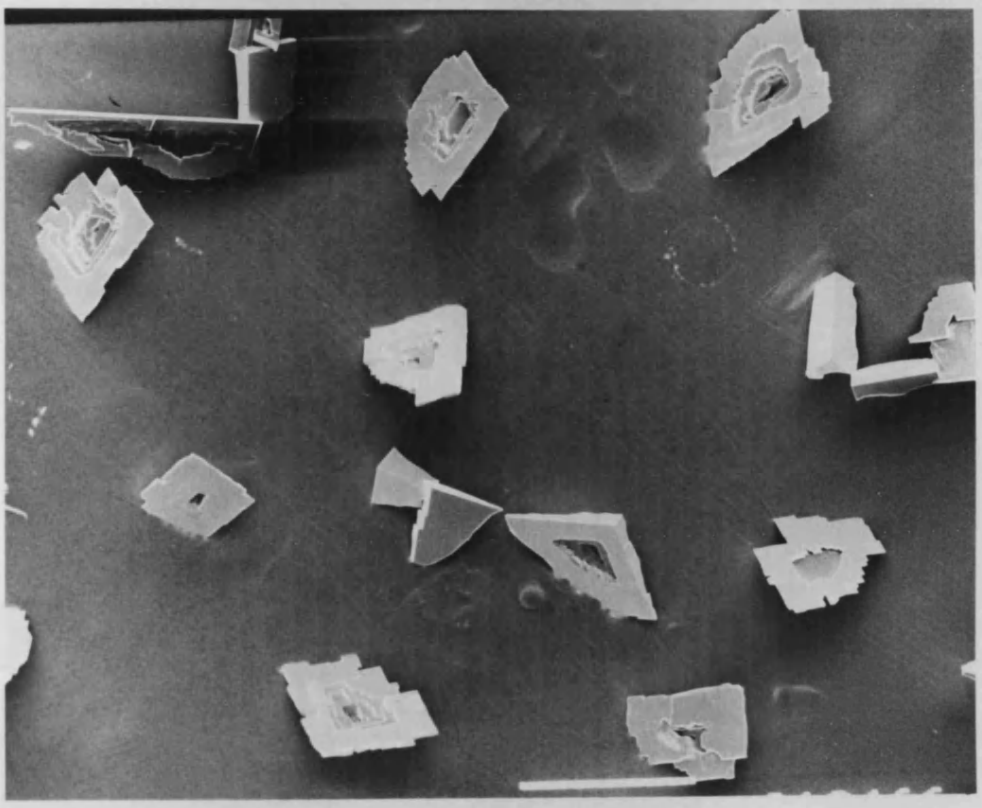

FIG. 3.25: SEM SHOWING THE SMOOTH VENTRAL SURFACE OF THE CALCITE PLATES (Scale bar = 100 μm)

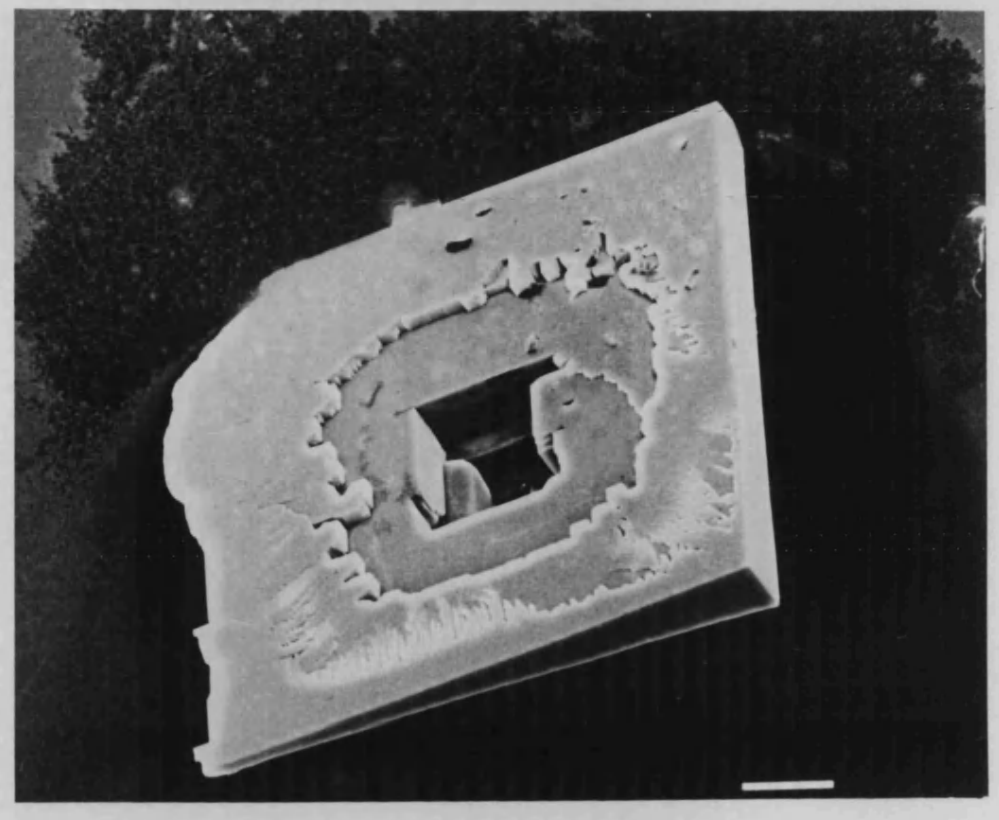

FIG. 3.26: SEM SHOWING THE BACK OF THE CALCITE PLATE WITH CENTRAL CAVITY (Scale bar = 10 μm)

FIG. 3.27: SEM OF THE CENTRAL ELEVATION OF AN ORIENTED CALCITE PLATE. DETAILS OF THE THREE INCLINED RIDGES AND STEPPED FACES ARE SHOWN. (Scale bar = 10 μm)

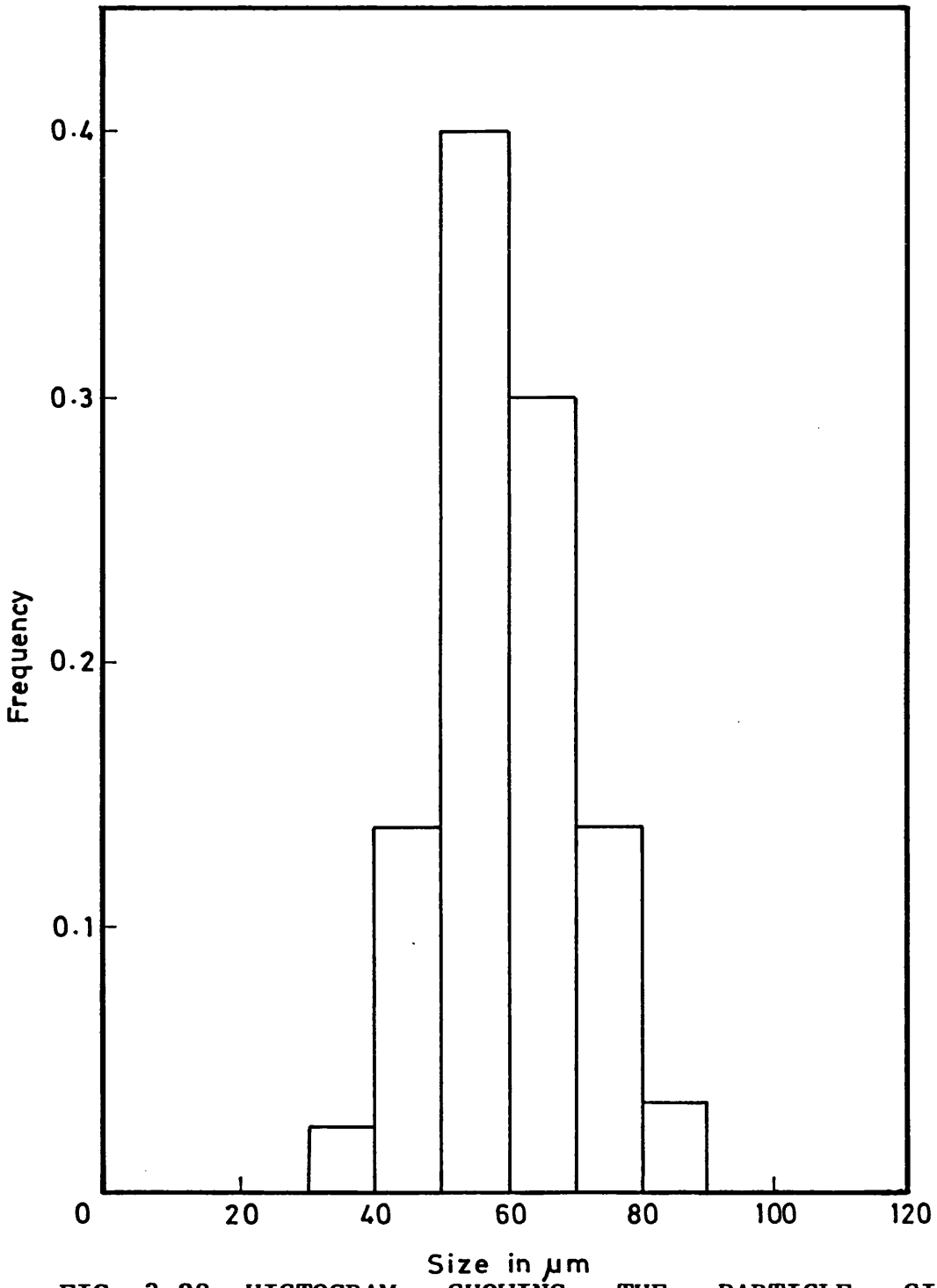

FIG. 3.28: HISTOGRAM SHOWING THE PARTICLE SIZE (Length) DISTRIBUTION OF CALCITE PLATES.

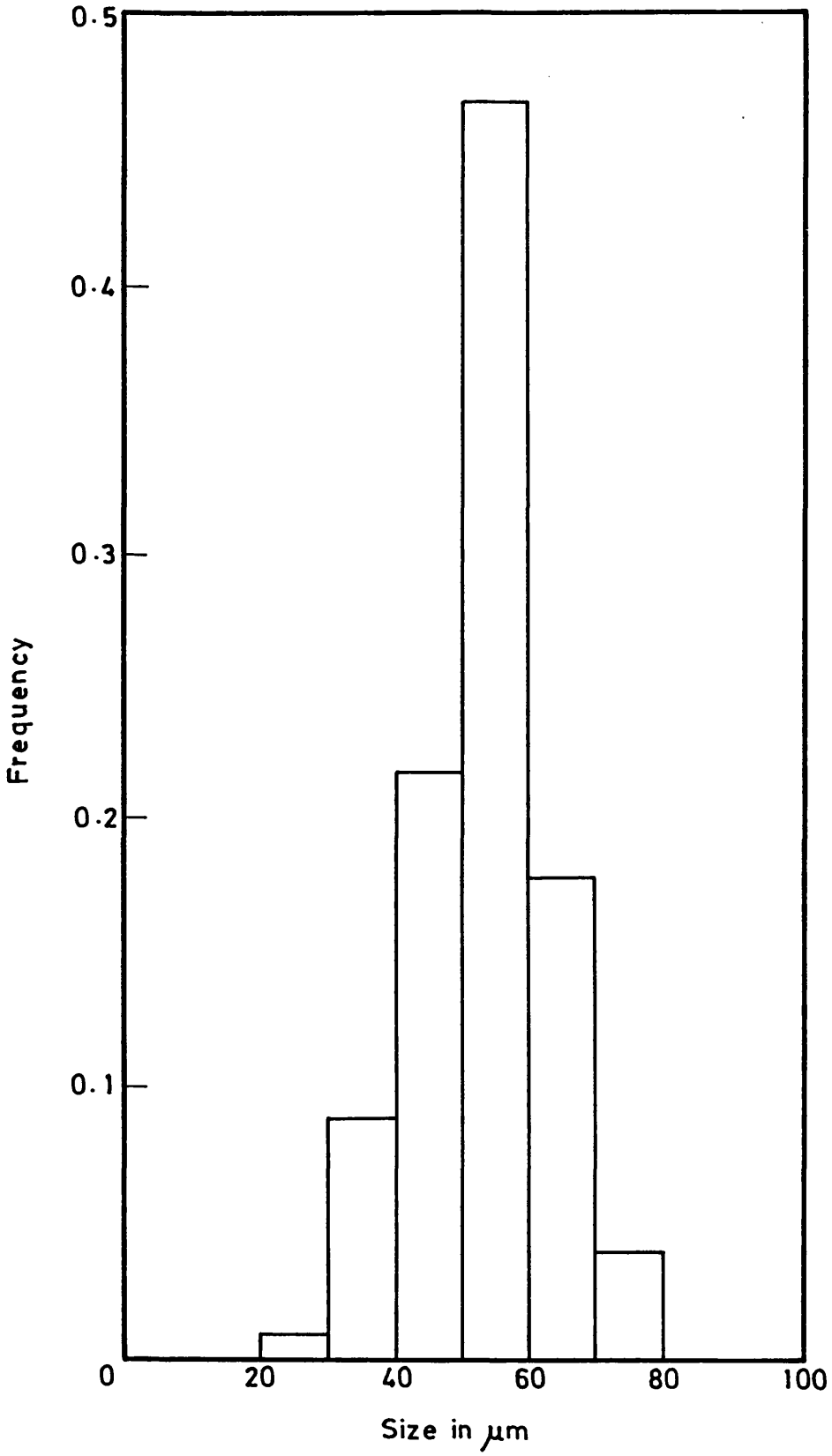

FIG. 3.29: HISTOGRAM SHOWING THE PARTICLE SIZE (Width) DISTRIBUTION OF CALCITE PLATES.

The base plate thickness was ≈ 5 μm in size along the thicker side of the crystal (Fig. 3.30). The top surface of the crystal which was in contact with the monolayer had a roughened texture indicating the fast growth rate of the crystal probably due to the interaction of the monolayer. The nucleation density of the calcite plates was 6850 per cm^2 and is slightly higher than that of vaterite florets (Table 3.5). In some experiments a morphologically related form of type II crystals were observed. The type II calcite crystals did not show the plate-like morphology characteristic of type I crystals. SEM micrographs of these plates clearly showed the base plates and the centrally elevated rhombohedral crystals. These crystals had psuedo c_3 symmetry and were triangular in projection with only two of the four basal {10.4} faces being developed (Fig. 3.31). The upper roughened surface of type II crystals was elevated across the entire crystal and the side faces were smooth {10.4} faces. Three inclined faces equivalent to those present on the central elevation of type I crystals were observed. In some crystals, smooth rhombohedral faces decorated along the shorter inclined ridge (Fig. 3.32). This enabled the orientation of these faces to be determined from the morphological analysis (Fig. 3.33). The a and c axes of the decorated rhombs were in the plane of the monolayer. Thus the face aligned parallel to the monolayer surface was of $(1\,\bar{1}.0)$ form which is a first order prismatic face. Hence, nucleation on the $(1\,\bar{1}.0)$ face is preferentially stabilized by the stearate monolayer. Once nucleated the crystals seemed to have grown the same way to a critical size after which in some experiments the crystal started to grow away from the

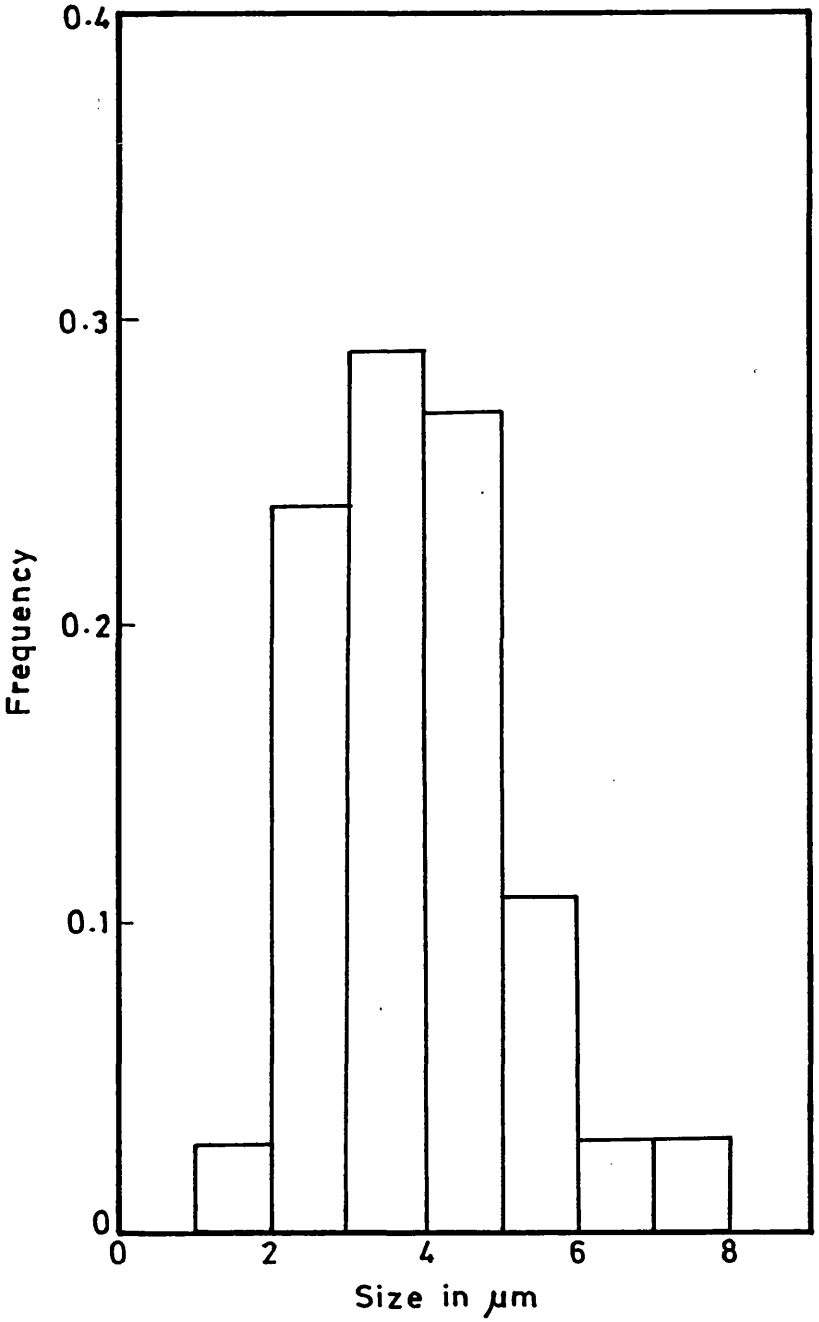

FIG. 3.30: HISTOGRAM SHOWING THE SIZE (Thickness) DISTRIBUTION OF CALCITE PLATES (Measurements were made on the thicker side of the crystal).

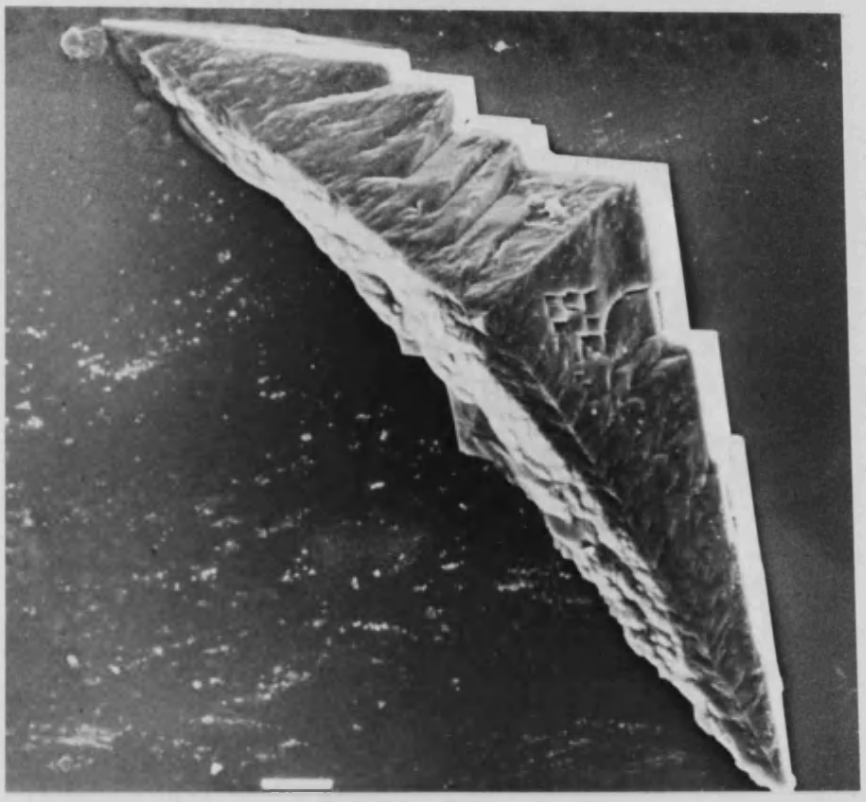

FIG. 3.31: SEM OF CALCITE TYPE II CRYSTAL (Scale bar = 10 μm)

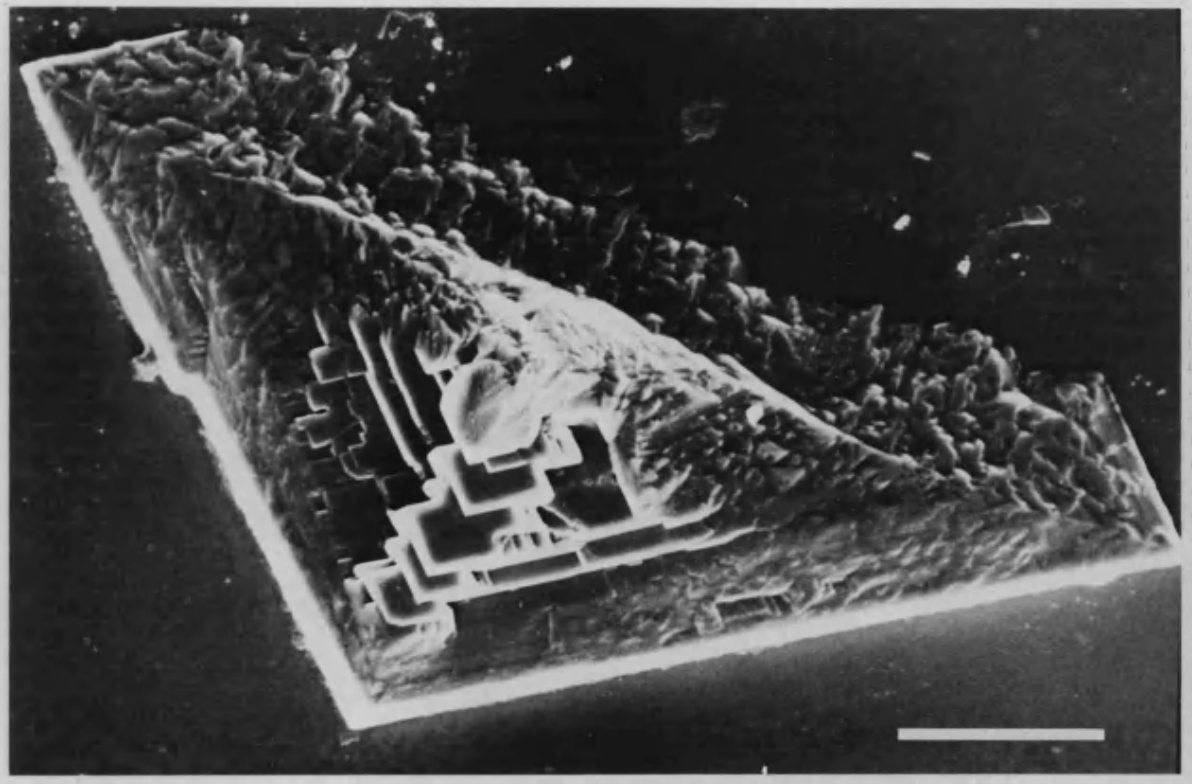

FIG. 3.32: SEM OF CALCITE TYPE II CRYSTAL SHOWING RHOMBOHEDRAL DECORATION ALONG ONE OF THE INCLINED RIDGES (Scale bar = 20 μm)

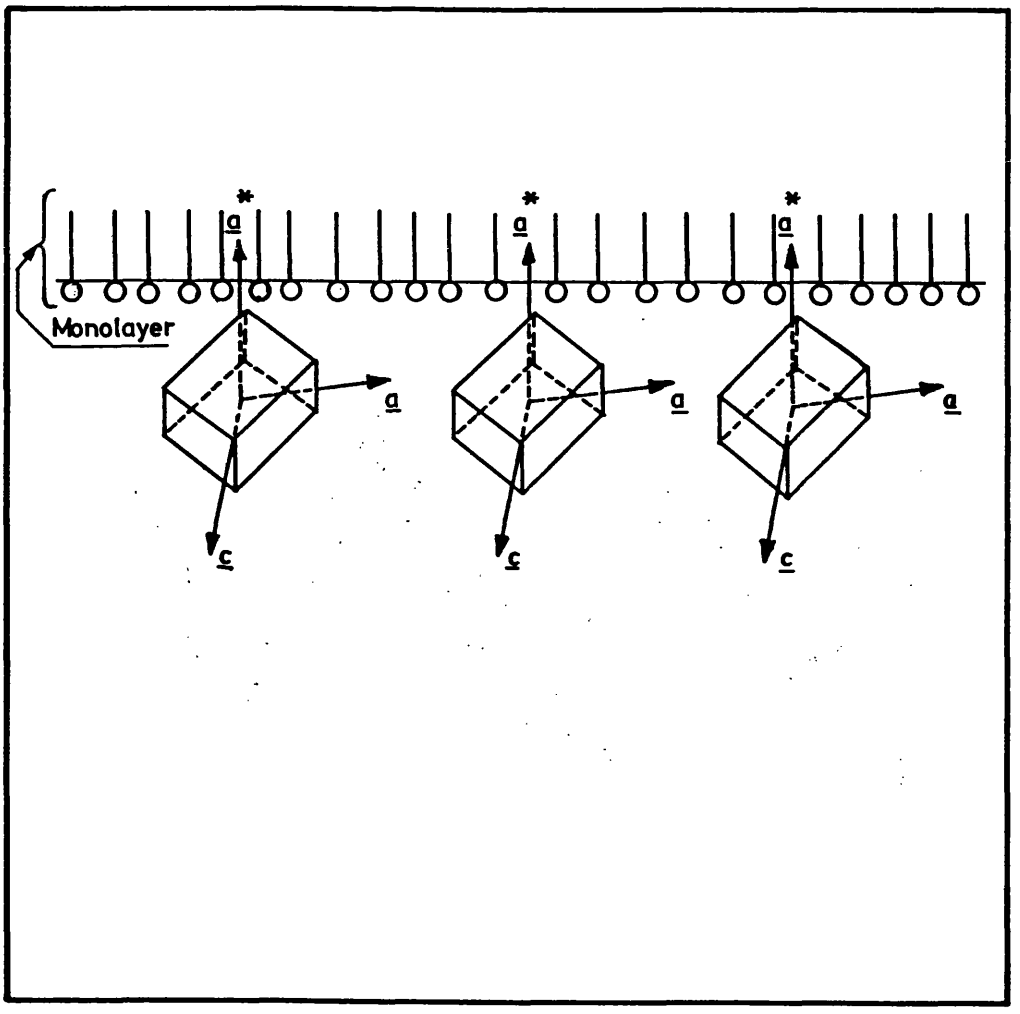

FIG. 3.33: SCHEMATIC DIAGRAM SHOWING THE ORIENTATION OF THE CALCITE PLATE WITH RESPECT TO THE MONOLAYER SURFACE.

monolayer, which led to the development of full plates. The inclination of the central elevation to the base plate at around 45° showed that feature of the crystal (Fig. 3.34). This inclination developed the wedge shaped type I calcite crystals. The trough calcite crystals were similar to type II crystals except that they had extended growth along the in-plane a axis direction and developed mountain range type of calcite (Fig. 3.35) crystals. This could be due to the difference in the surface concentration ratio of calcium to bicarbonate ions.

When there was slight fluctuation in the concentration of calcium, the populations of the crystal types obtained were slightly different and variable. For example, when there was 8.4 mM concentration of calcium, the two types of calcite crystals along with some non-oriented calcite crystals and vaterite florets were observed under the monolayer (Fig.3.36). For some reason the nature of the solution had prevented the type II crystals from growing into a full plate. When there was a small change in room temperature the coherence of the monolayer molecules slightly decreased and that was shown by the presence of small aggregates of non-oriented control-like, normal and truncated rhombohedral crystals. The presence of non-oriented crystals were only seen in some dish experiments, and at the edges of the monolayers near the barrier belt in the trough experiments. However, even in the non-oriented crystals the surface roughening and a slight elevation in the centre could be seen indicating a physical interaction with the surface. When the calcium

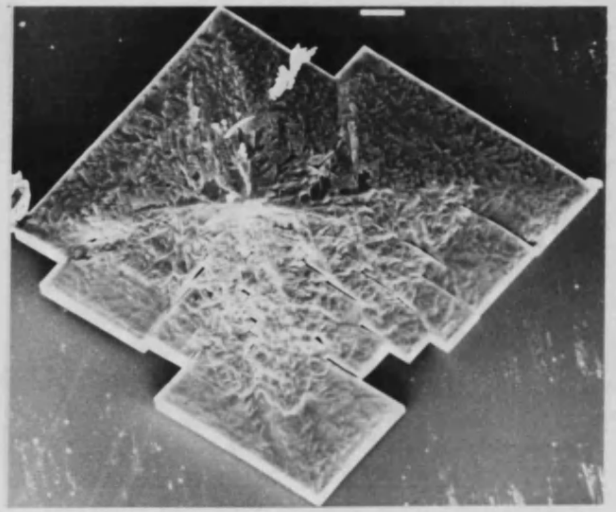

FIG. 3.34: SEM OF TYPE I CALCITE VIEWED FROM THE SIDE SHOWING WEDGE-SHAPED PROFILE AND THE VARYING SURFACE TEXTURE OF DIFFERENT SIDES (Scale bar = 10 μm)

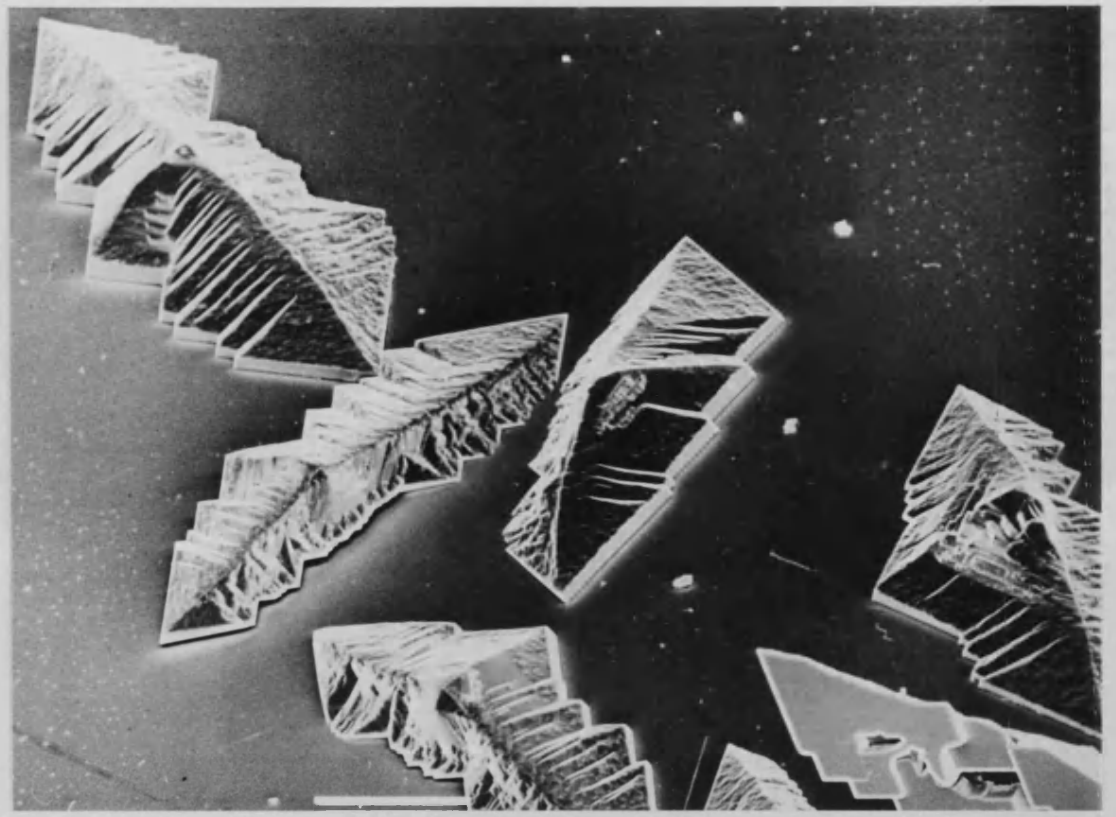

FIG. 3.35: SEM OF TYPE II CALCITE CRYSTAL WHICH HAS GROWN OUT ALONG THE a AXIS (Scale bar = 10 μm)

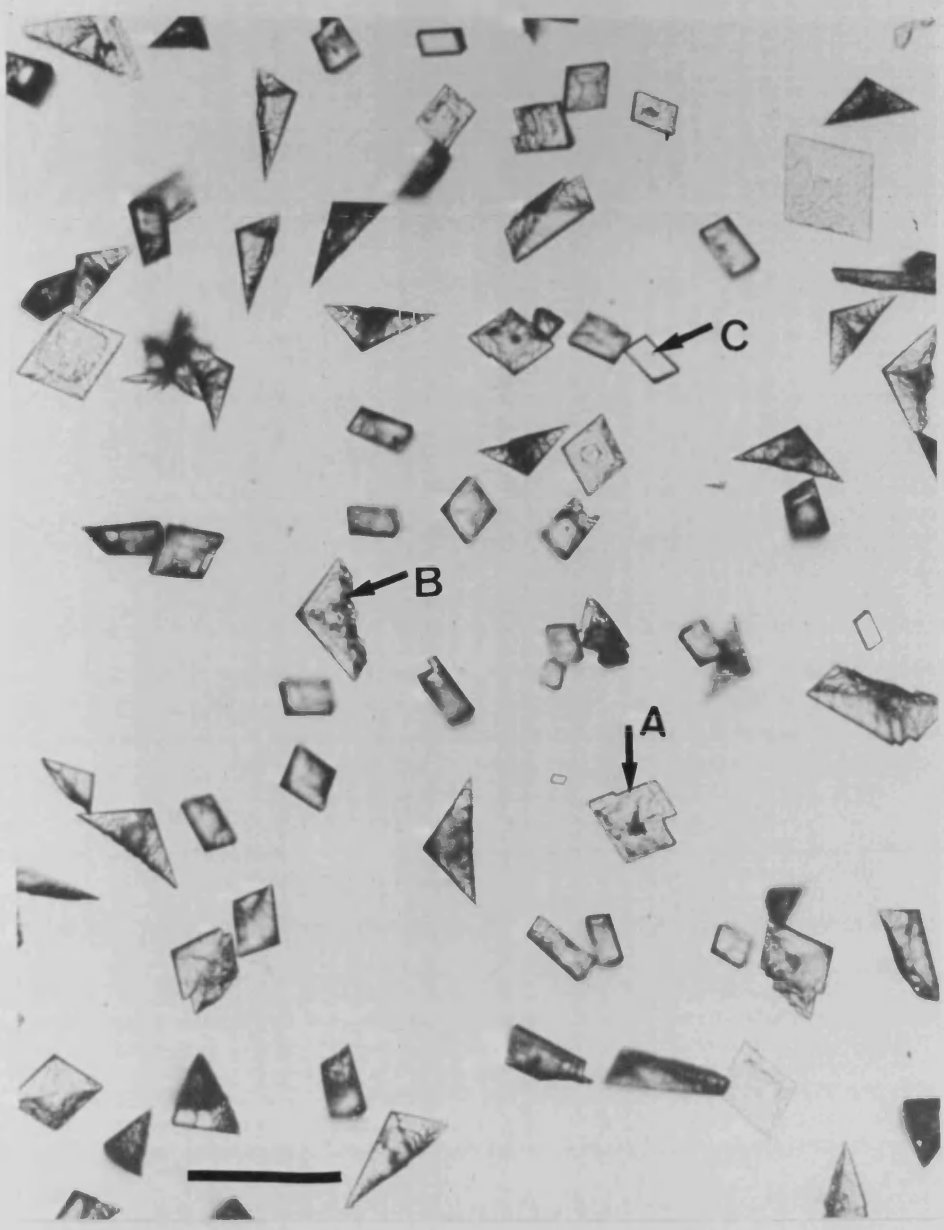

FIG.3.36: OPTICAL MICROGRAPH SHOWING ORIENTED TYPE I (A) AND TYPE II (B) CALCITE CRYSTALS AND SOME TYPE III NON-ORIENTED TRUNCATED RHOMBS (C).
(Scale bar = 10 μm)

concentration was reduced to half at around 4.5 mM the system completely switched to nucleate vaterite as described in section 3.3 (iii) (b).

From the experimental results, it is seen that both calcium concentration and calcium/bicarbonate concentration ratio has influence to some extent in dictating the structure of the crystal formed. However the experiments show that it is possible to get both oriented calcite and vaterite crystals under suitable solution conditions in stearic acid monolayers which are clearly different from the control crystals.

3.3.5 **DILUTION EXPERIMENTS:** The typical experiments done in the glass dishes have shown that it is possible to get both vaterite and calcite crystals under suitable dilutions. In the experiment where the calcium bicarbonate solution of 9mM calcium concentration was prepared and diluted to four different concentrations the results obtained were remarkable. At 9 mM concentration complete full plates were nucleated and grown on the surface. The vaterite crystals, calcite half plates, and the non-oriented truncated rhombs were completely absent. When the solution was diluted to 4.5 mM and the monolayer spread the crystals were exclusively vaterite.

At lower concentration of calcium at 2.3 mM the crystals grown were a mixture of calcite plates, vaterite florets and non-oriented rhombs. However the nucleation density was very low (Table 3.2) and the sizes of the crystals were very small which was expected of at a low concentration. Further when the solution was diluted to 1.2 mM calcium

concentration the crystals could not be identified at around normal 20 hours under optical microscope. When they were allowed to grow upto 44 hours, small, non-oriented rhombohedral crystals were mainly seen along with some calcite plates. However the vaterite formation was mainly eliminated. The system was so sensitive that a small change in the concentration of the solution reduced the reproducibility of the results. However, the calcite full plates were reproducibly obtained which are at present unique for stearic acid monolayers. It was so sensitive that at intermediate concentrations from 9 to 4.5 mM concentrations, mixture of calcite and vaterite crystals, mixture of full plates, half plates and non-oriented truncated rhombs were present (Fig. 3.36).

(vi) THE EARLY CRYSTAL GROWTH STUDY OF THE CALCITE PLATES:

The calcite crystals grown under acid monolayers were analysed for their structure and morphology in their early growth stage. The XRD data of the early crystals (Table 3.7) had shown that the crystals were mainly calcite. The early crystals were too small to identify them under optical microscope. The SEM micrographs of the crystals collected between 20 to 40 minutes showed (Fig. 3.37) that the crystals were thin calcite plates with a rhombohedral extension which were similar in orientation and morphology of the mature crystals. This indicates that the crystals nucleated were stable at 20 minutes and continue to grow without any changes in the growth processes.

Table 3.7: XRD data of the early crystals at higher concentration of calcium (9.0 mM). [Grown under acid monolayer].
(d-spacing in Å)

d-spacing	Calcite	Vaterite
3.853	3.852	4.245
3.592		3.577
3.296		3.296
3.039	3.030	
2.746	2.834	2.735
2.497	2.495	
2.277	2.284	2.219
2.093	2.094	2.212
1.918	1.907	2.065
1.877	1.872	1.857

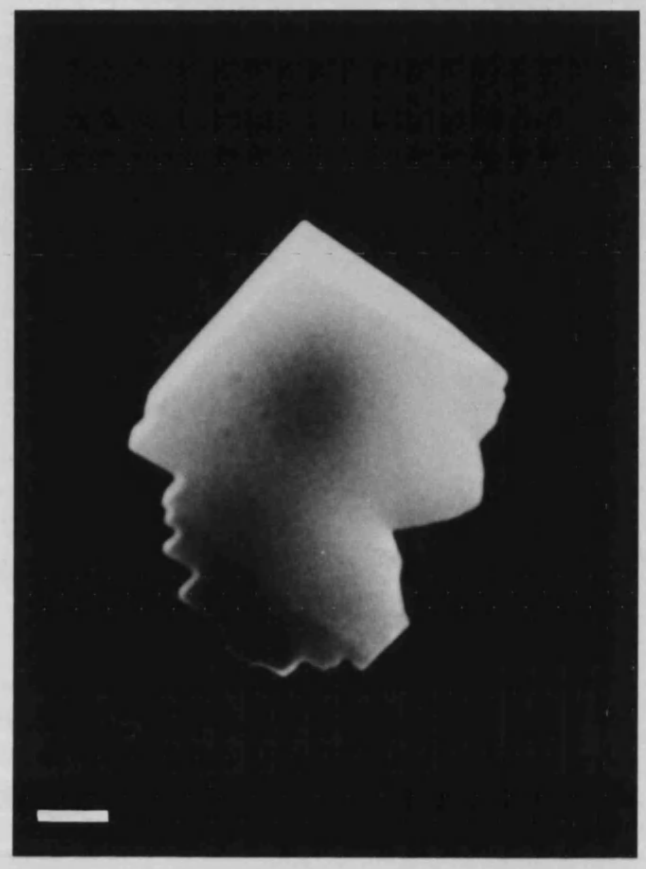

FIG. 3.37: SEM OF AN EARLY CALCITE PLATE COLLECTED AT t = 20 MINUTES (Scale bar = 1 μm)

Crystals grown at the bottom of the dishes were similar to control bottom crystals. They were small, smooth, discrete rhombohedral crystals and were adhered to the bottom surface of the containers.

3.4 DISCUSSION:

The results shown above indicate the formation of stable stearate films and elucidated the controlled crystallization of calcium carbonate under the monolayer. At low [Ca] of 4.5 mM, vaterite is formed and is specifically oriented on the (00.1) face parallel to the monolayer surface. At higher [Ca] of 9 mM, Ca^{2+} binding to the COO^-group is effected and at this juncture the oriented calcite nucleation occurs. Hence, it is vital to analyse the results and identify the reasons for the formation of vaterite and its specific orientation with respect to monolayer at low supersaturation and the formation of highly oriented calcite crystals at higher supersaturation under the monolayer. Some possible factors that could be responsible for the specific crystal formation and its orientation are discussed below.

3.4.1 ION BINDING:

Changing the composition of the subphase solution with $CdCl_2$, $CaCl_2$ and $Ca(HCO_3)_2$ solution resulted in some condensing effect on the isotherm. The condensed nature of the monolayer in the liquid phase might be due to the incorporation of divalent cations, and the cross-linking actions of Cd^{2+} and Ca^{2+} ions, which require two stearate ions for electroneutrality. Incorporation of these ions into the structure also accounts for a small change in surface area/molecule. At pH 6.4 formation of a homogeneous mixture of stearic acid and a high proportion of calcium stearate have also been reported [135]. Slightly more condensed film formation under $Ca(HCO_3)_2$ solution subphase observed in comparison with

$CaCl_2$ solution was due to the higher [Ca] in the bicarbonate solution. The possible effect by HCO_3^- ions in the solution could also be responsible for higher condensation.

It is known from previous studies that the uptake of calcium by stearic acid films and calcium induced binding to form a calcium Stern layer depends on the amount of calcium, the nature of other cations present (competitive adsorption) and on the nature of the anions present in the subphase [186]. Hence, the difference in the increased condensation in the liquid phase and increased area/molecule in solid phase on calcium bicarbonate solution can be explained by a) higher [Ca] levels and b) an effect due to HCO_3^-/CO_3^{2-} interactions at the monolayer headgroups. Slight expansion of the isotherm at marginally higher experimental temperature indicates a small thermal mobility of the molecules on the surface. Similarly increased amount of CO_2 in the solution causes small increase in the surface area (data not shown) which might be due to the increased permeability of CO_2 hindering the highest possible close packed monolayer formation [138].

3.4.2 **PHYSICO-CHEMICAL FACTORS AFFECTING THE CRYSTAL FORMATION IN THE ABSENCE OF MONOLAYER:** The question of conditions governing the polymorphic forms of calcium carbonate in natural environments has prompted numerous studies on the effect of various factors on calcium carbonate precipitation in aqueous solutions. These studies have a rather lengthy history, dating well back into the last century. The precipitation of calcium carbonate in aqueous solutions is a problem attracting the

attention of many investigators in a variety of fields. Its importance stems from the fact that $CaCO_3$ is encountered in numerous situations both in industry and in biological environments. A thorough understanding of the mechanism of precipitation of $CaCO_3$, although of paramount importance has not yet been established.

The present control experiments were very sensitive to factors such as supersaturation, temperature, purity of the system, organic/inorganic additives, pH of the solution and the CO_2 flux. Kitano's detailed study on calcium carbonate precipitation shows the influence of these factors on the polymorphic forms of $CaCO_3$. It was reported [187] that the temperature has profound effect on the supersaturation and the rate of nucleation of the solution. Prompted by this observation the temperature of the solution was maintained constant throughout this work at 301 K by using a cold water bath. The main polymorph formed in the control experiment being thermodynamically stable calcite, indicates that the crystal nucleation is thermodynamically controlled. However the formation of a small amount of more soluble vaterite crystals suggests that localized kinetic effects on nucleation are also present. The heterogeneous size distribution of calcite crystals indicates a continuous nucleation event. Changes in supersaturation effected by varying the flow rate of CO_2 and the bubbling time showed that the over-all ionic concentrations and possibly the relative ratio of [Ca] and [HCO_3^-] in solution mainly determined the nucleation rate and hence the polymorph formed. However, the factors that slowed the system down such as reduced temperature greatly favoured the

formation of calcite [188]. The factors that increased the rate of evolution of carbon dioxide from the solution such as high temperature, high flow rate and slow stirring increased the proportion of vaterite. In summary these studies indicate the sensitivity of the system under investigation to a wide range of physical and chemical factors.

The control crystals formed without any specific orientation at the air/water interface. They were aggregated, clustered and highly heterogeneous in population indicating a random growth process. The presence of truncated rhombohedral crystals in some areas on the surface occasionally showed that the normal form in growth habit was occasionally perturbed. As no specific truncated faces were observed, these effects were possibly due to spatial restrictions in growth at the air/water boundary.

The presence of acicular needle-like bunches of aragonite in some experiments may be due to a kinetic effect or possibly arises from the presence of trace amount of magnesium in the solution [189]. The discrete well defined rhombohedral calcite crystals formed at the bottom of the containers indicate a slower precipitation rate probably due to the slower supersaturation generated by diffusion limitations at the glass/water interface.

3.4.3 **CRYSTALS GROWN UNDER STEARATE MONOLAYERS AT 4.5 mM CONCENTRATION:** The XRD data of the polymorph collected from dish experiments at [Ca] = 4.5 mM under fully compressed films indicate the preferred formation of vaterite under stearate monolayer at this supersaturation level. Highly oriented and homogeneously grown crystals

show that the nucleation has occurred as one single event within a small time span. The absence of disk crystals and hat-like outgrowths at t=16 hours, indicate the absence of any secondary/later nucleation event. This also shows that nucleation is catalytic under the monolayer. Stoppage of secondary nucleation might be due to the quick fall in supersaturation levels. It has been well established that higher supersaturation levels give fast nucleation rate. Thus the localized supersaturation level under the monolayer could be higher when compared to subphase solution. The increase in supersaturation at the surface is possible due to the charged surface generating high localized levels of ions by electrostatic interactions. This induced supersaturation on the surface then reduces the surface free energy of nucleation and thus kinetically favours vaterite nucleation. The increased charge accumulation may further give a value < 1 for Ca_{2}^{+}/HCO_{3}^{-} ratio which enhances the formation of kinetic phase vaterite [170] under the monolayer.

Preferential formation and inevitable presence of vaterite at various [Ca] up to 8.4 mM, shows that the system itself prefers to form vaterite nuclei at certain conditions which is not too dependent on [Ca] of the solution alone. Some preliminary experiments with excess of HCO_{3}^{-} ions in solution, have shown the preferred formation of vaterite. Also similar experimental studies suggested that increasing the speed of precipitation by increasing HCO_{3}^{-} ions with condensed CO_{2} may assist in the formation of vaterite although no detailed experiments have been performed on this problem [172]. Lippmann [170] has reported that vaterite may

nucleate and grow at ordinary temperature under suitable conditions containing non-stoichiometric proportions of ions having excess of CO_3^{2-} ions in solution. The open arrangement of carbonate groups in vaterite, whose planes are orientated parallel to c axis can tolerate the electrostatic repulsion due to excess surface carbonate, quite different from the coplanar arrangement in calcite, which is destabilized by mutual repulsion. Furthermore, the vaterite structure appears to be naturally more tolerant to slight disorientations.

In short, a negative charge caused either by sufficiently dissolved CO_3^{2-} or by the formed layer of COO^- ions creating a negatively charged surface for the nuclei seems to be the condition for vaterite formation. Once formed it is further stabilized by the charged layer of carboxylate ions. The specific binding of calcium ions to COO^- does not seem to be a vital factor for the formation of vaterite.

However the orientation of the vaterite crystals with the [00.1] axis perpendicular to the monolayer surface is also influenced strongly by the stearate monolayer. This suggests that along with electrostatic interaction between the stearate surface and the vaterite nuclei, structural and stereochemical relationships may be important at the nuclei-monolayer interface.

3.4.3 **STEREOCHEMICAL CORRELATION:** The formation of (00.1) face - oriented vaterite under stearic acid monolayer could be explained as follows. Once vaterite is nucleated under charged monolayer, stereochemical and structural correlation between the caboxylate head group and the

crystal lattice of the nuclei formed stabilises it in the most preferred orientation. In the case of vaterite, there is no structural matching between the head group spacing of the carboxylate head group and the Ca-Ca distances in the (00.1) face of vaterite (Fig.3.38.A). Head group spacing at the compressed monolayer is ≃ 5 Å which is close to the Ca-Ca distance in (00.1) face of calcite (4.96 Å) but not of vaterite which is 4.13 Å. So the effect of structural matching on the nucleation of vaterite is not possible as the lowest possible limiting head group spacing is higher than the Ca-Ca distances in (00.1) face of vaterite. However, in spite of the mismatch between stearate layer and (00.1) face of vaterite, the vaterite nuclei are oriented and stabilised on the (00.1) face. One possibility is that such preferred orientation may be favoured by a stereochemical relation between carboxylate groups and carbonates in the (00.1) face (Fig.3.38.B). The planar CO_3^{2-} group is perpendicularly orientated to the calcium in (00.1) layer which is similar to the orientation of the carboxylate head group at the monolayer-solution interface. At pH ≃ 6 and [Ca] = 4.5 mM, it is unlikely that strong calcium binding to form calcium stearate monolayer occurs. Furthermore, similar oriented vaterite crystals formed under positive-charged monolayer (see in Chapters IV), show that although the above stereochemical relation may exist, other factors may be important in stabilizing the orientation of (00.1) face. For example the (00.1) face is unicharged; so a net of negatively charged stearate headgroups can preferentially stabilize this face. (A similar argument can account for this effect on octadecylamine monolayer, see chapter IV).

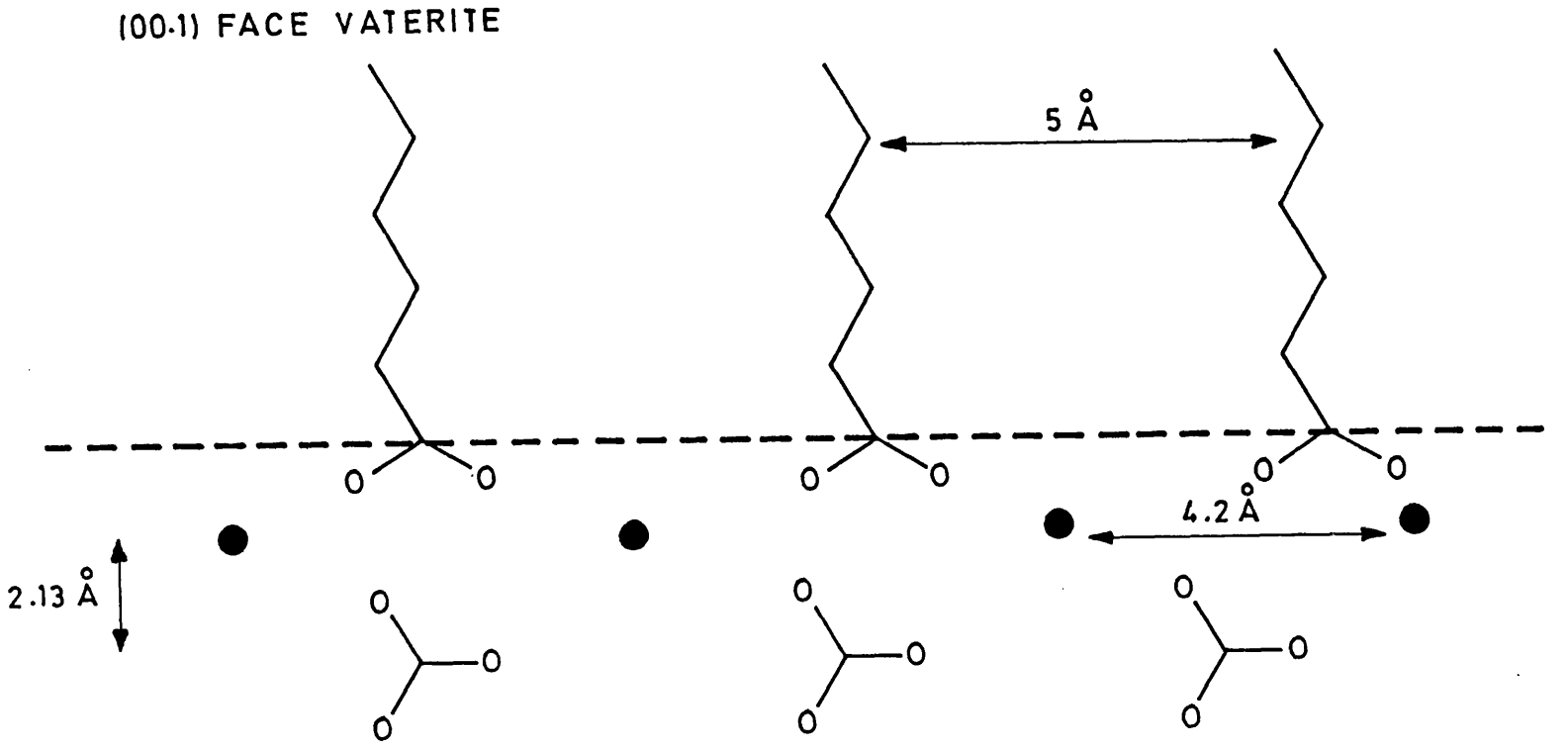

FIG. 3.38: (A) SCHEMATIC DIAGRAM SHOWING THE STEREOCHEMICAL CORRELATION AND THE STRUCTURAL MISMATCH THAT PREVAILED BETWEEN THE CARBOXYL HEADGROUP AND THE (00.1) FACE OF VATERITE.

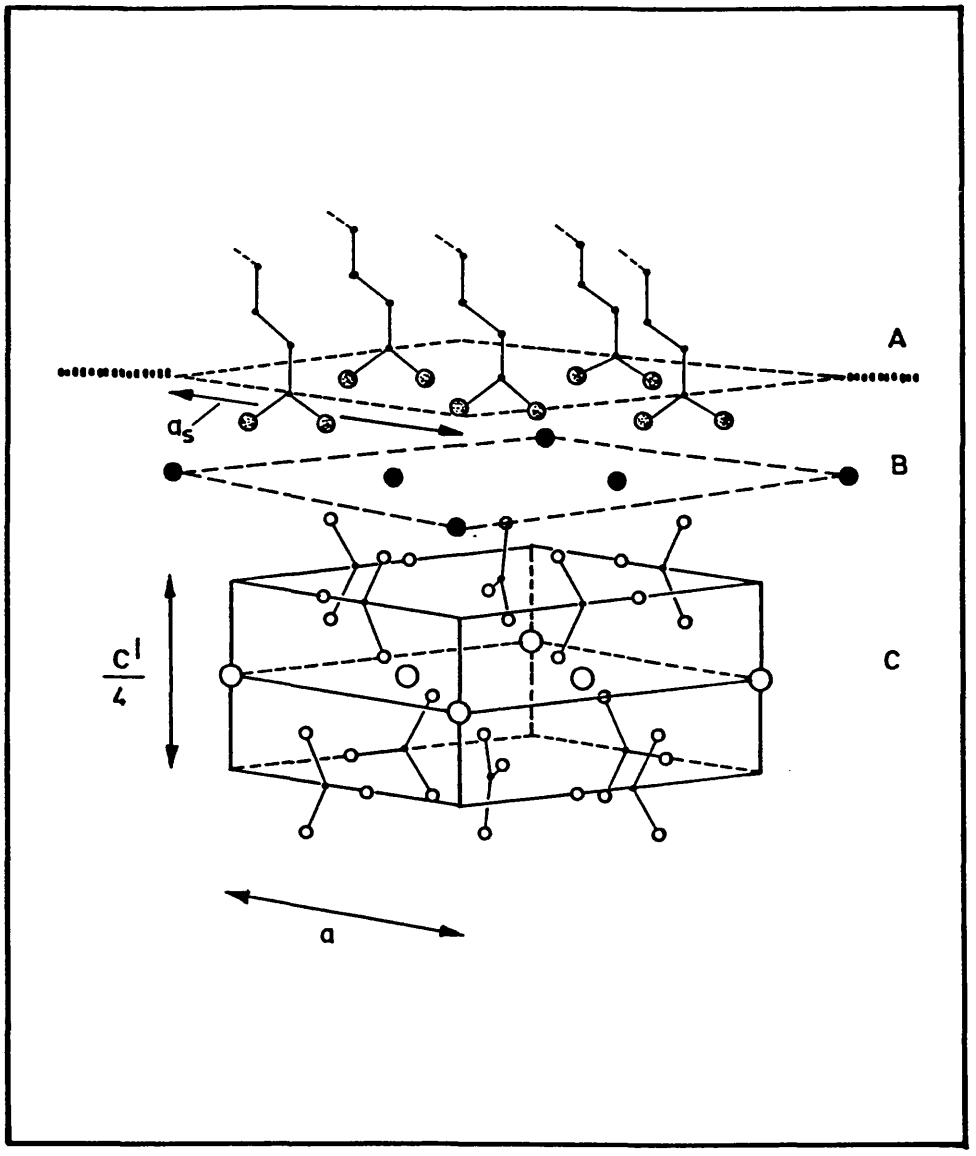

FIG. 3.38: (B) (00.1) FACE OF VATERITE.

(APPOSED TO THE MONOLAYER SURFACE)

3.4.4 EFFECT OF PACKING DENSITY OF THE MONOLAYER:

Changes in the packing density by increasing the surface area/molecule of the monolayer did not change the structure or orientation of the vaterite formed. However the reduction in nucleation density (Table 3.5) shows that the rigidity of the monolayer increases the charge density on the surface and thus accumulated the nuclei formed, in greater number, and this has led to slightly less homogeneously formed early crystals, when compared to highly homogeneous early crystals formed under the liquid phase. The flexibility in the liquid phase monolayer, led to the mobility of the ions with an increase in the encounter time and thus reduced the growth rate and organised the crystal nucleus under the monolayer in a preferred orientation and thus increased the homogenity. However there are no differences in the sizes of final crystals formed at t=21 hours. This implies that films of increased dynamic freedom up to an optimum level, might have aided uniform nucleation after which it continued to grow by diffusion controlled process.

The presence of discrete nucleation sites, oriented growth and homogeneous size distribution indicates a cooperative effect caused by electrostatic and stereochemical interactions under the stearate monolayers. The crystals grow at similar rates and growth is limited by the reduction in supersaturation levels within 21 hours. Although the surface of the crystals are in contact with the monolayer in the early stages of crystal growth the later outgrowths are into solution.

Variable extent of surface roughening on the mature crystals indicates a diffusion controlled growth into the solution. Although the initial crystals are single domain disks, the dendritic outgrowths are misaligned indicating a polycrystalline nature for the matured florets.

The formation of crystals under uncompressed films was slow, and a mixture of vaterite, orientated and non-orientated calcite was identified. The formation of some oriented vaterite crystals under uncompressed films suggests that there is localised organisation of the stearic acid molecules even at low surface pressure. Furthermore, this effect may be enhanced by calcium binding. Similar observations have been reported in the crystallization studies of glycine under chirally resolved palmitoyl lysine monolayers, and had been shown that both compressed and uncompressed films form oriented nucleation [95]. Surface diffraction studies of the monolayer surfaces [184,185] showed that the film contains polycrystalline surface of microdomain size and suggested that some degree of localized domain formation also occurs in the gaseous phase. Probably because of this reason in the uncompressed monolayer surfaces, the local islands of ordered monolayer and the non-ordered molecules give oriented and non-oriented crystals respectively.

3.4.5 EFFECT OF SUPERSATURATION CHANGES:

(i) Low supersaturation levels:

At [Ca] = 2.3 mM, main crystals formed were vaterite, but the nucleation densities were highly reduced. Crystals were not identified under optical microscope at t = 21 hours and it was not possible to

observe the crystals clearly at t = 44 hours. At [Ca] = 1.2 mM, very few normal and truncated rhombohedral calcite crystals were formed. Oriented vaterite and calcite crystal were rarely noticed. This implies that the nucleation and growth were reduced at this low supersaturation level which is close to vaterite solubility limit. The influence of the monolayer appears to be minimal at these low levels. This shows that the electrostatic attraction between the monolayer and the crystal nuclei formed is reduced or absent at this very low concentration.

The marginally different proportion of vaterite crystals formed in trough experiments compared to dish crystals can be explained as follows. A non-equilibrium condition of the solution is established and the CO_3^{2-}/Ca^{2+} ratio increases further due to the charged monolayer. This is further enhanced in the trough experiments because the amount of CO_2 lost per unit time is greater due to the surface area coverage of the monolayer.

(ii) High supersaturation levels:

At supersaturation levels of [Ca] = 9 mM the change from vaterite florets to calcite plates is dramatic. At first this seems to contradict Ostwald's law of stages [190]. Ostwald's law states that the least stable polymorph having the highest solubility value is formed preferentially under kinetic conditions of precipitation. Hence, when supersaturation was increased vaterite should be formed rather than calcite.

A schematic diagram based on simplified version of the nucleation equation

$J_N = Ae^{(-\Delta G/kT)}$, is given in Figure 3.39, where,

(J_N = Rate of nucleation

ΔG^* = The energy of activation required for a phase formation/transformation,

'A' is Pre-exponential factor, 'T' the temperature and 'k' the constant introduced.)

Fig. 3.39 represents the obedience of Ostwald's law. This predicts that at [Ca] = 4.5 mM only calcite should be formed as indicated by A in Figure 3.39. At 9 mM concentration kinetically favoured vaterite represented by C in the figure should be precipitated. At intermediate supersaturations represented by B it should give a mixture of calcite and vaterite. However this law does not necessarily apply at all supersaturation levels in the same system or between different systems. A modified behaviour shown in Figure 3.40 is more appropriate to explain the present system. The difference in the figures relates to changes in pre-exponential factor 'A' and ΔG^*. Similar observations have been recently reported by Cardew and Davey for sodium thiosulphate dihydrate system [191].

At supersaturation levels of [Ca] < 4.5 mM, a mixture of calcite and vaterite of variable proportion is formed as represented by A'. At [Ca] = 4.5 mM vaterite is exclusively formed as shown by point B', whereas at 9 mM of [Ca] completely calcite is formed as shown by point D'. At intermediate concentrations as shown by C' both polymorphs are formed.

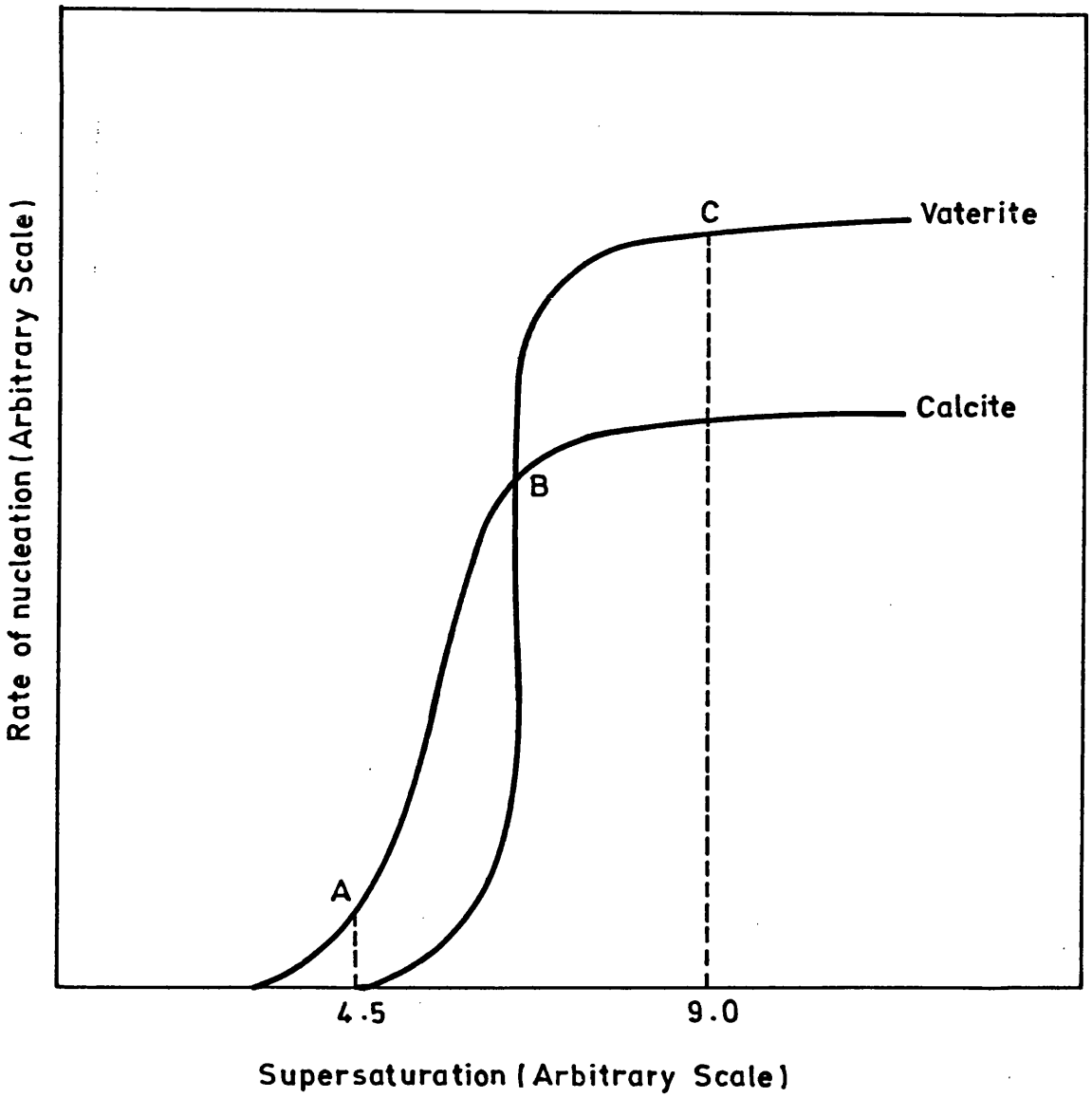

FIG. 3.39: GRAPHICAL REPRESENTATION OF SUPERSATURATION EFFECT ON THE RATE OF NUCLEATION OF DIFFERENT POLYMORPHS, (OBEYS OSTWALD'S LAW).

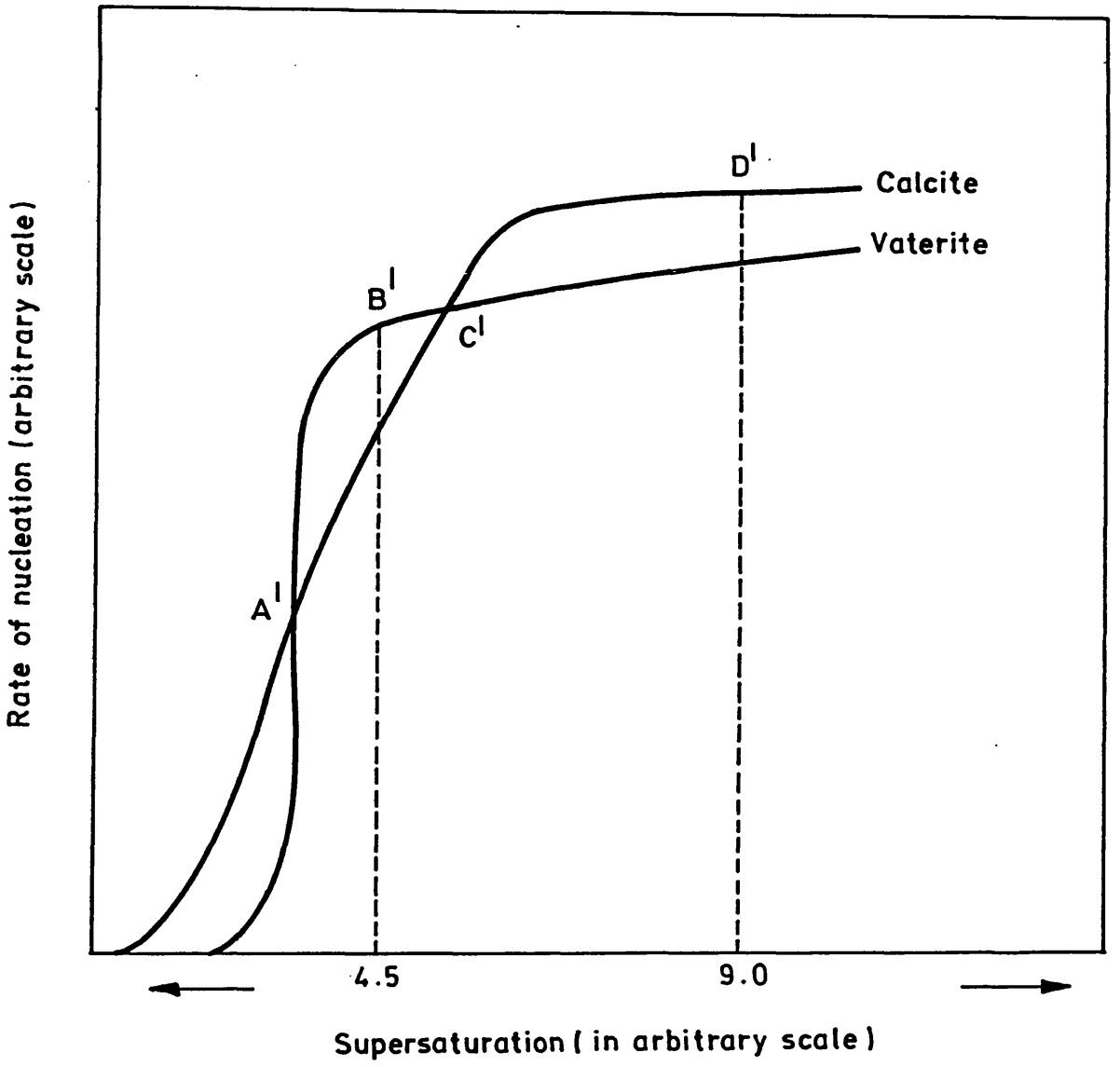

FIG. 3.40: MODIFIED GRAPH SHOWING THE EFFECT OF SUPERSATURATION ON POLYMORPHIC NUCLEATION REPRESENTING THE PRESENT SYSTEM.

The rapid rise in J_N for vaterite around [Ca] = 4.5 mM reflects the effects of electrostatic charge accumulation at the monolayer surface. The increase in nucleation rate of calcite after point C' is due to the lowering of the activation energy of the calcite phase formed. This lowering of activation energy is effected by the charged monolayer via calcium binding and structural and stereochemical correlations as discussed below.

The crystallographic orientation of calcite type I and type II crystals with the rhombohedral (10.4) and prismatic $(1\bar{1}.0)$ faces parallel to the surface of the stearate film, have been determined by morphological analysis.

Type II crystals represent the nucleation orientation of type I crystals, formed by realignment during growth stages. Fig. 3.31.B show type II crystals, where the secondary growth perpendicular to the a axis has been developed at the monolayer. The development of this secondary growth fills in the other side of the crystal, and establishes the two additional (10.4) faces and the plate like morphology (Fig.3.41). The growth development of this side of the type II crystals forms the wedged (10.4) side faces. The formation of elongated straits perpendicular to a axis and the in-built structural irregularities seen in the mature type I crystals are the consequences of the secondary growth in type II crystals. The nature of the elevated features on the upper surfaces of type I and type II crystals were identical and the apex of the elevated faces probably represents the initial point of contact with the monolayer surface.

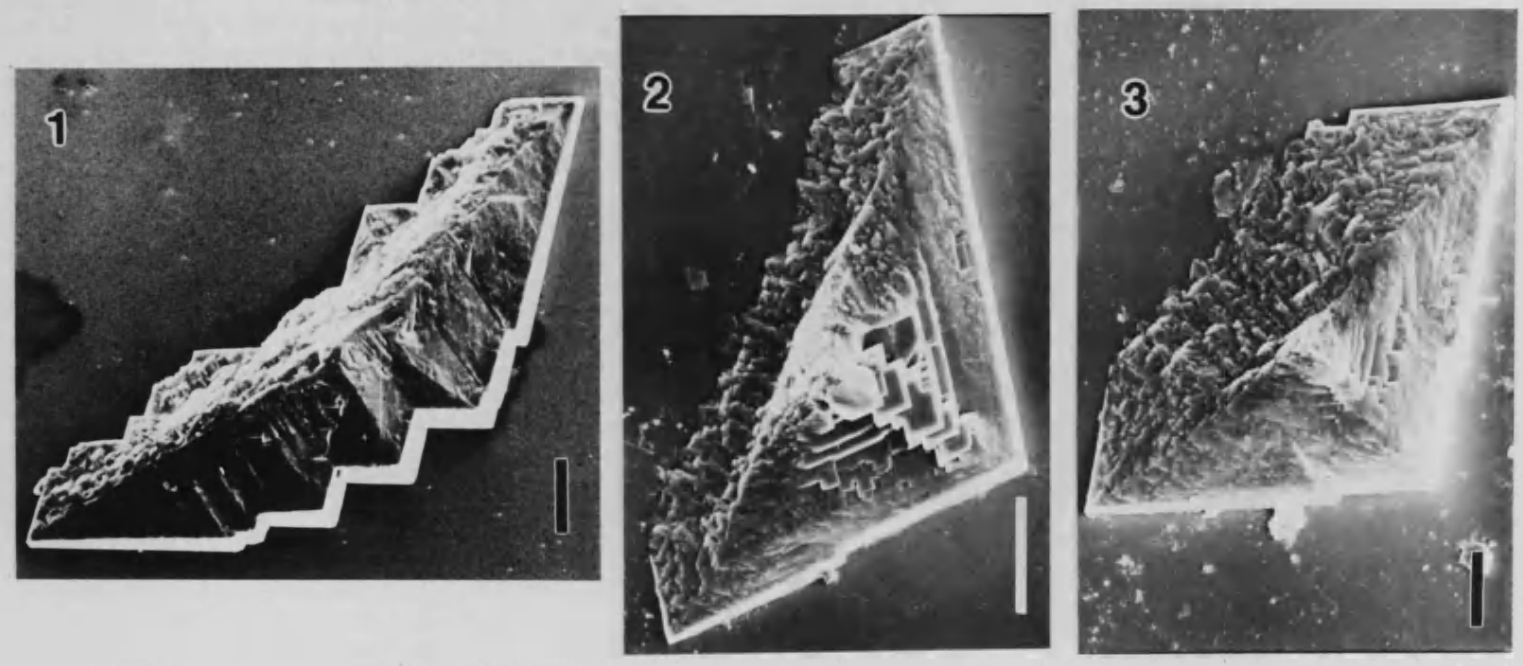

FIG. 3.41: SEMS SHOWING THE STAGES OF DEVELOPMENT FOR TYPE II CALCITE CRYSTALS GROWING INTO TYPE I (Scale bar = 10 μm)

From this, it is clear that both type I and type II crystals nucleated along the same crystallographic direction.

The nucleation of both type I and type II crystals on the $\{1\bar{1}.0\}$ face reflects specific interactions at the stearate head groups. The oriented crystals aligned at $\{1\bar{1}.0\}$ face, then forms smooth $\{10.4\}$ faces aligned at 45° to the monolayer/solution interface. This is clearly seen in the orientation and the surface texture of the central elevated structure of type I and type II crystals. However, the orientation of inclined faces and the ridges in between the faces show that these faces are of negative rhombohedral form $\{01.4\}$ rather than the $\{10.4\}$ faces of positive rhombohedra. Further alignment of these faces to bring them into contact with the monolayer might be due to surface tension/hydrodynamic forces effected on the developed crystal surfaces. Also, there is noticeable difference in the texture between the central elevation and the upper surface of the type I base plates, which agrees well with a realignment of the crystal such that one of the $\{10.4\}$ faces becomes physically in contact with the film surface.

The change from vaterite to calcite nucleation on stearate film at higher [Ca] suggests that the extent of calcium binding is important for oriented calcite nucleation. A well defined Ca-bound layer appears to be required to mimic the first layer of the $(1\bar{1}.0)$ face of calcite, but it is not a prerequisite for the formation of vaterite.

Compressed acid monolayers on supersaturated bicarbonate solutions at the experimental pH and temperature showed changes in the

surface pressure-area isotherms indicating partial calcium binding prior to nucleation. The ion binding may aid nucleation of this face by restricting the arrangement of Ca atoms in two dimensions. If it is assumed that the carboxyl head groups adopt a hexagonal or psuedohexagonal lattice of interhead group spacing ≃ 5 Å, when compressed on aqueous subphases, then there is a close epitaxial match between the Ca-Ca distances and the coplanar atoms in the $(1\bar{1}.0)$ face (4.96 and 8.6 Å in two dimensions) and the periodicity of binding sites ≃ 5Å (Fig 3.42). As previously described, (Fig 3.38) no such match can be identified for the (00.1) face of vaterite apposed to a stearate monolayer.

Geometric matching cannot be fully responsible for $(1\ 1.0)$ oriented calcite nucleation. For example, the (00.1) face of calcite comprises a hexagonal lattice of coplanar Ca atoms of 4.96 Å periodicity and such an arrangement also matches the periodicity of the monolayer binding sites. A significant difference between the $(1\ \bar{1}.0)$ and (00.1) faces is the orientation of the carbonate anions; they lie perpendicular to the $(1\ \bar{1}.0)$ (Figs. 3.42, 3.43) surface but parallel to (00.1) face. Thus the stereochemistry of the carboxylate head groups mimics that of the anions in the $(1\bar{1}.0)$ crystal face but not (00.1) face of calcite. Addadi and Weiner [81] have proposed a similar mode of interaction in the crystal growth of calcium dicarboxylate salts in the presence of acidic macromolecules. Thus, the possibility of geometric and stereochemical matching created within the calcium stearate layer can account for the preferential formation and stabilization of the calcite $(1\bar{1}.0)$ face during nucleation.

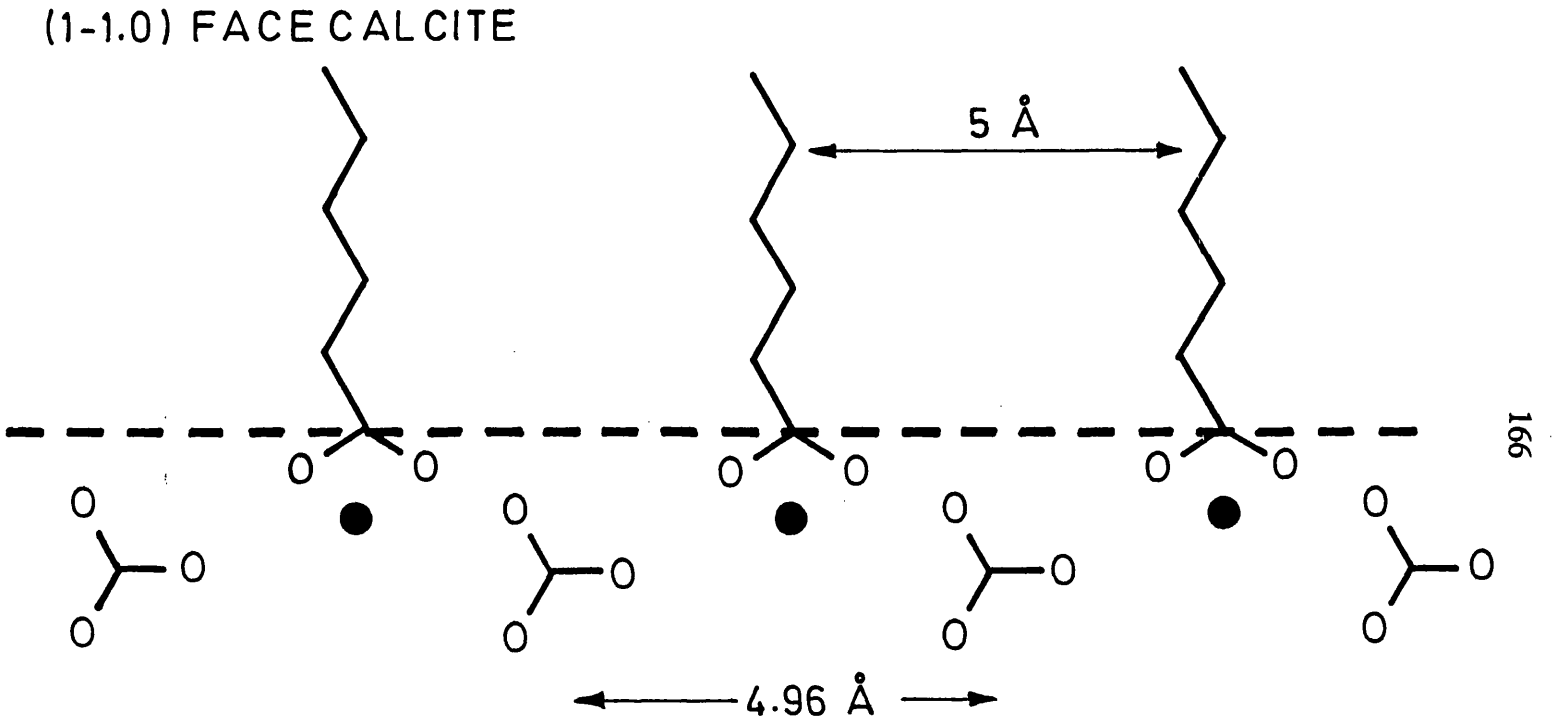

FIG. 3.42: A TWO DIMENSIONAL DIAGRAM SHOWING THE STEREOCHEMICAL CORRESPONDENCE AND STRUCTURAL CORRESPONDENCE THAT EXISTS BETWEEN THE COO^- GROUP AND THE (1-1.0) FACE OF CALCITE.

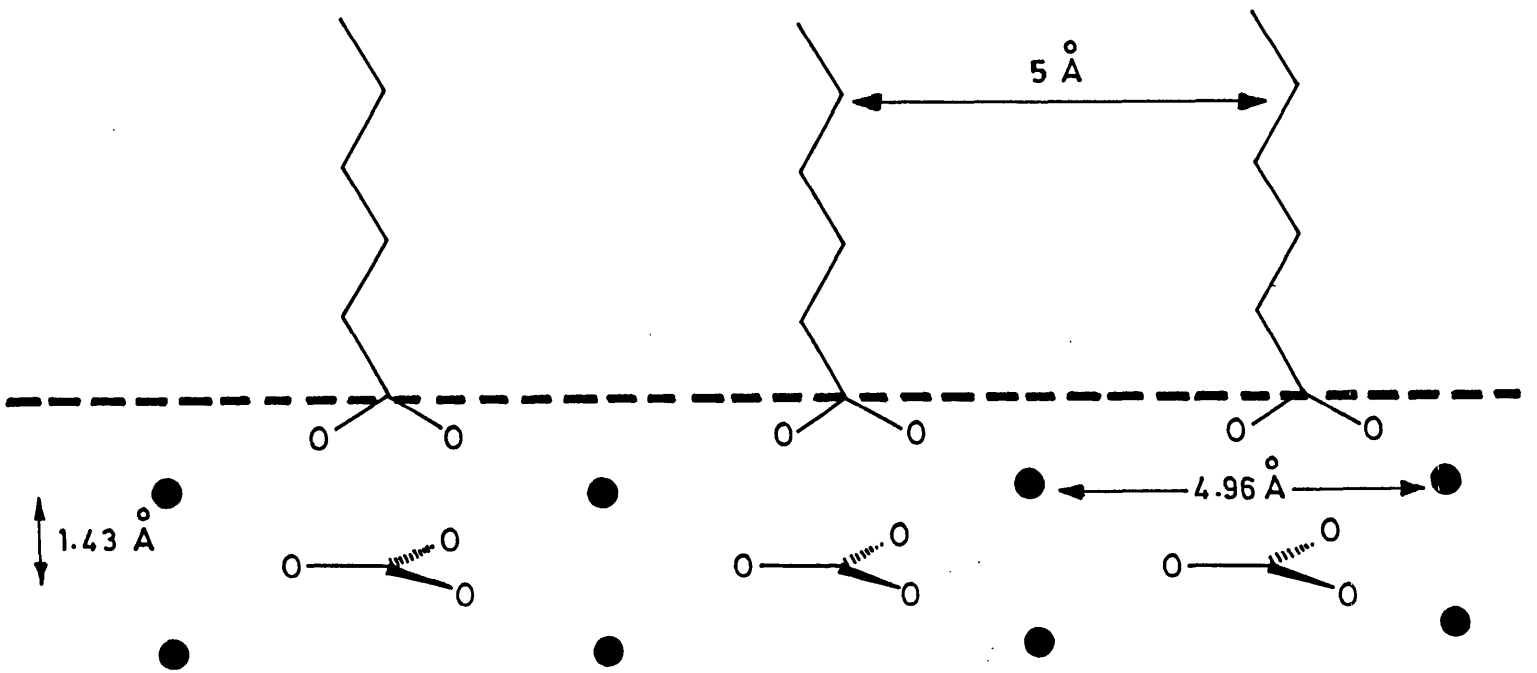

FIG. 3.43: (00.1) FACE OF CALCITE THAT SHOWS NO STEREOCHEMICAL CORRELATION BETWEEN THE CARBOXYLATE GROUP AND THE CARBONATE LAYER IN THE FACE.

Changing the packing density from solid to liquid phase monolayer, did not change the orientation and structure of the calcite crystals formed indicating similar binding effects are present in the liquid phase monolayer. However the nucleation density was reduced with slightly increased proportion of non-oriented calcite crystals. This shows the orientation of the COO^- group is not changed in the liquid phase monolayer and the packing in micro-patches is available for local oriented nucleation.

3.4.6 SUMMARY: The preferred orientation of vaterite and calcite under stearate monolayers may involve the interplay of several factors. In the case of vaterite formed at [Ca] = 4.5 mM, the (00.1) face of the oriented crystals observed is unicharged and could be kinetically favoured by electrostatic accumulation of calcium ions. No structural relationship between the monolayer and crystal is clearly apparent but there is a stereochemical correspondence of carbonates and carboxylates which is observed at [Ca] = 9 mM for the $(1\,\bar{1}.0)$ face of calcite. Hence, the stereochemistry of carboxylates is important in dictating both the (00.1) and $(1\,\bar{1}.0)$ orientations of vaterite and calcite crystals respectively.

Furthermore, the oriented $(1\,\bar{1}.0)$ face of calcite is also favoured by other factors. Calcium binding to the carboxylate creates a charged surface and the geometrical matching of Ca-Ca distances in two dimensions in $(1\,\bar{1}.0)$ face of calcite with carboxylate head groups favour the nucleation of calcite on the $(1\,\bar{1}.0)$ face.

To elucidate these possibilities, studies of calcium carbonate crystallization under positive and neutral monolayers were undertaken and these are reported in chapter IV and V.

CHAPTER IV

CRYSTALLIZATION UNDER AMINE MONOLAYERS

4.1 INTRODUCTION:

The interesting and important observations in the crystallization of calcium carbonate under stearate monolayers have provided some insight into the factors that control nucleation and growth at organised organic surfaces as discussed in the previous chapter. The primary factor was that the carboxylate group is involved in dictating controlled crystallization in terms of structure, morphology and orientation, through various physico-chemical and stereochemical interactions. The above mentioned control is also present in the biological processes, through various mechanisms involving acidic organic molecules. Hence, the understanding of specific processes in these model systems might lead to some clarification of controlled biomineralization. Thus, it would be appropriate to study the effect of changing the carboxylate group in the monomolecular film without altering the hydrophobic alkyl chain, to a positively charged amino group. In addition, any differences noted in crystal formation may to some extent pinpoint the specific effect of the carboxylate groups in crystal formation. Furthermore, introducing the amino group into the system as monolayers is relevant as it is a commonly encountered group in many organic matrices along with acidic residues associated with biomineralization.

Monomolecular films of octadecylamine $CH_3(CH_2)_{17}NH_2$ have been studied and some aspects of these monolayers have been reported

[193, 194]. It is interesting as they are bases and therefore give cations in the presence of acidic subphase solutions. Their behaviour is accordingly to some extent a mirror image of the behaviour of acids. In particular, they are most stable on subphases with high pH value and form easily dissolved expanded monolayers, on highly acidic subphases. As with acids, they can be stabilized by a multiply charged counter ions, for example, sulphate, carbonate and hydrogen phosphate [193]. At room temperature and neutral pH, all amines with chain length longer than 13 carbon atoms give reasonably stable monolayers which are normally condensed. When the temperature is raised, an expanded film formation occurs. For amines surface pressure (π) - area (A) isotherm behaviour changes with pH. At pH <5 the amine monolayer expands [194].

Adam [102] reported a pronounced and bewildering dependence of the properties of ionized amine films on the specific chemical nature of the subphase. In amine monolayers, the condensation of the monolayer is shown in the presence of the anions like SO_4^{2-} [193]. It is obvious that counterion effects on ionized monolayers must involve many factors including the ionization of the films, the structure of the ionic double layer, the possibility of complexing hydrolysis or incomplete dissociation of the counterions in solution

(which may, of course, be altered in the region of the interface), the effect of ions on water microstructure [195] and the possibility of true specific chemical binding.

Attempts to evaluate ionization constants of amine monolayers are incomplete and complicated by the fact that the pH in the bulk solution does not accurately reflect the conditions at the interface. Betts and Pethica [182] estimated the ionization constants of n-nonadecylamine monolayers and obtained pKa values of ca 10.1. Since the value for amines in aqueous solution is ca 10.6, they concluded that in the amine layer, the ionization constants shifted towards neutrality, but only by a small value of 0.5. On acidic substrates (0.01 M H_2SO_4), the amines form RNH_3^+ ions, resulting in electrostatic repulsions between the ionized molecules giving very expanded monomolecular films [124]. However, strong evidence was presented for association in the monolayers of amines and amine oxides at a low pH where the monolayer is largely in the protonated form. This gave less expanded films over much of the area range [82].

Under unionized or partially ionized conditions or in the presence of divalent anions, they form condensed monolayers with a limiting area similar to acid and alcohol monolayers (≃20Å), whereas in the presence of monovalent anions and at pH <3 they form expanded monolayers with an area around 30 $Å^2$.

Crystal growth studies of sodium chloride under amine monolayers have recently been reported [94]. The limiting molecular area in a 6 M NaCl solution, suggests that the chloride ions penetrate between octadecyl ammonium molecules giving expanded monomolecular films comprising alternate positive and negatively charged ionic layer on the surface. This correlates with the similar arrangement in NaCl which has evenly distributed positive and negative charge on the (100) face of sodium chloride grown under the monolayer.

This chapter is aimed at studying the crystallization of $CaCO_3$ under NH_3^+ headgroups in order to assess the influence of charge effects at the monolayer surface. Furthermore, unlike carboxylate headgroups the ammonium headgroups do not have any direct stereochemical correlation with $CaCO_3$ crystals. So, studying this system will aid elucidation of the interplay of geometric, charge and stereochemical factors involved in the controlled crystallization of $CaCO_3$

4.2 EXPERIMENTAL:

4.2.1 PURITY OF THE SUBSTANCE: Octadecylamine exists in the solid form at ordinary temperature and is freely soluble in chloroform. Octadecylamine obtained from Lancaster Synthesis Ltd was recrystallized from $CHCl_3$ and the purity of the material determined by microelemental and IR spectral analysis.

4.2.2 PRESSURE-AREA ISOTHERMS: The surface pressure-area curves of amine monolayers on pure water and bicarbonate solution subphases were recorded using Langmuir mini-trough similar to acid monolayers. (See sections 2.5 and 3.2 for experimental details on monomolecular film preparation.) Preparation of supersaturated bicarbonate solution was as described in section 2.6. The pH and the temperature of pure water and the bicarbonate solution were recorded before running each isotherm. A dilute solution of amine (1 mg cm^{-3}) in chloroform was prepared and 60 µl of the solution was spread to form the film. One main difficulty encountered in these film formations was that even a small interaction/vibration caused the film to be destabilized. Hence, care was taken to run the barrier at speed level less than one and the external vibrational disturbances were reduced as much as possible. The pH of water and bicarbonate solution subphases were 6.5 and 6.1 respectively. The temperataure of the solution was kept at 290 ± 1 K. Maintaining the temperature was crucial for plotting π-A curves for amines, as higher temperature in the range 295 ± 1 K caused much more

expansion in the film. Hysteresis was also checked for amine films on pure water.

4.2.3 CRYSTAL GROWTH EXPERIMENTS UNDER AMINE MONOLAYERS:

Crystallization studies were done under compressed monomolecular films on bicarbonate solution subphases at different compression levels to give fully and partially compressed films. Calcium carbonate crystallization occurred under the monolayer by the slow loss of carbon dioxide from the supersaturated bicarbonate solution having a total [Ca] = 9.0 mM. Immature crystals were collected at t = 45 minutes and mature crystals at t = 21 hours for analyses. Early crystals were studied under scanning electron microscopy for the orientation of the crystals. Mature crystals were studied by optical and scanning electron microscopy. Bulk samples of the mature crystals were collected for quantitative and qualitative XRD analyses, and FT-IR studies. In determining the polymorphic composition of the crystals the measurements were made using a calibration curve based on the intensities of the {10.4} and {118} reflections of calcite and vaterite respectively.

To study the effects of supersaturation, the crystallization experiments were done in thoroughly cleaned glass crystallizing dishes. Bicarbonate solution of total [Ca] = 9.0 mM was prepared and diluted to [Ca] = 4.5, 2.3 and 1.2 mM. Fully compressed amine films were formed on the surfaces of these solutions. This enabled to study the influence of supersaturation and the changes effected in crystals grown under identical experimental environments.

For comparison, the crystals were also grown in the absence of monolayers at these concentrations. Crystals grown after t = 21 hours were collected and analysed for the structure, morphology, orientation, nucleation density and size distribution. The crystals in the glass dish experiments at 9 mM calcium concentration were compared with trough crystals grown at the same concentration.

The influence of packing density and orientation of the amine molecules on crystallization was studied by changing the compression of the films from fully compressed solid phase to partially compressed liquid phase level by spreading films with the surface pressures of around 40 mN m^{-1} and around 15 mN m^{-1} respectively.

The crystals grown under amine monolayer at [Ca] = 9.0 mM were left undisturbed in solution for 15 days prior to analysis. The consequences of any phase transformations were therefore studied.

The nucleation densities were determined as an average of several experimental results (for both glass dish and trough experiments) and the number of crystals counted was more than 2000. Crystals grown under monolayers were selected at random and the sizes were measured from optical and SEM micrographs. The hexagonal cross sections of the vaterite florets grown under the monolayer were measured for more than 250 crystals. For the second morphological form of vaterite (type II), over 150 crystals were measured along the crystal length viewed from above the monolayer. Detailed experimental analysis

of the crystals formed, sample collection, size distribution measurements and the density calculations are given in section 3.2.

4.3 RESULTS:

The purity of the octadecylamine >99% was established by the microelemental analysis. The % compositions of the elements were given.

Calculated for $C_{18}H_{39}N$: C = 80.30; H = 14.50 and O = 5.20.

Experimental value : C = 79.92; H = 14.86 and O = 5.22.

The FI-IR analysis of the amine sample (Fig. 4.1) showed the following characteristic absorption peaks corresponding to amine group. The N-H stretching vibrations of the amine group was observed at 3330 cm^{-1}. The peaks at 816 and 1569 cm^{-1} were due to the presence of the out-of plane bending of the $-NH_2$ group and in-plane bending of N-H stretching respectively. Other peaks corresponding to hydrocarbon chain including methyl and methylene groups were described in section 3.3.

The surface pressure-area curves of amine monolayer on pure water gave an area of 20 $Å^2$ at a surface pressure of 40 mN m^{-1} (Fig. 4.2A). The curve obtained was smooth and contained three regions similar to acid monolayers. The amine monolayers existed in the gas phase up to 40 $Å^2$ and the pressure was less than 1 mN m^{-1}. When the surface area was reduced from 40 $Å^2$, the liquid phase formation started and the surface pressure increased steadily up to a pressure of 20 mN m^{-1}, with an area of 30 $Å^2$/molecule. Above 20 mN m^{-1}, there was a steep rise in surface pressure and the monolayer area remained almost

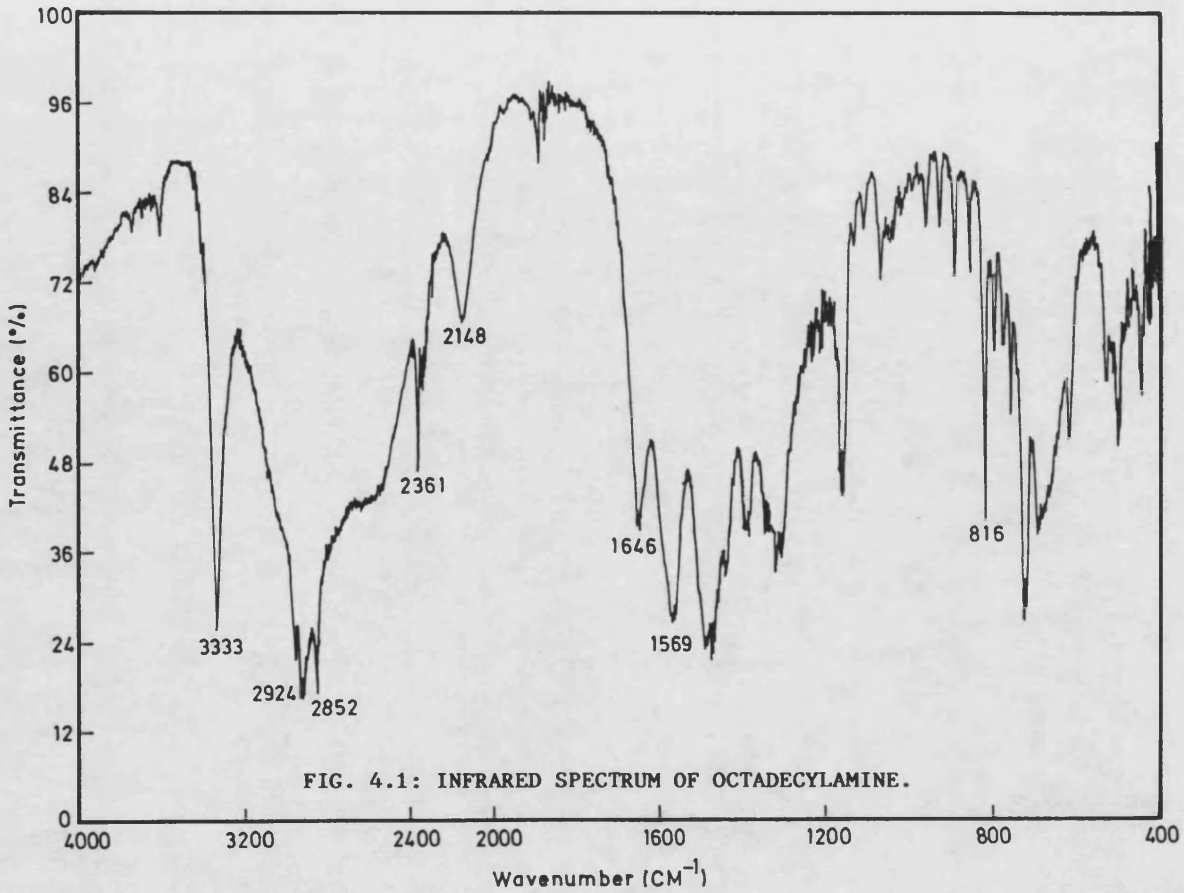

FIG. 4.1: INFRARED SPECTRUM OF OCTADECYLAMINE.

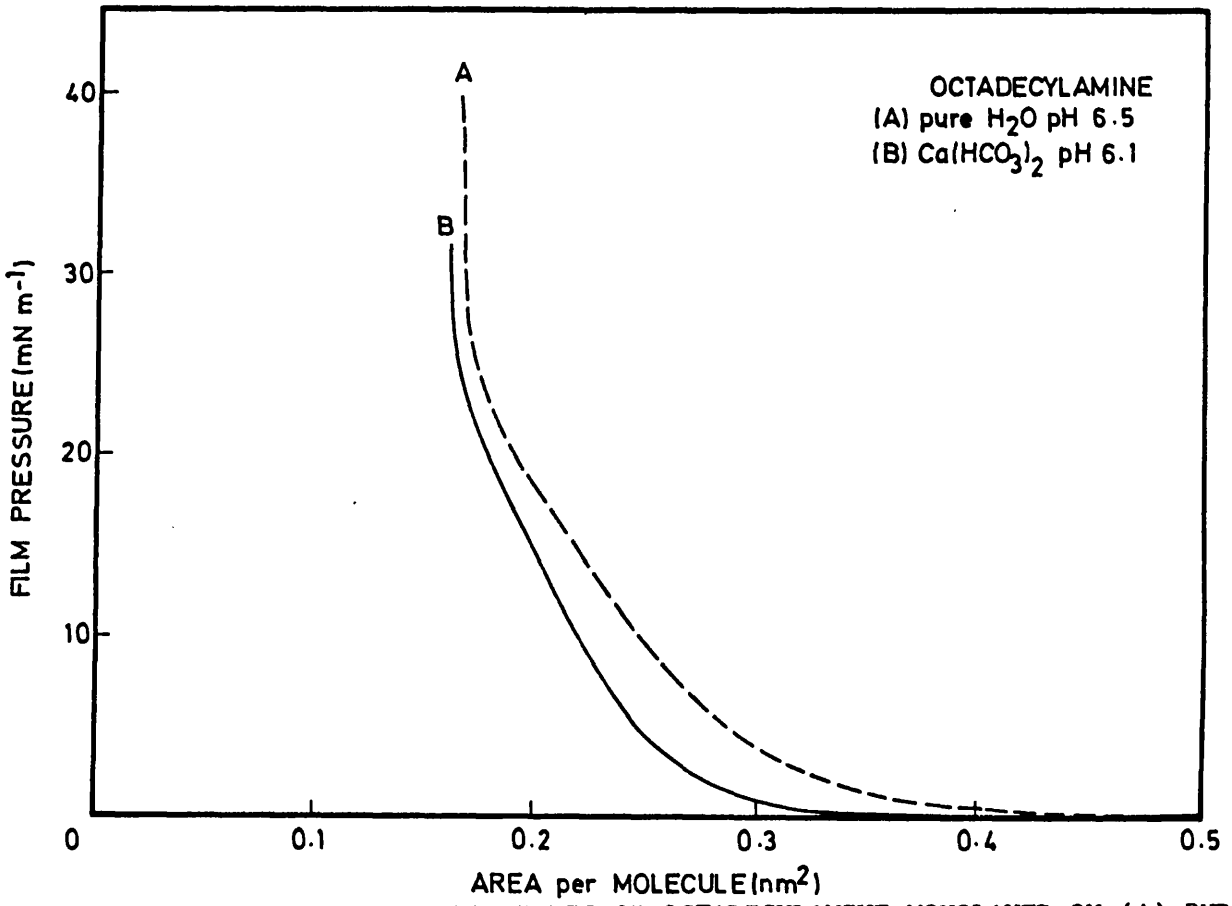

FIG. 4.2: SURFACE PRESSURE-AREA CURVES OF OCTADECYLAMINE MONOLAYER ON (A) PURE WATER AND (B) CALCIUM BICARBONATE SOLUTION SUBPHASE.

constant at this region and gave a limiting value of 20 $Å^2$/molecule. When the pH was lowered or the temperature was increased, an expanded film formation with an increased area was observed. The film formation on $Ca(HCO_3)_2$ solution with a [Ca] = 9mM gave a similar pressure-area plot (Fig. 4.2B). However, a slight condensation was observed in the liquid phase, but the area per molecule remained essentially the same giving a limiting value of 19.6 Å. When the partial pressure of CO_2 in the bicarbonate solution was increased, the film stability and coherence was lost and a continuous isotherm could not be obtained. For example, when CO_2 gas was bubbled through the $CaCO_3$ suspension in water for four hours and 24 hours and the bicarbonate solutions used as subphases, film coherence was lost. Slight hysteresis in amine films was also noticed.

The amine molecules were assumed to have a hexagonal close packed structure, in their highest pressure phase and on that basis, the inter-headgroup spacing was calculated as ca. 5 Å. The pK_a value for amine is 10.6. Hence, it is possible that at the working pH of 6, the majority of amine molecules would be in the ionized form. However, it is difficult to estimate the exact percentage of ionization from the pressure-area curves as it occurs over a range of pH.

Crystals formed under amine monolayer at [Ca] = 9.0 mM were collected on glass slides both from the trough and from crystallizing dishes. They were analysed for polymorphic composition. XRD powder patterns with strong lines showed that the polymorph formed was the metastable phase vaterite (Table 4.1). No lines for calcite or

Table 4.1: XRD data of the mature crystals grown under amine monolayer at high concentration of calcium (9.0 mM)

d-spacing (Å)	Calcite (Å)	Aragonite (Å)	Vaterite (Å)
4.180		4.212	4.245
3.562		3.396	3.577
3.288		3.273	3.296
3.029	3.030		
2.736	2.834	2.700	2.735
2.495	2.495	2.481	2.219
2.313	2.284	2.328	2.122
2.068	2.094	2.106	2.065
	1.907	1.977	1.857
1.857	1.873	1.882	1.825
1.824	1.626	1.814	1.825
1.651	1.604	1.698	1.648

aragonite were present. However, some calcite crystals were observed by optical microscopy. XRD quantitative analysis was done using the calibration curve with known compositions of calcite and vaterite. It showed that 95% by weight of the crystals formed were vaterite, within an experimental error of 5%. The remaining weight % was calcite. (Table 4.2). The calcite crystals as observed under optical microscope were small, non-oriented, smooth and rhombohedral in morphology with a wide size distribution.

FT-IR spectra of the product vaterite (Fig. 4.3) showed four distinct absorption bands at 713 & 749 cm^{-1} due to doubly degenerate planar bending, 850 & 874 cm^{-1} due to out-of-plane bending, 1089 cm^{-1} due to symmetric stretching and 1457 cm^{-1} due to doubly degenerate anti-symmetric stretching. Vaterite has a characteristic absorption band at 1089 cm^{-1} which is totally absent for calcite.

Crystals grown in glass crystallizing dishes were observed *in situ* at various time intervals starting from t = 2 hours to 21 hours. Figure 4.4.A shows the *in situ* crystals grown for 2 hours. Although the images are not of high quality due to surface vibrations, they clearly show two different types of dendritic morphologies resulting from discrete oriented nucleation. Figures 4.4.B and 4.4.C show the crystals collected on glass slides from glass dish and trough respectively. Type I crystals were vaterite florets, exhibiting hexagonal symmetry and were similar to the vaterite florets obtained

Table 4.2: XRD quantitative analysis of polymorphic composition of $CaCO_3$ crystals

Crystals grown	[Ca] mM	% weight	
		Calcite	Vaterite
Control	9.0	68	24
Control	4.5	82	15
Monolayer	9.0	5	95
Monolayer	4.5	10	90

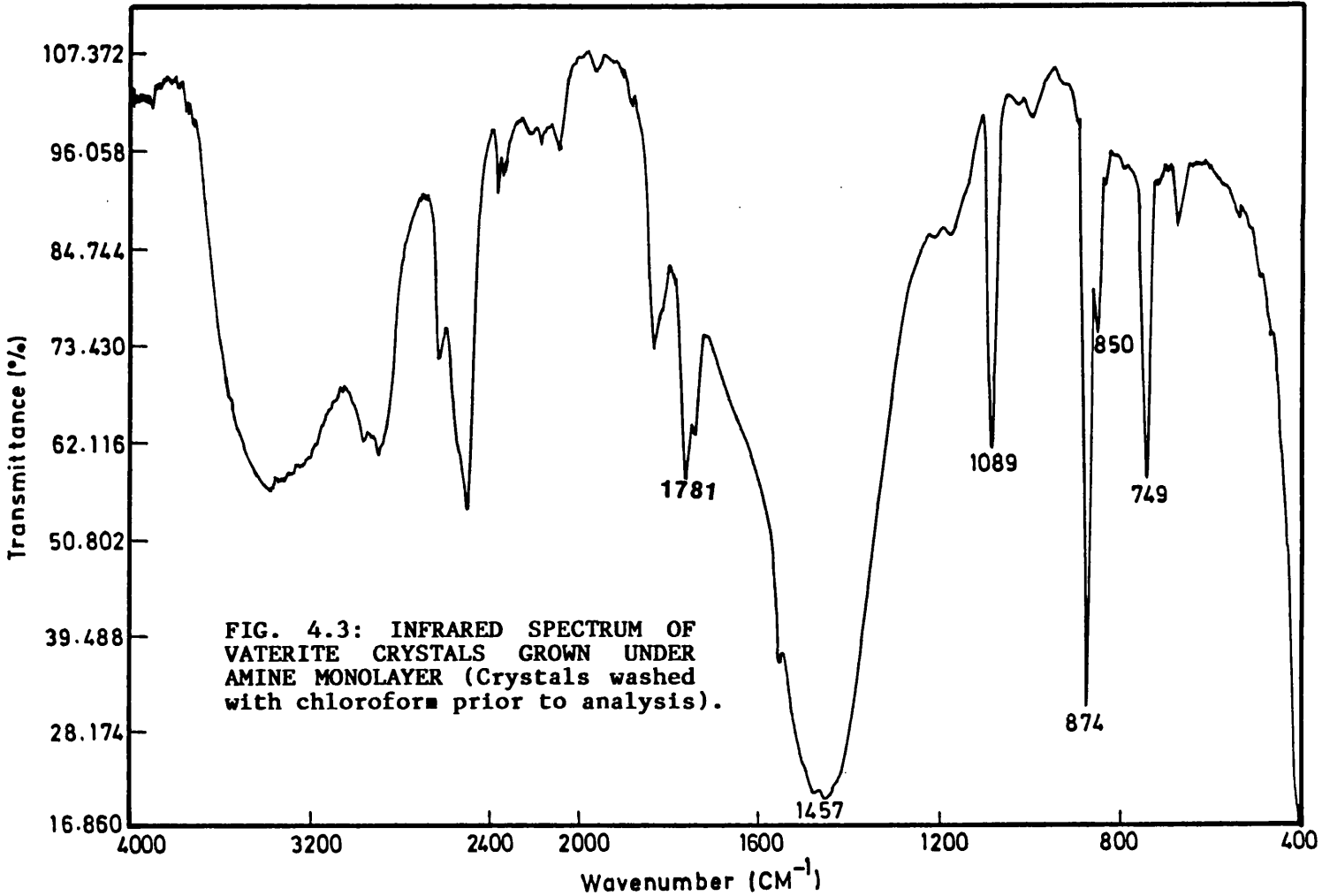

FIG. 4.3: INFRARED SPECTRUM OF VATERITE CRYSTALS GROWN UNDER AMINE MONOLAYER (Crystals washed with chloroform prior to analysis).

FIG. 4.4: (A) *IN SITU* PICTURE SHOWING THE TWO DIFFERENT ORIENTATIONS OF VATERITE CRYSTALS EVIDENT AT THE EARLY STAGES OF GROWTH. (Scale bar = 100 μm)

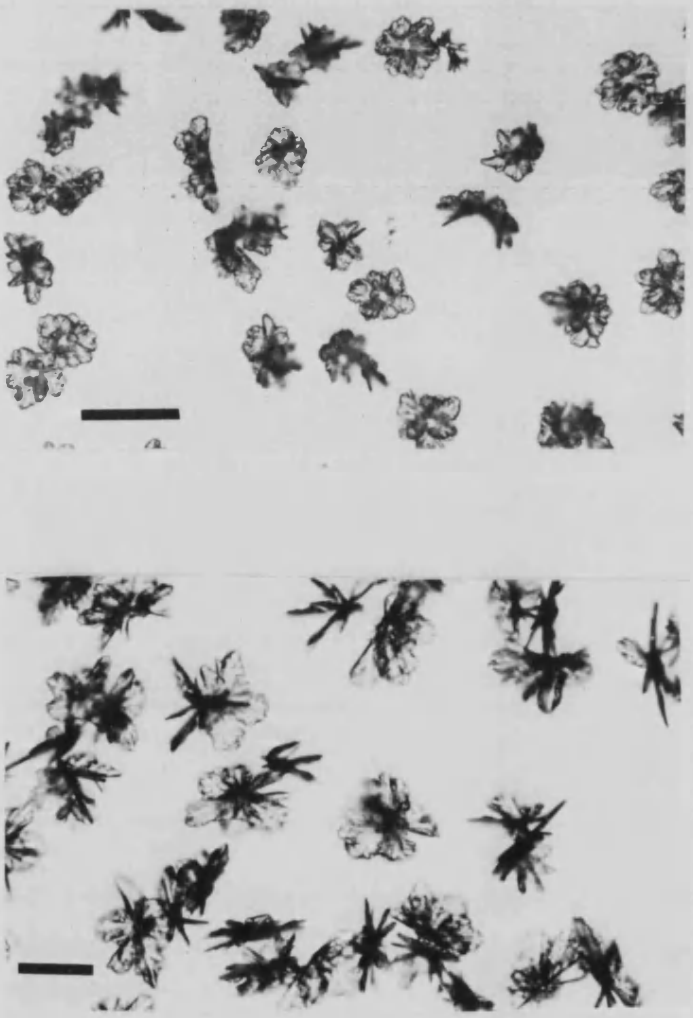

FIG. 4.4: (B,C) OPTICAL MICROGRAPHS OF MATURE VATERITE CRYSTALS COLLECTED AT t = 21 HOURS FORM GLASS DISH (B) AND TROUGH EXPERIMENTS (C). (Scale bars = 100 μm)

under stearate monolayers. Type II crystals were "butterfly-like" crystals and exhibited a two fold vertical axis of symmetry. The proportion of type I and type II crystals were slightly variable but in most of the experiments they were in 3:2 ratio (Table 4.3).

Vaterite crystals when viewed under SEM, showed two different orientations relating to type I and type II vaterite crystals. Type I crystals (Fig. 4.5) were oriented in the similar manner as was observed in crystals under acid monolayers. They had a hexagonal symmetry, when viewed as if from above the monolayer (Fig. 4.6.); they consisted of radial outgrowth resulting in a complex floret shaped morphology. They had an elevated centre in the form of a disk from which the radial outgrowths developed and resulted in the final morphology. The outer crystal extensions were parallel to the monolayer surface; however, the interior of the radial outgrowths were slightly inclined to the monolayer surface into the solution. The radial outgrowth with hexagonal faces aligned parallal to the monolayer (Fig. 4.6b) could be seen clearly and this indicated that the orientation of the crystals was such that the c axis was aligned perpendicular to the monolayer surface. Furthermore it indicated that the a axes of the crystal lie in the plane of the monolayer. The orientation of these crystals was consistent and the crystallographic a and c axes were thus aligned parallel and perpendicular to the monolayer surface respectively.

Table 4.3: Nucleation density of crystals grown under octadecylamine monolayer.

[Ca] mM	Monolayer state	Calcite		Non-oriented calcite	Vaterite		Total
		Type I	Type II		Type I	Type II	
9.0	Solid	---	---	---	2800	1950	4750
9.0	Liquid	---	---	---	1625	1350	2975
4.5	Solid	---	---	---	2875	2000	4875
4.5	Liquid	---	---	275	1375	925	2575
2.3	Solid	---	---	300	700	950	1950
1.2	Solid	---	---	100	175	200	475

Nucleation density = Number of crystals/1 cm^2

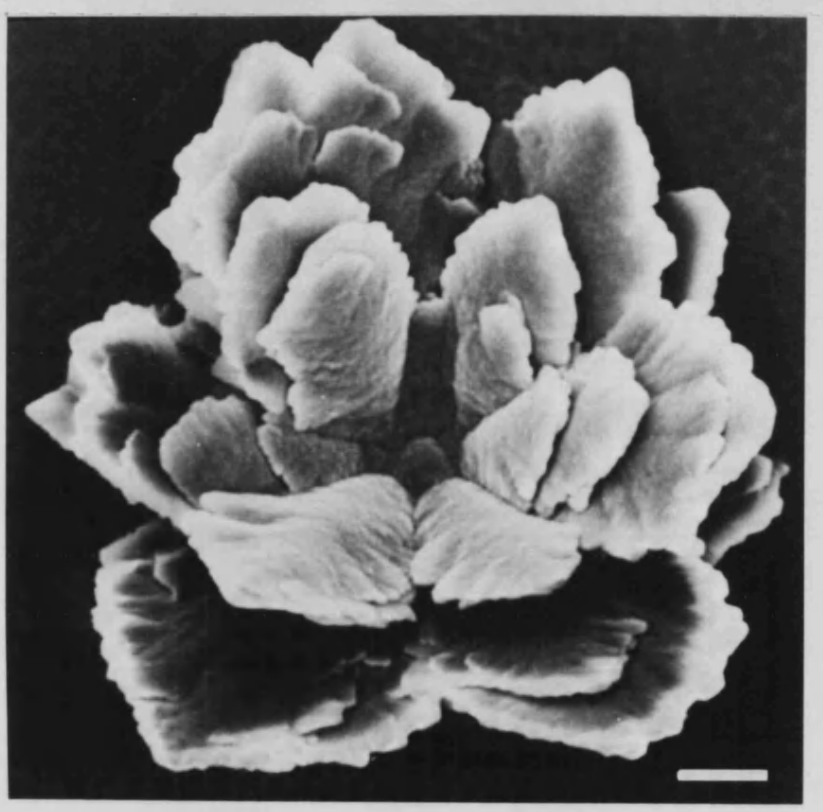

FIG. 4.5: SEM MICROGRAPH OF VATERITE TYPE I CRYSTAL ORIENTED WITH THE (001) FACE APPOSED TO THE MONOLAYER. (Scale bar = 10 μm)

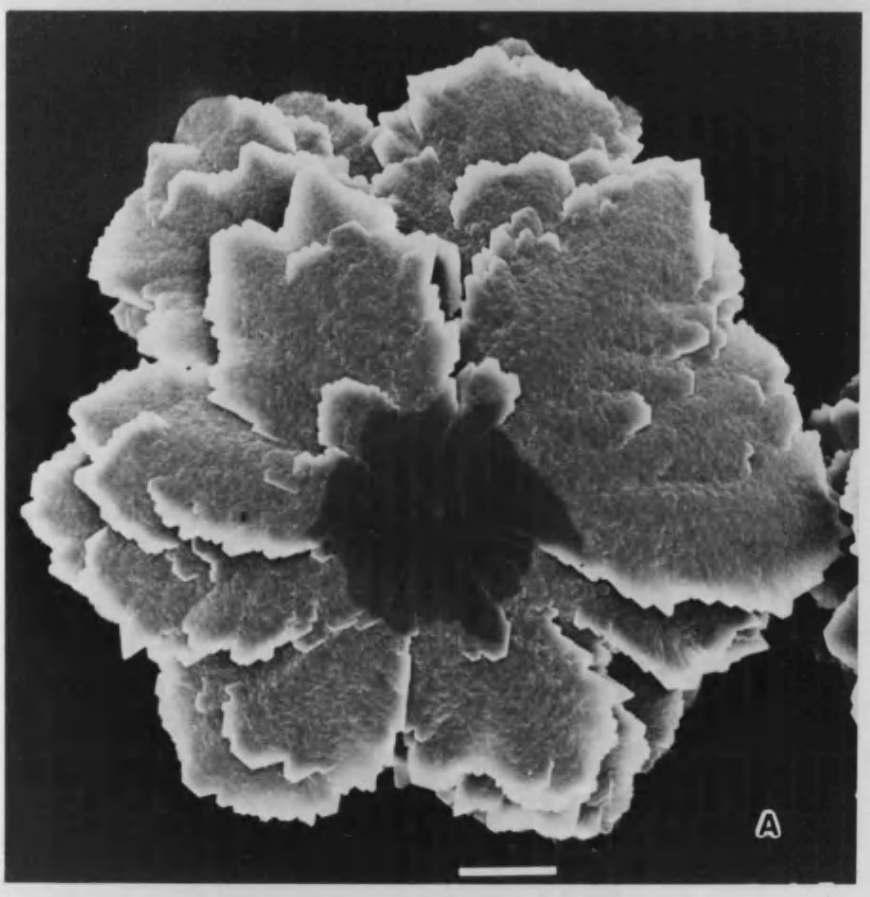

FIG. 4.6: SEM MICROGRAPH OF VENTRAL VIEW OF TYPE I VATERITE FORM SHOWING THE HEXAGONAL SYMMETRY OF THE CRYSTAL. (Scale bar = 10 μm)

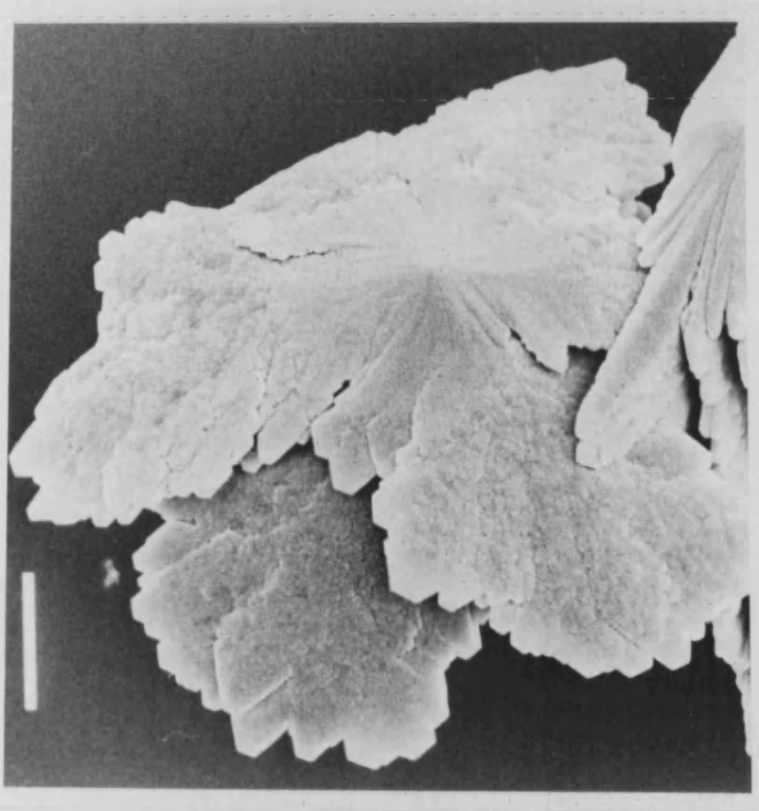

FIG. 4.6.(B) SEM MICROGRAPH SHOWING THE RADIAL OUTGROWTH WITH HEXAGONAL FACES PARALLEL TO THE MONOLAYER SURFACE. (Scale bar = 10 μm)

The crystals were highly homogeneous and had narrow size distribution. Size measurements of type I crystals gave a mean size of 70 μm with a standard deviation of 12 μm (Fig. 4.7).

Type II vaterite crystals when studied by SEM showed a different orientation with respect to monolayer surface. They exhibited psuedo C_{2v} symmetry when viewed from above the monolayer (Fig. 4.8). The central disk like formation was elongated and opened up at the edges and extended along four different directions and were within 25° deviation on both sides of the long axis of the disk, but parallel to the monolayer surface. When viewed from above, this elongated growth along the surface was smooth and no surface roughening was noticed on the disk and on the elongated growth. Further growth of the crystal resulted in hexagonal outgrowths into solution which were aligned nearly perpendicular to the monolayer/solution interface. These hexagonal outgrowths could be viewed from below the monolayer (Fig. 4.9), and the alignment of the outgrowths showed that the crystallographic c axis lies parallel to the monolayer surface and perpendicular to the long axis of the central disk. In addition, the prismatic side faces of the hexagonal plates are of second order prismatic form {11.0} in vaterite and show that they are aligned perpendicular to the a axis of the psuedo hexagonal unit cell. One of these prismatic faces was aligned parallel to the organic surface (Fig. 4.10). So it can be inferred that type II crystals are aligned with the a axis perpendicular to the monolayer/solution interface.

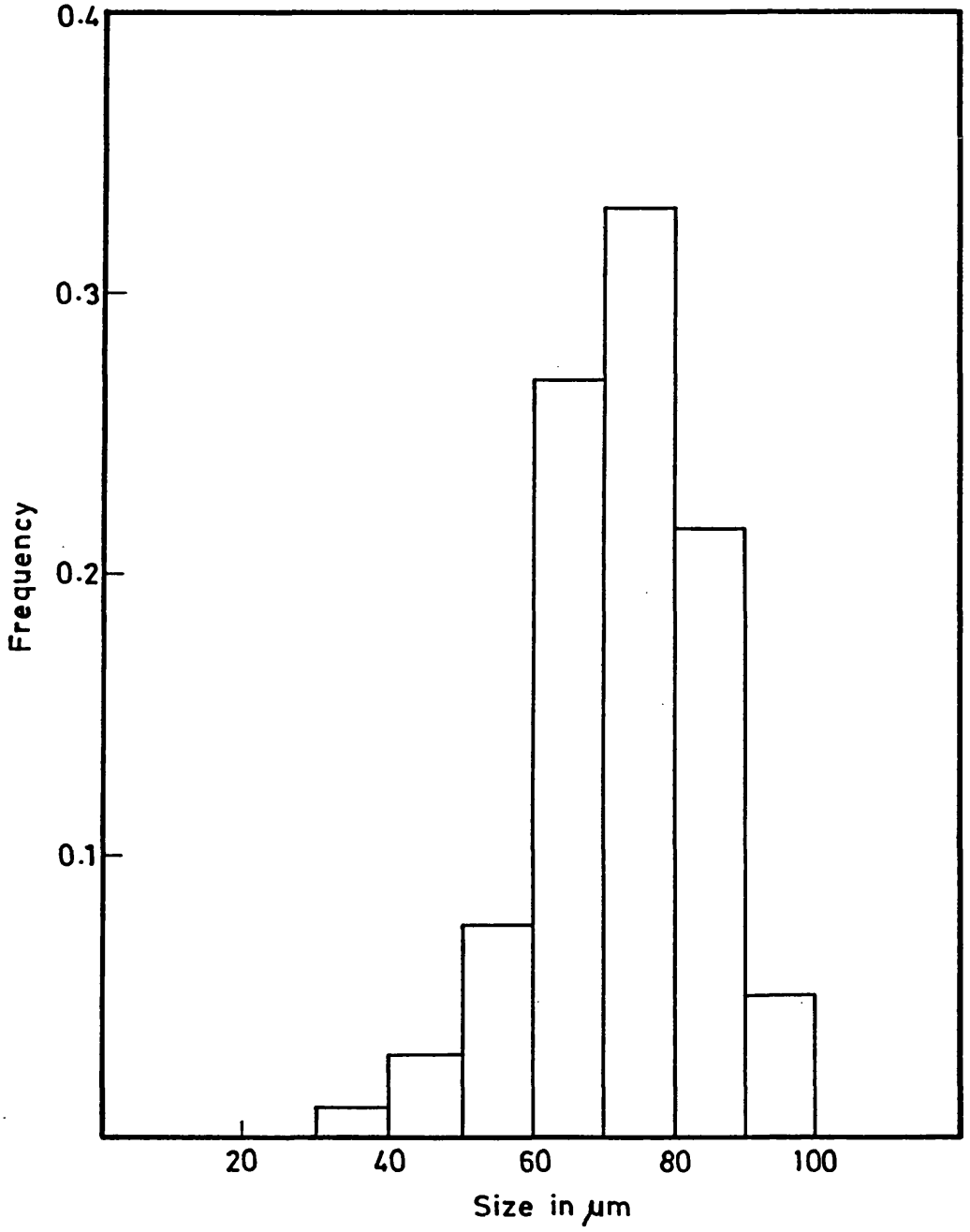

FIG. 4.7: HISTOGRAM SHOWING THE SIZE DISTRIBUTION OF MATURE TYPE I VATERITE CRYSTALS GROWN AT [Ca]=9.0 mM SOLUTION (Hexagonal cross section of the crystals were measured from micrographs).

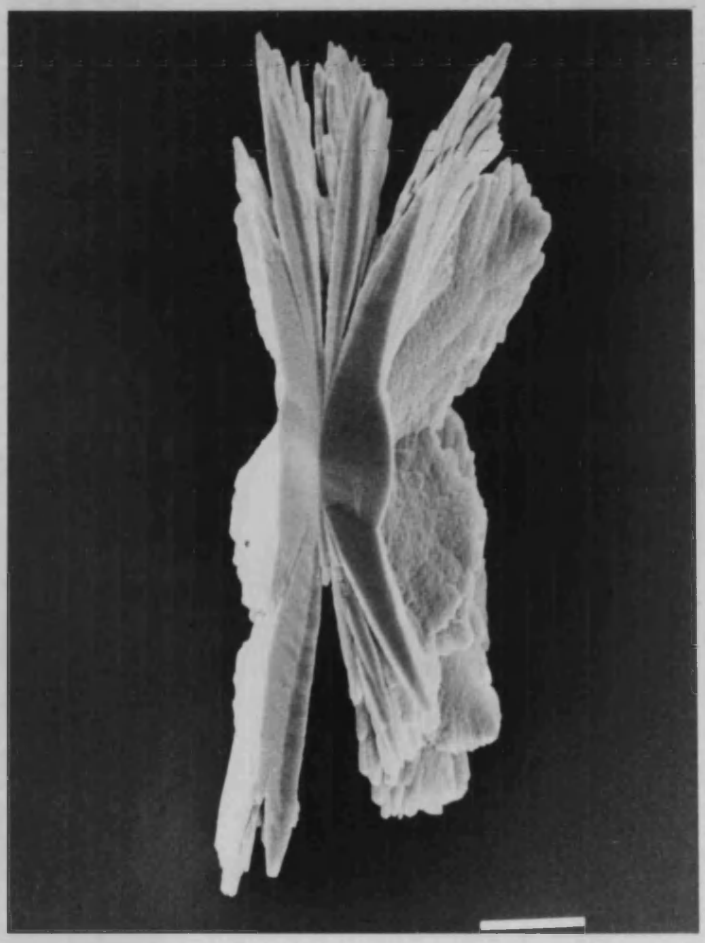

FIG. 4.8: SEM MICROGRAPH OF TYPE II VATERITE CRYSTAL; VIEW FROM ABOVE THE MONOLAYER (Scale bar = 10 μm)

FIG. 4.9: SEM MICROGRAPH SHOWING THE HEXAGONAL OUT-GROWTH WITH [00.1] DIRECTION OF THE CRYSTAL PARALLEL TO THE MONOLAYER. (VIEW FROM BELOW THE MONOLAYER). (Scale bar = 10 μm)

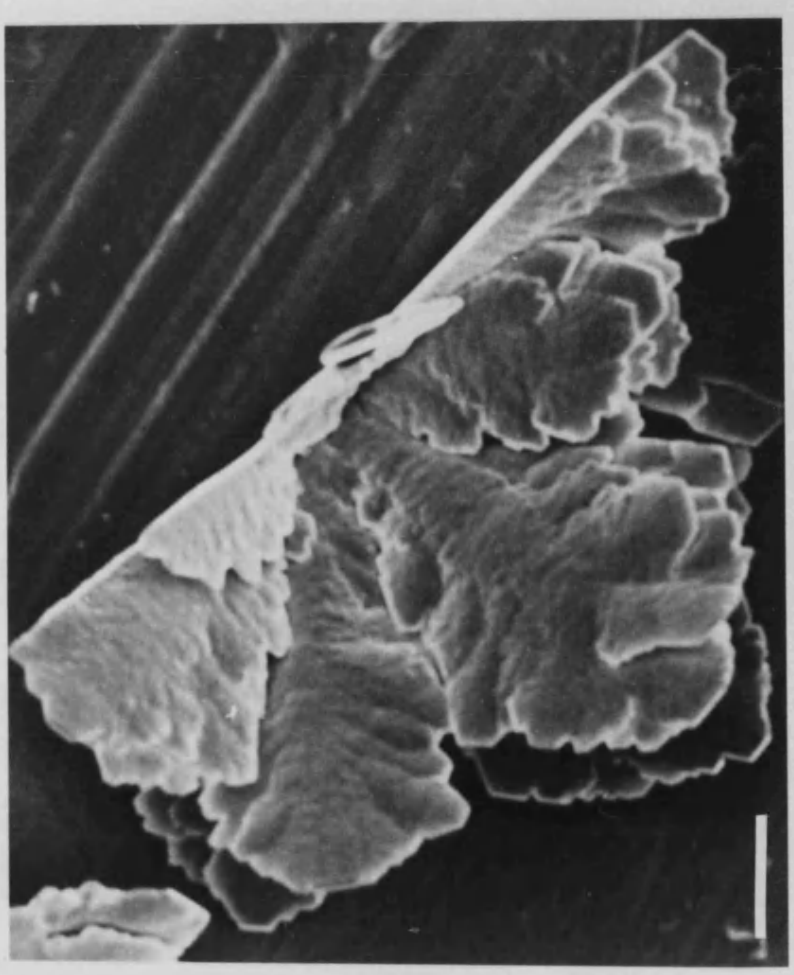

FIG.4.10: SEM MICROGRAPH OF TYPE II CRYSTAL SHOWING SECOND ORDER PRISMATIC (11.0) FACE ALIGNED PARALLEL TO THE MONOLAYER SURFACE. (Scale bar = 10 μm)

Early crystals collected at t = 30 minutes showed type I biconvex disks and type II elongated oval shaped disks (Fig. 4.11). Crystals viewed *in situ* at t = 1 hour exhibited clearly the two different morphological forms and showed the peripheral edge development (Fig 4.12) leading to mature vaterite florets and "butterfly-type" crystals at t = 21 hours. It appears from this that these two forms nucleate in the same orientation as was observed in the mature crystals and maintained their respective orientations throughout the growth process. These observations were further confirmed by parallel work done by Heywood [196] using transmission electron microscopy on the early crystals collected from trough and dish experiments.

Type II crystals showed slightly less homogeneity when compared with type I crystals in size distribution mainly due to the orientational differences of the crystals. Mean size of these crystals were 80 μm with a standard deviation of 14 μm (Fig. 4.13). However the absolute size of the crystals varied depending on the total amount of calcium and carbonate ions available for crystal growth under the monolayer. For example the crystals grown in the trough experiments were larger by 20 μm on an average when compared to dish crystals.

When the film pressures were reduced and the monolayer formation was changed to the liquid phase, no change in the polymorphic formation or in the two morphological form was observed. However, the nucleation density was reduced by around 30% (Table 4.3).

FIG. 4.11: EARLY CRYSTALS COLLECTED FROM SOLID PHASE AMINE MONOLAYER AT t = 30 MIN. (Scale bar = 5 μm)

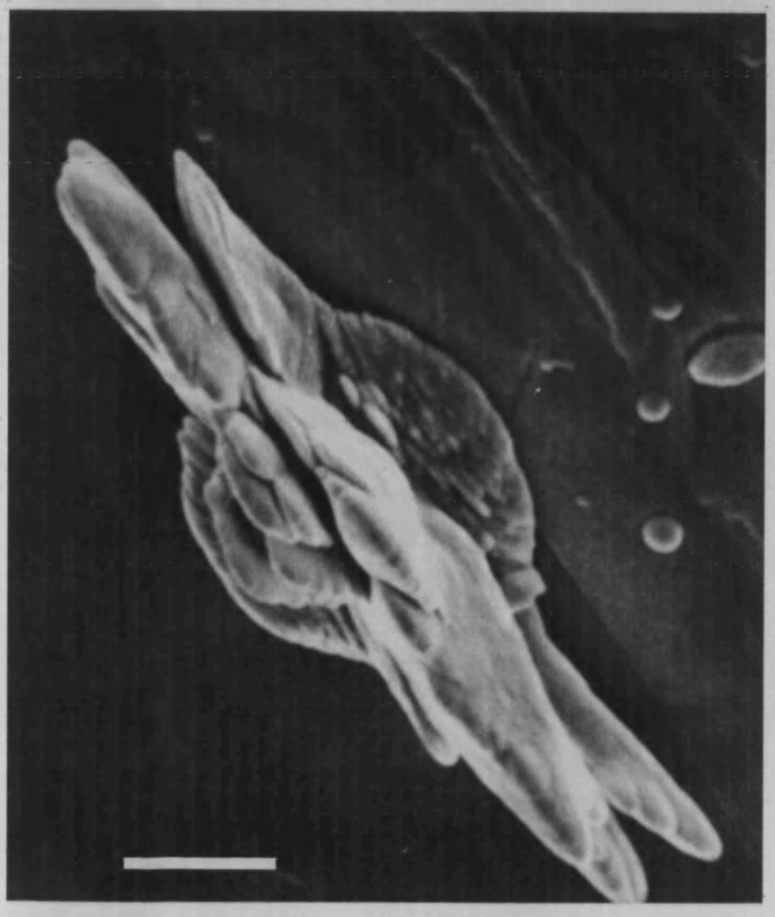

FIG. 4.12: SEM MICROGRAPH OF A SINGLE CRYSTAL COLLECTED AT t = 1 Hour. (Scale bar = 5 μm)

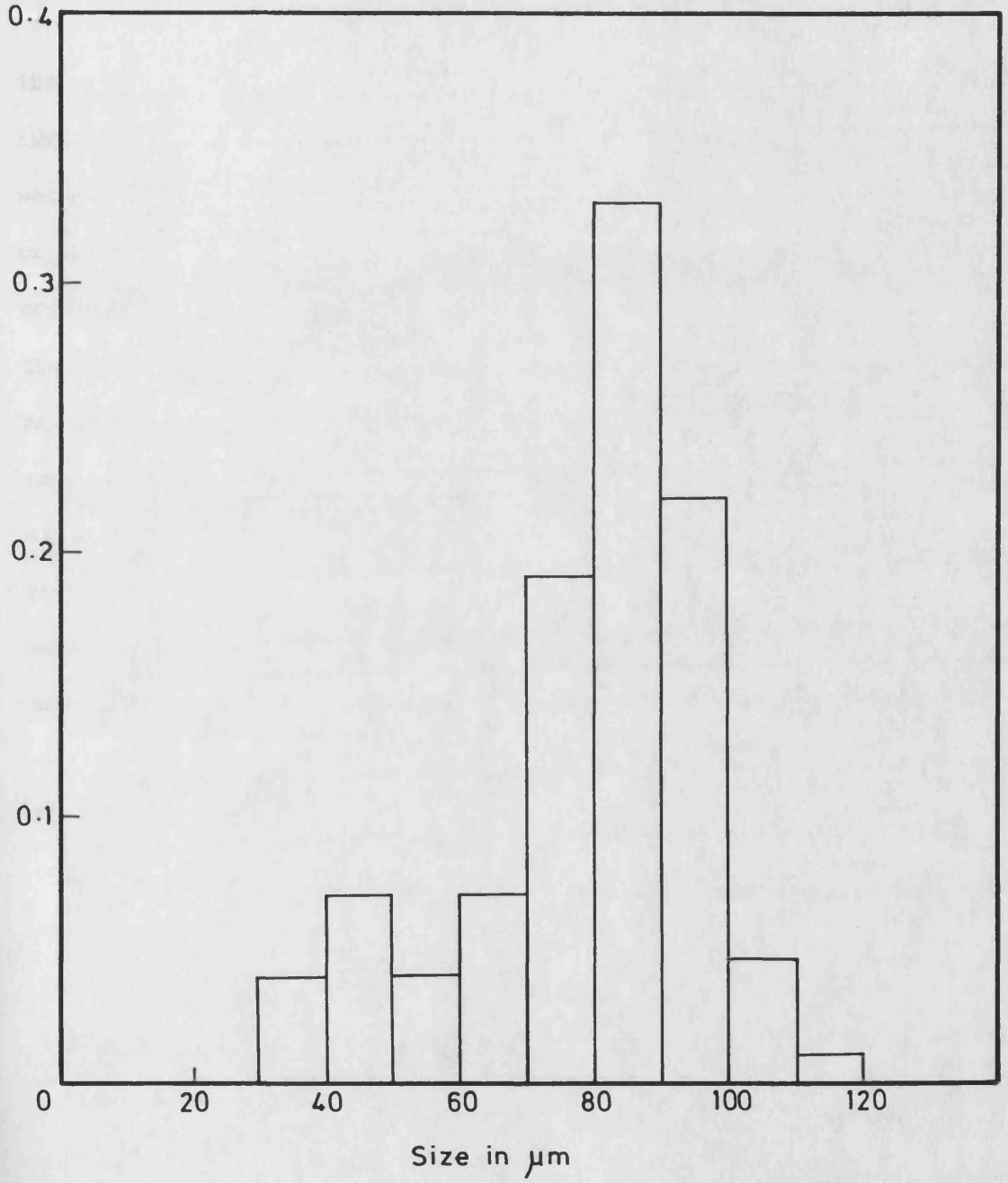

FIG. 4.13: HISTOGRAM SHOWING THE SIZE DISTRIBUTION OF TYPE II VATERITE CRYSTALS GROWN AT [Ca]=9.0 mM.

The changes in supersaturation from [Ca] = 9 mM to 4.5 mM, did not affect the formation of vaterite (Table 4.2, & Fig 4.14) or the two morphological forms. Crystals grown at 4.5 mM calcium concentration were almost exclusively vaterite (Table 4.3) and exhibited the same crystallographic and morphological orientations with respect to the monolayer surface (Fig. 4.15). There was no difference in the nucleation density of the crystals or in the relative numbers of the two morphological forms (Table 4.3). However the size of the crystals was reduced (Figs. 4.16 and 4.17). Type I and type II crystals had mean size 50 and 60 μm respectively. The crystals were less complex and surface roughening was slightly reduced (Fig. 4.18). Increasing or decreasing the partial pressure of CO_2 by changing the flow rate did not have any effect on vaterite formation.

Vaterite nucleation of the two different morphological forms occured even at a concentration as low as 2.3 mM calcium concentration. But the nucleation densities and sizes of the two forms were highly reduced (Table 4.2). However, when the concentration was further reduced to 1.2 mM, vaterite formation was negligible and some non-oriented calcite crystals were formed (Table 4.3), which showed very little surface interaction with the monolayer. The nucleation density and size of crystals were significantly reduced and the crystals could be observed under optical microscope only after t = 44 hours.

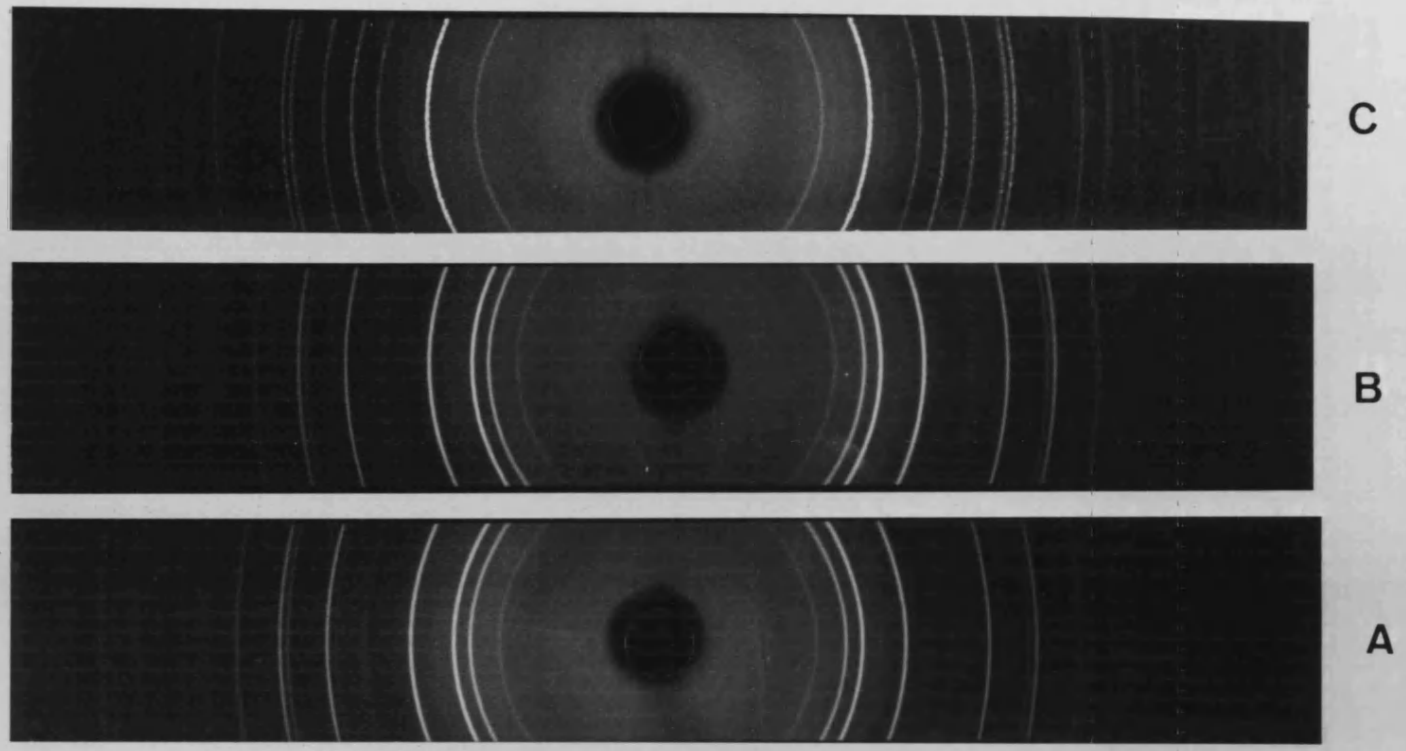

FIG. 4.14: XRD PHOTOGRAPH OF CRYSTALS GROWN AT (A) [Ca] = 4.5 mM COMPARED WITH (B) CRYSTALS GROWN AT = 9 mM, AND (C) CRYSTALS GROWN IN THE ABSENCE OF A MONOLAYER.

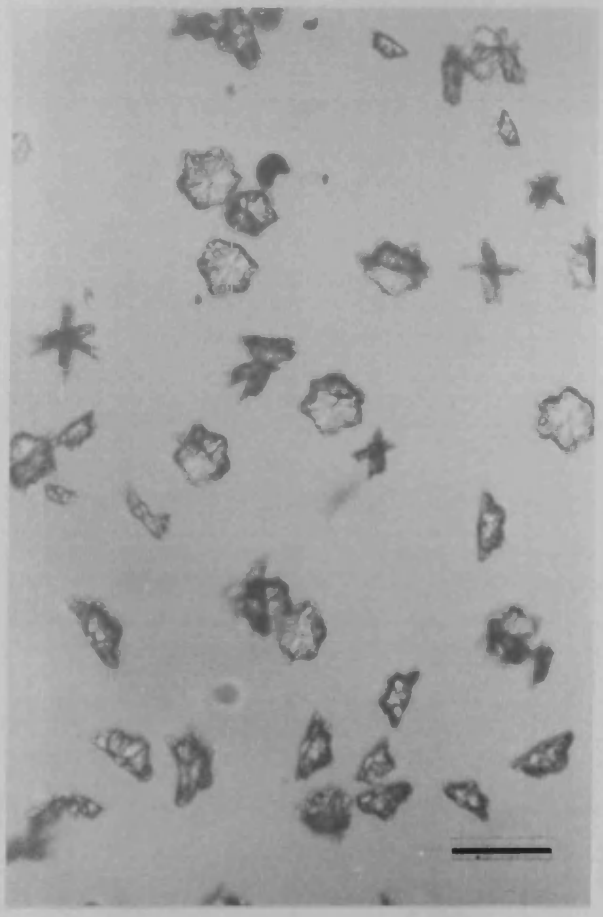

FIG. 4.15: OPTICAL MICROGRAPH OF CRYSTALS GROWN AT [Ca] = 4.5 mM. (Scale bar = 100 μm)

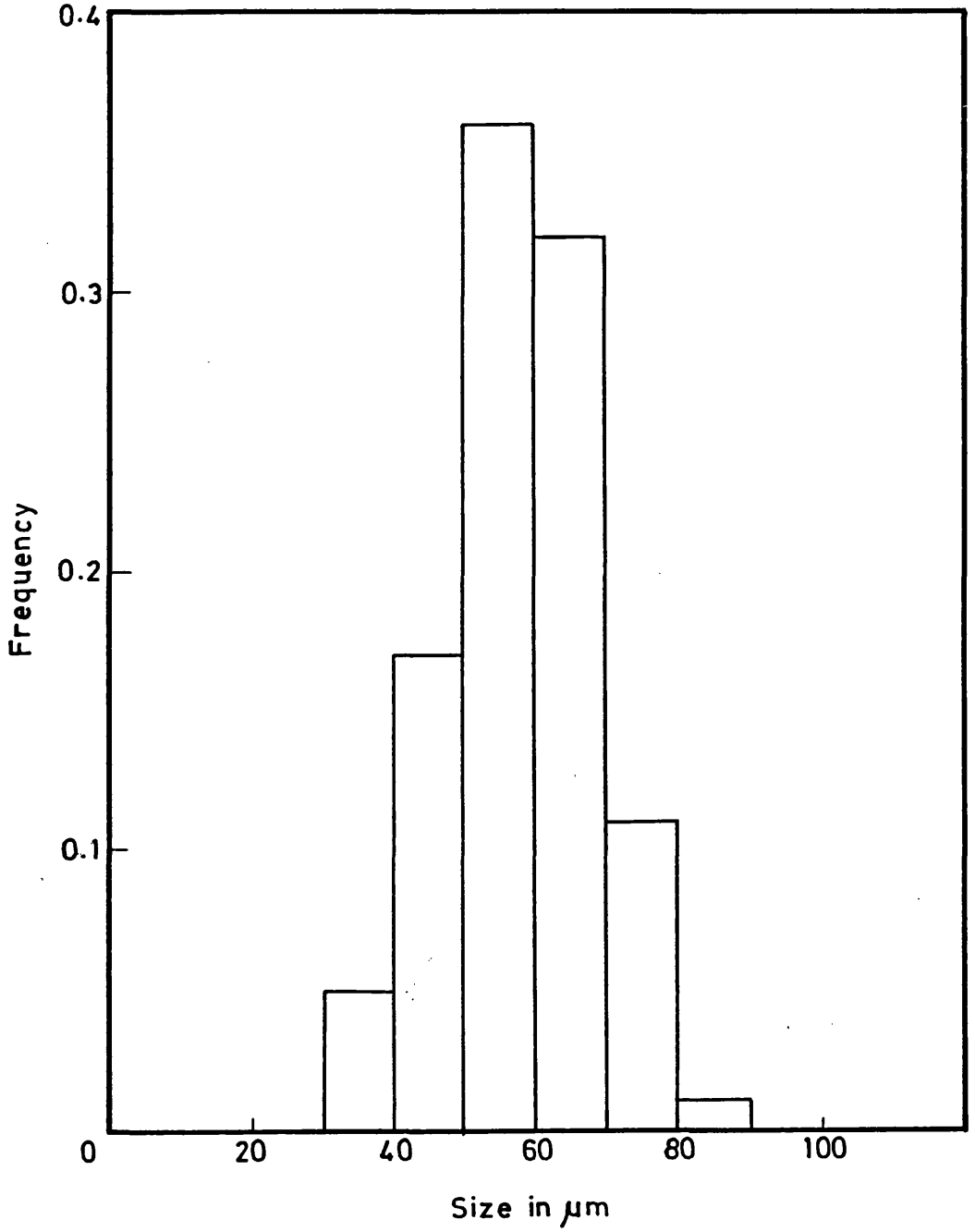

FIG. 4.16: HISTOGRAM SHOWING THE SIZE DISTRIBUTION OF TYPE I CRYSTALS GROWN UNDER OCTADECYLAMINE MONOLAYER AT [Ca]=4.5 mM SOLUTION.

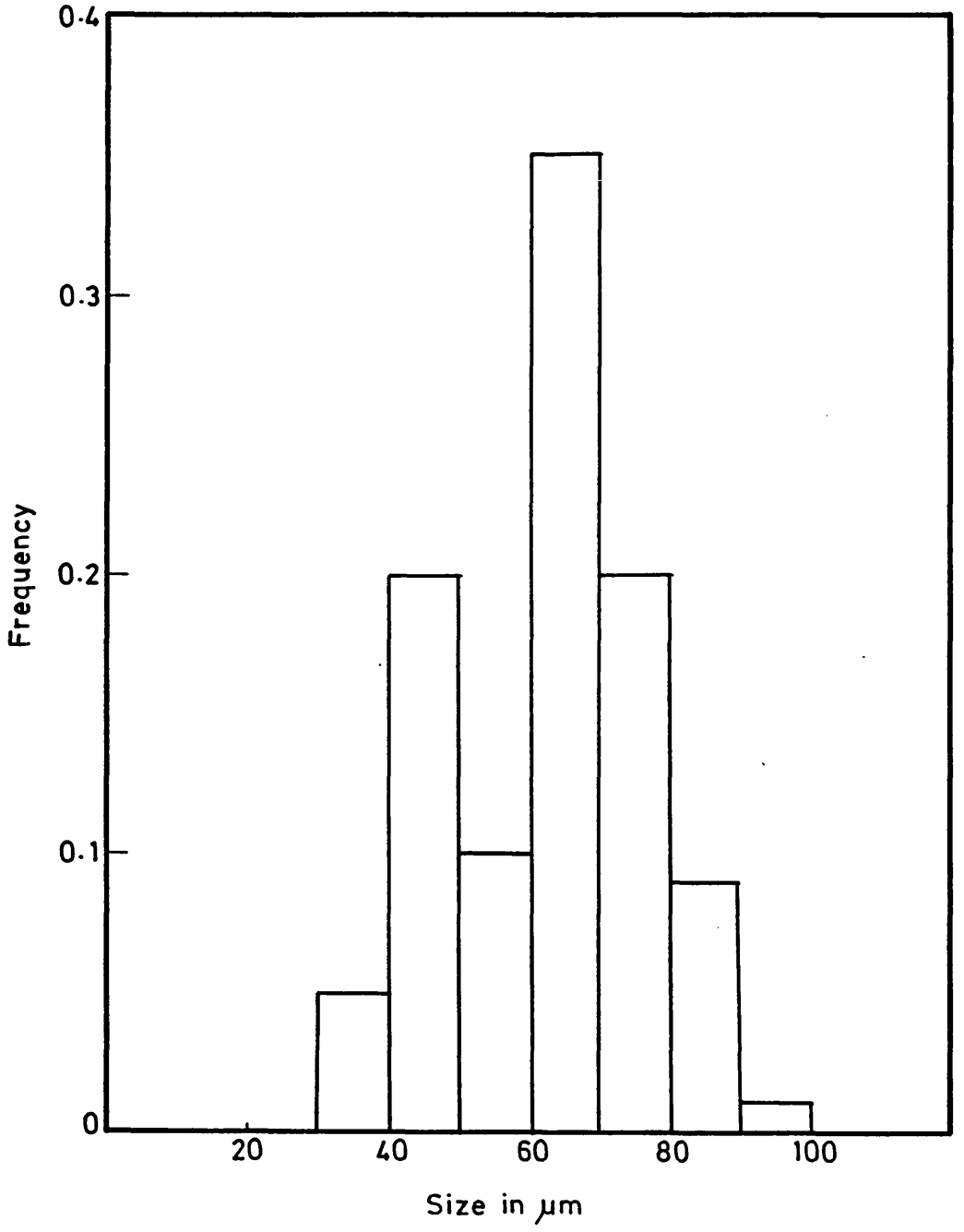

FIG. 4.17: HISTOGRAM SHOWING THE SIZE DISTRIBUTION OF TYPE II CRYSTALS GROWN AT [Ca]=4.5 mM (The longest dimension of the crystals measured from micrographs).

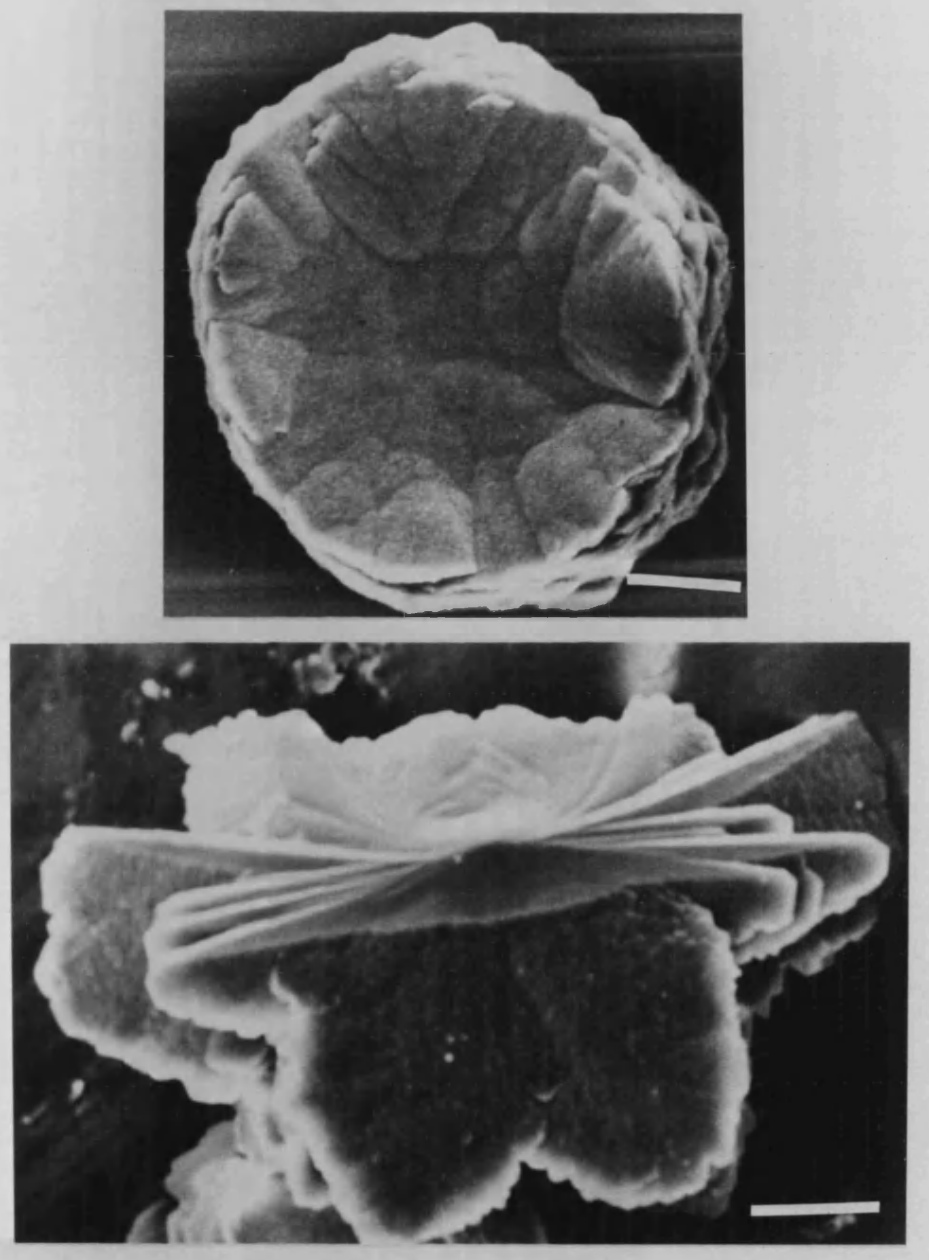

FIG. 4.18: SEM MICROGRAPHS OF TYPE I CRYSTAL (A) AND TYPE II CRYSTAL (B), GROWN AT [Ca] = 4.5 mM. (Scale bar = 10 μm)

Formation of rhombohedral calcite crystals was noticed in some experiments where the external temperature was lowered slightly, but no specific orientation was observed. Furthermore, a small reduction in temperature slightly increased the proportion of type II crystals. However, these observations in terms of a temperature effect were only preliminary and were less reproducible.

4.4 DISCUSSION:

The results presented in the previous section show that oriented vaterite formation is favoured under octadecylamine monolayers and the two morphological forms are consistently formed under the film. The two forms show specific morphlogical and crystallographic orientations with respect to monolayer. Hence, there are some specific interactions by the monolayer on the nucleation orientation of vaterite. The possible physico-chemical and stereochemical interacting factors are discussed below.

The formation of solid/liquid phase monolayers on pure water indicates that the monomolecular films of octadecylamine are stable under the conditions used. The intercalation of bicarbonate ions with ammonium ions might be a possible explanation for the formation of partially expanded monolayers occasionally observed in the system.

There is a possibility for weak binding between the ions which probably could lead to the formation of diffuse layer containing both bicarbonate and carbonate ions. However, with CO_3^{2-} ions, the intermolecular attraction increases and the area/molecule decreases, when compared with monovalent bicarbonate ions.

Formation of vaterite at [Ca] = 9.0 and 4.5 mM suggests that the amine films create a local environment below the monolayer of increased supersaturation which is higher than in the bulk solution. This increased supersaturation is effectively created by carbonate and bicarbonate interactions at the amine monolayers over a range of

concentration levels. As it is possible to form vaterite at higher supersaturation levels, amine monolayers preferably favour the vaterite nucleation by a similar mechanism discussed for stearate films at low calcium concentration (See section 3.4).

Alternatively, it is possible to assume that the charged amine monolayers could be highly catalytic in reducing the activation energy for vaterite formation. In this context, we can assume that vaterite nucleation is activated by the formation of a negatively charged diffused layer underneath the monomolecular film. As it is reported [159] that a negatively charged surface favours the formation of vaterite which has a much more open and defective structure, the diffuse layer in the present system might have led to this polymorphic selectivity.

Formation of two different morphological forms of vaterite was present in this system. Type I vaterite crystals were also formed in variable proportions under acid films. This shows that the type I crystals are not specific to the sign of headgroup charge and calcium binding or carbonate binding to the monolayer is not necessary for oriented nucleation. Hence, there must be some common phenomena which may involve structural or stereochemical correlations between the amine and stearate monolayers and the (00.1) face of vaterite. However, there can be no direct stereochemical relationship on amine films as the amine group has no stereochemical equivalent in the crystal structure of $CaCO_3$.

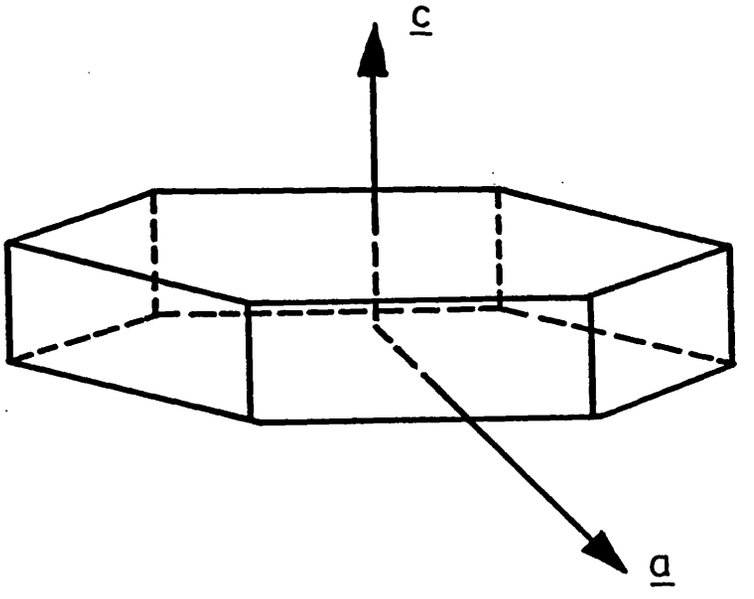

FIG. 4.19: DRAWING SHOWING DISPOSITION OF a AND c AXES OF VATERITE WITH RESPECT TO THE HAXAGONAL PLATE-LIKE HABIT. THE PRISMATIC (11.0) AND BASAL (00.1) FACES LIE PERPENDICULAR TO THESE AXES RESPECTIVELY.

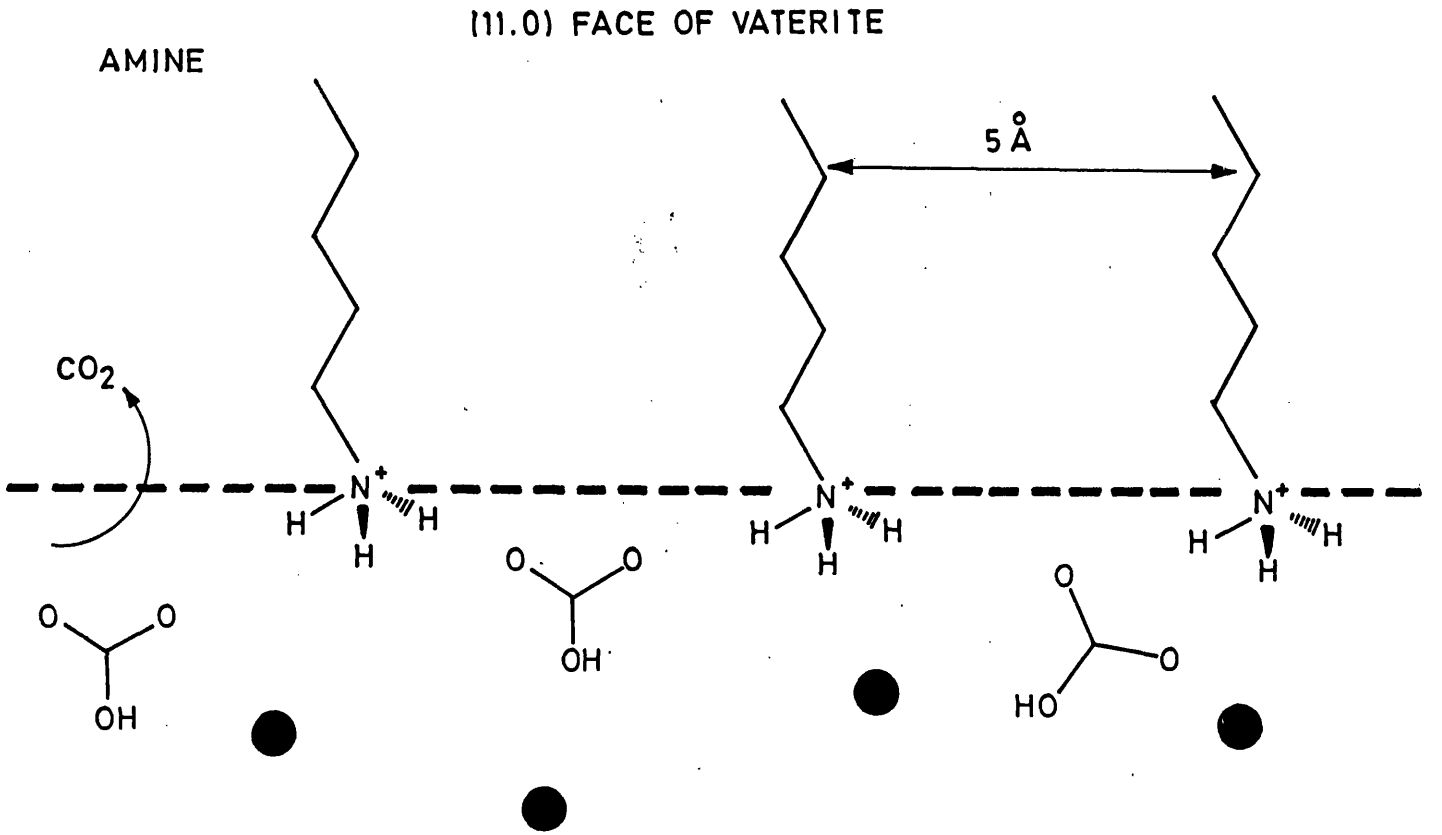

FIG. 4.20: (11.0) FACE OF VATERITE SHOWING THE POSITION OF Ca^{2+} AND CO_3^- IN THE CRYSTAL LATTICE.

The (11.0) face of vaterite has a similar feature as observed in the (00.1) face of vaterite and (1 $\bar{1}$.0) face of calcite under stearate monolayers (Fig.4.19). This (11.0) face of vaterite has only a subset of carbonate anions aligned perpendicular to the crystal face. One probable explanation for (11.0) face nucleation could be that at the working pH of around 6.0 the binding mode of carbonate ions will be through bidentate HCO_3^- interactions orthogonal to the amine (NH_3^+) headgroups (Fig. 4.20). This indirect influence provides to some extent a possible stereochemical recognition between carbonate ions organised within the boundary layer below the amine groups and those contained in the developing nuclei. This effect is not highly specific since both (11.0) and (00.1) faces can be nucleated depending on the coherence of carbonate binding within localized domains under the monolayers.

In summary, monolayers with charged headgroups can control nucleation by (I) charge accumulation (either +ve or -ve) resulting in the formation of diffuse (octadecylamine) or Stern layers (stearic acid), (II) stereochemical effects, directly or indirectly related to the monolayer headgroups, and (III) geometric factors (stearate only). The question then arises as to the possible effect of neutral headgroups such as -OH. The following chapter addresses this question and describes the effect of increases in inter-headgroup spacing on $CaCO_3$ nucleation.

CHAPTER V

INFLUENCE OF MODIFIED MONOLAYERS IN CONTROLLING THE CRYSTALLIZATION OF CALCIUM CARBONATE

5.1 INTRODUCTION:

The influence of charged monolayers on the polymorphic and morphological forms of calcium carbonate crystallized from supersaturated calcium bicarbonate solution had been discussed in chapter III and IV.

Both positive and negatively charged monolayers induce oriented vaterite nucleation, whereas, negatively charged stearate monolayers effectively control the oriented calcite formation through structural and stereochemical factors. To understand further and confirm the mode of influence on oriented vaterite and calcite formation, neutral monolayers such as octadecanol and cholesterol had been used and crystallization under these monolayers was studied and discussed in this chapter. Furthermore, to understand the influence of hydrocarbon chain length on oriented crystal formation, the C_{20}, C_{22} and C_{24} acids have been used as monolayers. The epitaxial importance on the formation of oriented crystals has been studied by using isostearic acid as the monolayer forming substance. Thus, this chapter aims to confirm and extend the results obtained in previous chapters and elucidate the hypothesis proposed for the mechanism of oriented crystallization.

Octadecanol ($C_{18}H_{37}OH$) has an identical chain length to the stearate molecule. Hence the headgroup spacing is expected to remain the same as the acid monolayer, the only change in the molecule being that the charged COO^- group is replaced by the neutral 'OH' group.

Cholesterol ($C_{27}H_{45}OH$), has a 'OH' group similar to octadecanol, but differs in the hydrocarbon moiety having a bulky steroid

ring structure. Hence, the limiting area per molecule will be greatly increased over that for octadecanol.

Eicosanoic acid ($C_{19}H_{37}COOH$), docosanoic acid ($C_{21}H_{39}COOH$), tetracosanoic acid ($C_{23}H_{41}COOH$), all have the COO^- headgroup, but with increasing chain lengths. These molecules are similar to stearic acid but are increasingly insoluble giving more stable monolayer films.

Isostearic acid ($C_{18}H_{37}COOH$) has a COOH headgroup but differs from stearic acid due to the 'CH_3' group on carbon (2) and hence has increased headgroup spacing because of the branched hydrocarbon chain.

5.1.1 Octadecanol: Fatty alcohols have the general formula $C_nH_{2n+1}OH$, their monolayer properties form the same trends as the acid monolayer, except that they are not subject to dissociation, so that the subphase pH is largely immaterial. Similar to acid films, alcohol monolayers are formed for members of the series with 13 carbon atoms or more and stability increases with chain length.

Alcohols have special advantages to be used as films; i) their pressure-area curves are simple with two approximately straight lines and relates to the simplicity of the film structure and ii) the effect of ions in the subphase should be less than on films with more reactive types of headgroups [123]. Octadecanol forms stable monolayers over a range of pH. The stability studies of octadecanol films on water of various pH by measuring the area of the film under constant pressure, were carried out and was reported that octadecanol films are much more stable

with high collapse pressure when compared to stearic acid [142]. Alcohol monolayers had been studied both as a function of surface pressure at various temperatures and as a function of temperature at one (high) surface pressure and confirmed the stability of the monolayer [154]. The data providing valuable information regarding molecular interaction and orientation of various films at different pressures, revealing the two dimensional phase transformations as observed in Π-A curves of alcohol monolayers had been reported [134]. It has been shown that alcohol monolayers reduce the rate of evaporation of water which is dependent on film pressure [126, 140].

The structure of the alcohol monolayer ($C_{21}H_{43}OH$) on water in the region near close packing, by grazing incidence in-plane X-ray diffraction has been reported recently and suggested a hexagonal to pseudo-hexagonal structural transition within the molecular layer [154]. Similar studies by Bohonon et al [149] have shown that henicosanol ($C_{20}H_{41}OH$) pack into distorted-hexagonal structure in the close packed arrangement.

Even though the formation, stability and structure of alcohol monolayers are being studied for sometime, no attempt was made to use these monolayers for crystal growth studies.

5.1.2 **Cholesterol:** Cholesterol ($C_{27}H_{45}OH$) is a natural widespread component of cell membranes but little is known about the formation and structure of monomolecular films. Some studies made on monolayer properties of cholesterol established the close packing of vertically

oriented cholesterol molecules and the condensed state of the monolayer based on pressure-area isotherms and demonstrated [197] that the overall geometry and the favourable location of the polar hydroxy groups are undoubtedly responsible for the strong film properties of such a relatively complex structure.

A study [198] of the monolayer characteristics of cholesterol has shown that when the polar headgroup is suitably located in the molecule so as to allow close packing, it formed a condensed monolayer. Measurements on the dynamic behaviour of cholesterol revealed the dependence of hysteresis on the compression rate of the monolayer [141].

Mixed monolayers of cholesterol with fatty acids had been examined at various compositions and temperatures [139] and showed that fatty acid and cholesterol are miscible in the expanded state and immiscible in the condensed state and the interaction between the molecules is not specific but large enough to form homogeneous monolayers. Phosphatidic acid and cholesterol mixed monolayers had been studied and reported the possible existence of ion-dipole interaction between cholesterol and phosphatidic acid [199]. Furthermore, it was shown that the addition of cholesterol had reduced the binding of calcium to lecithin monolayers [199]. The immiscibility of cholesterol with either octadecanol or stearic acid had been shown by the surface potential measurements [200].

Crystal growth studies were done recently using cholesterol moiety as monolayers and showed the inhibitory effect of these monolayers on the crystal nucleation of sodium chloride [94].

5.1.3 **Modified fatty acid monolayers:** It is well known that hydrophobicity increases with the length of the alkyl group (n) and the stability of the film increases with chain length. Hence, when C_{20}, C_{22}, and C_{24} acids are used as monolayers, they are expected to form highly stable rigid and coherent films as compared to stearic acid. Thus, it is possible that the relative ratio of type II and type I (realigned) calcite crystals may increase as the monolayers become more stable.

Isostearic acid also forms close packed monolayers with an area/molecule 31$Å^2$ [201]; a higher monomolecular area compared to stearic acid monolayers (20-22 $Å^2$), probably due to an additional methyl group in the tail position. Use of this molecule enables the study of the effect of packing arrangement of molecules containing an active functional group, on the crystallization of $CaCO_3$.

5.2 CRYSTAL GROWTH STUDIES UNDER OCTADECANOL MONOLAYERS:

5.2.1 **Experimental:** Octadecanol ($C_{18}H_{37}OH$) was obtained in pure form [BDH, specially pure] and recrystallized from chloroform and the purity checked by microelemental analysis and I.R. spectral analysis. Compressed monolayers of octadecanol were formed on pure water at pH 6.3 and at T = 291 K and on $Ca(HCO_3)_2$ solution having [Ca] = 9 mM, at pH 6.0 and T = 291 K. Experimental procedure for film formation and supersaturated $Ca(HCO_3)_2$ solution preparation is described in sections.2.5 and 3.2. Crystals of calcium carbonate grown under octadecanol monolayers on calcium bicarbonate solution subphase in the Langmuir trough were collected after 21 hours of growth and analysed by X-RD, OM and SEM

techniques. The bicarbonate solution was diluted to give [Ca] = 4.5, 2.3 and 1.2 mM and 100 ml of each solution was taken in glass crystallizing dishes, the compressed monolayers of octadecanol were spread on these solutions and the crystals grown up to 21 hours were analysed under optical microscopy.

5.2.2 **Results:** The purity of recrystallized octadecanol was confirmed to be >99% by elemental analysis and by I.R. spectral analysis. The micro-elemental analysis results are shown below.

	C%	H%	O%
Calculated value:	80.00	14.07	5.93
experimental value:	79.90	14.20	5.90

I.R spectra of octadecanol is shown in Fig.5.1. Absorption bands of terminal methyl group due to asymmetric and symmetric modes appeared at 2900 and 2850 cm^{-1} respectively. The methylene ($-CH_2-$) groups in a linear aliphatic chain gave the sharp absorption bands at 720 and 730 cm^{-1} due to the weak rocking motion. Peaks at 1440 and 1370 cm^{-1} confirmed the presence of a terminal $-CH_3$ group. The most important absorption band was due to the stretching frequency of O-H broad band at 3281-3384 cm^{-1}.

i) Monomolecular films of octadecanol: Octadecanol formed stable monolayers on pure water and on bicarbonate solution subphases and the pressure-area isotherms recorded were similar in both cases (Fig 5.2) and gave areas/molecule around 20.5 and 20 $Å^2$ respectively. No specific condensation of the isotherm was noticed. This indicated the absence of any strong molecular interaction between the monolayer and the ions in the

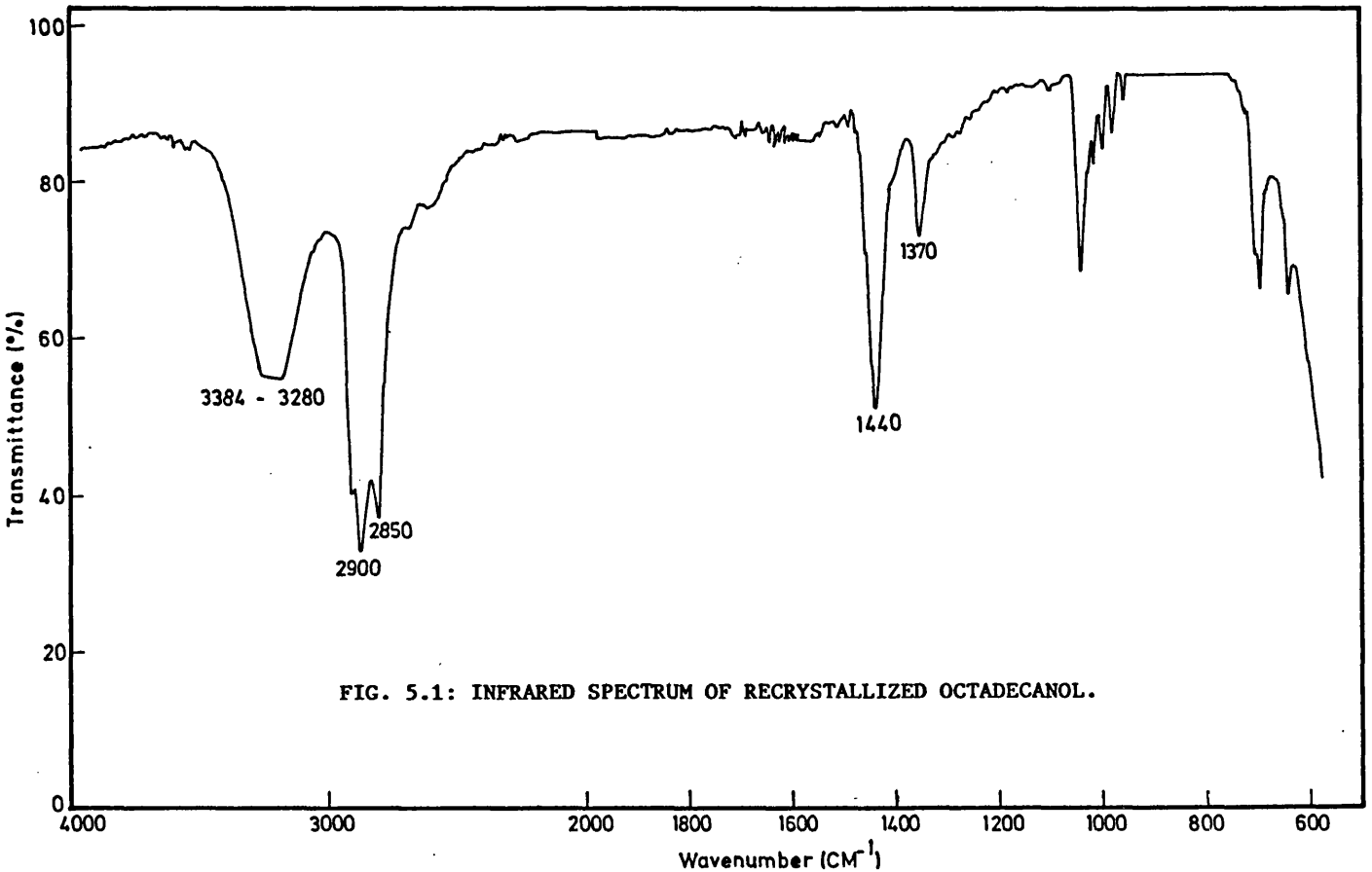

FIG. 5.1: INFRARED SPECTRUM OF RECRYSTALLIZED OCTADECANOL.

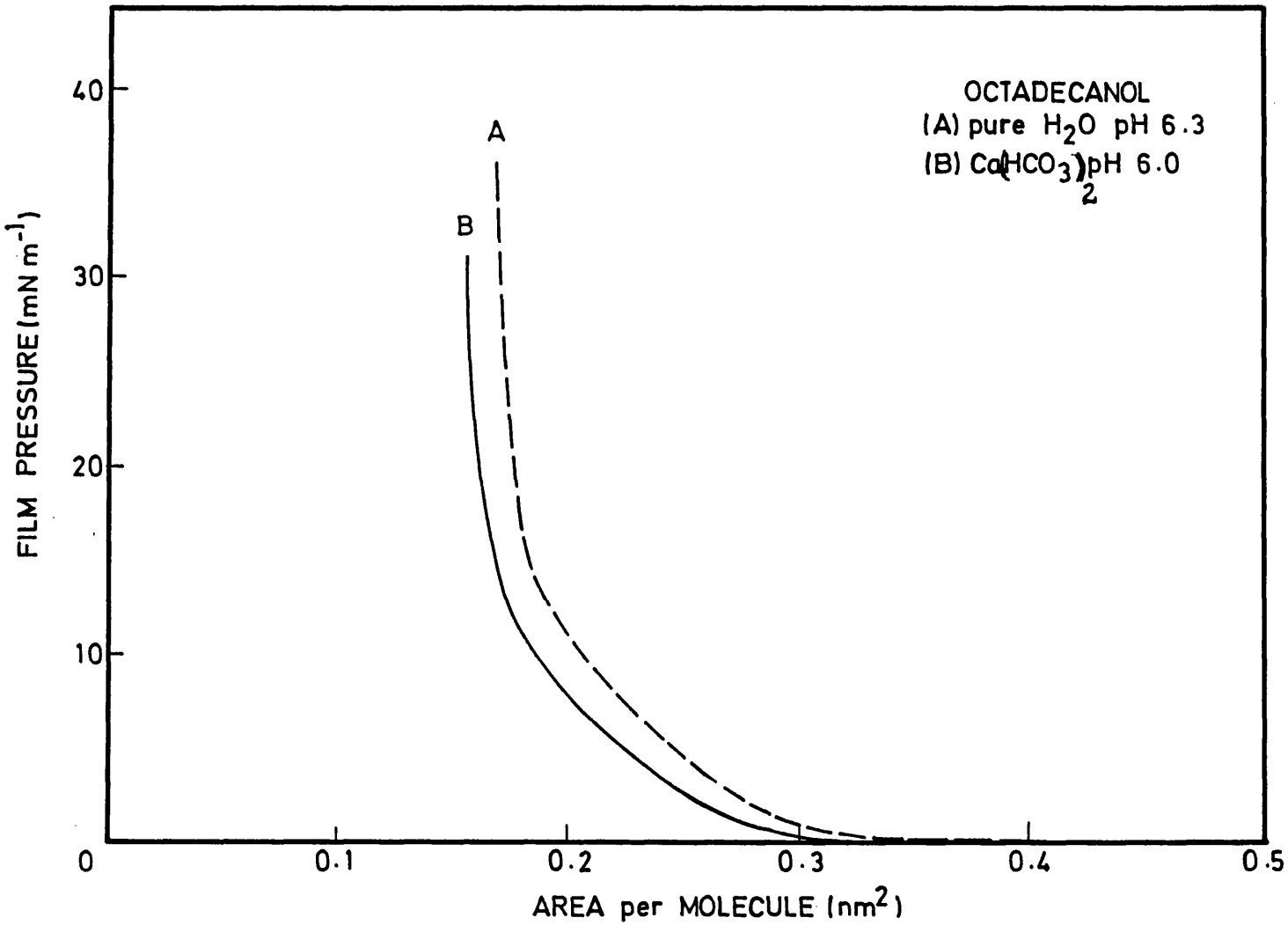

FIG. 5.2: SURFACE PRESSURE-AREA CURVES OF OCTADECANOL ON (A) PURE WATER AT pH 6.3 AND CALCIUM BICARBONATE SOLUTION AT pH 6.0 SUBPHASES.

subphase solution which is to be expected from a neutral molecule like octadecanol. The isotherms recorded in several experiments consistently gave the same area/molecule within ± 0.5 $Å^2$ and no hysteresis was observed. This showed the stable and rigid film formation and the absence of loss of molecules from the monolayers by dissolution.

ii) Crystal growth under octadecanol monolayers: Calcium carbonate crystals grown under octadecanol monolayers at [Ca] = 9 mM were collected on glass slides for optical microscopy and X-RD analysis and on stainless steel stubs for SEM analysis. X-RD analysis showed strong lines for calcite. However a few lines for vaterite were also observed (Table 5.1).

Optical microscopic observations showed (Fig. 5.3) that the crystals were mainly calcite with the occasional presence of vaterite florets. The calcite crystals were of rhombohedral form without any specific orientation of {10.4} faces with respect to monolayer surface. Crystal surfaces did not show any surface roughening (Fig. 5.4). They were smooth on all faces of the crystal. SEM micrographs further showed regular growth faces of the crystals with slow growth in the direction perpendicular to the monolayer surface. No elevation or holes were noticed on the crystal faces (Fig. 5.5). These crystals looked similar to the crystals formed at the bottom of the dishes in control experiments, and showed that the crystals were formed at a slow growth rate. Crystal sizes were not homogeneous. Crystal length and width had heterogeneous size distribution (Figs. 5.6 & 5.7) with a mean length and width of 40 and 35 μm and σ = 16 and 20 μm respectively. They showed preferential growth along

Table 5.1: XRD data of the mature crystals grown under octadecanol monolayer [calcium] (9.0 mM)

d-spacing (Å)	Calcite	Aragonite	Vaterite
3.839	3.852	4.212	4.245
3.556		3.396	3.577
3.258		3.273	3.296
3.029	3.030		
2.728	2.834	2.700	2.735
2.483	2.495	2.481	2.219
2.274	2.284	2.328	2.122
2.095	2.094	2.106	2.065
1.912	1.907	1.977	1.857
1.871	1.873	1.882	1.825
1.626	1.626	1.814	1.825
1.600	1.604	1.698	1.648

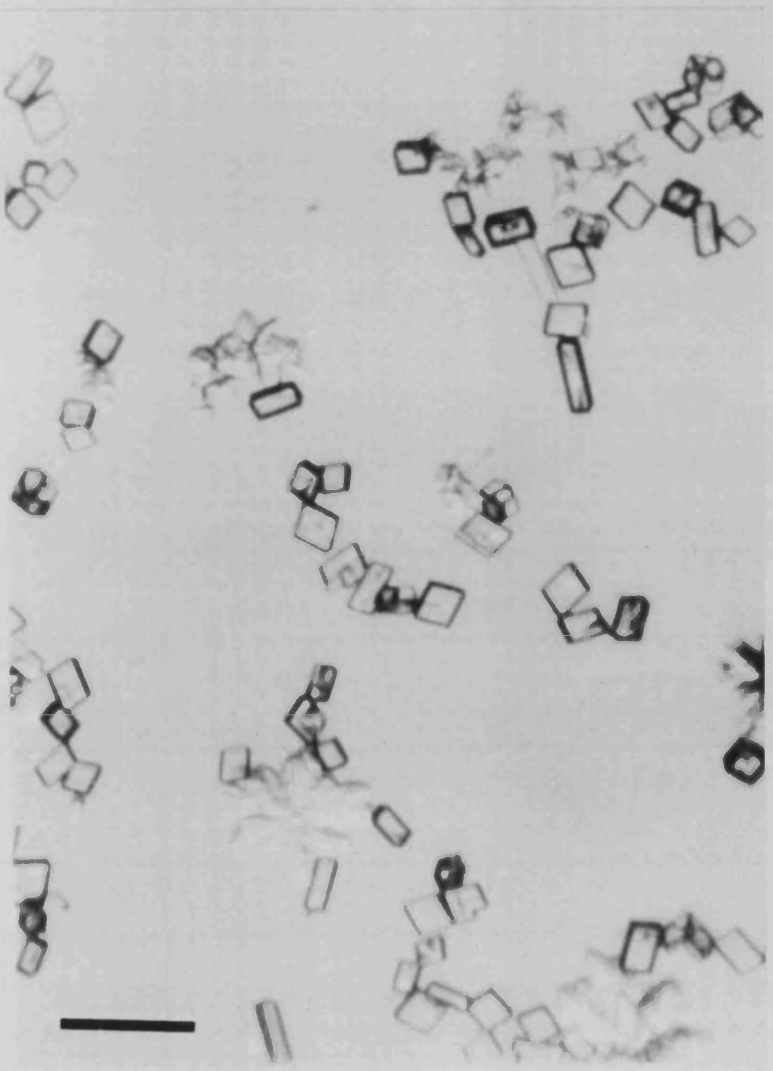

FIG. 5.3: OPTICAL MICROGRAPH SHOWING NON-ORIENTED RHOMBOHEDRAL CALCITE CRYSTALS AND SOME VATERITE FLORETS ([Ca] = 9mM, Scale bar = 100 μm)

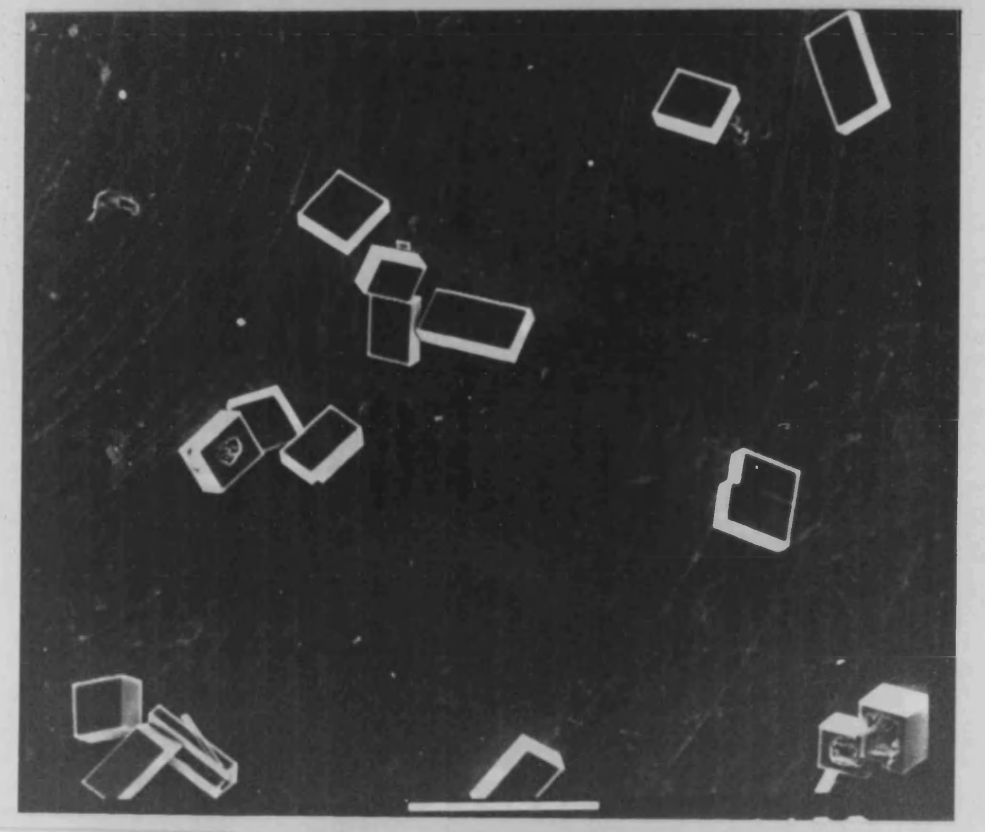

FIG. 5.4: SEM MICROGRAPH OF RHOMBOHEDRAL CALCITE (The smooth surfaces of the crystal suggest that there was minimal interaction between the crystals and the monolayer.) (Scale bar = 100 μm)

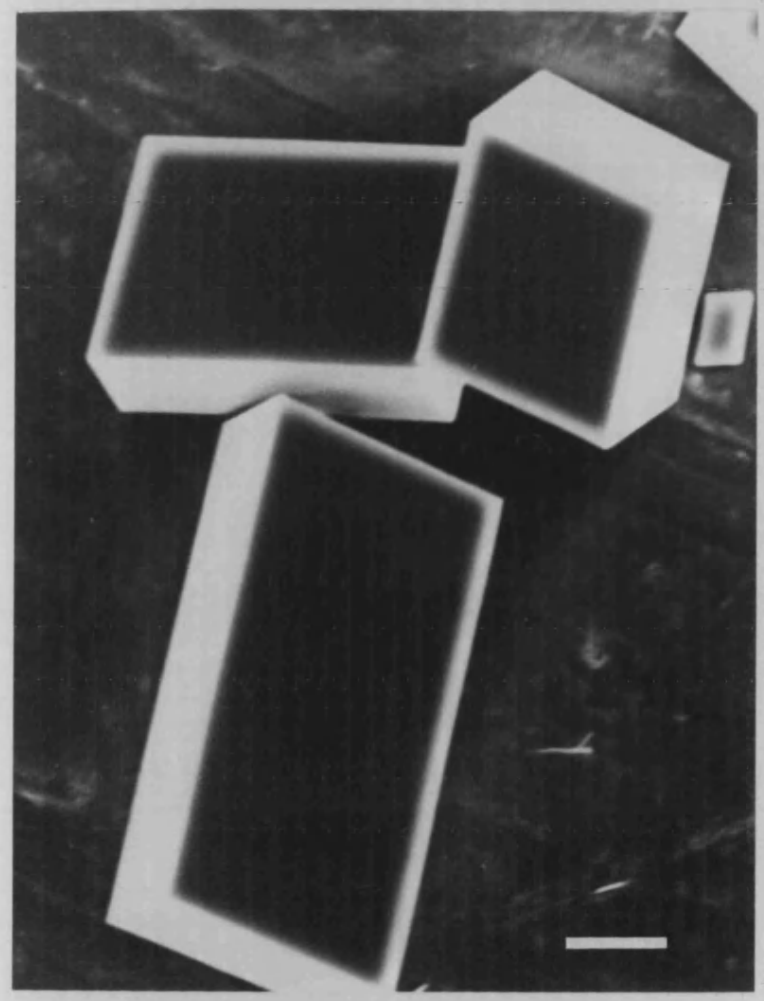

FIG. 5.5: SEM OF MONOLAYER-GROWN CALCITE CRYSTALS. THE MICROGRPAH SHOWS THAT THE LENGTH AND WIDTH DIMENSIONS OF THE CRYSTALS ARE VARIABLE WHILE THE THICKNESS IS RELATIVELY CONSTANT. (Scale bar = 10 μm)

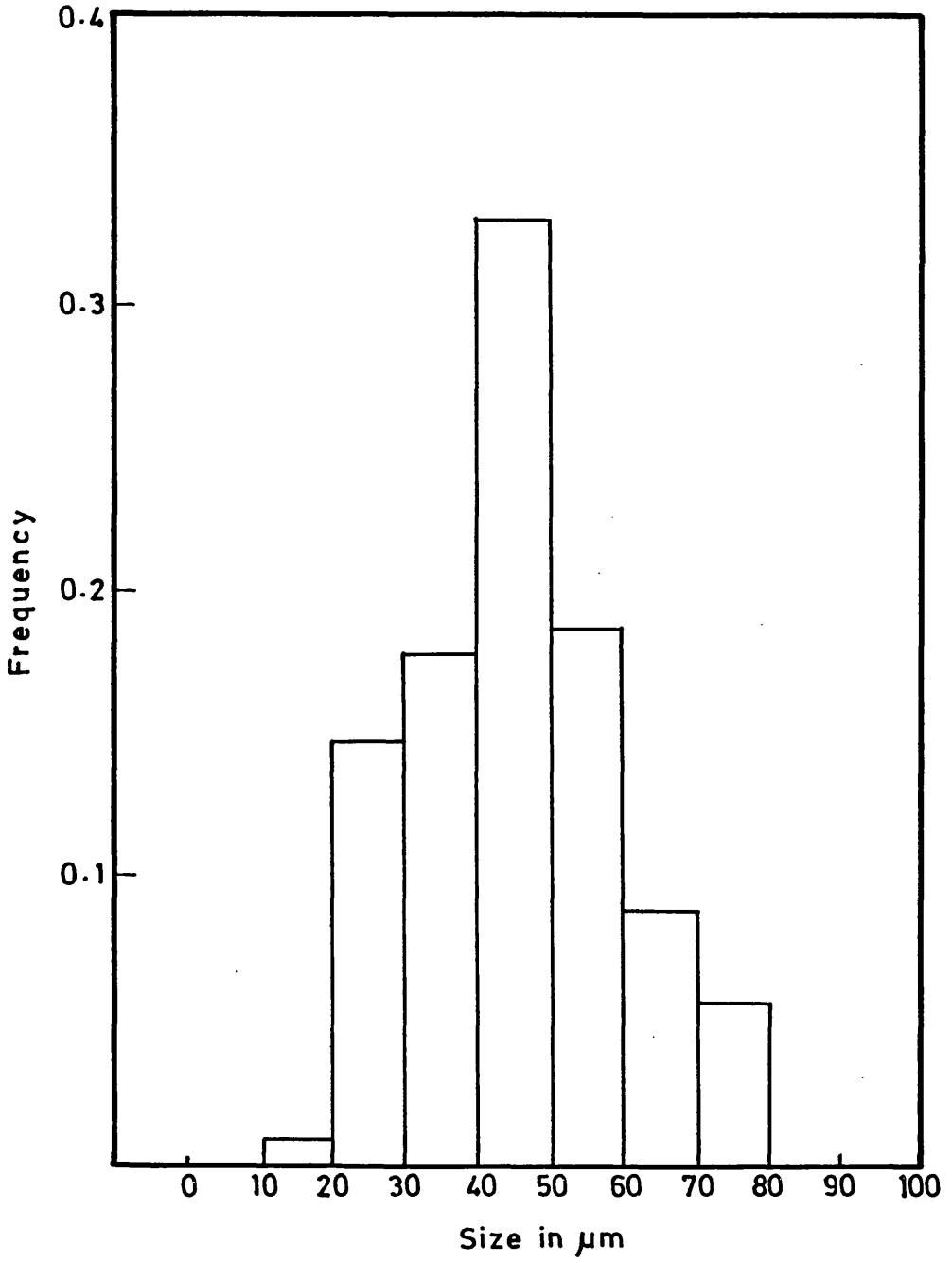

FIG. 5.6: HISTOGRAM SHOWING THE SIZE DISTRIBUTION (LENGTH) OF CRYSTALS GROWN UNDER OCTADECANOL MONOLAYER.

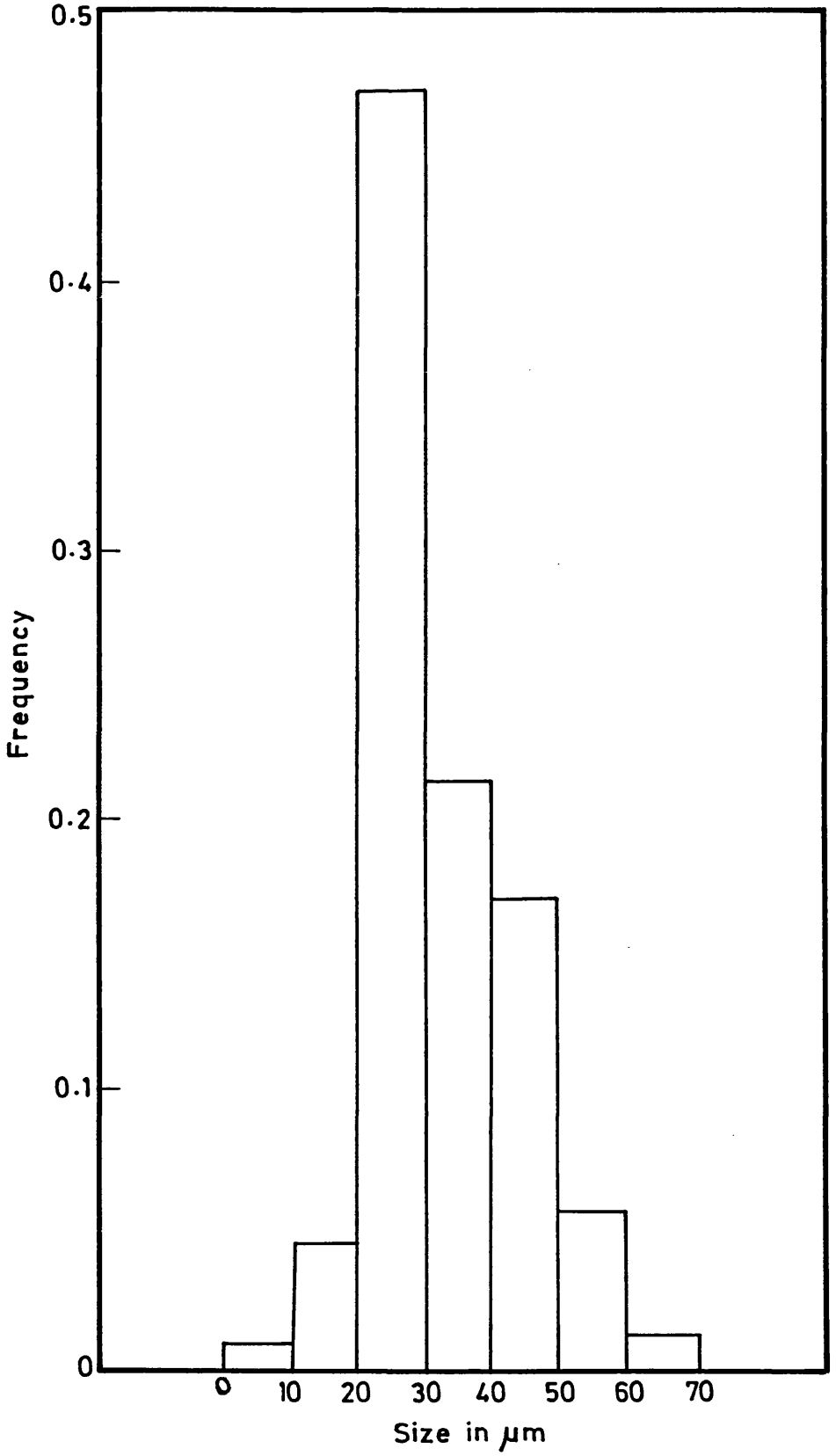

FIG. 5.7: HISTOGRAM SHOWING THE SIZE DISTRIBUTION (WIDTH) OF CALCITE CRYSTALS GROWN UNDER OCTADECANOL MONOLAYER.

the directions parallel to the monolayer surface. Growth along the direction perpendicular to the monolayer surface was restricted and had a limited growth range into the bulk solution. The crystals were less than 10 μm in thickness with a mean size of 5 μm (Fig 5.8).

Along with the main polymorph calcite, some vaterite florets as observed in stearate monolayers were also seen. They had the similar hexagonal symmetry with complex morphology and were oriented with the c axis perpendicular to the monolayer surface (Fig. 5.9). However no central elevation was noticed when viewed from the ventral side of the floret (Fig. 5.10). This shows the absence of any specific interaction of the monolayer with the crystal face nucleated. The crystal sizes of these florets were comparable to type I florets grown under amine monolayers and were around 100 μm.

X-RD quantitative analysis showed 68 ± 5 % were calcite the remaining weight percent being vaterite. However, this did not correlate with the number of nucleation sites as the crystal sizes of vaterite crystals were much larger with complex morphological structure when compared to the thin calcite crystals.

One distinct observation made was that the nucleation density of the crystals grown was noticeably reduced, when compared with acid and amine monolayers (Fig. 5.11).

When the total [Ca] was reduced to 4.5, 2.3 and 1.2 mM, the nucleation density was further diminished (Fig 5.11). No specific changes

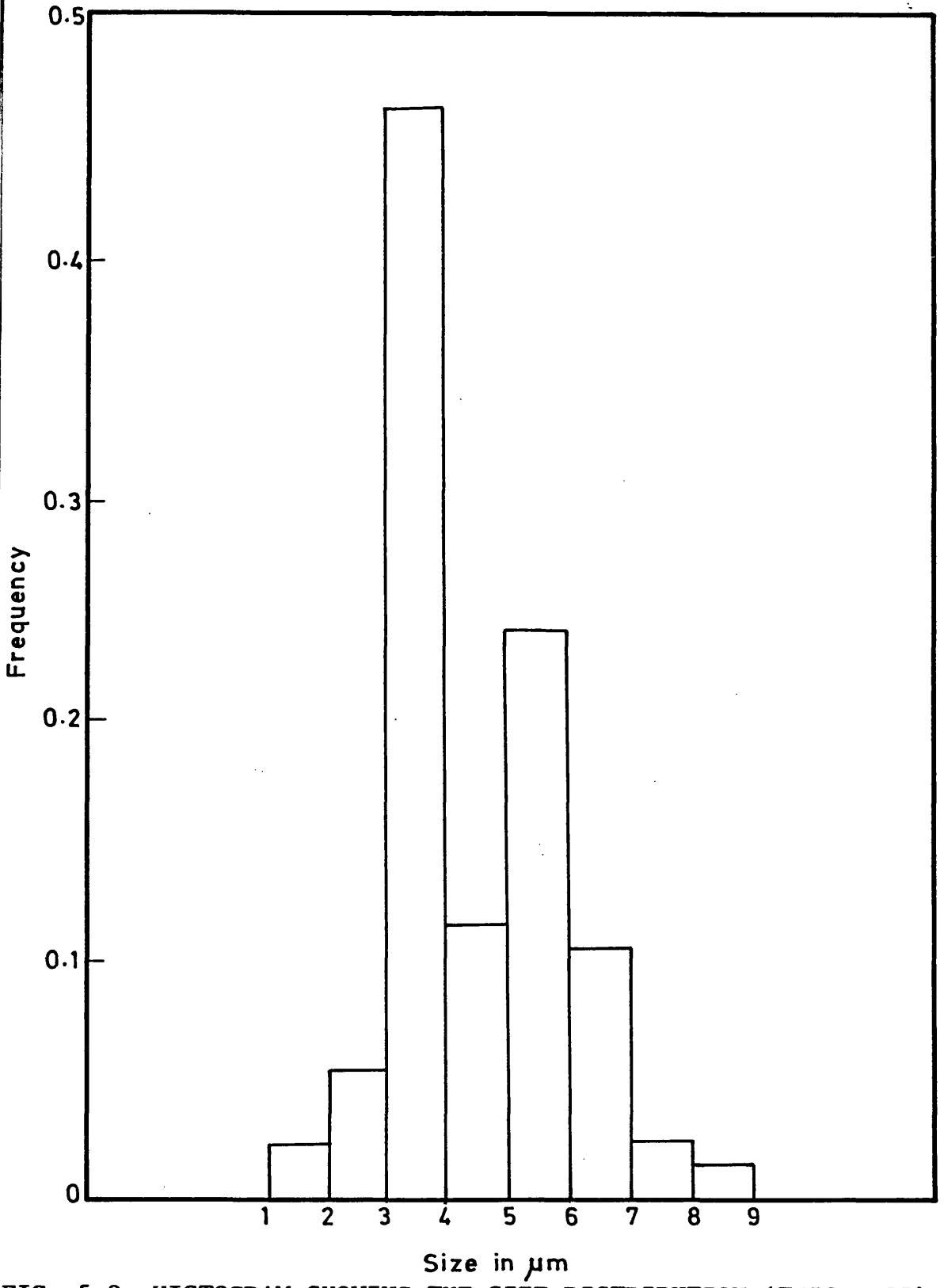

FIG. 5.8: HISTOGRAM SHOWING THE SIZE DISTRIBUTION (THICKNESS) OF CALCITE CRYSTALS GROWN UNDER OCTADECANOL MONOLAYER.

FIG. 5.9: SEM MICROGRAPH OF VATERITE FLORET FORMED UNDER OCTADECANOL MONOLAYER. VIEWED FROM BELOW THE MONOLAYER. (Scale Bar = 50 μm)

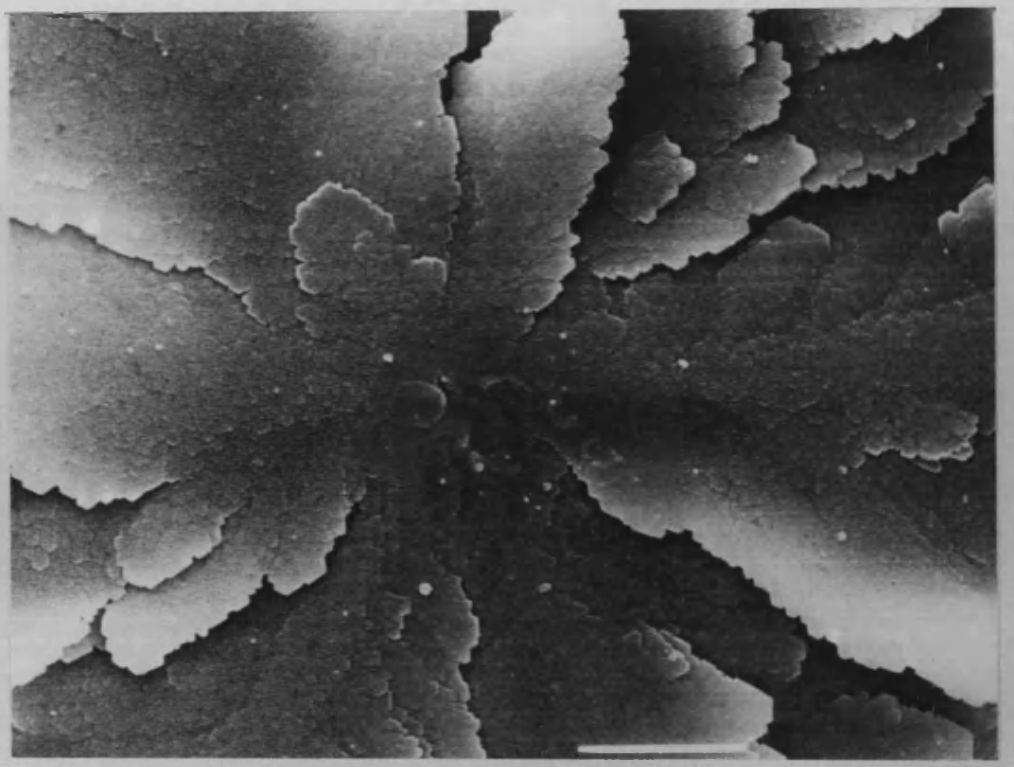

FIG. 5.10: SEM MICROGRAPH OF VATERITE FLORET; THE VENTRAL VIEW SHOWS THE ABSCENCE OF A CENTRAL ELEVATION. (Scale bar = 10 μm)

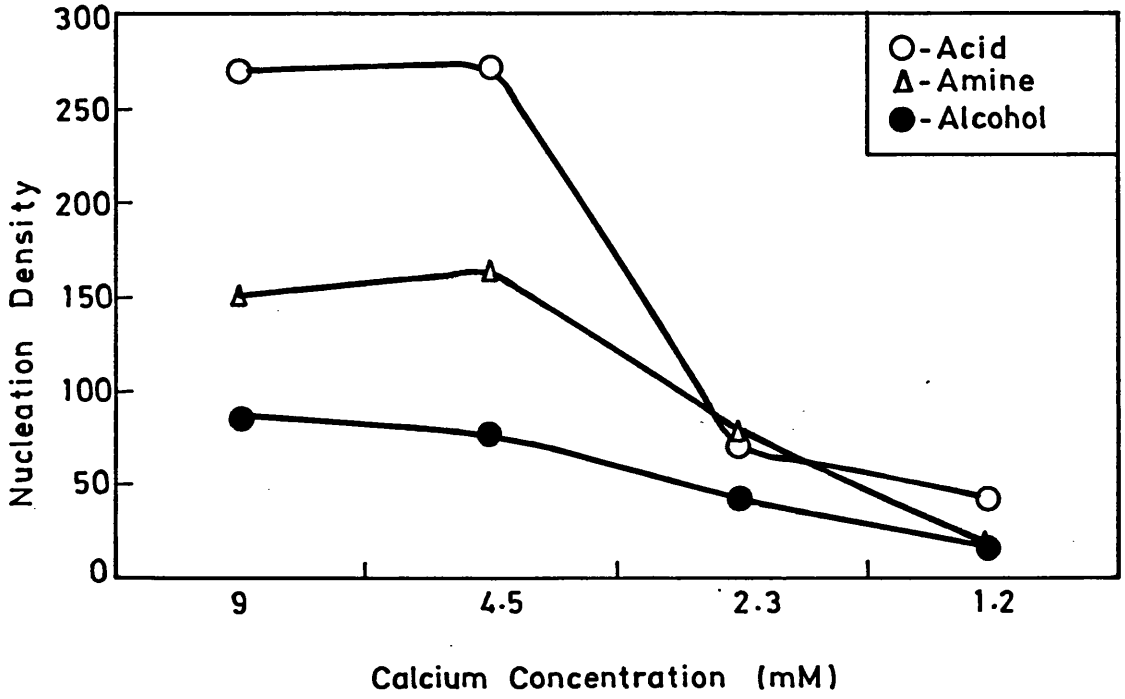

FIG. 5.11: THE EFFECT OF SUPERSATURATION ON THE NUCLEATION DENSITY OF CRYSTALS FORMED UNDER OCTADECANOL AND COMPARED WITH THE DENSITY OF CRYSTALS FORMED UNDER ACID AND AMINE MONOLAYERS.

were observed in the calcite rhomb formation. However the crystal sizes were smaller and the proportion of vaterite was further reduced (Table 5.2).

d) Discussion: Octadecanol being a neutral polar molecule formed rigid monolayer and was not affected by the presence of Ca^{2+}, HCO_3^- and CO_3^{2-} ions. This indicates the absence of any structured ionic layer under the film. Calcite crystals formed were comparable to the control crystals grown at the bottom of the crystallizing dishes where the crystal formation and growth were slow and restricted by diffusion limitations. Absence of any surface interaction on the crystals at the air/water interface shows that octadecanol is not physico-chemically or stereochemically involved in the crystallization phenomenon.

A low nucleation density value indicates that the monolayer has an inhibitory effect on crystallization. This inhibition is clearly not involved with any chemical, stereochemical or structural factors between the monolayer and the rhombohedral crystals formed. The 'OH' group is not charged and there is no correlation between the {10.4} faces of calcite and the headgroups of the monolayer. One possibility for reduction in nucleation density and slow growth might be that the octadecanol monolayer acted as a neutral inert "monomolecular lid" covering the surface of the subphase solution and creating an atmosphere of restricted diffusion at the interface and thereby reducing the rate of CO_2 evolution. Similar observations were noticed when heavy hydrocarbon lids were laid on the surface of bicarbonate solution [202]. Alternatively, the neutral surface

Table 5.2: Nucleation density of crystals grown under octadecanol monolayer.

[Ca] mM	Monolayer state	Calcite		Non-oriented calcite	Vaterite		Total
		Type I	Type II		Type I	Type II	
9.0	Solid	---	---	1875	275	---	2150
4.5	Solid	---	---	1625	300	---	1925
2.5	Solid	---	---	500	550	---	1050
1.2	Solid	---	---	400	---	---	400

Nucleation density = Number of crystals/1 cm^2

may provide an increase in the activation energy for nucleation when compared to air/water interface.

Polymorphic and morphological forms grown in the system are not much different from the control experiment crystals; in both they are mainly calcite with some occasional formation of vaterite. From this, it can be implied that octadecanol, is not catalytic to the formation of any one specific polymorph. However the vaterite crystals formed under octadecanol monolayer are slightly different from those occasionally observed in the control crystals. These were dendritic in morphology and were aggregated with control calcite crystals. The vaterite crystals formed under octadecanol monolayer, although few, were discrete and well developed. This can be explained in two different ways. One possibility is that octadecanol monolayer might have contained some acid molecules as impurities which would have favoured the vaterite formation. However, oriented calcite plates which are probable at this [Ca] level were not located. Furthermore, FTIR spectral analysis did not show the presence of C=O group in the octadecanol sample. Alternatively, a few vaterite nuclei could have been formed kinetically as in the control system and these nuclei might have grown slowly to give individual vaterite florets.

In summary, the formation of rigid octadecanol monolayer acts as a thin inert membrane that reduces the rate of formation of CO_2, according to the equation

$$2HCO_3^-{}_{(aq)} \text{ ------> } CO_3^{2-}{}_{(aq)} + H_2O_{(aq)} + CO_{2(g)}$$

indirectly reducing the rate of kinetics of crystalliation. The monolayer was not involved structurally or stereochemically in $CaCO_3$ crystallization. These results are consistent with the proposed influence of COO^- headgroups (chapter III) in dictating the oriented nucleation of vaterite and calcite under suitable conditions. It also confirms the catalytic and stereochemical effect caused by octadecylamine monolayers in vaterite formation. Thus a charged functionality is crucial to the oriented nucleation of calcium carbonate under Langmuir monolayers.

5.3. CRYSTALLIZATION STUDIES UNDER CHOLESTEROL MONOLAYERS:

Cholesterol, a compound having a similar 'OH' headgroup like octadecanol but differing in the hydrocarbon moiety was chosen for film formation and crystal growth studies to observe the influence of headgroup packing on nucleation.

5.3.1 Experimental:

Monolayers of high purity cholesterol (> 99%) were spread from chloroform solution (1mg/1ml) on pure water and pressure area curves were recorded at pH 6.8 and at T = 291 K. Mixtures of cholesterol and stearic acid were also prepared. They were spread as mixed monolayers on pure water subphases.

Mixture I	CHL. 75%	Acid. 25%
Mixture II	CHL. 50%	Acid. 50%
Mixture III	CHL. 25%	Acid. 75%

The ratios were taken as number percentages of molecules of both the substances and were prepared in chloroform. Mixed and pure monolayers

were also spread on calcium bicarbonate solution subphases at pH 6.2 and at T = 290 K and pressure-area curves were plotted.

Crystal growth studies under pure cholesterol and mixed monolayers from supersaturated $Ca(HCO_3)_2$ solution having [Ca] = 9.8 mM. were undertaken. The 21 hours grown crystals were collected on glass slides for optical microscopic observations.

5.3.2 Results:

a) Pure and mixed cholesterol monolayers: Cholesterol having only a single hydroxyl group in the same position of the ring system yielded stable and incompressible monolayers. Vertical orientation of cholesterol molecule (Fig.5.12) and the condensed state of the monolayer had been established fron the pressure-area isotherm of pure cholesterol on pure water (Fig.5.13.A). The area/molecule was 38 ± 1 $Å^2$. The molecular area observed with cholesterol agreed well with (≃ 40 $Å^2$) from previous studies [97, 203].

Mixed monolayers with stearic acid also formed condensed films with monolayer areas gradually reducing from 38 to 22 $Å^2$, for pure stearic acid monolayer. The limiting areas/molecule of 75%, 50%, 25% cholesterol mixtures with acid on pure water subphases were 36, 32 and 29 $Å^2$ respectively (Fig. 5.13 B,C,D). The reduction in area/molecule could not be correlated linearly to the cholesterol concentration. Cholesterol and stearic acid are so different in chemical structure that they do not form an ideal mixed film. It can be inferred that they form immiscible condensed monolayers at all ratios. However, previous studies [139] show that the reduction in areas with the number of cholesterol molecules obey

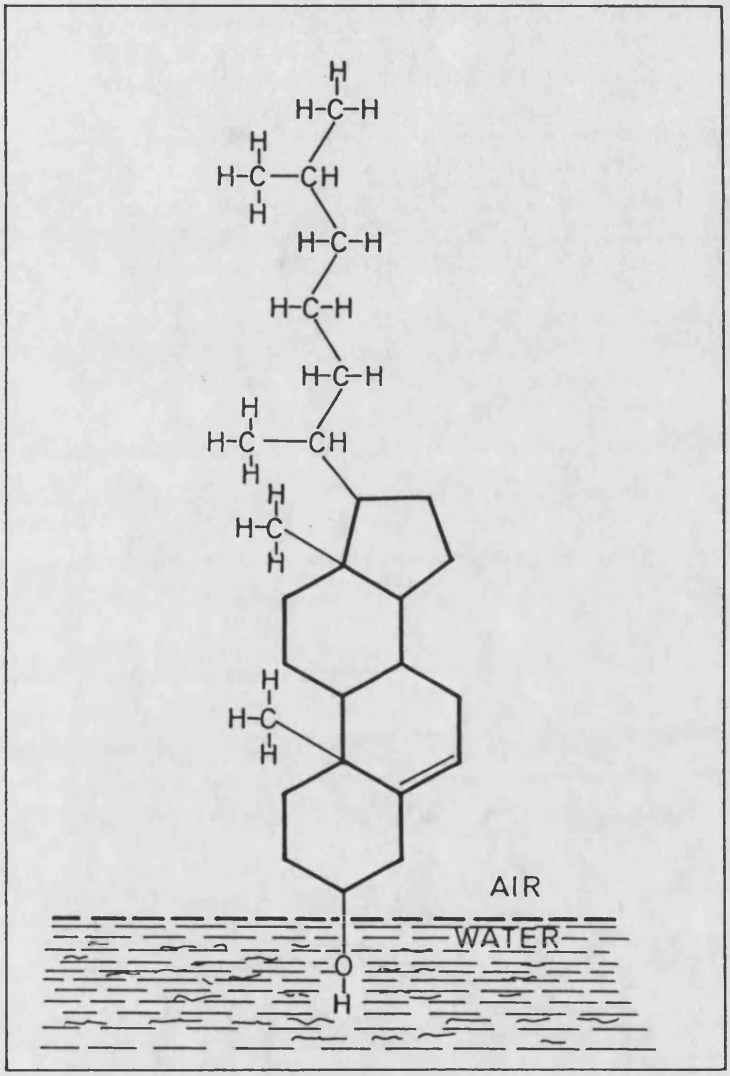

FIG. 5.12: STRUCTURAL ORIENTATION OF CHOLESTEROL AT AIR/WATER INTERFACE.

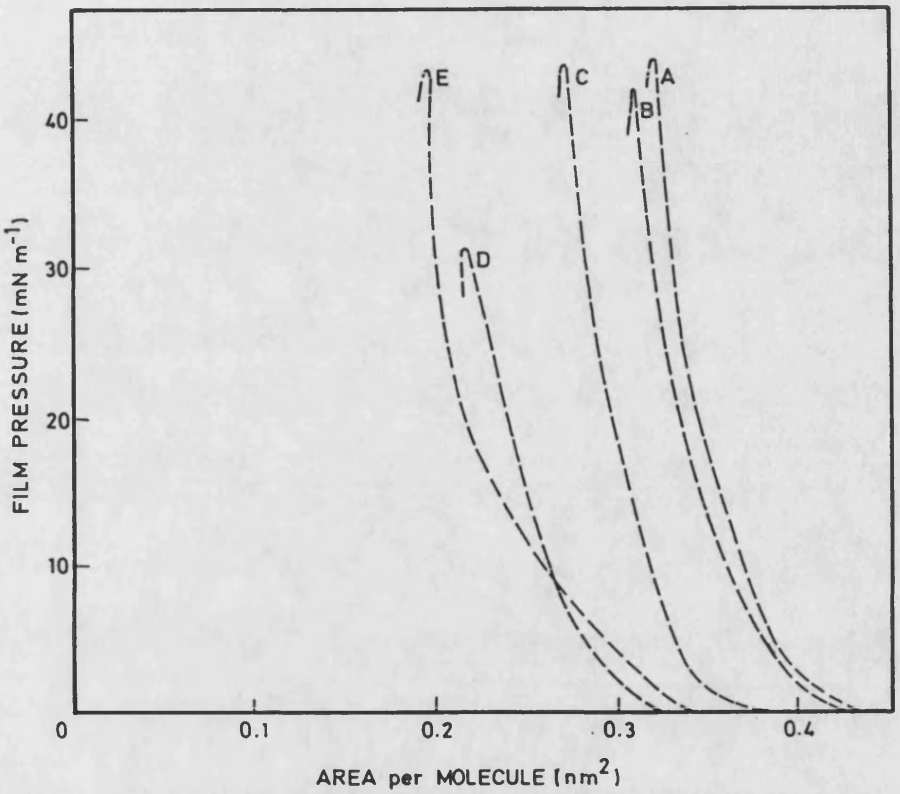

FIG. 5.13: SURFACE PRESSURE-AREA CURVES OF CHOLESTEROL ON PURE WATER SUBPHASE AT T=291 K AND pH=6.8: (A) PURE CHOLESTEROL MONOLAYER; MIXED MONOLAYER OF DIFFERENT PERCENTAGE COMPOSITIONS OF CHOLESTEROL AND STEARIC ACID: (B) 75 and 25, (C) 50 and 50, (D) 25 and 75, AND (E) PURE STEARIC ACID MONOLAYER.

an additive rule. We did not find a similar correlation from our limited results.

Monomolecular films on $Ca(HCO_3)_2$ solution subphases on compression gave similar isotherms (Fig.5.14). Increased condensation was observed when the proportion of acid molecules was increased. The area/molecule was 39.5 $Å^2$ and was comparable with the value obtained on pure water subphase. The areas/molecules of 75%, 50%, 25% cholesterol in mixed monolayers were 39, 38 and 29 $Å^2$ respectively, and did not show any correlation with the amount of cholesterol present in the mixed monolayers One possibility for not observing proportionate reduction in area/molecule as the amount of cholesterol decreased might be that some stearate molecule might have occupied the vacant positions between two cholesterol molecules (Fig 5.15).

b) Crystal growth studies under cholesterol monolayers: $CaCO_3$ crystals grown under pure cholesterol were observed by optical microscopy. These crystals were mainly control-like calcite crystals with some dendritic vaterite formation (Fig. 5.16). Some crystals resembled the calcite crystals grown under octadecanol film. The crystal sizes were heterogeneous with mean length of 30μm and σ = 13μm (Fig. 5.17) and were aggregated. This clustered formation made the nucleation density determination difficult.

Crystals grown under mixed monolayers were a mixture of oriented calcite plates and non-oriented control-like crystals (Fig.5.18) Crystal sizes did not change with varying compositions of the mixtures.

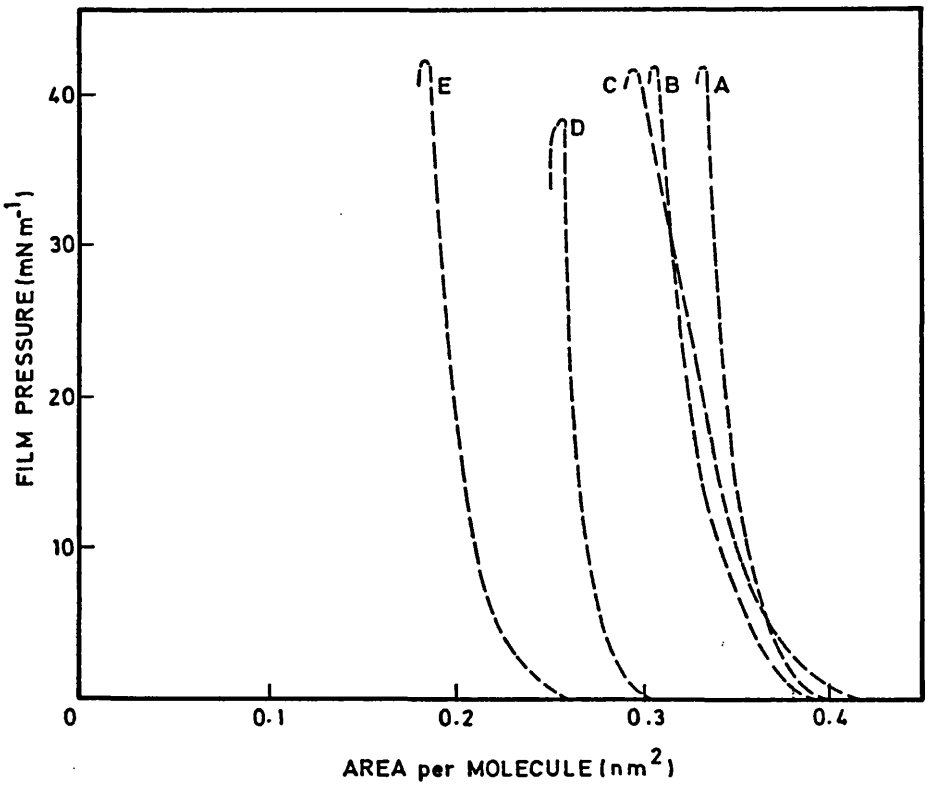

FIG. 5.14: SURFACE PRESSURE-AREA CURVES OF CHOLESTEROL ON CALCIUM BICARBONATE SOLUTION SUBPHASE AT T=290K AND pH=6.2: (A) PURE CHOLESTEROL MONOLAYER; MIXED MONOLAYER OF DIFFERENT PERCENTAGE COMPOSITIONS OF CHOLESTEROL AND STEARIC ACID: (B) 75 and 25, (C) 50 and 50, (D) 25 and 75 AND (E) PURE STEARIC ACID MONOLAYER.

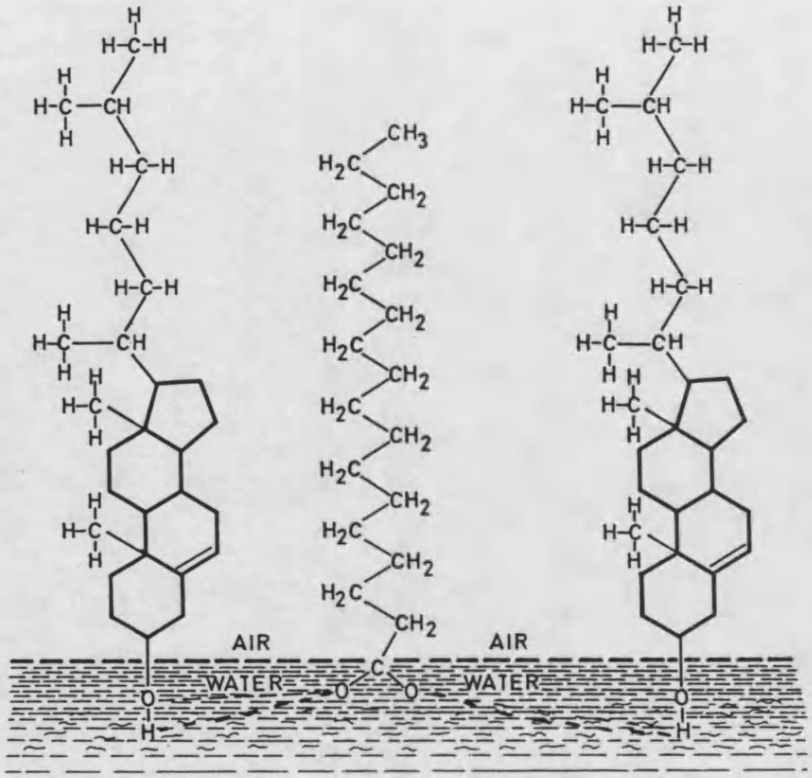

FIG. 5.15:REPRESENTATION OF MOLECULAR ARRANGEMENT OF CHOLESTEROL AND STEARIC ACID IN THE MIXED MONOLAYER (THE BROKEN LINE INDICATES A POSSIBLE ION-DIPOLE).

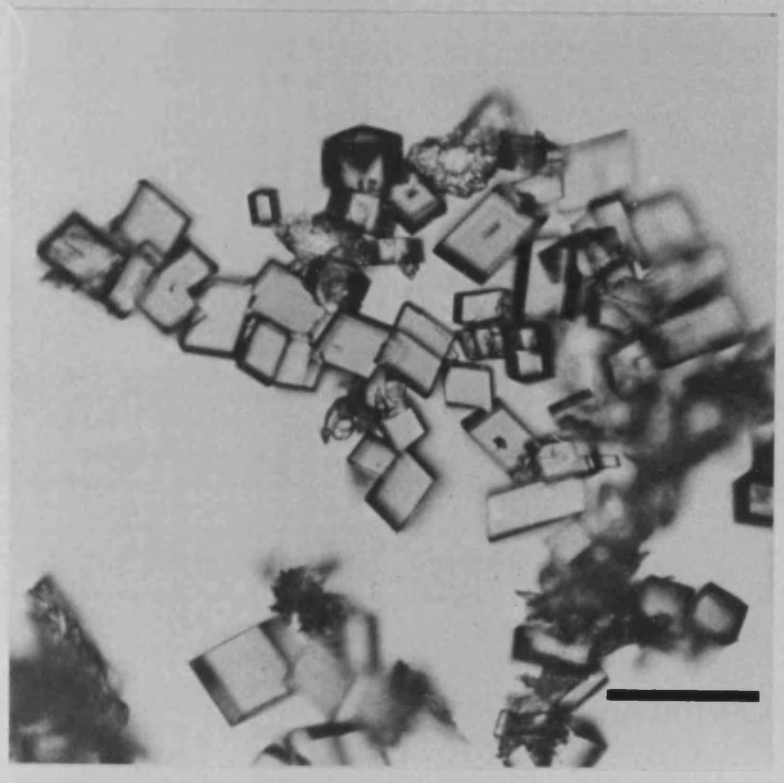

FIG. 5.16: OPTICAL MICROGRAPH OF CRYSTALS GROWN UNDER PURE CHOLESTEROL MONOLAYER. (Scale bar = 100 μm)

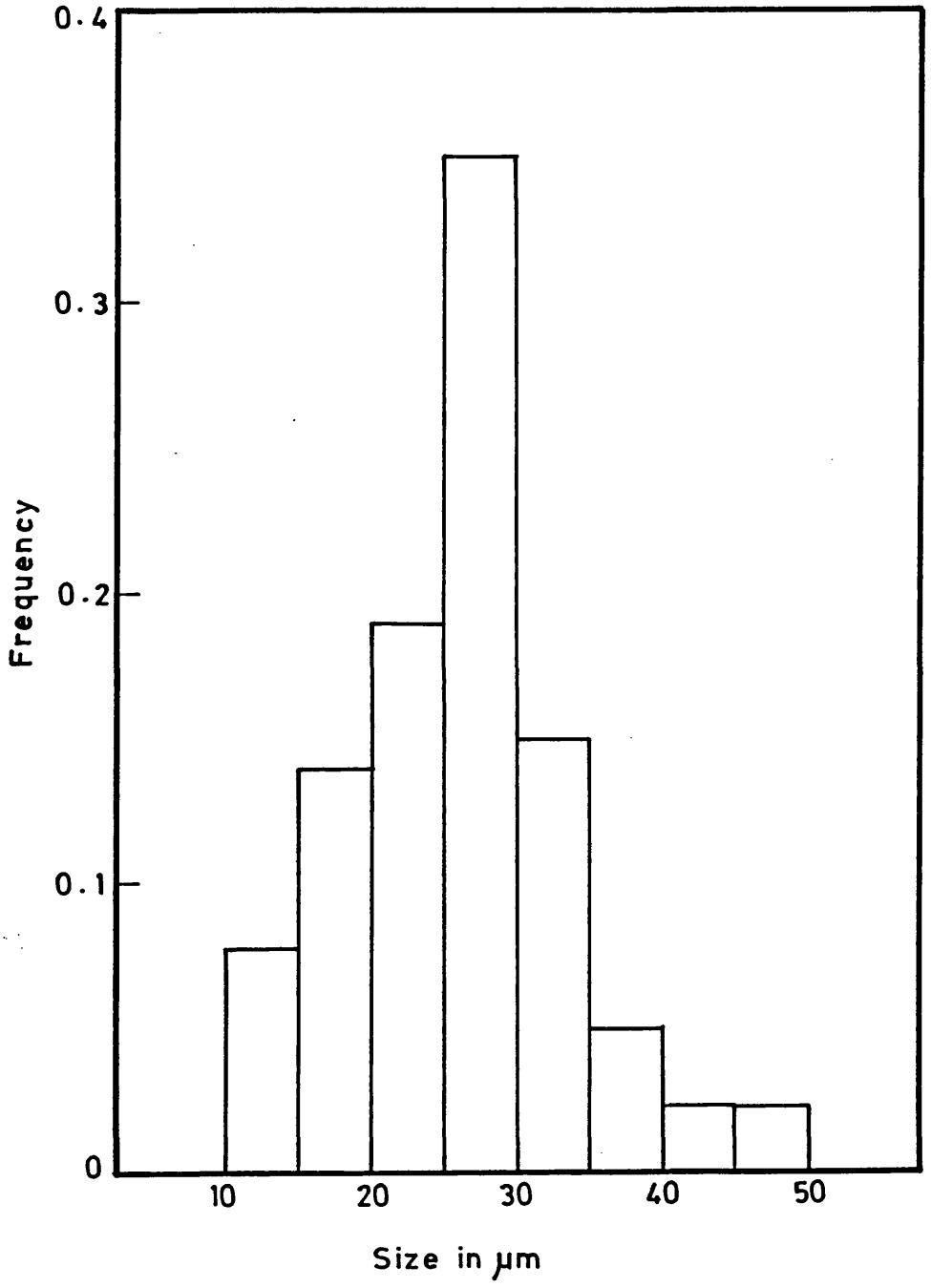

FIG. 5.17: HISTOGRAM SHOWING THE SIZE DISTRIBUTION OF CALCITE CRYSTALS GROWN UNDER CHOLESTEROL MONOLAYER (MEASUREMENTS WERE MADE AT THE LONG SIDE OF THE CRYSTAL).

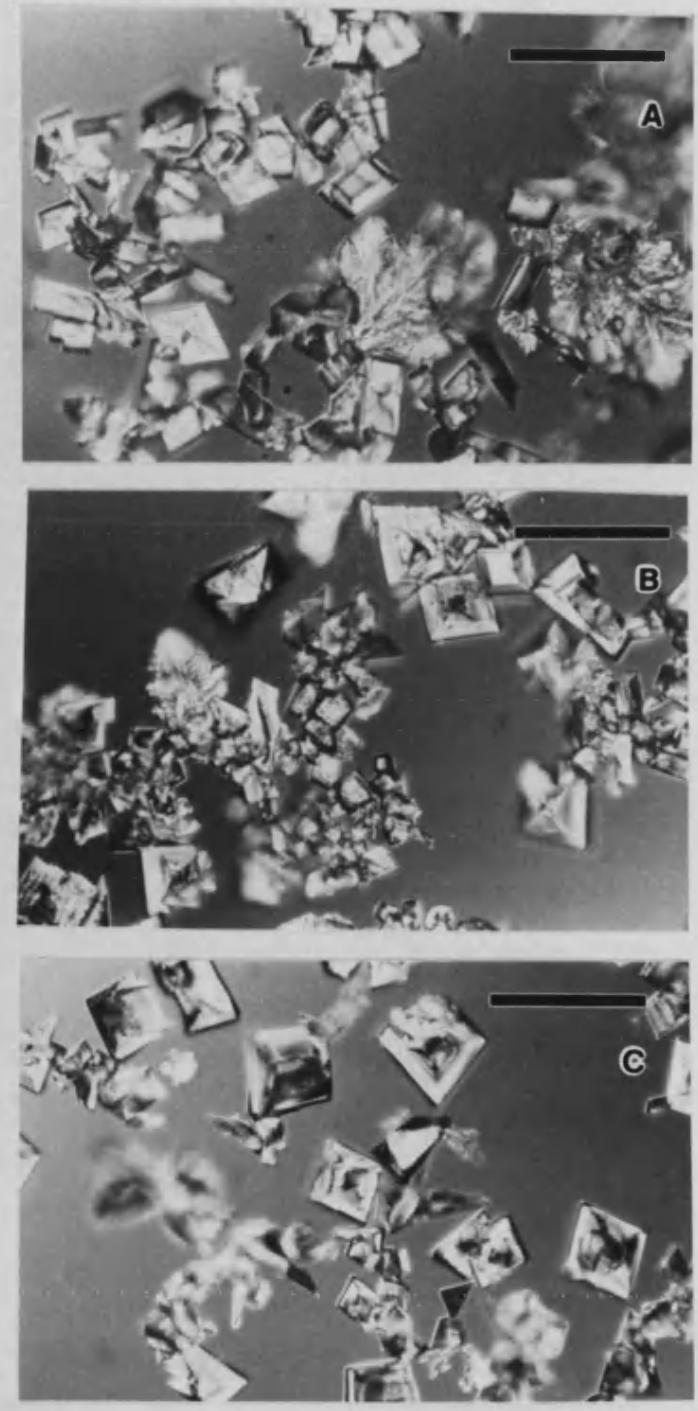

FIG. 5.18: OPTICAL MICROGRAPHS OF CRYSTALS GROWN UNDER MIXED MONOLAYERS OF CHOLESTEROL AND OCTADECANOIC ACID. (A) 75:25 (B) 50:50 (C) 25:75 (%) CHOLESTEROL:OCTADECANOIC ACID. (Scale bar = 100μm)

However, the number of oriented plates/unit area decreased as the cholesterol number increased in the mixture (Fig. 5.19), but did not show any linear relation between them (Table 5.3). The crystals grown in the mixtures composed localized areas of oriented plates and non-oriented calcite crystals. No regular arrangement of these crystals under the monolayer could be seen. The few vaterite crystals located were dendritic and did not show any specific orientation with respect to monolayer.

5.3.3. Discussion:

Results from these cholesterol experiments show that this molecule is inert towards crystallization of $CaCO_3$ at the experimental conditions chosen. When mixed with stearic acid, it did not interfere with the influence of stearic acid on oriented crystallization. Similarly stearic acid had no effect on the activity of cholesterol monolayer in the crystallization process.

Cholesterol films were highly stable and condensed. The molecular areas observed seem to be the smallest obtained with any of the cyclic compounds like saturated sterols, but correspond well with the areas to be expected for closely packed vertically oriented molecules.
The condensing effect/monomolecular area at different surface pressures in mixed monolayers did not show any numerical relationship with the amount of cholesterol. It is possible that the condensation and area/molecule is based on more than one assumption i.e., equilibrium and homogenety in the spread film.

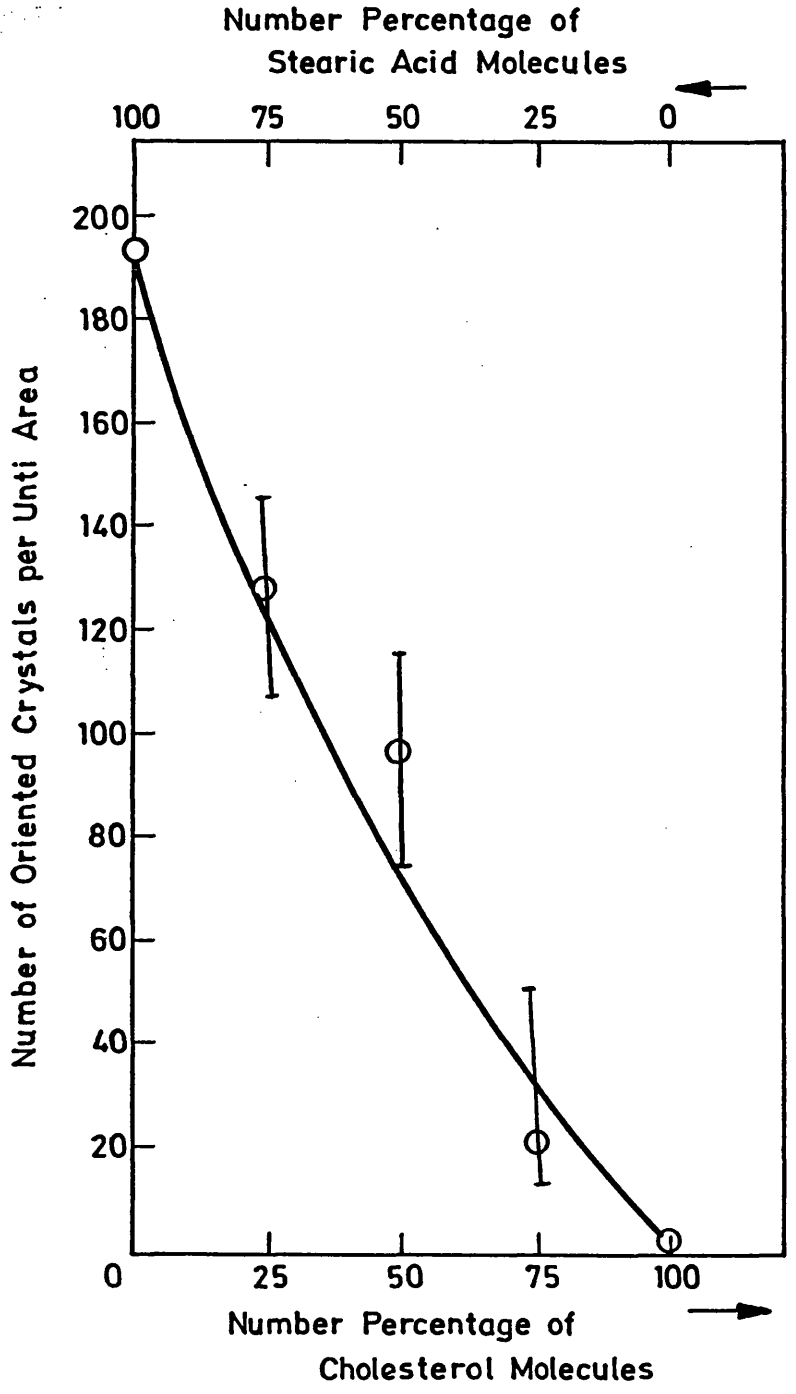

FIG. 5.19: EFFECT OF MIXED MONOLAYER OF CHOLESTEROL AND STEARIC ACID ON THE FORMATION OF ORIENTED CRYSTALS.

Table 5.3: Number of oriented crystals Vs cholesterol percentage (Number %).

CHL %	ACID %	Oriented Calcite Plates per unit area. Experimental	Calculated/Expected
100%	0%	0	0
75%	25%	20	39
50%	50%	96	97
25%	75%	128	145
0%	100%	194	194

Crystals grown under cholesterol were no different from control crystals but different from octadecanol experiments. Cholesterol has a single hydroxy group but a much more complex and bulky hydrocarbon geometry than the simple octadecanol. The hydroxy group being neutral did not show any specific interaction with crystal nucleation/orientation, as seen from octadecanol monolayer. However, cholesterol films did not inhibit the nucleation rate unlike octadecanol films. This indicates that the dissociation of HCO_3^- ions to give CO_2 gas was not affected by cholesterol monolayer. The absence of this inhibitory effect is presumably due to the bulky ring system having increased headgroup spacing of ca 6.8 Å assuming hexagonal packing arrangement of the molecules in the monolayer.

Crystals grown under mixed monolayers indicate that the monolayer is not homogeneously formed as discussed in the section above. However decreasing amount of cholesterol and increasing that of acid in the mixed monolayers showed an increase in oriented nucleation revealing the non-interference of both the substances. Furthermore, it confirms the unique nature of stearate molecules in dictating the oriented calcite nucleation under the monolayer.

5.4. INFLUENCE OF HOMOLOGUES OF STEARIC ACID MONOLAYERS ON ORIENTED CRYSTALLIZATION OF $CaCO_3$:

The aim of this piece of work was to determine the influence on crystallization of $CaCO_3$ by increases in hydrocarbon chain length. The increase in chain length increases the overall hydrophobic nature of the molecules and hence is expected to give rigid monolayers.

Crystal growth under C_{20}, C_{22} and C_{24} acids is thus expected to give similar results as observed in stearic acid system. However, since type I calcite crystals were considered to arise from realignment of type II crystals (section 3.3), increasing chain lengths may increase the type II/I ratio.

5.4.1. **Experiment**: Crystal growth experiments were carried out on $Ca(HCO_3)_2$ solutions having [Ca] = 9.4 mM. Solid phase monolayers of C_{20}, C_{22} and C_{24} fatty acids were spread on the surface of bicarbonate solutions in glass crystallizing dishes and the crystals formed were collected in glass slides after 22 hours and observed under optical microscopy. The amount of acid molecules required to form the solid phase were calculated assuming that the acid molecules of different chain lengths had similar limiting area/molecule and headgroup spacing. The number and types of oriented crystals and their relative ratios were calculated from optical microscopic observations. The nature of orientation of the crystals was analysed by SEM microscopy.

5.4.2 **Results and discussion**: Crystals grown under three different acid monolayers were observed under optical microscopy and compared with the crystals grown under stearic acid monolayers grown under similar experimental conditions. Oriented calcite crystals were similar in all the monolayers in their polymorphic forms morphological types and crystallographic orientation with respect to monolayer surface. However, there were small variations in nucleation densities and in the sizes of the crystals and the relative proportions of type I and type II crystals.

These changes did not show any correlation with the increase in chain length of the acids.

The optical micrograph in Fig. 5.20 (A) shows the crystals grown under (C_{24}) tetracosanoic acid and is compared with the crystals grown under stearic acid monolayer (Fig.5.20 [B]). SEM micrograph of calcite plate grown under tetracosanoic acid showed the similar oriented crystal formation having central elevation and three inclined ridges with ($1\bar{1}.0$) face of the crystal nucleated under the monolayer (Fig.5. 21); they were mainly type II crystals grown without the realignment to form type I crystals. Crystals from eicosanoic acid and docosanoic acid were no different from crystals grown under stearic acid monolayer and type II crystals had dendritic growth. These observations provide additional evidence and confirm the hypothesis proposed for the oriented nucleation of calcite crystals under stearate monolayers and show that the formation of type I and type II crystals is not primarily influenced by the rigidity of the monolayer.

5.5. CRYSTAL GROWTH UNDER ISOSTEARIC ACID MONOLAYERS:

This work was undertaken to determine the importance of spacing of the carboxyl group in stearate monolayers on $Ca(HCO_3)_2$ solution subphases in the oriented nucleation of $CaCO_3$. The possibility of controlling/modifying the packing mode of the COO^- group by chemical modifications of the hydrophobic side chains can provide a suitable approach for the systematic investigation of the structural correspondence for oriented crystal nucleation.

FIG. 5.20: OPTICAL MICROGRAPHS OF CALCITE CRYSTALS FORMED UNDER (A) OCTADECANOIC ACID, (B) TETRACOSANOIC ACID. (Scale bar = 50 μm)

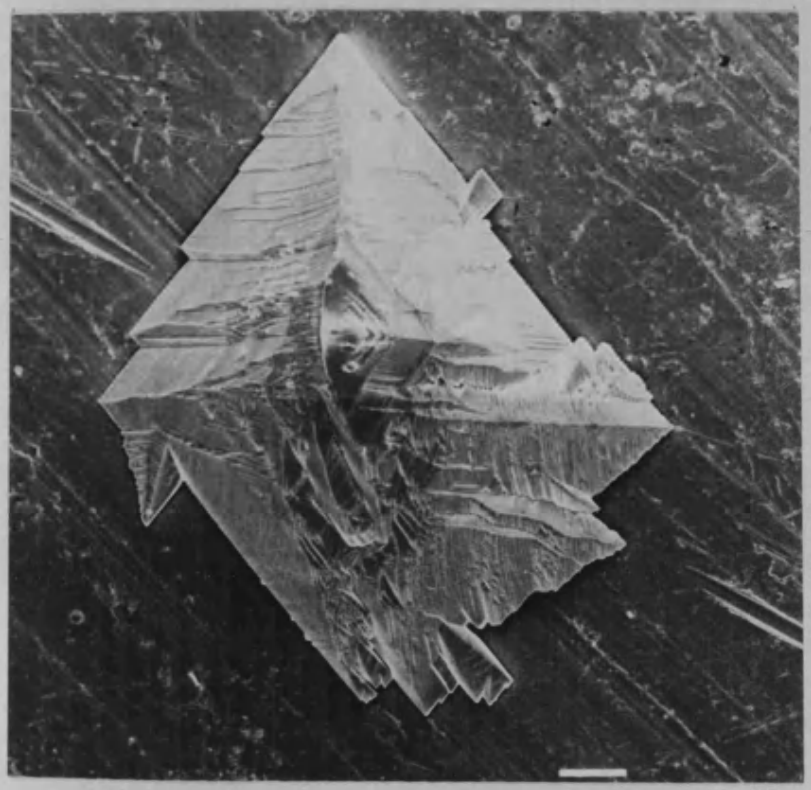

FIG. 5.21: SEM OF ORIENTED CALCITE CRYSTAL FORMED UNDER TETRCOSANOIC ACID. THE CENTRAL ELEVATION WITH THREE INCLINED RIDGES IS CLEARLY SEEN INDICATING THAT THE CRYSTAL IS ORIENTATED WITH THE (1-1.0) FACE PARALLEL TO THE MONOLAYER. (Scale bar = 10 μm)

5.5.1 Experimental: Isostearic acid (2-methyl octadecanoic acid) was obtained from Pfaltz & Bauer, Inc., and is in the liquid form at room temperature. 1mg/1ml of the acid solution was prepared in $CHCl_3$ and used to form the monomolecular films. Monomolecular layers of isostearic acid were formed on pure water at pH 6.8 and at T = 293 K and on supersaturated $Ca(HCO_3)_2$ solution at pH 6 temperaure 291 K and [Ca] = 9.3 mM. A control system using stearate monolayer was also prepared for comparison. Crystals of $CaCO_3$ grown for 22 hours under isostearic acid were collected in glass slides and were analysed using optical microscopy.

5.5.2 Results and discussion: Isostearic acid formed good monolayers (Fig 5.22) giving an area of 29 A^2, with a headgroup spacing of 5.8 A (assuming hexagonal packing), which is slightly lower than the value reported in the literature [201]. However, at high pressures the collapse of the monolayer was observed from the continuous reduction in the monolayer area.

Crystals grown under isostearic acid were mainly control-like calcite crystals as viewed from optical microscopy. Crystal aggregation and heterogeneous nature, typical of control crystals were observed. (Fig. 5.23 A) A few oriented type II calcite crystals were occasionally observed (Fig. 5.23. B).

An increase of ca 0.8-1.0 A in interheadgroup spacing has a profound effect on oriented nucleation of calcite under carboxylate monolayers. The results indicate that a close structural match between

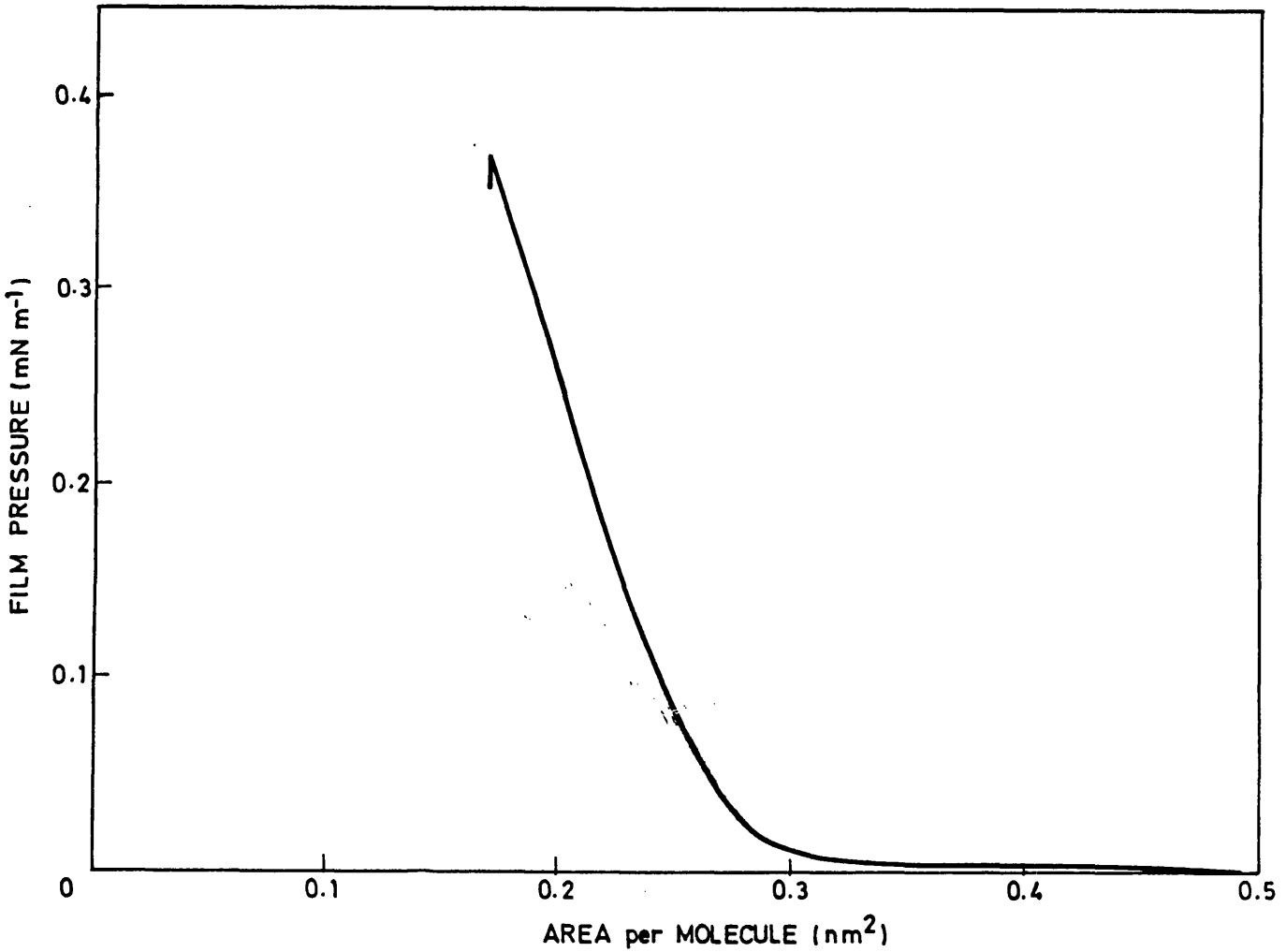

FIG. 5.22: SURFACE PRESSURE-AREA CURVE FOR ISOSTEARIC ACID MONOLAYER ON CALCIUM BICARBONATE SOLUTION SUBPHASE AT [Ca]=10 mM, TEMPERATURE=293K AND pH=6.1.

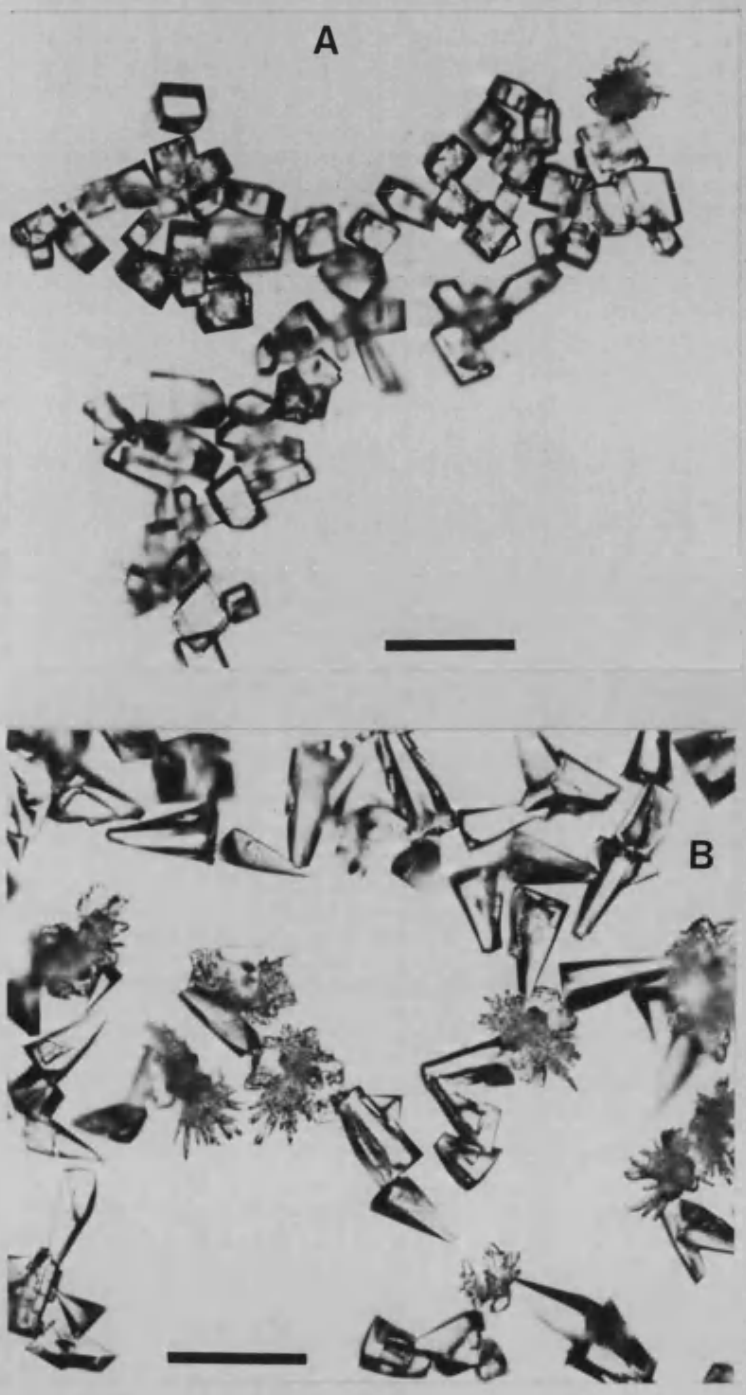

FIG. 5.23: OPTICAL MICROGRAPH OF CRYSTALS FORMED UNDER ISOSTEARIC ACID MONOLAYERS. (A) NON-ORIENTED CRYSTALS REPRESENTING MAJOR AREA OF THE MONOLAYER SURFACE. (B) MICROGRAPH SHOWS SOME ORIENTED BUT AGGREGATED CALCITE CRYSTALS FORMED.
(Scale bar = 100 μm)

Ca-Ca distances in the $(1\ \bar{1}0)$ face and the binding sites under the monolayers is critical to the generation of a preferred orientation. Thus the structural correlation along with charge accumulation and stereochemical correspondence are key features of oriented nucleation at inorganic-organic interfaces.

CHAPTER VI

INFLUENCE OF CATIONS ON THE ORIENTED CRYSTALLIZATION OF CALCIUM CARBONATE UNDER CHARGED MONOLAYERS.

6.1 INTRODUCTION

The previous chapters have involved the studies of controlled crystallization of $CaCO_3$ under charged and neutral monolayers. Changes by reducing [Ca] in the bulk solution, by dilution, on the controlled crystallization have been examined. Charged monolayers effected oriented crystallization of calcite and vaterite depending on [Ca], whereas, neutral monolayers did not effect controlled nucleation. When the inter-headgroup spacing was increased the orientation effect was lost or reduced in neutral and acidic monolayers respectively. The rigidity of monolayers by increasing chain length did not affect the morphological types or oriented calcite nucleation under acid monolayers.

The aim of the present chapter is to study the effect of competitive ion-binding on the oriented nucleation of $CaCO_3$ crystals under charged monolayers. Sodium and lithium cations are used at various [Ca] : [M^+] ratios.

Many geological minerals and some biological minerals are known to contain foreign ions such as Na, Li, K, Rb, Mg, Sr, Zn, Fe and Mn. The composition of these ions in biominerals is reported to be biologically controlled [204]. Kitano and Wood studied [205] the precipitation of synthetic $CaCO_3$ in presence of Na and reported that Na reduced the rate of precipitation and favoured the formation of calcite. The presence of Na^+ in biogenic calcite has been studied by Land and Hoops [206] and Pilkey and

Harris [207] and others. In the study by White, [208] the Na^+ levels of the synthetic calcite precipitated from NaCl solution were reduced which suggested that the presence of organics may be responsible for the higher levels of Na^+ in biogenic calcite. This study further showed the possible interference of sodium in biomineralization processes. Hence, it is interesting to study the role of these ions in controlled mineralization through *in vitro* systems.

The co-precipitation of alkali metal ions (Li^+, Na^+, K^+, Rb^+) with $CaCO_3$ by inorganic methods was studied [209] experimentally and it was shown that alkali metal ions are not readily co-precipitated with calcite. The amount of alkali metal ions precipitated decreased with increasing ionic radius of alkali metals. Changes in the morphologies of calcite and aragonite crystals to spherulitic and dendritic forms were studied in the presence of cations and it was suggested that the substitution of cations in the crystal lattice could be responsible for the changes in morphologies [189].

Interaction of ions with charged monolayers has long been studied and it has been shown that ion binding of specific ions to the monolayer headgroups depends on charge/radius effects and other ions present in the bulk solution [186]. An example of this effect has been provided by the observation that the condensation of an α-iodostearic acid monolayer by Ba^{2+} is inhibited by the presence of excess potassium iodide in the subphase [210]. Counter-ion effects had also been studied for fatty acids and amines and the nature of the monolayers formed were analysed

[211, 212]. However, crystal growth studies under the monolayer in the presence of foreign ions have not been studied to date. This chapter analyses the crystallization of $CaCO_3$ with added lithium and sodium chlorides at various concentrations under the charged monolayers and in the control experiments. Group IA cations were used rather than group IIA cations because of the known structural effects of the latter cations. For example, low levels of Mg^{2+} kinetically favour aragonite over calcite crystallization from supersaturated solutions [189]. The morphologies of the crystals formed in the absence of monolayers were examined and compared with crystals formed under charged monolayers under the same experimental conditions. These studies will enable an understanding of the binding effect of Ca to stearate monolayers in the presence of lithium and sodium and the influence of cationic species on the oriented crystallization of $CaCO_3$ under amine monolayers.

6.2 EXPERIMENT:

Crystal growth studies of $CaCO_3$ with added lithium and sodium from supersaturated calcium bicarbonate solutions were carried out in the absence of monolayers (control sodium and control lithium expts). The preparation of bicarbonate solution is given in section 2.6. The [Ca] of the bicarbonate solution determined was in the range of 8.5-10 mM.

100 ml or 1 dm^3 of bicarbonate solution was taken in each crystallizing dish. Solutions of NaCl were prepared and added to the crystallizing dishes prior to pouring bicarbonate solution to give final concentrations of 0.04, 0.08 0.1, 0.12, 0.15, 0.16, 0.2, 0.25, 0.3, 0.4M for sodium. These were calculated to give the ratios, [Ca]:[Na] = 1:4, 1:8, 1:10, 1:12, 1:15, 1:16, 1:20, 1:30, and 1:40 in the solution. A set of similar solutions were taken and solid phase stearic acid monolayers were spread at the air/water interface. The dishes were left undisturbed for 22 and 44 hours and the crystals grown were collected for XRD, EDXA, atomic absorption IR and optical and scanning electron microscopy.

Amine monolayers were spread on the surface of bicarbonate solutions containing, 0.04, 0.08, 0.12, 0.16, 0.20, 0.24 molar concentrations of sodium chloride to give [Ca]:[Na] ratio of 1:4, 1:8, 1:12, 1:16, 1:20, 1:24 in the bulk solution.

Crystals grown in the presence of sodium, and in the presence and absence of monolayers were collected and analysed for their structural and morphological changes and the orientational nature of the crystals grown under the monolayers.

Crystallization of $CaCO_3$ in the presence of lithium were carried out in a similar manner. The concentrations of lithium in bicarbonate solutions were 0.02, 0.04, 0.06, 0.08, 0.10, 0.15, 0.20, 0.40M with corresponding [Ca] : [Li] ratios = 1:2, 1:4, 1:6, 1:8, 1:10, 1:15, 1:20, 1:40. Crystals grown in the presence of lithium, in the absence/and presence of the stearate and amine monolayers were collected after 24 and 44 hours and analysed for their morphological and structural changes, by XRD, IR and optical and SEM microscopy. The effect on the orientational influence of the monolayer and the changes in the oriented crystals under the monolayer in the presence of lithium were determined.

6.3 RESULTS

6.3.1 Crystallization of $CaCO_3$ in the presence of Na and Li in control experiments:

Polymorphic and morphological forms of $CaCO_3$ grown in presence of various amounts of sodium and lithium in the control solutions gave very interesting and marked results.

6.3.1.1 Control experiments in presence of sodium:

Control experiments in presence of sodium with increasing amounts from 0.04 to 0.4 molar concentrations in bicarbonate solution were observed by optical microscopy. The crystals were mainly rhombohedral, control-like calcite crystals and were similar to the control experiments in the absence of Na. Crystals grown in the presence of sodium having [Ca] : [Na] = 1:10 are shown in Fig.6.1. Crystals were similar in all concentrations of sodium except that they were increasingly smaller and grew more slowly as the concentrations of sodium increased.

At [Ca] : [Na] = 1:40, crystals were only observed around 40 hours by optical microscopy. However, there were no differences in the polymorphic and morphological forms of $CaCO_3$ crystals formed. Calcite crystals grown at [Ca] : [Na] = 1:10, were washed with distilled water and elemental analysis by X-ray spectroscopy was carried out. The EDXA spectrum (Fig.6.2) shows the presence of a very small amount of sodium in the crystal. A corresponding peak for chlorine was not observed.

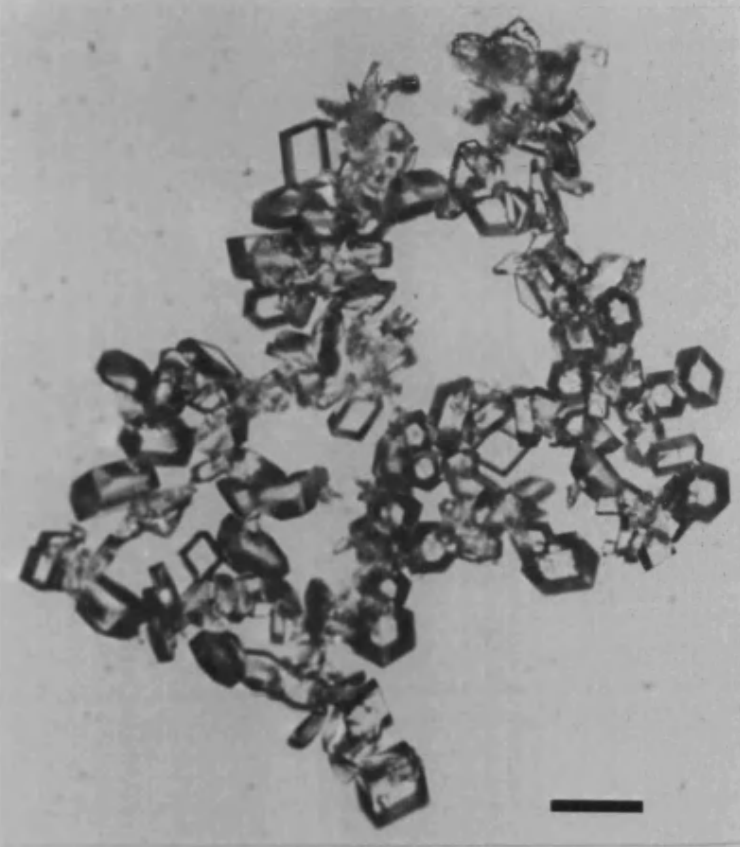

FIG. 6.1: OPTICAL MICROGRAPH OF CALCITE CRYSTALS GROWN FROM SUPERSATURATED $Ca(HCO3)_{2(aq)}$ IN THE PRESENCE OF SODIUM IONS. [Ca]:[Na] = 1:10. (Scale bar = 100 μm)

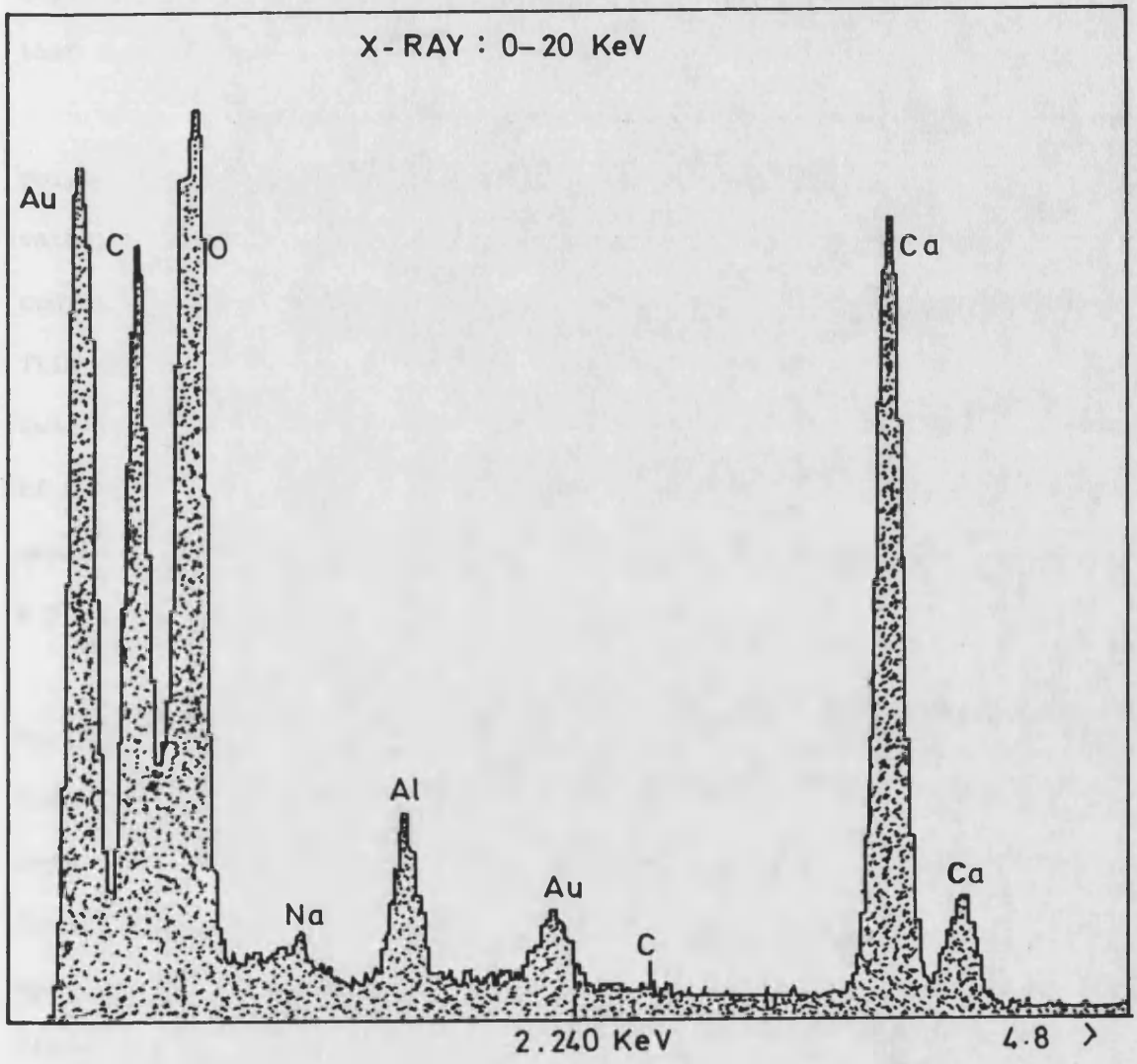

CALCITE CRYSTALS 15 KV

FIG. 6.2: EDAX SPECTRUM FROM THE SURFACE OF A CALCITE CRYSTAL (ALUMINIUM AND GOLD PEAKS ORIGINATE FROM THE SAMPLE HOLDER).

This indicates that sodium is adsorbed on the surface and is not a NaCl drying artefact. Atomic absorption spectrophotometric analysis also showed that 0.039 mole % of sodium ions were present in calcite crystals.

XRD analysis of the same crystals showed the main polymorph as calcite (Table 6.1). However, two lines corresponding to vaterite crystals were also observed. An overlapping line corresponding to sodium chloride at 2.822 Å with the calcite line at 2.834 Å was observed. This one line is insufficient to predict the presence of NaCl. Qualitative observations showed that the nucleation density and growth rate of $CaCO_3$ crystals decreased and vaterite formation reduced as the concentration of sodium in the bulk solution increased.

6.3.1.2 Control experiments in presence of lithium:

Crystallization of calcium carbonate in the presence of various concentrations of lithium in control experiments analysed by qualitative XRD showed that the crystals were mainly calcite. Analysis of crystals grown in the presence of lithium at [Ca] : [Li] = 1: 20 is shown in Table 6.2. The absence of LiCl and Li_2CO_3 was noticed. An overlapping 'd' spacing at 4.122 was observed which is close to vaterite and Li_2CO_3. However, the line can be correlated to vaterite rather than to lithium carbonate as the strongest intensity line of Li_2CO_3 at 2.812 was absent. Furthermore, slight deviation of 'd' spacing values of calcite was also observed.

Table 6.1: X-RD data of $CaCO_3$ crystals grown in presence of sodium. [Ca] : [Na] = 1 : 10. [Ca] = 0.01 M.

d-spacing (Å)	Calcite (d in Å)	Sodium chloride (Å)	sodium carbonate (Å)
4.078			
3.842	3.852		
3.534			
3.220			
3.012	3.030		2.908 (I=100%)*
2.822	2.834	2.821 (I=100%)**	
2.491	2.495		2.545 (I=100%)#
2.280	2.284		
2.091	2.094		
1.995			
1.912	1.907		
1.870	1.877		
1.625	1.604		

* = Intensity value corresponds to hydrated sodium carbonate.

= Intensity value corresponds to unhydrous sodium carbonate.

** = Intensity value corresponds to sodium chloride

Table 6.2: X-RD data of $CaCO_3$ crystals grown in presence of lithium. [Ca] : [Li] = 1 : 10. [Li] = 0.1 M. (d- spacing in Angstroms,[Å])

d-spacing	Calcite	Li_2CO_3	LiCl
4.122		4.160 (I=85%)	
3.887	3.852		
3.047	3.030 (I=100%)	2.918 (I=80%)	2.967 (I=100%)
		2.812 (I=100%)	
2.501	2.495		
2.288	2.284		2.570 (I=86%)
2.102	2.094		
1.923	1.926		
1.884	1.873		1.817 (I=58%)
1.610	1.604		
1.530	1.524		

I = Intensity of diffracted X-ray lines

Optical microscopic observations of calcite crystals grown at [Ca] : [Li] = 1:20, showed a remarkable change in the morphology of the crystals grown. Instead of normal rhombohedral {10.4} faces of crystals being formed, hexagonal (00.1) faces of calcite crystals were developed (Fig.6.3). Qualitative observations showed that at this ratio almost exclusively all the calcite crystals had developed hexagonal faces. Crystals aligned with their hexagonal faces oriented perpendicular to the direction of incidence of cross-polarized light became extinct indicating that the expressed faces were normal to the isotropic calcite $\underline{c}$ axis. The proportion of fully developed hexagonal faces of crystals increased, as the concentrations of lithium in the solution were increased. When the [Ca] : [Li] in the mother solution was in the ratio of 1:2, the majority of the crystals had developed triangular (00.1) faces of calcite (Fig. 6.4). As the concentration was increased to [Ca] : [Li] = 1:20, the triangular faces were changed and the truncation of all six {10.4} faces resulted in hexagonal tabular crystals (Fig.6.5). Furthermore, when the crystals were allowed to grow for 44 hours almost all the crystals were fully developed hexagonal calcite. This shows that the crystal growth process is constant through the crystallization period. In general, the (00.1) faces were smooth, but unlike the {10.4} faces they contained surface steps. In some crystals particularly at higher lithium concentrations the stepping resulted in a depressed central region of the (00.1) face indicating that the effect of lithium in inhibiting crystal growth perpendicular to the $\underline{c}$ axis was more pronounced in the centre of the crystal face than at the edges. When

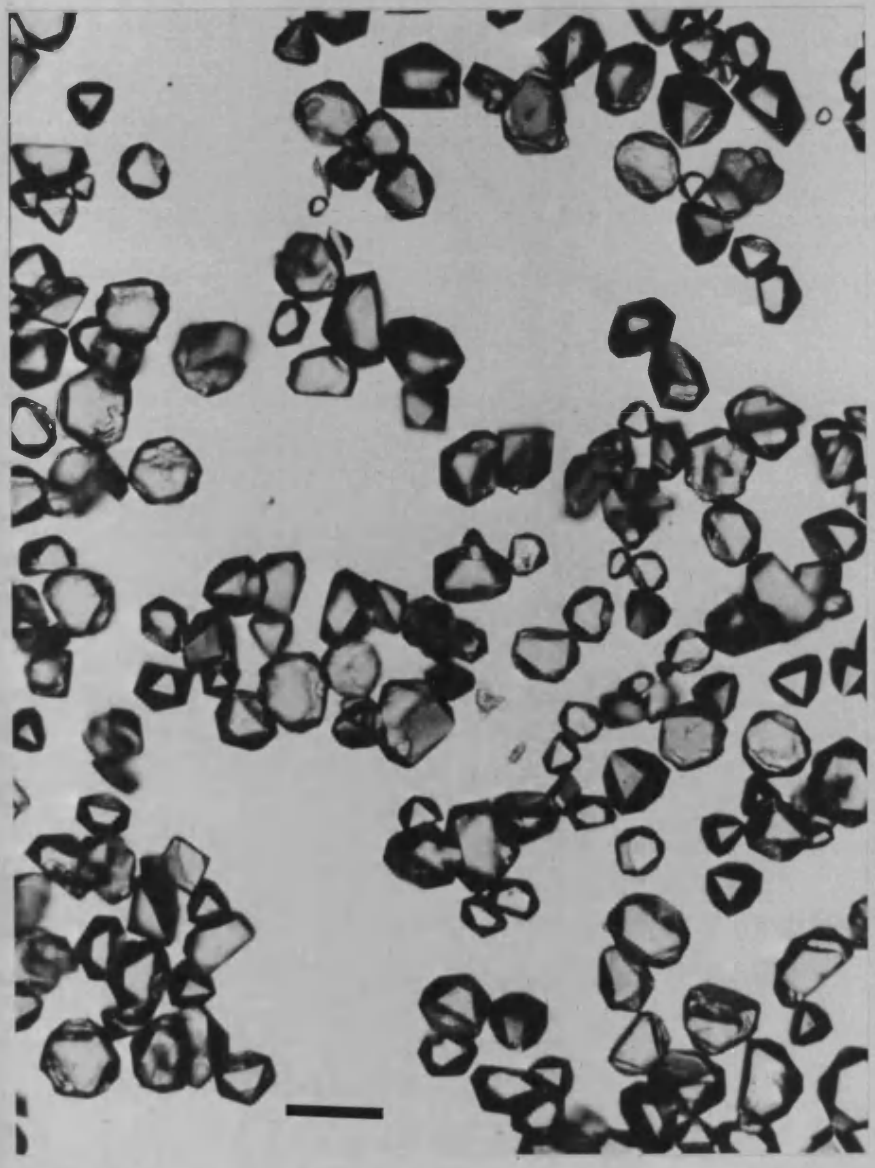

FIG. 6.3: OPTICAL MICROGRAPH OF CALCITE CRYSTALS GROWN IN THE PRESENCE OF LITHIUM IONS. THE NORMAL RHOMBOHEDRAL {10.4} MORPHOLOGY IS MODIFIED BY THE Li^+, PROMINANT HEXAGONAL (00.1) FACES ARE OBSERVED ON THESE CRYSTALS. THE CRYSTALS WERE WASHED WITH DISTILLED H_20 PRIOR TO ANALYSIS. [Ca]:[Li] = 1:20. [Ca] = 0.01 M. (Scale bar = 50 µm)

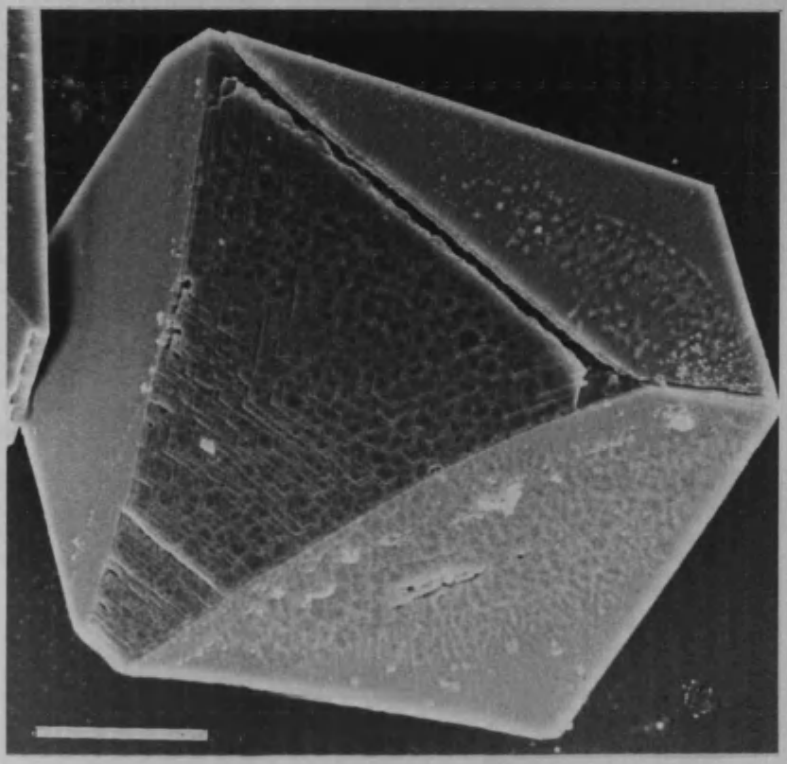

FIG. 6.4: SEM MICROGRAPH SHOWING THE DEVELOPMENT OF THE (00.1) FACES OF CALCITE GROWN IN THE PRESENCE OF LITHIUM. [Ca]:[Li] = 1:2. (Scale bar = 20 μm)

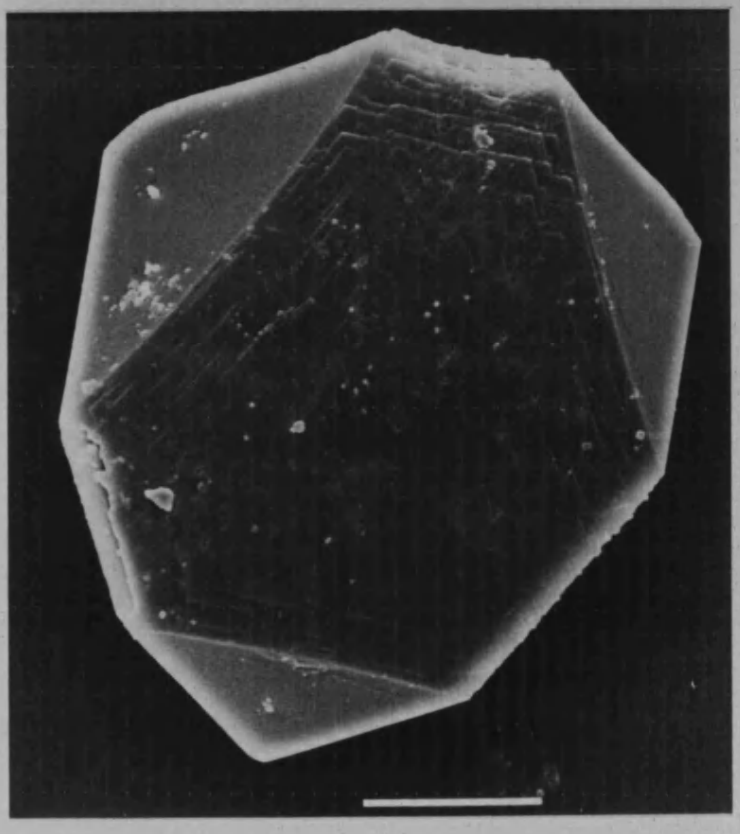

FIG. 6.5: SEM MICROGRAPH SHOWING A FULLY DEVELOPED (00.1) FACE OF CALCITE GROWN IN THE PRESENCE OF LITHIUM. [Ca]:[Li] = 1:20. [Ca] = 0.01 M. (Scale bar = 10 μm)

the lithium concentration was increased to [Ca] : [Li] = 1:40 aggregates of hexagonal calcite crystals were observed (Fig.6.6). Further, the atomic absorption spectrophotometeric analysis showed the presence of 0,06 mole % of lithium in the calcite crystals.

IR spectra of calcite crystals collected from pure control experiments and crystals grown in presence of [Ca] : [Li] = 1:20 showed some features (Figs. 6.7 and 6.8). First of all, the spectrum was highly resolved for the crystals grown in presence of Li. Secondly, pure control crystals had absorption peaks typical of calcite crystals (see section 3.3). But for crystals grown in the presence of Li, the peak at 1374cm^{-1} was very weak and at 1439cm^{-1}, it was noticeably sharper. Furthermore, the peaks at 1014cm^{-1} were resolved clearly. Vaterite and Li_2CO_3 have absorption frequencies at 1452 cm^{-1} and 1475 cm^{-1} respectively but, these would be additional peaks with measurable intensities in the spectrum. These changes are insignificant and it was not possible to determine any distortion in the crystal lattice from these results. However, some observations giving a resolved spectrum with higher frequencies of disordered calcite in presence of ferric gel have been reported [213]. High resolution XRD analysis of $CaCO_3$ crystals grown in the absence of lithium and the surface and bulk crystals grown in presence of lithium at Ca : Li = 1 : 20 are shown in figures 6.9, 6.10 and 6.11. The intensities

FIG. 6.6 : CALCITE CRYSTALS GROWN AT HIGH CONCENTRATION OF LITHIUM. [Ca]:[Li] = 1:40. [Ca] = 0.01 M. (Scale bar = 10 μm)

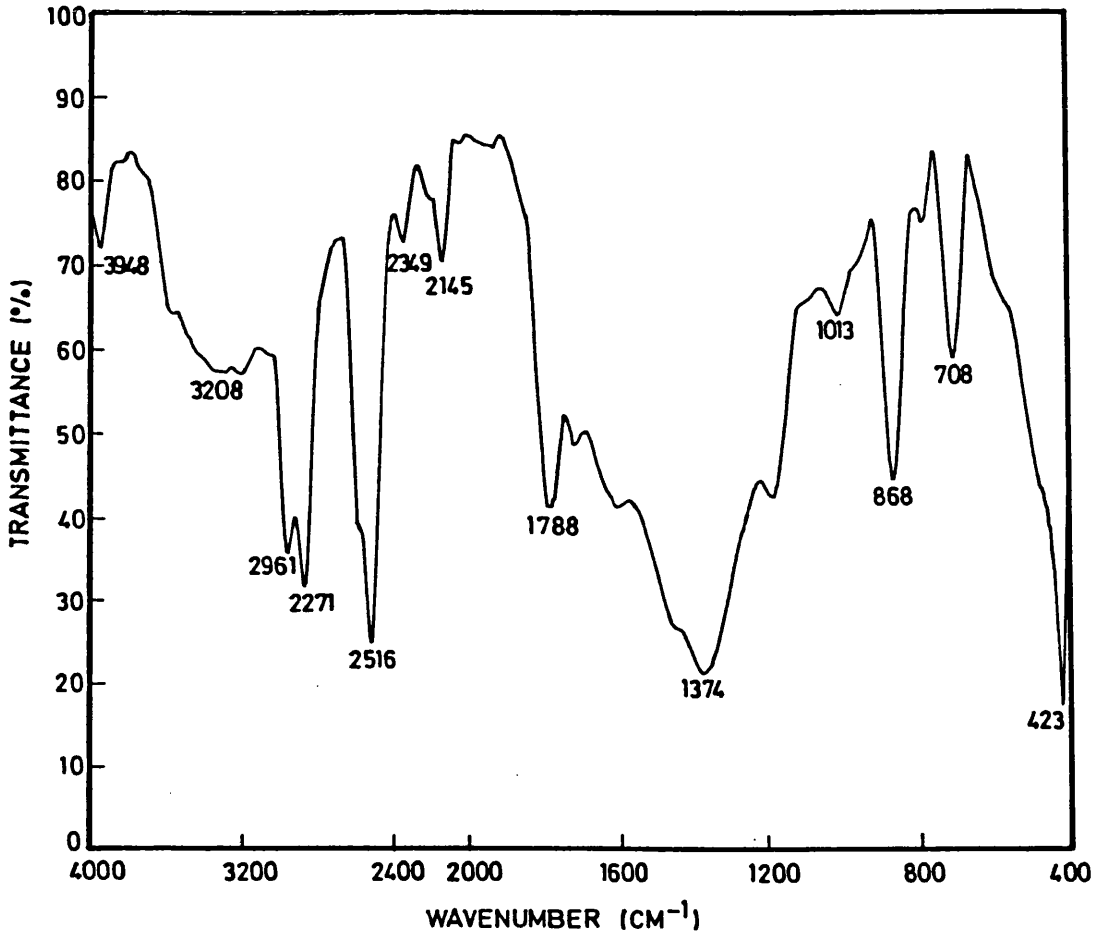

FIG. 6.7: INFRARED SPECTRUM OF CALCITE CRYSTALS GROWN IN THE ABSENCE OF ADDITIVES.

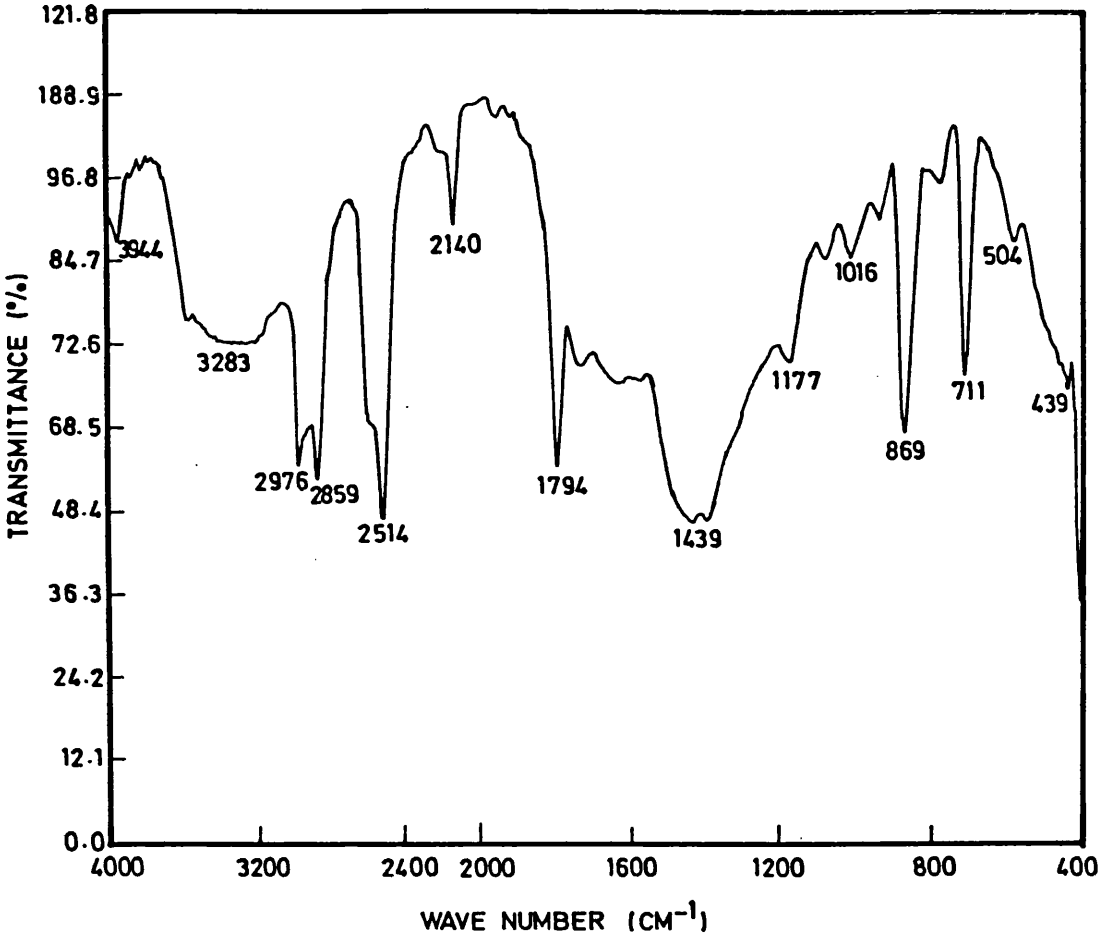

FIG. 6.8: INFRARED SPECTRUM OF CALCITE CRYSTALS GROWN IN THE PRESENCE OF LITHIUM.

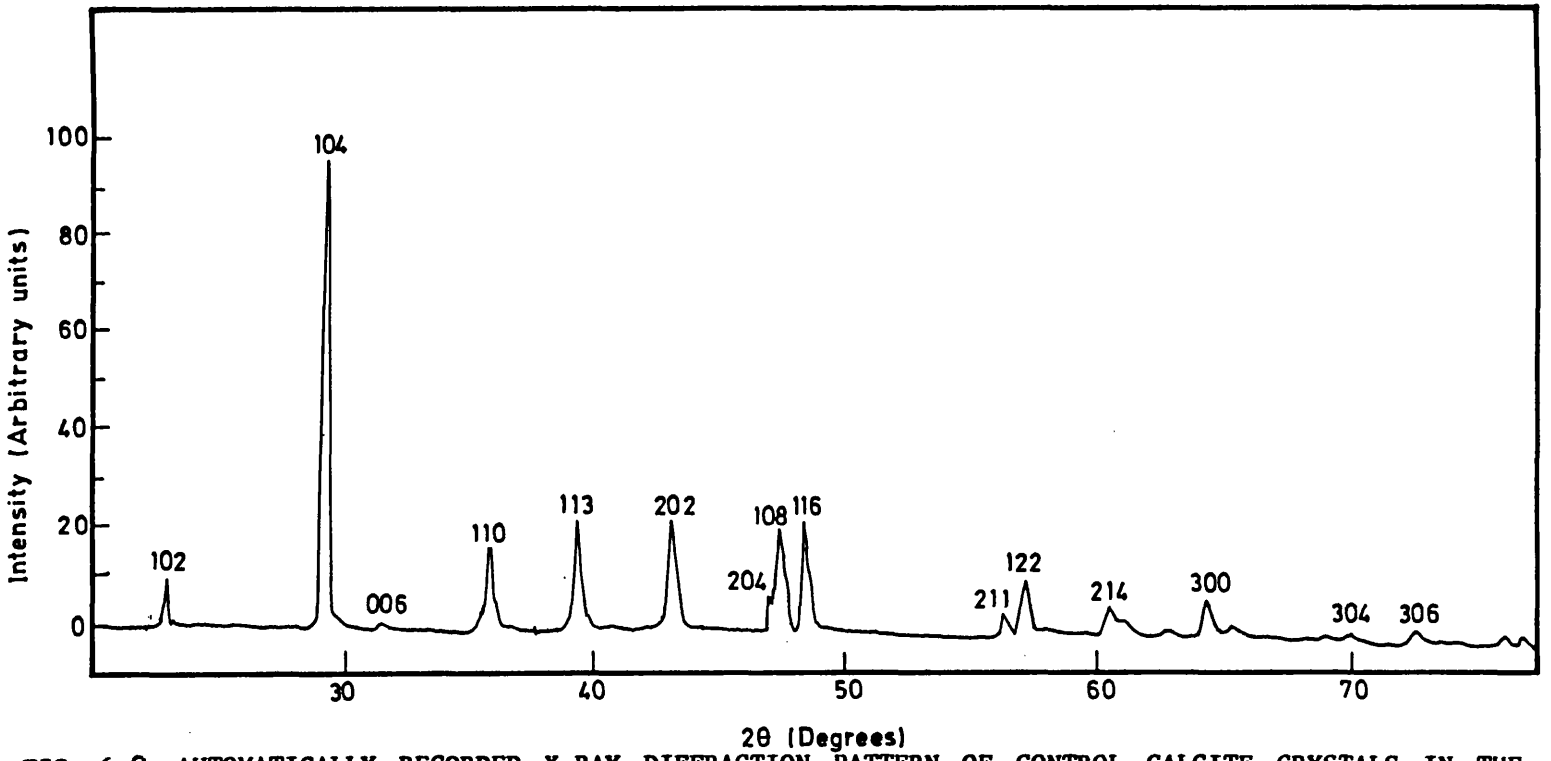

FIG. 6.9: AUTOMATICALLY RECORDED X-RAY DIFFRACTION PATTERN OF CONTROL CALCITE CRYSTALS IN THE ABSENCE OF ADDITIVES (CuK_{α} RADIATION AND NICKEL FILTER WERE USED).

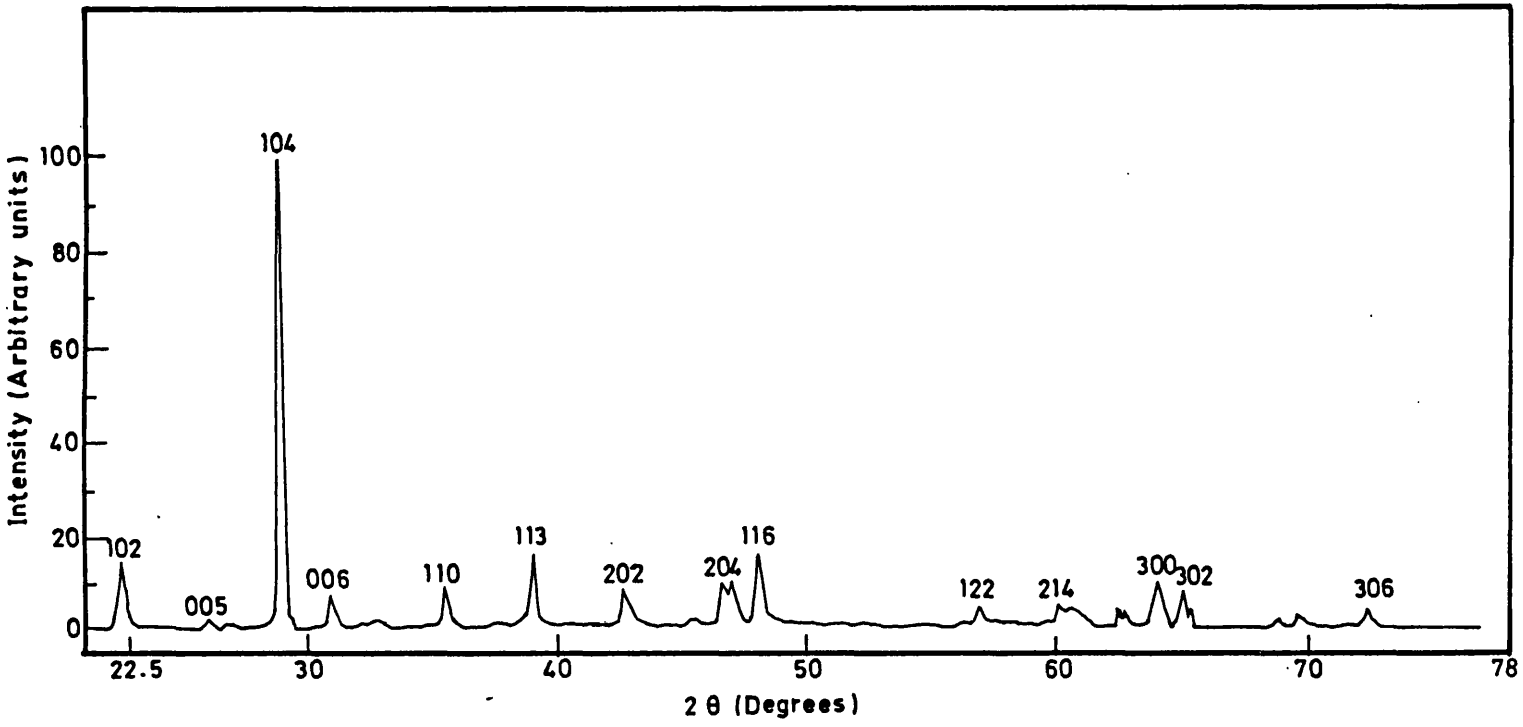

FIG. 6.10: XRD PATTERN OF CALCITE CRYSTALS GROWN IN THE PRESENCE OF LITHIUM. CRYSTALS WERE COLLECTED FROM THE SURFACE (CuK_{α}-RADIATION AND NICKEL FILTERS WERE USED).

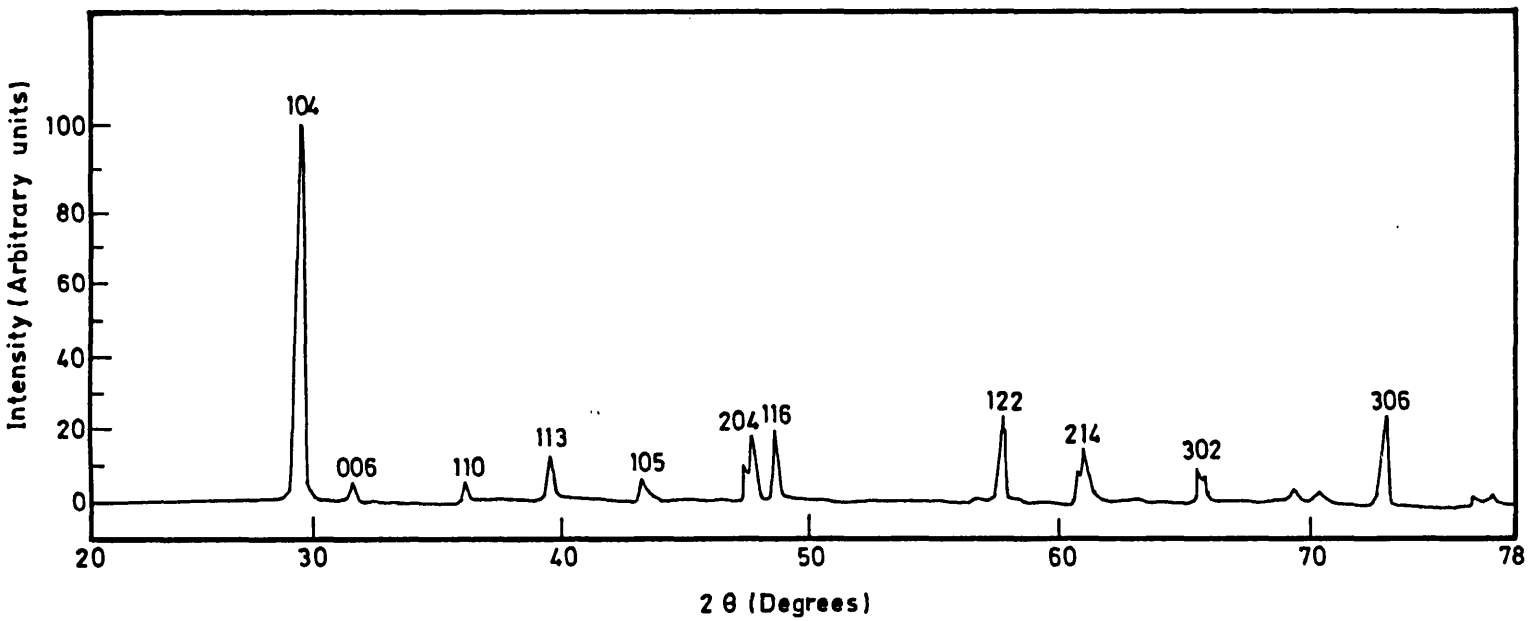

FIG. 6.11: XRD PATTERN OF CALCITE CRYSTALS GROWN IN THE PRESENCE OF LITHIUM. CRYSTALS WERE COLLECTED FROM THE BULK OF THE SOLUTION (CuK_{α}-RADIATION AND NICKEL FILTERS WERE USED).

of peaks corresponding to (hkl) planes of the crystal were different between the control crystals and crystals grown in the presence of lithium. The main peak intensity values corresponding to specific (hkl) planes are given in table 6.3. The values clearly show differences between normal control and lithium control crystals and show a general trend of decrease in intensity value from pure control crystals. However, the intensity values corresponding to (00.6) plane has increased. Further, the values of (10.2), (30.6), (20.4), (30.0) planes remained nearly equal.

The changes in line intensities could have been caused by the following factors; the surface roughness would have caused a change on relative line intensities (as occurs in the case of a coarse powder compact) and if the linear absorption coefficient was high, the intensities of low angle reflections would be abnormally low because of the absorption of the diffracted rays in each projecting portion of the surface. But in the present result, the reflection of (00.6) plane (low angle reflection) shows 120% increase in the intesity value. This shows that more number of tabular crystals were preferentially oriented in the sample holder giving rise to the increase in the intensity of the (00.6) reflection. Thus, it indicates the presence of significant proportion of tabular crystals in the sample. The determination of the unit cell lattice parameters (Table.6.4) showed only very small deviations from the theoretical values. As there are theoretical values [159, 214] which show a deviation of 0.06 Å in c_{hex} unit cell dimensions, it is difficult to infer that the 0.026 Å deviation from control crystals to crystals grown in the presence of lithium is

Table 6.3: Intensity values of d-spacing lines of (hk.l) planes of calcite crystals grown in presence of lithium. (Maesurements made from X-ray diffraction) and CuK_{α} radiation was used.

(hk.l) Planes of Calcite crystals	% 'I' values Normal control crystals (I.C)	% 'I' values Lithium control (From surface.) crystals (I.Li)	(I.Li-I.C) / I.C % (ΔI %)
(10.2)	12.0	15.3	27.5
(00.6)	2.5	5.5	120.0
(11.0)	19.6	10.0	-49.0
(11.3)	25.5	14.8	-42.0
(20.2)	25.8	6.4	-75.5
(20.4)	9.0	8.0	-11.0
(10.8)	24.8	8.9	-64.0
(11.6)	27.5	10.5	-11.0
(21.1)	4.7	1.3	-72.0
(12.2)	12.5	4.0	-68.0
(21.4)	7.7	5.0	-35.0
(30.0)	10.0	10.0	-0.0
(30.6)	4.4	4.0	-9.0
(11.12)	3.4	1.6	-43.0

Intensity values of (10.4) planes were taken as standard as 100% and other values were calculated from that.

Table 6.4: Unit cell dimensions (in Å) of calcite crystals grown in the presence and absence of lithium.

Type of crystals formed	Hexagonal cell dimensions a_{hex}	c_{hex}
Calcite crystals (literature value)	4.990	17.061 (c/a = 3.419)
Calcite crystals (normal control)	4.990	17.070 (c/a = 3.421)
Calcite crystals (lithium control)	4.997	17.097 (c/a = 3.421)

significant. However, previous data [159] with magnesian calcite show that a change of 0.2% in the lattice constant is significant enough to show the presence of ≃ 2.5% of foreign ions that would have created a disordered lattice structure giving change in the lattice constant values. Our data show similarly a small change in lattice parameters (Table 6.4) indicating a possible presence of lithium on the crystal face. However, confirmation of these results requires more detailed data collection in these experiments.

6.3.2 Influence of sodium on the formation of crystals under stearic acid monolayers:

Calcium carbonate crystals grown under stearate monolayers in the presence of sodium were observed by optical microscopy. Crystals grown at 1:10 and 1:20 are shown in (Figs. 6.13. A,B & C). When compared to the number of oriented calcite crystals under acid monolayers in the absence of sodium the number of oriented crystals per unit area reduced gradually as the concentration of sodium increased. Figure 6.14 shows the reduction in oriented crystals as the concentration of sodium increased. Apart from reduction in the number of oriented crystal forms, the total nucleation density was also reduced. However, there were no changes in the crystallographic orientation, with the $(1\bar{1}.0)$ face aligned parallel to the monolayer surface. This reduction was significant even at [Ca] : [Na] = 1:10, although at [Ca] : [Na] = 1:40 there were still some oriented crystals formed. Hence, sodium ions did not change the orientational effect of stearate monolayers on $CaCO_3$ nucleation, but reduced

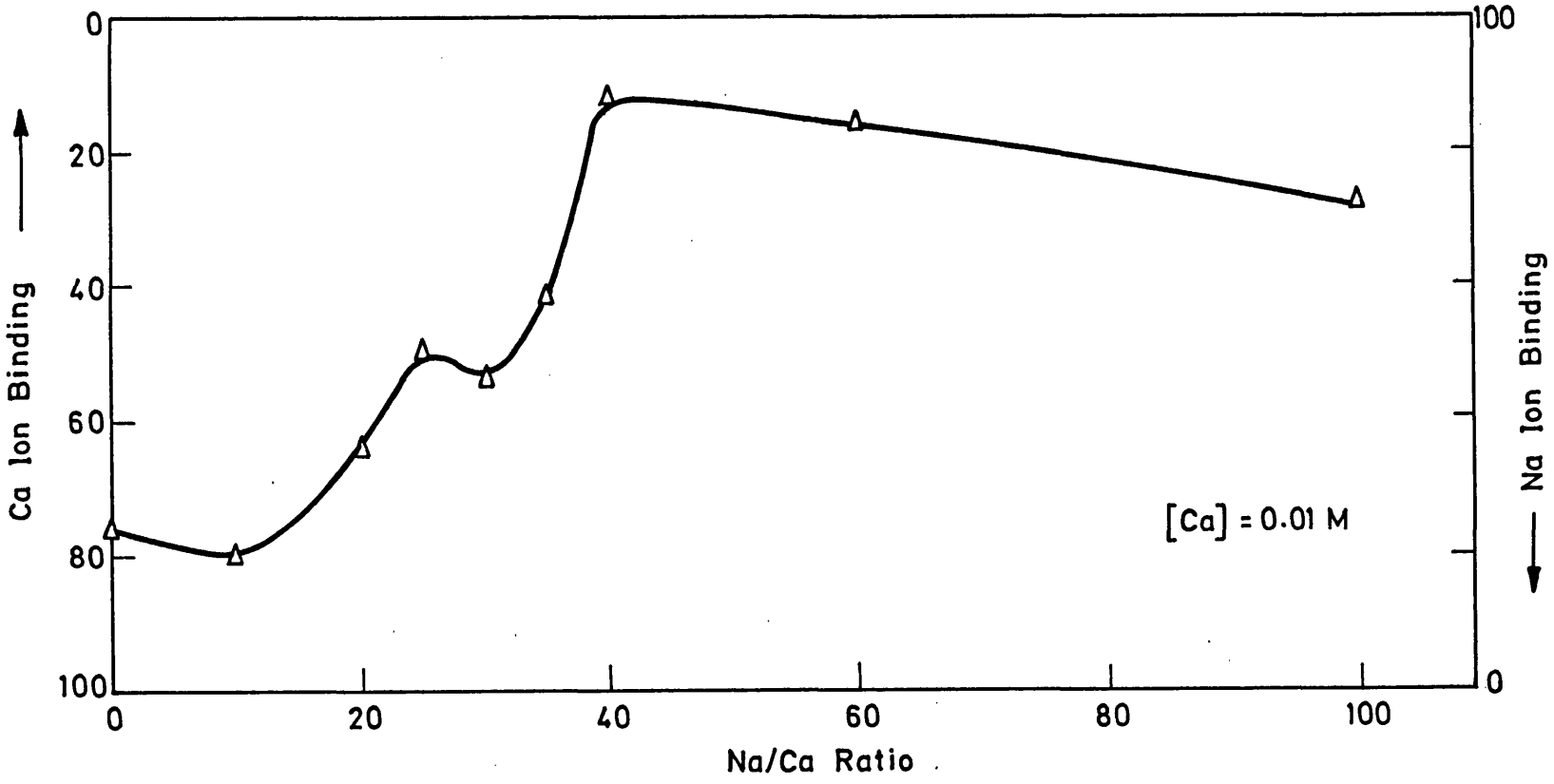

FIG. 6.12: DATA SHOWING THE BINDING RATIO OF Ca AND Na UNDER STEARIC ACID MONOLAYER (REPRODUCED WITH PERMISSION FROM Dr. S. ROSER). (See text page 314)

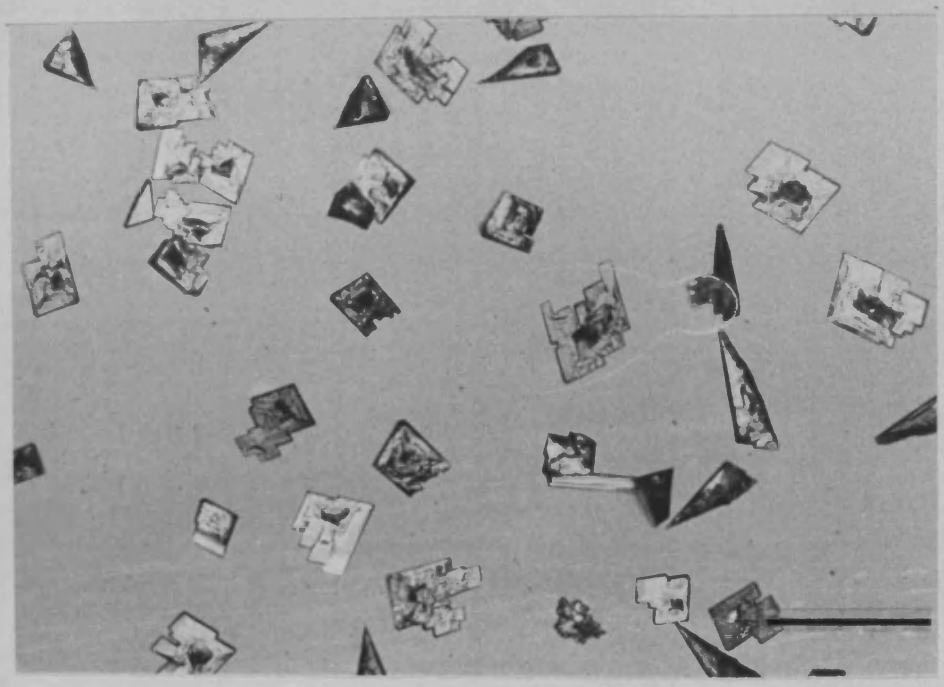

FIG. 6.13.(A). OPTICAL MICROGRAPH OF CRYSTALS GROWN UNDER STEARIC ACID MONOLAYER IN THE ABSENCE OF SODIUM IONS. (Scale bar = 100 μm)

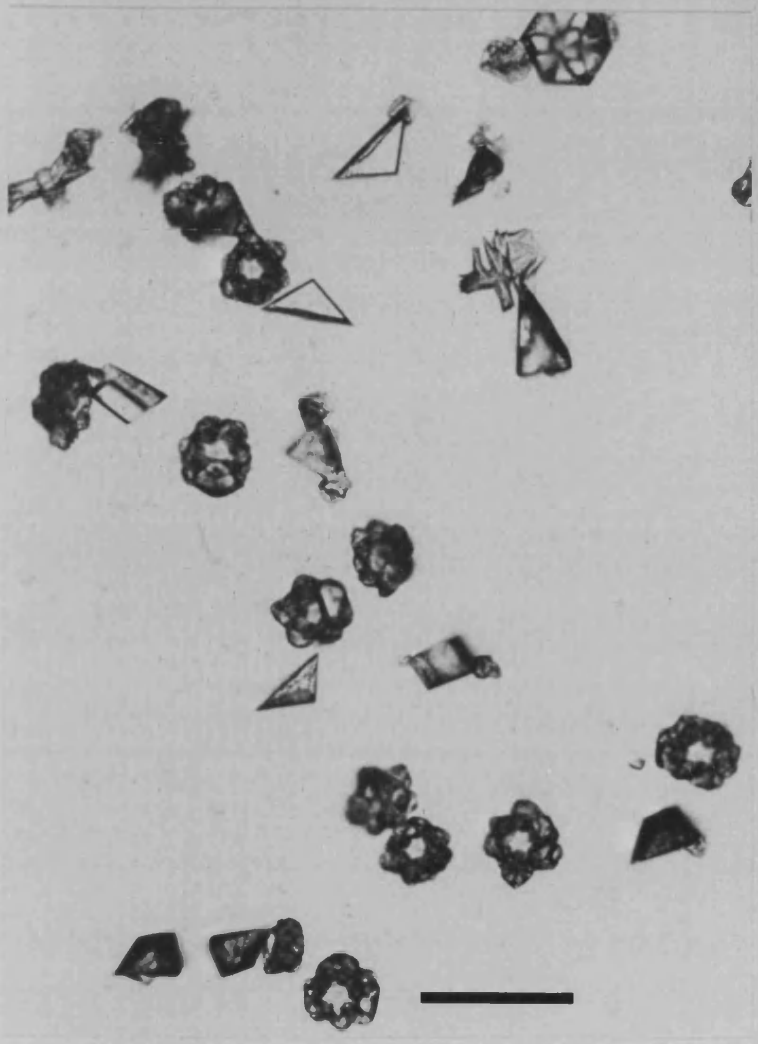

FIG. 6.13.(B). OPTICAL MICROGRAPH OF CRYSTALS GROWN UNDER STEARIC ACID MONOLAYER IN THE PRESENCE OF SODIUM IONS. [Na] = 0.1 M. [Ca]:[Li] = 1:10
(Scale bar = 100 μm)

FIG. 6.13.(C). OPTICAL MICROGRAPH OF CRYSTALS GROWN UNDER STEARIC ACID MONOLAYER IN THE PRESENCE OF SODIUM IONS. [Na] = 0.2 M. [Ca]:[Li] = 1:20
(Scale bar = 100 μm)

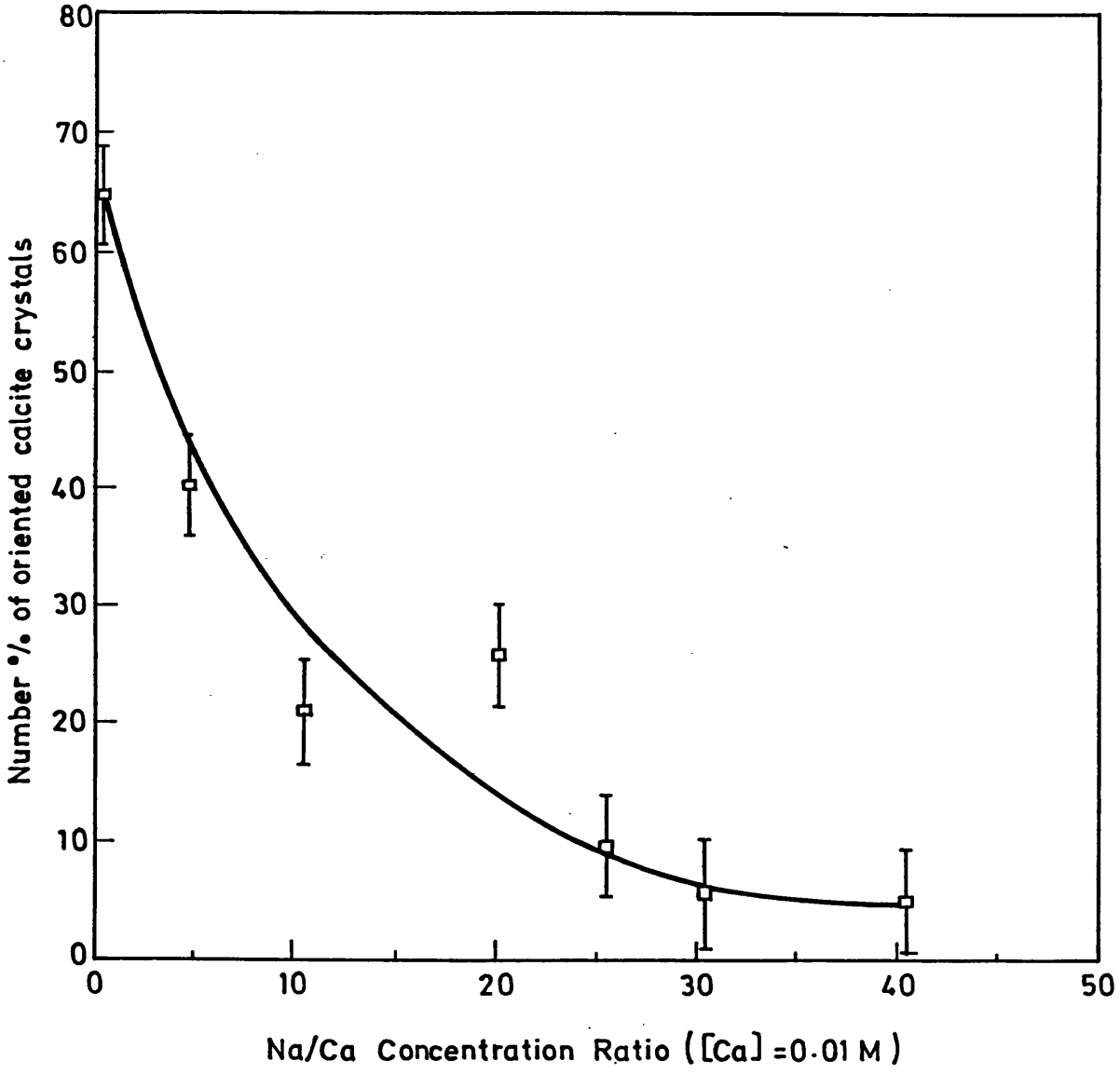

FIG. 6.14: GRAPH SHOWING THE INFLUENCE OF SODIUM IONS ON ORIENTED CALCITE CRYSTALS GROWN UNDER ACID MONOLAYER.

the total nucleation density of the crystals and increased the proportion on non-oriented crystals. Similarly, the small number of vaterite crystals formed in presence of sodium were not changed in their hexagonal morphology. Their sizes were reduced and the number of crystals formed were decreased (Fig. 6.15) as the concentration of sodium increased.

6.3.3 **Influence of lithium on oriented crystallization of $CaCO_3$ under stearic acid monolayer:**

Crystallization of $CaCO_3$ under a stearate monolayer in the presence of lithium gave similar effects as for Na except that the (11.0) face oriented calcite crystallization contained truncated (00.1) faces.

At low concentrations of lithium (Ca : Li = 1 : 2) the influence of lithium was not noticed on the morphological nature of the crystals. Calcite crystals formed were oriented on their $(1\bar{1}.0)$ faces. However the number of oriented crystals was reduced as the concentration of lithium increased. Furthermore as the concentration of lithium increased to [Ca] : [Li] = 1:10 the development of truncated (00.1) faces on the oriented calcite crystals were noticed (Fig.6.16). An interesting feature in these crystals was that the calcite crystals showed the specific $(1\bar{1}.0)$ orientation due to the interaction of the monolayer, and were aligned parallel to the monolayer surface, with the truncated (00.1) face developed in a perpendicular direction to the monolayer surface (Fig.6.17). This

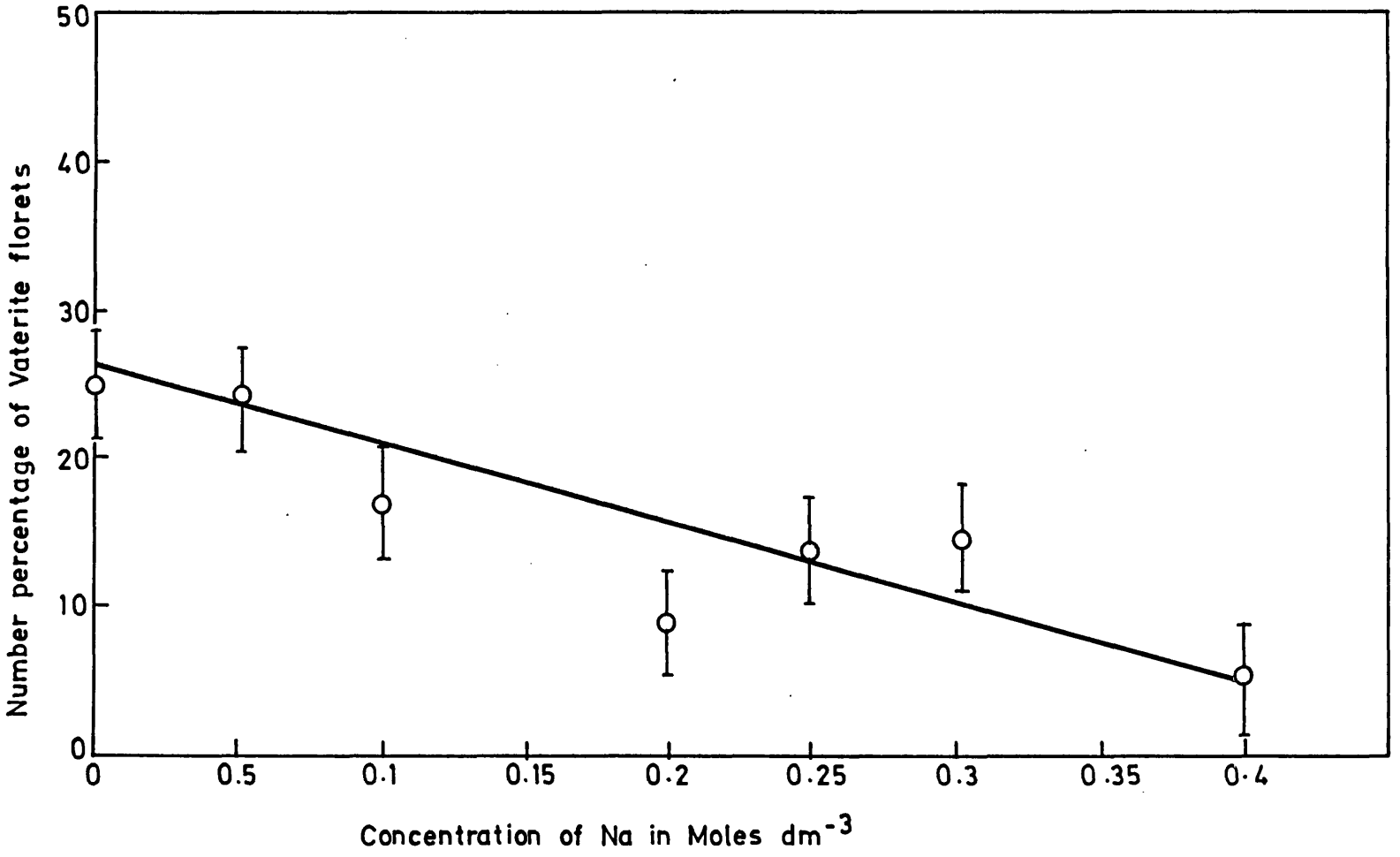

FIG. 6.15: GRAPH SHOWING THE PRESENCE OF SODIUM IONS ON ORIENTED VATERITE CRYSTALS GROWN UNDER STEARIC ACID MONOLAYER.

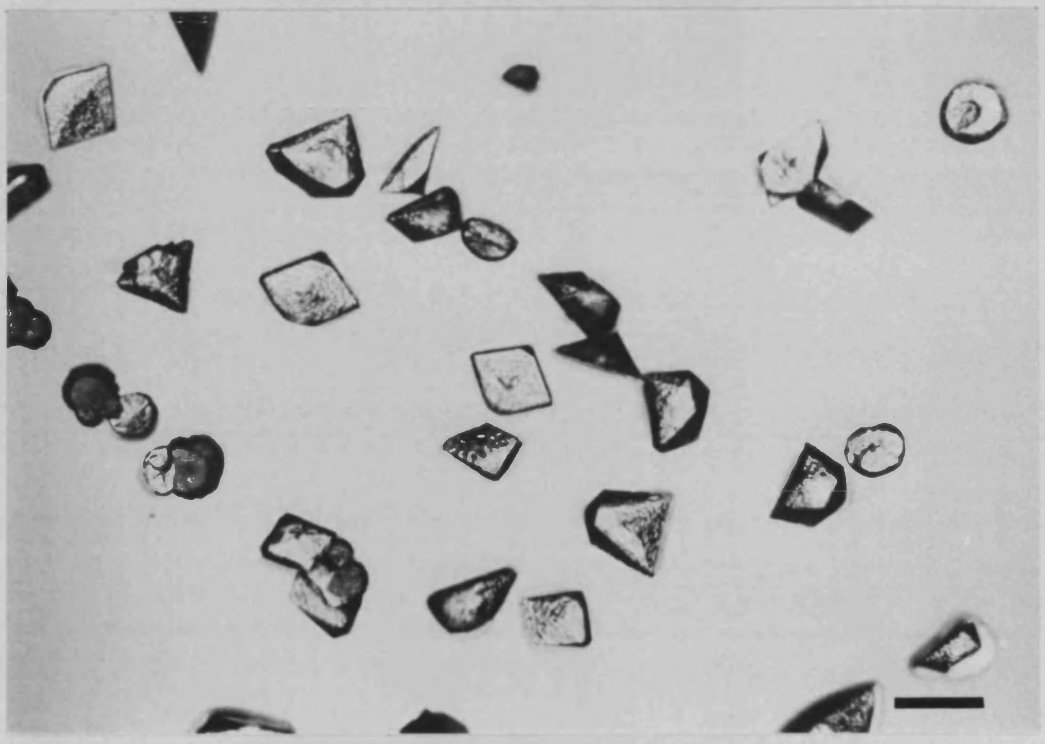

FIG.6.16. OPTICAL MICROGRAPH OF CRYSTALS GROWN UNDER STEARIC ACID MONOLAYER IN THE PRESENCE OF LITHIUM. CRYSTALS SHOW THE SURFACE ROUGHENING AND THE CENTRAL ELEVATION. NOTE THAT MANY CRYSTALS ARE ORIENTED AND THE SMALL TRUNCATED (OO.1) FACES ALIGNED PARALLEL TO THE VIEW DIRECTION. (Scale bar = 100 μm)

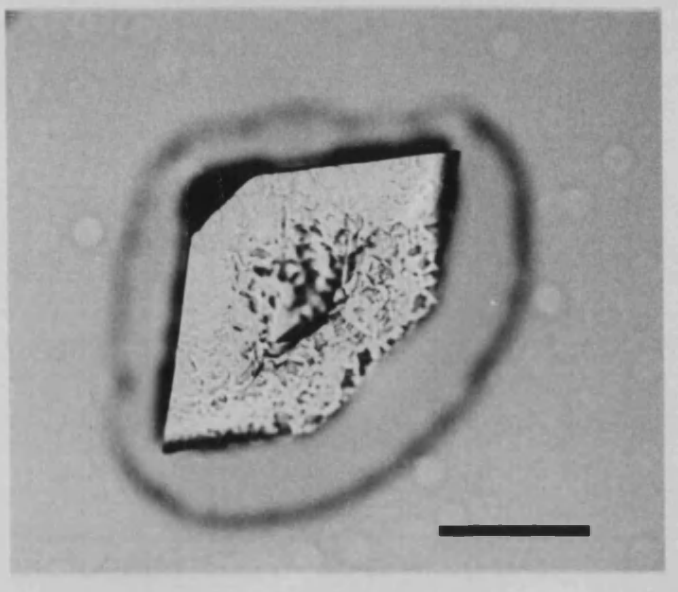

FIG. 6.17: THE DEVELOPMENT OF A TRIANGULAR (00.1) FACE EFFECTED BY LITHIUM IS CLEARLY SEEN AT THE EDGE OF AN ORIENTED CALCITE CRYSTAL. *THE RING AROUND THE CRYSTAL IS A DRYING ARTEFACT*. (Scale bar = 50 μm)

indicated that the c axis was running nearly parallel to the monolayer surface. Furthermore, the roughness on the surface of the crystals specific to the monolayer interaction was clearly seen.

As the concentration of lithium was increased (e.g. Ca : Li = 1 : 10) a significant number of crystals showed the changes in the nature and type of crystals formed under the monolayer. As explained above, lithium favoured the development of (00.1) face of calcite, and stearate molecules favoured ($1\bar{1}.0$) face of calcite and both were noticed in the crystals formed. Furthermore, the reduction in total nucleation density of crystals and the decrease in the number of oriented crystals (Fig.6.18) as the Li concentration was increased were noticed (Fig.6.18). The figure shows the gradual decrease in the oriented calcite crystals that finally dropped down to 6% at [Ca]:[Li] = 1:20. However, the proportion of vaterite formed under the monolayer did not change much in the presence of lithium even though the amount of vaterite crystals formed is less when compared to calcite. Furthermore, the nucleation density and sizes of vaterite crystals were reduced as the lithium concentration increased. There were no orientational or morphological changes in the vaterite crystals formed. Comparitively lithium effect on oriented crystallization was observed at a low concentration ratio than with sodium.

6.3.4 Crystal growth studies of $CaCO_3$ under amine monolayer in presence of sodium: Crystals grown in the presence of sodium were not changed in structure and morphology compared with the vaterite crystals formed under the amine monolayer with no sodium. There were some subtle

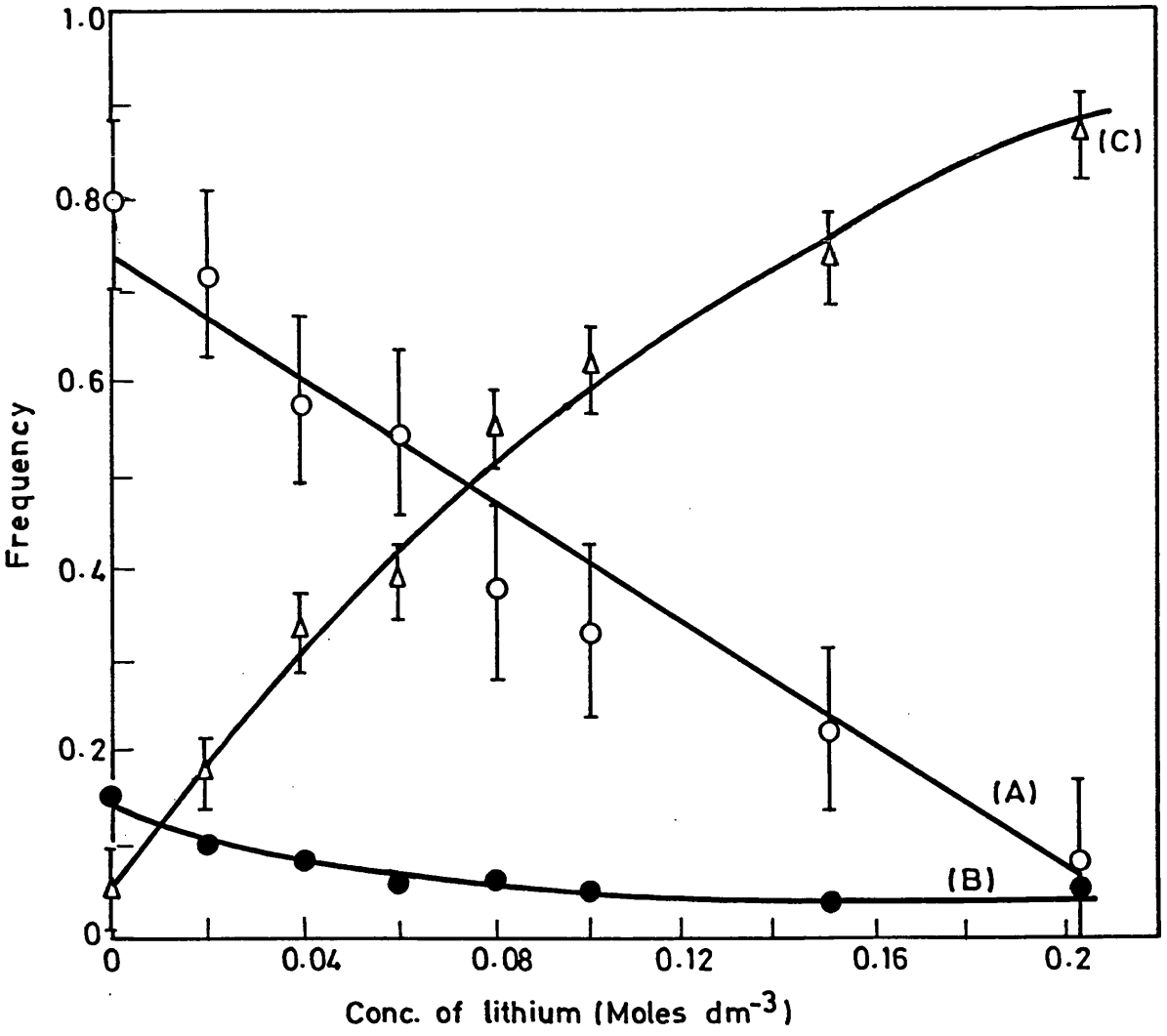

FIG. 6.18: FREQUENCY DISTRIBUTION OF TYPES OF CRYSTALS GROWN UNDER STEARIC ACID MONOLAYERS IN THE PRESENCE OF LITHIUM: (A) ORIENTED CALCITE CRYSTALS, (B) ORIENTED VATERITE CRYSTALS AND (C) NON-ORIENTED CALCITE CRYSTALS.

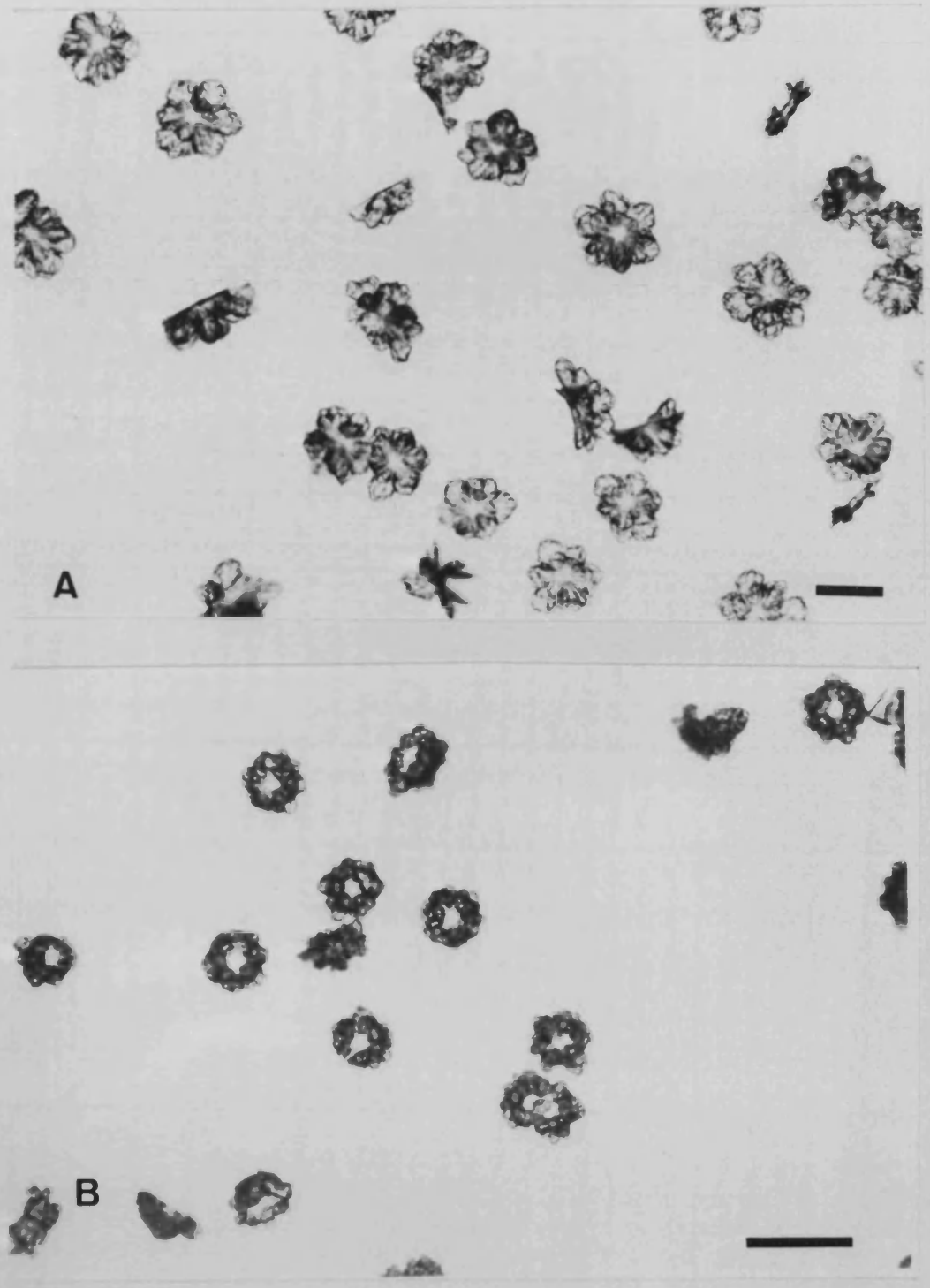

FIG. 6.19: OPTICAL MICROGRAPHS OF CRYSTALS GROWN UNDER AMINE MONOLAYERS:(A) CRYSTALS GROWN IN THE ABSENCE OF SODIUM, (B) CRYSTALS GROWN IN THE PRESENCE OF SODIUM. [Ca]:[Na] = 1:6. [Ca] = 0.01 M. (Scale bars = 100 μm)

differences in morphology (Fig 6.19 A and B). Nucleation density was reduced as the concentration of sodium was increased. The presence of sodium changed the complexity of the morphological form and the dendritic nature of the oriented crystals. Sizes of the crystals were also reduced. Figure 6.20 show the two types of crystals grown in presence of sodium under the monolayer. The distribution of vaterite type I crystals decreased predominantly. After [Ca] : [Na] = 1 : 20, there were no further changes (Fig. 6.21). The frequency distribution of type II crystals showed a similar trend and reduced to 5% at [Ca] : [Na] = 1 : 12 (Fig. 6.22). Further increase in the amount of sodium did not show any change in the density of vaterite type II crystals. A further noticeable difference was an increased appearance of non-oriented calcite crystals (Fig. 6.23). This indicates that the kinetic influence of the monolayer on vaterite nucleation was reduced and calcite crystals were formed in the bulk solution.

6.3.5 Crystal growth studies in presence of lithium under amine monolayers:

Crystallization of oriented vaterite formation under the monolayer was not affected at lower concentrations of lithium ([Ca]:[Li] = 1 : 4. The morphological type I and type II crystals were unchanged except that their sizes were reduced as the concentration of lithium increased. Furthermore, a secondary growth in vaterite crystals start to appear at [Ca] : [Li] = 1 : 10 (Fig. 6.24).

SEM micrographs showed no differences in the crystallographic orientation of the crystals with respect to the monolayer

FIG. 6.20: SEM MICROGRAPHS OF CRYSTALS GROWN UNDER AMINE MONOLAYER IN THE PRESENCE OF SODIUM. [Ca]:[Na] = 1:10. (A) VATERITE TYPE I CRYSTAL. (B) VATERITE TYPE II CRYSTAL. (Scale bars = 10 μm)

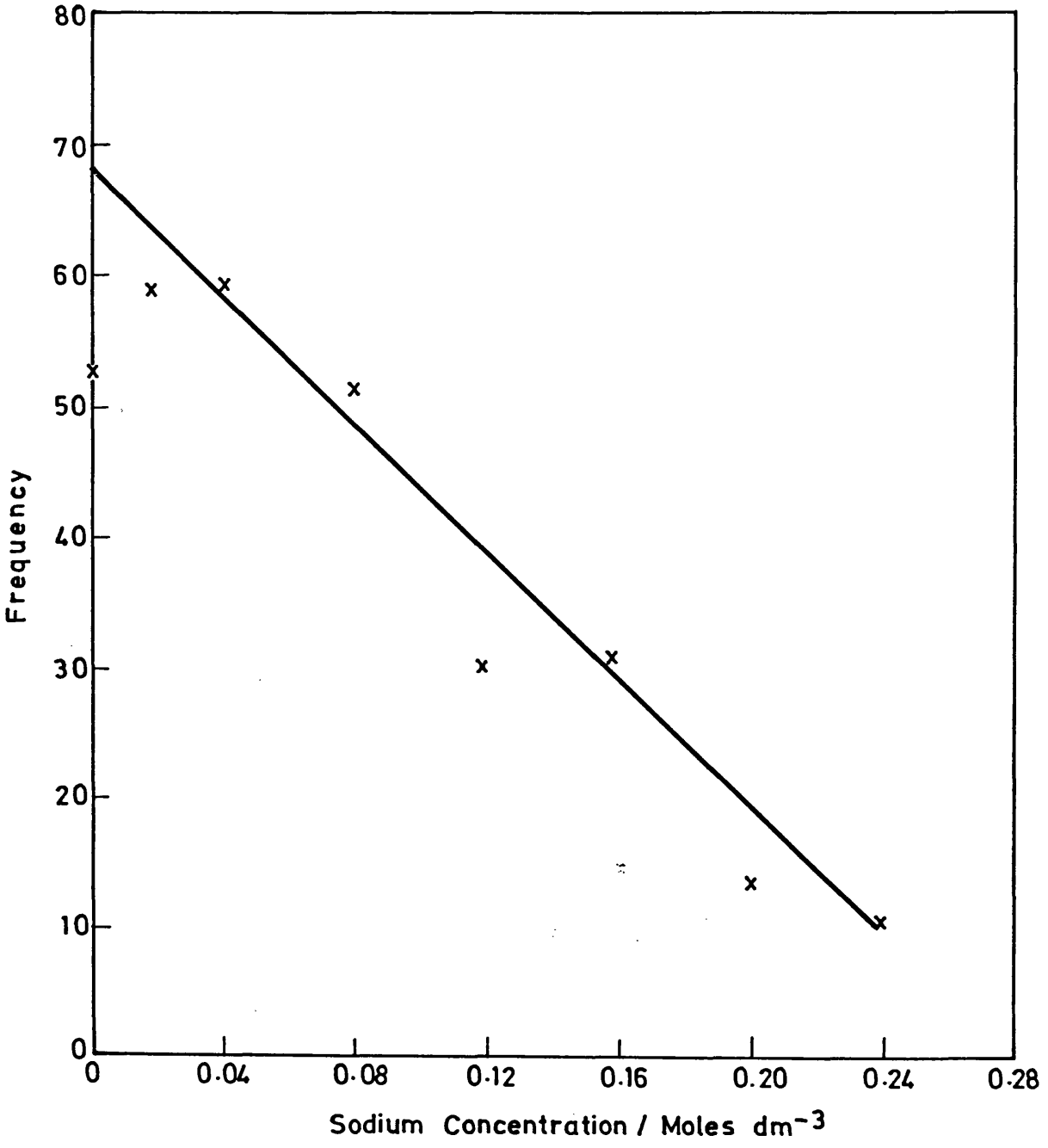

FIG. 6.21: FREQUENCY DISTRIBUTION OF ORIENTED VATERITE TYPE I CRYSTALS GROWN UNDER AMINE MONOLAYER IN THE PRESENCE OF SODIUM IONS.

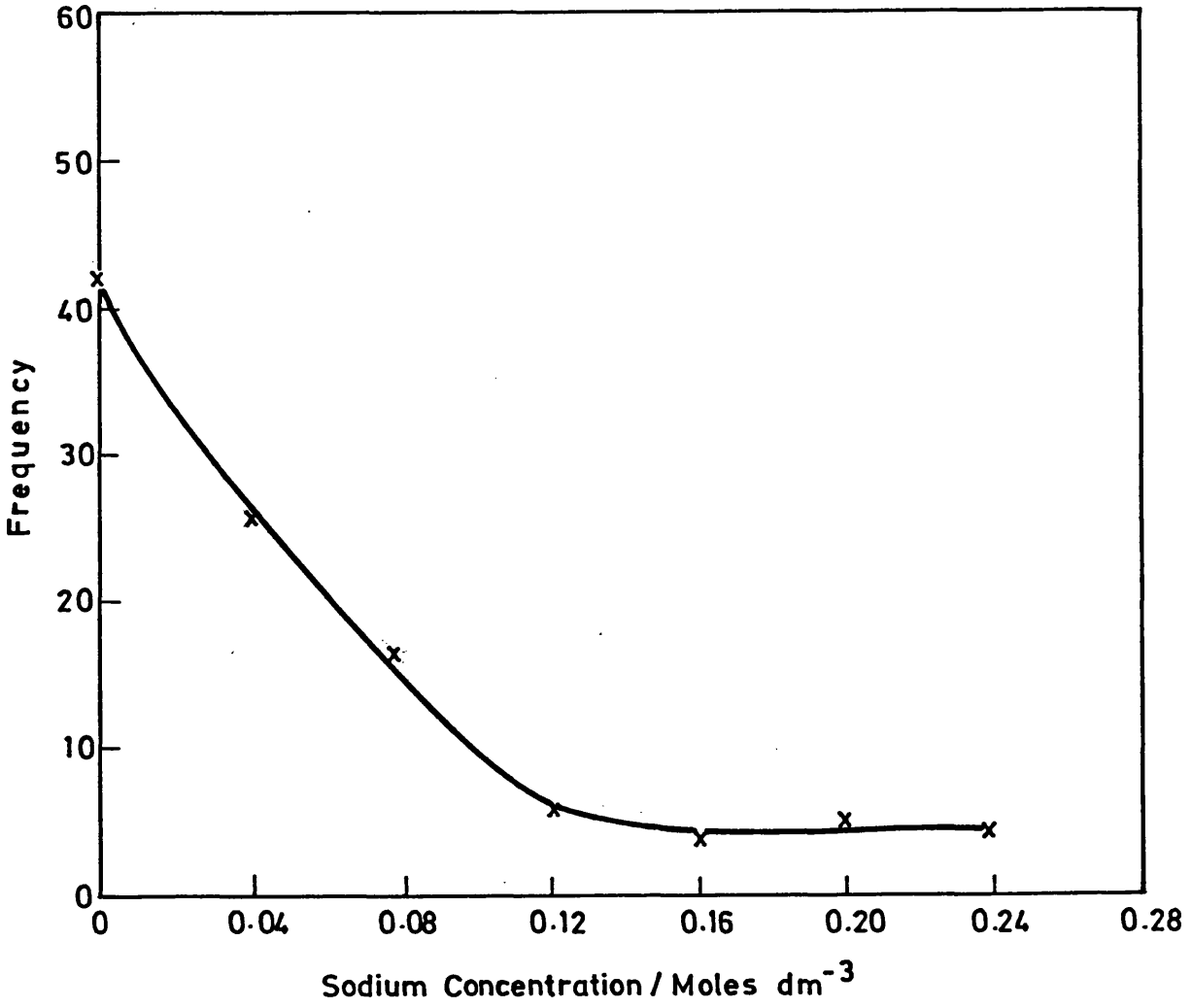

FIG. 6.22: FREQUENCY DISTRIBUTION OF ORIENTED VATERITE TYPE II CRYSTALS GROWN UNDER AMINE MONOLAYER INFLUENCED BY THE INCREASING CONCENTRATION OF SODIUM IONS.

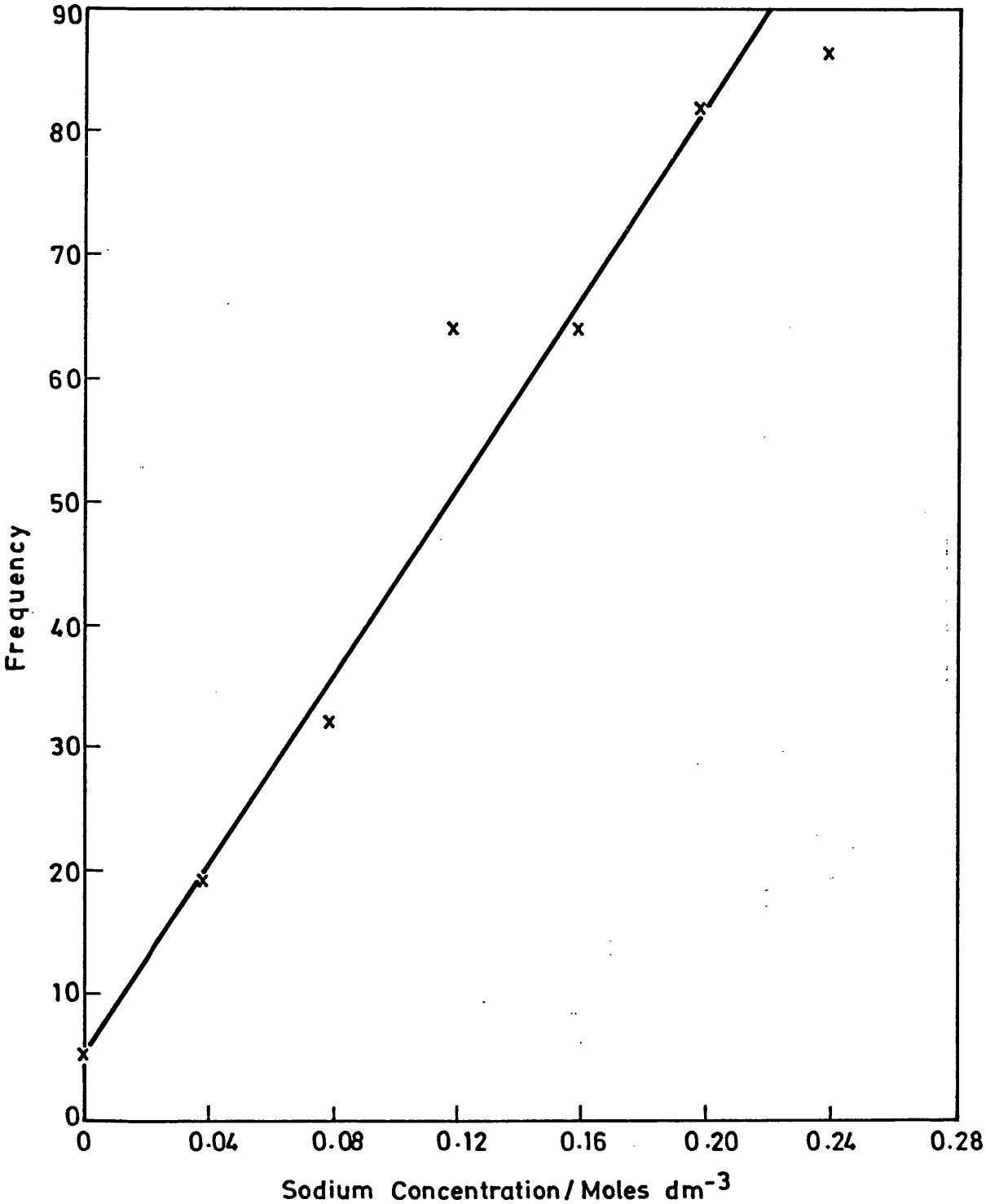

FIG. 6.23: FREQUENCY DISTRIBUTION OF NON-ORIENTED CALCITE CRYSTALS GROWN UNDER AMINE MONOLAYER IN THE PRESENCE OF SODIUM IONS.

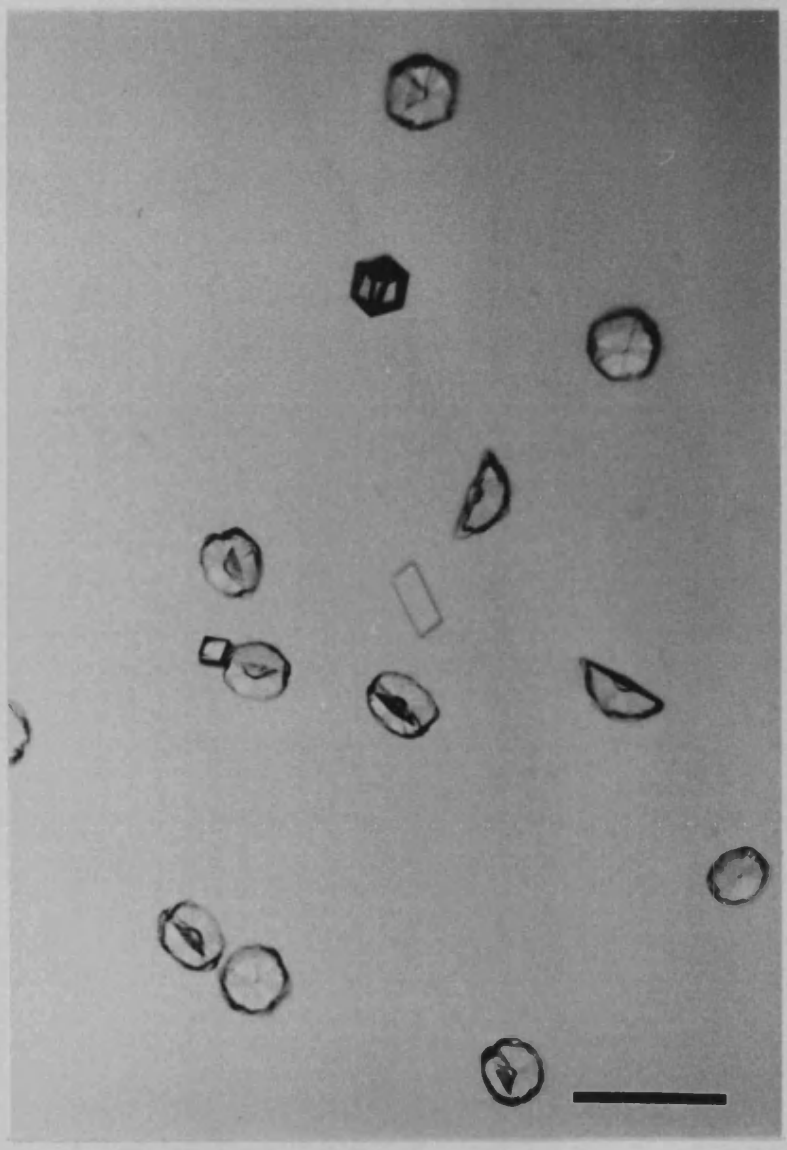

FIG. 6.24: VATERITE CRYSTALS GROWN UNDER AN AMINE MONOLAYER IN THE PRESENCE OF LITHIUM. SECONDARY GROWTH IS SEEN IN A SIGNIFICANT PROPORTION OF THE CRYSTALS. (Scale bar = 100 μm)

surface. Figures 6.25. A and B show the unaffected type I and type II crystals grown under amine monolayer in presence of lithium at [Ca] : [Li] = 1:10. Complex and dendritic nature is clearly reduced. Furthermore, some crystals showed a slight change in morphology, due to secondary growth developed along a direction nearly perpendicular to the original crystal surface (Fig. 6.25.C).

An interesting observation, noticed as the concentration of lithium increased further to [Ca] : [Li] = 1 : 20 was that a change from vaterite formation to complete calcite nucleation occured. Crystals formed were different from normal rhombohedral crystals and were comparable to the morphology of crystals formed in the presence of lithium in control experiments (Fig. 6.26). Many crystals had developed partially and fully formed hexagonal faces of calcite crystals. Figure 6.27 shows the distribution of types of crystals grown under amine monolayer at increasing concentration of lithium. There was no evidence that the truncated calcite crystals were oriented under the monolayer.

In summary the results showed that an increase in ionic strength of the solution by adding sodium or lithium disrupts the formation of oriented crystals. These reduced crystal nucleation by interfering with the arrangement of the Ca^{2+} and CO_3^{2-} ions to form the critical nucleus. The added ions also reduced the size and the density of oriented crystals formed. Furthermore, the important and interesting observation in the crystallization of $CaCO_3$ in the presence of lithium was the consistent

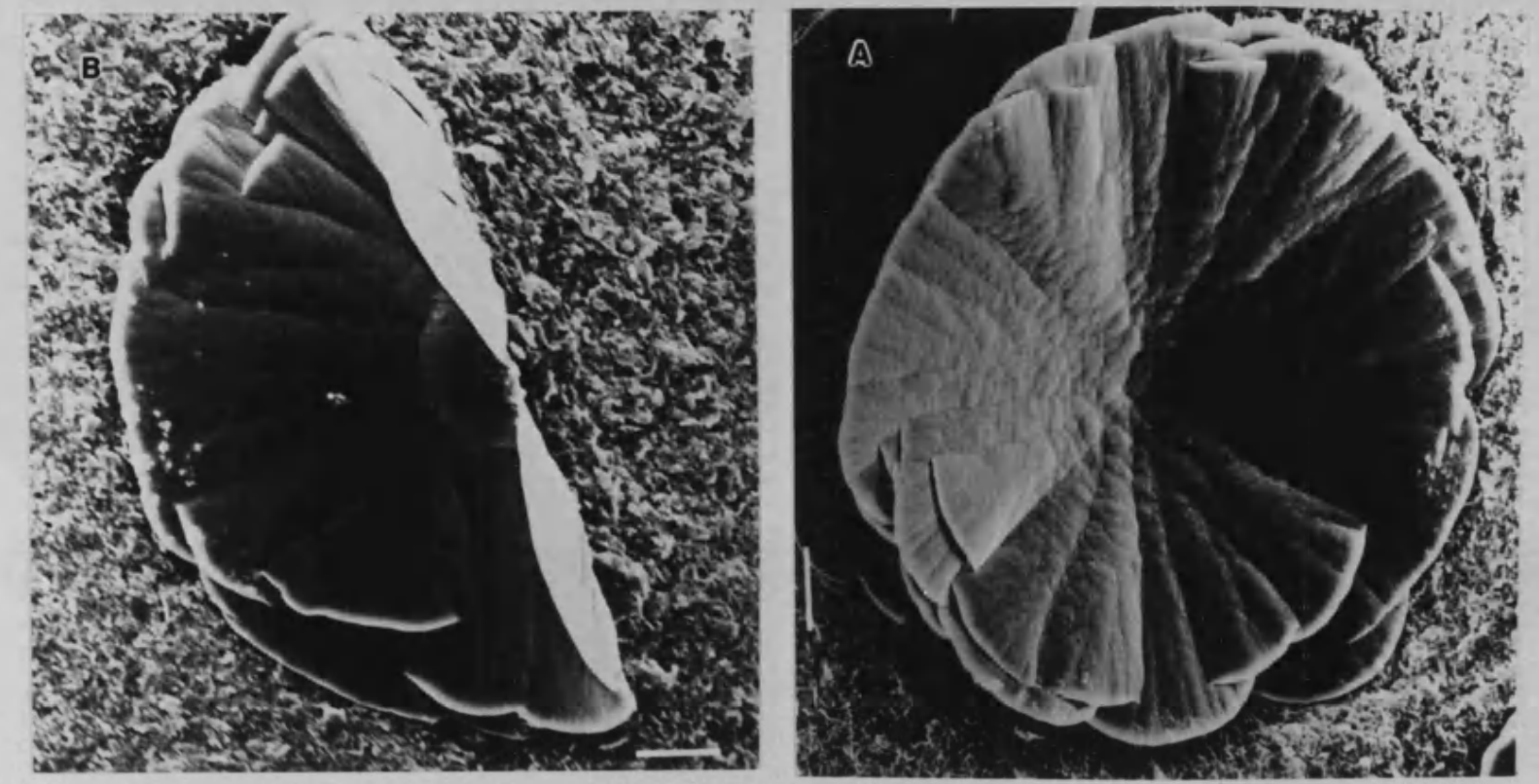

FIG. 6.25 (A) AND (B): SEM MICROGRAPHS OF MORPHOLOGICALLY UNAFFECTED TYPE I AND TYPE II VATERITE CRYSTALS GROWN IN THE PRESENCE OF LITHIUM AT [Ca]:[Li] = 1:10. (Scale bars = 10 μm)

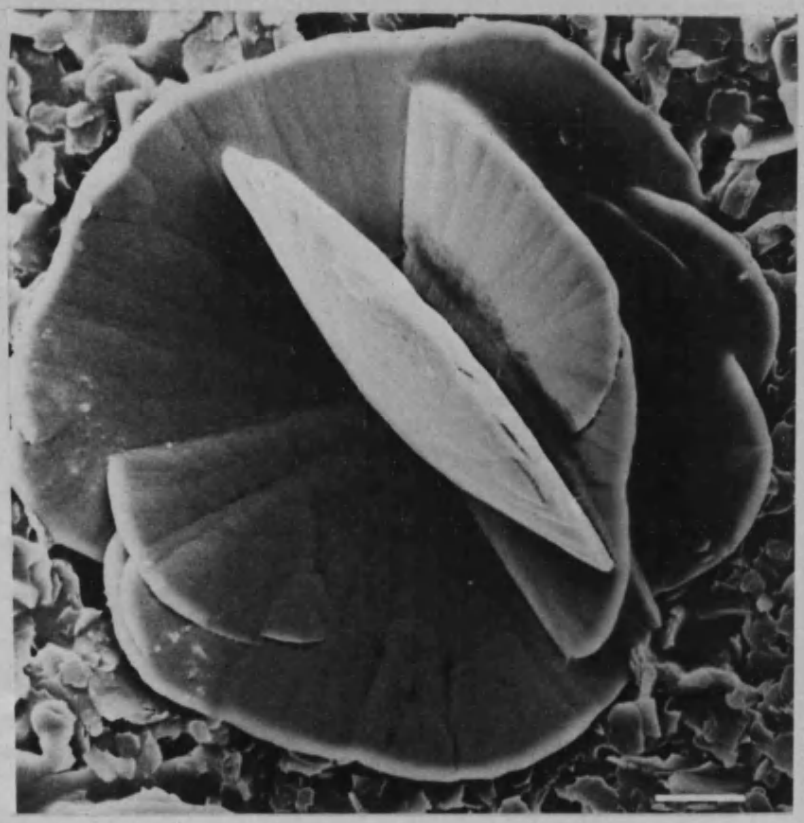

FIG 6.25 (C): SEM MICROGRAPH SHOWING THE EFFECT OF SECONDARY GROWTH UPON THE MORPHOLOGY OF THE VATERITE CRYSTALS. (Scale bar = 10 μm)

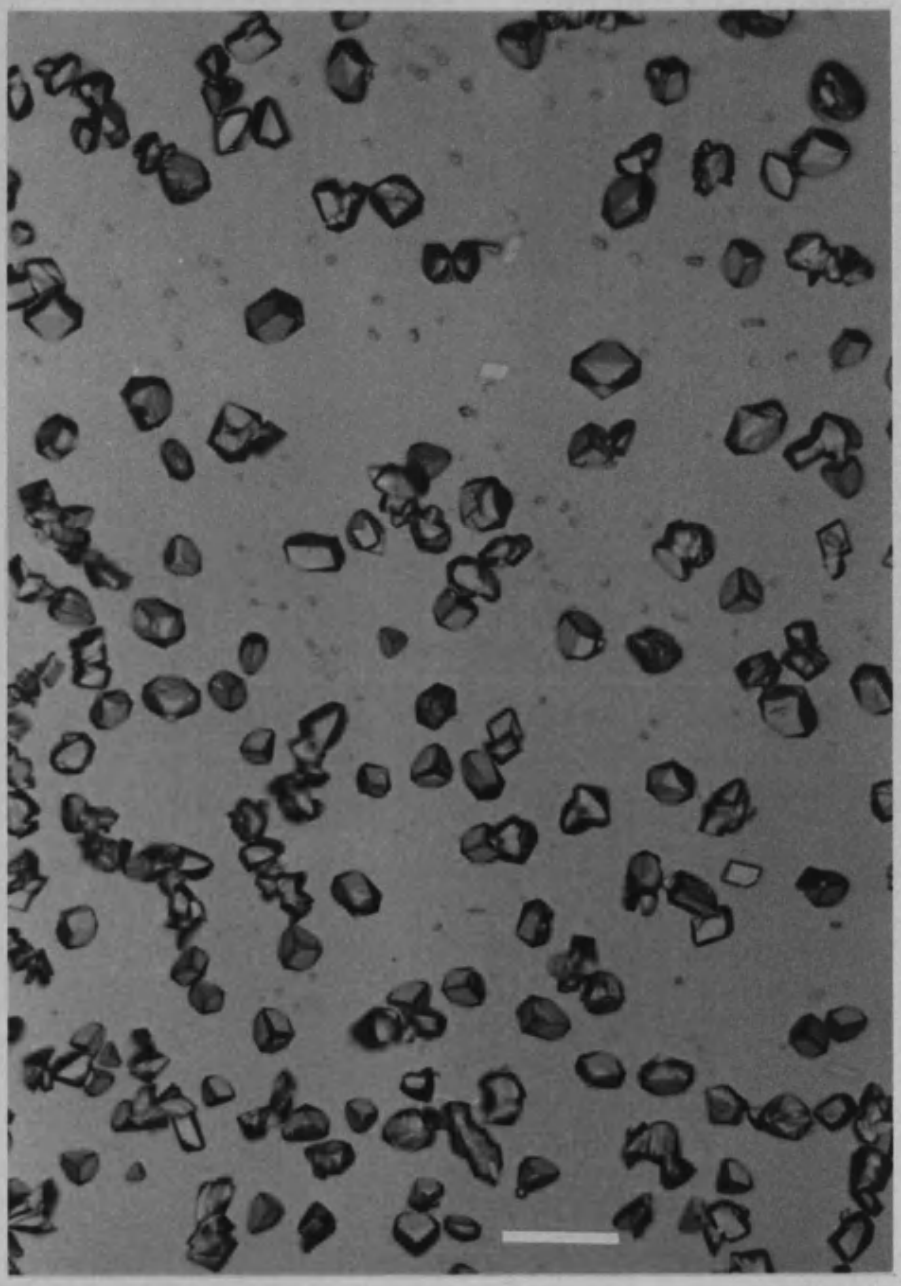

FIG. 6.26: OPTICAL MICROGRAPH OF CALCITE CRYSTALS FORMED UNDER AN AMINE MONOLAYER IN THE PRESENCE OF LITHIUM. [Ca]:[Li] = 1:20. [Li] = 0.2 M. THE MONOLAYER HAS NO EFFECT UPON $CaCO_3$ PRECIPITATION. THE CRYSTAL MORPHOLOGY IS INFLUENCED SOLELY BY THE PRESENCE OF LITHIUM. (Scale bar = 50 μm)

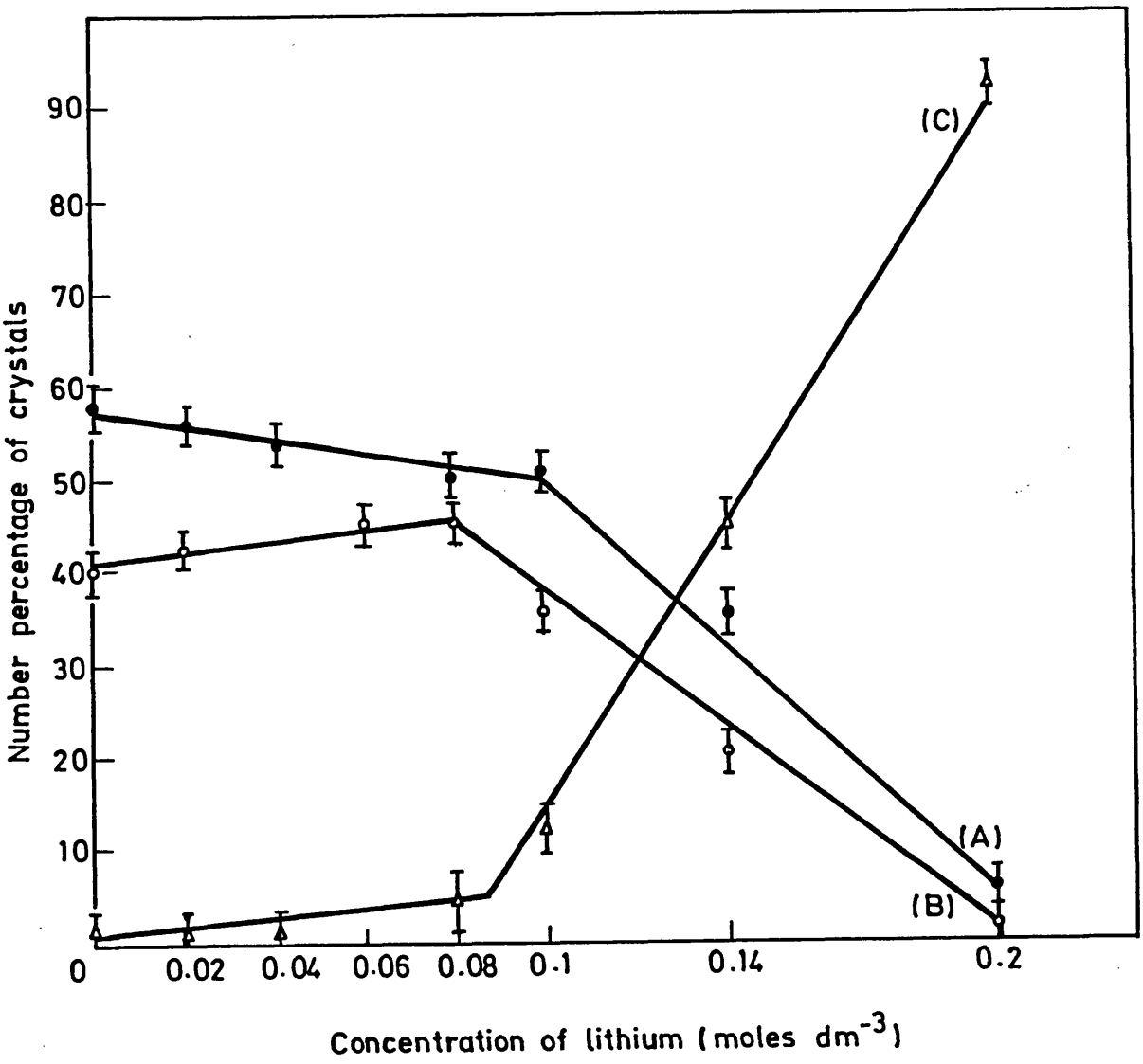

FIG. 6.27: FREQUENCY DISTRIBUTION OF THE TYPES OF CRYSTALS GROWN UNDER AMINE MONOLAYER IN THE PRESENCE OF LITHIUM: (A) VATERITE TYPE I CRYSTALS, (B) VATERITE TYPE II CRYSTALS AND (C) NON-ORIENTED CALCITE CRYSTALS. AS THE CONCENTRATION OF LITHIUM INCREASED, THE VATERITE NUCLEATION IS DIMINISHED.

formation of hexagonal (00.1) faces of calcite. This face is relatively unstable and generally not observed in synthetic calcite.

6.4 DISCUSSION:

From the above sections it is possible to infer that the chemical precipitation of $CaCO_3$ into its polymorphic and morphological forms from bicarbonate solution is greatly influenced by the presence of different ions on the surface and in the bulk solution. The understanding of the formation of the polymorphic and morphological types of $CaCO_3$ is important in terms of environmental and technological interest. Hence, it is vital to analyse the observations recorded in the above section. From the results three main conclusions can be drawn. (i) Lithium ions change the morphological type from normal rhombohedral (10.4) faces to the hexagonal (00.1) face of calcite crystals. (ii) Sodium and lithium ions reduced the number of oriented calcite crystals formed under a stearate monolayer and vaterite crystals formed under acid and amine monolayers; they increased the proportion of the non-oriented calcite crystals. (iii) Size and nucleation density of crystals formed under the monolayers were reduced, the complex and dendritic nature of the vaterite crystals changed and secondary growth of crystals appeared.

(i) Hexagonal calcite formation effected by lithium:

The (00.1) face of calcite is not generally expressed as the [00.1] direction is a fast growing direction. Along this direction alternate layers of calcium and carbonate are arranged in such a way that carbonate ions are in parallel arrangement to calcium ions. For this face to be expressed the fast growth should be slowed down in this direction.

This probably was effected by the specific adsorbtion of lithium ions onto the fast growing face thereby stabilizing the anionic charge of these crystal planes. Evidence from the atomic mass absorption shows the presence of lithium in the crystals and indicates the possibility of the adsorption of lithium ions on the surface. Lattice parameter determination showed some indication for the inclusion of lithium ions, but the effect was marginal suggesting that lithium was located in interstitial rather than lattice sites.

The schematic diagram in fig. 6.26 shows the $\underline{c}$ face of calcite with lithium ions adsorbed on to the surface and thus reduced the growth rate along the $\underline{c}$ direction enabling the (00.1) face to be developed. The position of lithium on the (00.1) face of calcite can be postulated from crystallographic measurements. The position indicated in the diagram shows that it is located between CO_3^{2-} ions and CaO_6 octahedra along the $\underline{c}$ direction. The position is surrounded by six O^{2-} ions and hence has a negative atmosphere. The size determined from crystallographic data is $\simeq$ 0.86 Å [214, 216] in radius and Lithium has an ionic radius 0.6Å (Pauling's radius). Hence, it could be located in these holes. This inclusion is more possible for lithium than sodium as the ionic radius of sodium is significantly larger (0.99 Å). If calcite crystals contained lithium in the interstitial positions, the positive excess charge should be compensated by other anionic species or by Ca vacancies (net charge -2). In the present system the possible anionic species are Cl^- and HCO_3^-. EDXA data showed the absence of any chloride in the crystal. Previous studies [216]

showed a similar effect with sodium and disregarded HCO_3^- to compensate for the charge as the incorporation of monovalent ions were independent of pH. Most probably Ca vacancies compensate for the excess charge.

Studies were carried out earlier to estimate the mechanism of the incorporation of monovalent and divalent ions in $CaCO_3$ crystals [216] and suggested the similar mechanism. However, there are controversial ideas on the inclusion of monovalent ions into crystal lattice. Onuma et al [217] suggest that the majority of alkali metals have no tendency to occupy the lattice site of the crystal structure as the isomorphic substitution of monovalent to divalent elements in $CaCO_3$ is hardly expected. However, they had analysed only with Na, K and Rb and have not mentioned lithium. Okuumura et al [209] have studied the coprecipitation of Li and sodium, showed a decrease in the amount of alkali metal precipitated as the ionic radius increased and supported the idea that alkali metals are placed in interstitial positions in the crystal structure of calcite and do not substitute for Ca in the lattice. Our results suggest the same idea that Na and Li may be present (in different proportions) on the crystal face. Lattice constants values also show similar trend and support the fact that lithium may be present in the crystal face and that determined the morphology.

Hence, it seems reasonable to suppose that eventually a different arrangement of the structural units became energetically more favourable and the new morphological form is assumed as the energy barrier had been overcome. The consideration outlined here apply only to crystal

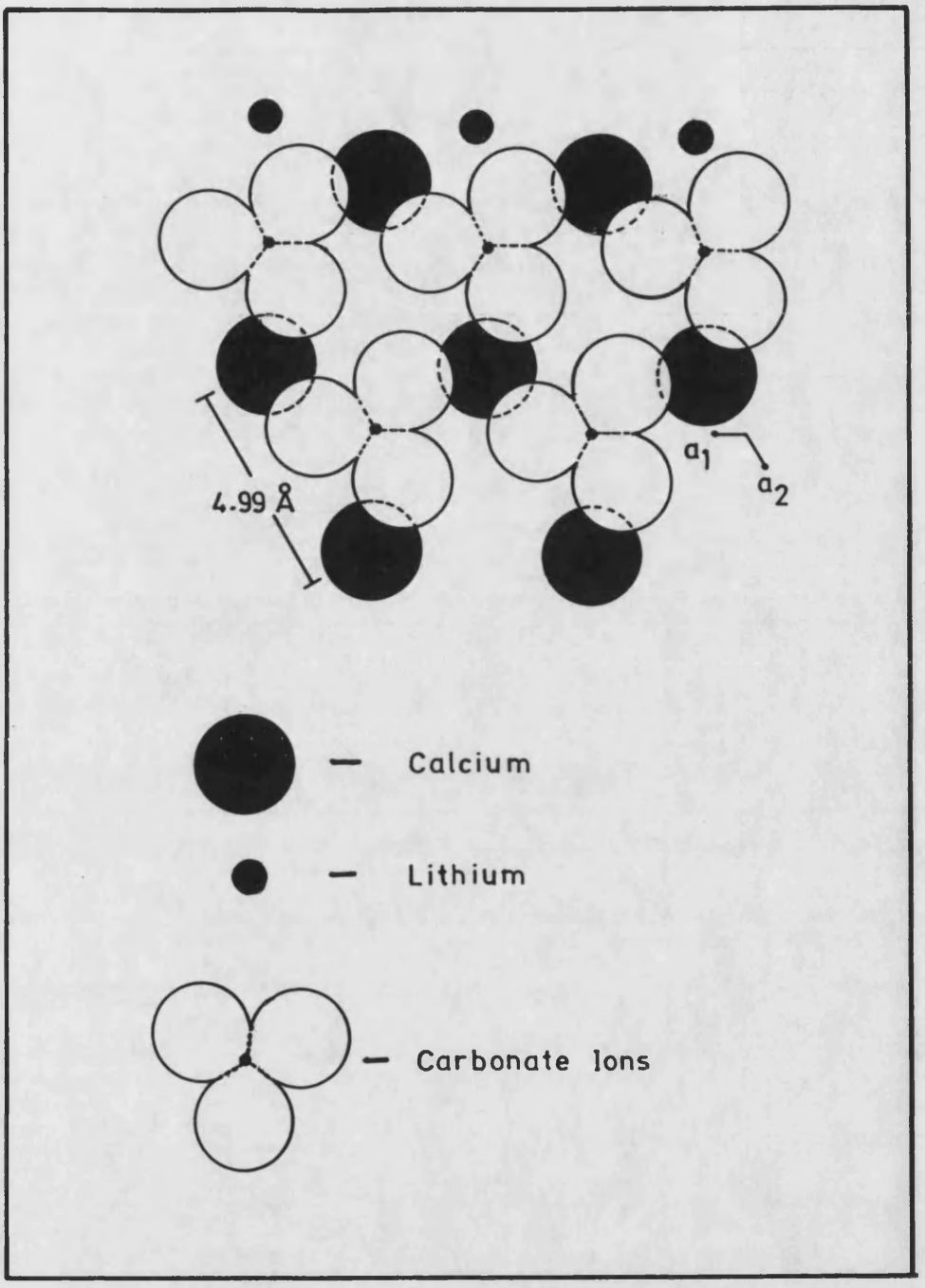

FIG. 6.28: HEXAGONAL UNIT CELL STRUCTURE OF CALCITE CRYSTAL. ● -SHOW THE POSSIBLE POSITIONS OF LITHIUM ABOVE THE TOP/FIRST LAYER OF CARBONATE. THE DISTANCE BETWEEN LITHIUM AND CARBONATE LAYER IS 1/8 OF THE DISTANCE BETWEEN THE TWO CARBONATE LAYERS.

type changes produced by ionic interactions. The general polymorphic transition produced by a change in surface or temperature or both, is considerably more complicated in as much as kinetics as well as thermodynamics are involved.

(ii) Crystallization under stearate monolayer in presence of sodium and lithium: The reduction in oriented crystallisation was possible as these ions weakly bind to stearate molecules. Previous studies [215] show that stearic acid forms good monolayers on calcium [illegible] solution in the presence of sodium [215]. As the amount of sodium increases, it is likely that the binding of calcium to stearate molecules is disrupted. Figure 6.12 shows the increase in the binding efficiency of sodium at the carboxylate headgroup as the concentration of sodium increased in the bulk solution. Competitive binding is controlled by the concentration of the ions present in the solution and so, as the concentration of the monovalent ion increased the binding of calcium to the stearate molecule decreased and the formation of Stern layer disrupted and hence the number of oriented crystals was reduced. Furthermore, the presence of these ions in solution would have increased the encounter time of Ca^{2+} and CO_3^{2-} for the critical nuclei formation and thus would have reduced the rate of formation and growth.

The oriented crystals formed under stearic acid in the presence of lithium showed that the (00.1) face developed nearly perpendicular to the monolayer surface and this face was perpendicular to the face nucleated under the monolayer. Hence the face nucleated which is

perpendicular to the (00.1) face is a prismatic face of calcite. Thus, this provides additional evidence for the earlier conclusion that the monolayer preferentially orients the $(1\bar{1}.0)$ face of calcite on the surface under the monolayer.

Formation of vaterite under the monolayers of acid and amine shows that the polymorphic selectivity is not primarily affected by either sodium or lithium. Slight morphological changes noted at high concentration of lithium might be due to the secondary growth which was not specifically controlled by the monolayer or by lithium. Probably, edge growth of the crystals is prevented by foreign ions thus facilitating a new growth direction into the bulk solution from the middle of the crystal.

The further increase in concentration of lithium under amine monolayers influences the ionic strength of the solution thereby reducing the rate of formation of crystal nuclei. As the slow rate of formation favours the formation of calcite, it is nucleated at the monolayer surface. Furthermore, lithium changed the morphology of the calcite crystals formed. The non-orientation of these crystals with respect to monolayer surface indicates the absence of any structural and stereochemical involvement in controlling the crystal orientation at this level of lithium. This change in polymorph is similar to dilution experiments where, at [Ca] = 1.2 mM the non-oriented calcite formation occured under amine monolayer (See chapter IV, section 4.3). Thus, the slow nucleation determines the calcite formation and lithium determines the morphology of the crystals under these conditions

The cations present in the solution act in two different ways. They break up the calcium binding under stearate monolayer and destabilise the charge accumulation under both the monolayers. This slows down the rate of nucleation by increasing the encounter time of crystal forming ions by the inclusion of Na^{+}or $Li^{+}$and Cl^{-} ions surrounding the Ca^{2+} and CO_3^{2-}ions in the solution. Additionally these foreign ions act as impurities which have a preferential affinity for particular crystal faces and thus favour growth in some directions more than in others.

Thus, we have demonstrated through this chapter that the organisation of charged monolayers, electrostatic charge accumulation under them and calcium binding to the stearate monlayers are critical for the formation of oriented nucleation. Additionally, we have shown that morphological change could be effected by inorganic cations (Li) possibly by the adsorption of these ions in interstitial sites.

CHAPTER VII

CONCLUSIONS

THE PRESENT SYSTEM:

The ability to modify the structure and morphology of crystals is an important aspect of biomineralization and materials science. In particular, $CaCO_3$ is an important inorganic, geological and bioinorganic mineral. Hence, the control of its crystal shape is fundamental to the industrial application of this material as a pigment, filler, etc, and in its biological function as a gravity detector, and structural support in exoskeletons.

The present system showed that the control of crystal structure and morphology can be effected by an organised monomolecular layer of amphiphilic molecules. The system gives good evidence for the effective control and modification of the structure and morphology of crystals formed, through structural, stereochemical and induced physico-chemical factors. The following modifications in this model system may aid future studies.

MODIFICATIONS IN THE MONOLAYER SYSTEM:

Although good monolayers were formed, the effective control in terms of surface pressure was not made as it was handled manually, hence, an automatic (computer-controlled) change in area as and when surface pressure is altered by environmental factors would be ideal for the system. Furthermore, because the monolayers were spread on aqueous surfaces, there were possibilities for the disruption of the

film forming molecules. If the film could be formed on rigid supports and then the crystals were allowed to grow under the influence of these supported monolayers highly reproducible results revealing the specific role of the monolayer might be obtained. Further changes could be to use micelles instead of monolayers to effect control on crystallization. Furthermore, studying the monolayers with a view to identifying the structural aspects and stereochemical nature of the film-forming molecules will be of immense value in elucidating similar interactions at the molecular level in biomineralization processes.

MODIFICATIONS IN THE BULK SYSTEM:

In the present work, we have used Kitano's procedure to crystallize calcium carbonate. It has immense value as it avoids the presence of any other ionic species other than those that come from $CaCO_3$, H_2O and CO_2. However the crystal nucleation which is determined by supersaturation is controlled by first order kinetics i.e by the CO_2 evolution from the system; hence maintaining constant purging/evolution of CO_2 to and from the bulk solution may possibly improve the system further by eliminating the error due to slightly uncontrolled purging of CO_2 to $CaCO_3$ suspension by the interference of atmospheric CO_2. This can possibly be done by keeping a closed atmosphere or by carrying out the experiments in a glove box. This method would also enable to control the partial pressure of CO_2 of required choice. Furthermore studying inorganic crystallization under a non-aqueous medium could be

of great interest as it can show the possible interactions of the common ions such as H^+, OH^- HCO_3 and other possible ionic additives.

DEVELOPMENT/CHANGES IN THE ANALYTICAL TOOLS USED:

In the present system electron microscopy was used as a main tool to analyse the morphological nature of the crystals formed. Being in the initial stages of system development, the work was mainly aimed at identifying the structure and morphology of the crystals formed under the organic monolayer and proposed possible mechanisms for the changes effected. The confirmation of these mechanisms requires more studies (on the controlled crystals formed) in terms of identifying the presence of any matrix/monolayer ionic species occluded in the crystal face. This can possibly be done by chromatographic and spectroscopic techniques where the organic material can be identified for its presence and the microquantities of the material can be quantitatively determined. This analysis in turn may lead to more confirmatory suggestions on the proposed mechanism.

APPLICATIONS OF THIS WORK:

Mention has been made of a few applications of this work in the relevant Chapters in this thesis. Control on the structural and morphological modifications is important in terms of its industrial uses, medical applications and in understanding the processes of biomineralization. The current interest in advanced materials is primarily directed towards synthesis of novel materials. However, the

main aim of this work was the crystallochemical recognition of the matrix molecules with the aim of achieving functional specificity in controlled crystallization. In this respect, it can be used in a wide area of work in controlling/developing features such as structural perfection, the shape, size and orientations that are important in optimising electrical, optical, magnetic and catalytic properties of materials. Thus it seems that a collaborative approach involving biological, chemical and materials science research is essential to the advancement of this area of work.

FURTHER WORK:

1) Immediate progress of the present system can be made in a few simple ways.

One aspect is that instead of using supersaturated $Ca(HCO_3)_2$ solutions, metastable solutions formed by addition of $CaCl_2$ and $NaHCO_3$ in aqueous medium can be used for the crystallization of $CaCO_3$ under the monolayers. This work has been taken up in this group and is in progress.

2) Another specific aspect for the progress of this work is to use polymeric substances instead of simple molecules as organised organic templates for growing crystals of biological and industrial interest. Monolayers of polymeric materials such as proteins and polypeptides are of main interest, for example, melittin is a peptide which has interaction with different cell membranes vesicles and bilayers. These macromolecules being the components closer to

biological systems can be taken up to study the nature of the monolayer formation and to use them for crystal growth studies.

All these pieces of work can finally lead us one step forward in unfolding the mysteries of biology/nature. And, who knows, as it was suggested [218], one day, we may make cars out of crystal growth.

APPENDIX:

(1) Principle of Scanning Electron Microscope:

The principle of scanning electron microscope (SEM) is shown in fig (A). Eelectrons from a thermionic or field emission cathode are accelerated by a voltage of 1-50 KV between cathode and anode. The smallest beam cross section at the gun - the cross over - with a diameter of the order of 10-50 μm for thermionic and 10-100 nm for field emission guns, is demagnified by a two or three stage eectron lens system, so that an electron probe of diameter 1-10 nm carrying an electron current of 10^{-10} - 10^{-12} A is formed at the specimen surface. For modes of operation that need a higher electron probe current of 10^{-9} - 10^{-8}, the elctron probe diameter increases to 0.1-1 μm.

The final probe-formiing lens has to operate with a relatively long working distance, that is, the distance between specimen and lower pole piece, so that the various particles and quanta emitted can be collected with the desired efficiency and if necessary, with zero magnetic field at the specimen. This requirement increases the spherical aberration of the probe-forming lens and, therefore, the smallest attainable electron-probe size. Electron-probe current, aperture and size can all be varied but not independently by changing the excitations of the first condenser lens and the aperture-limiting diaphragm in the last probe forming lens. Apertures of the order of ten milliradians are used for routine work and high resolution. For, one to two orders of magnitude smaller apertures are necessary to increase the depth of focus and

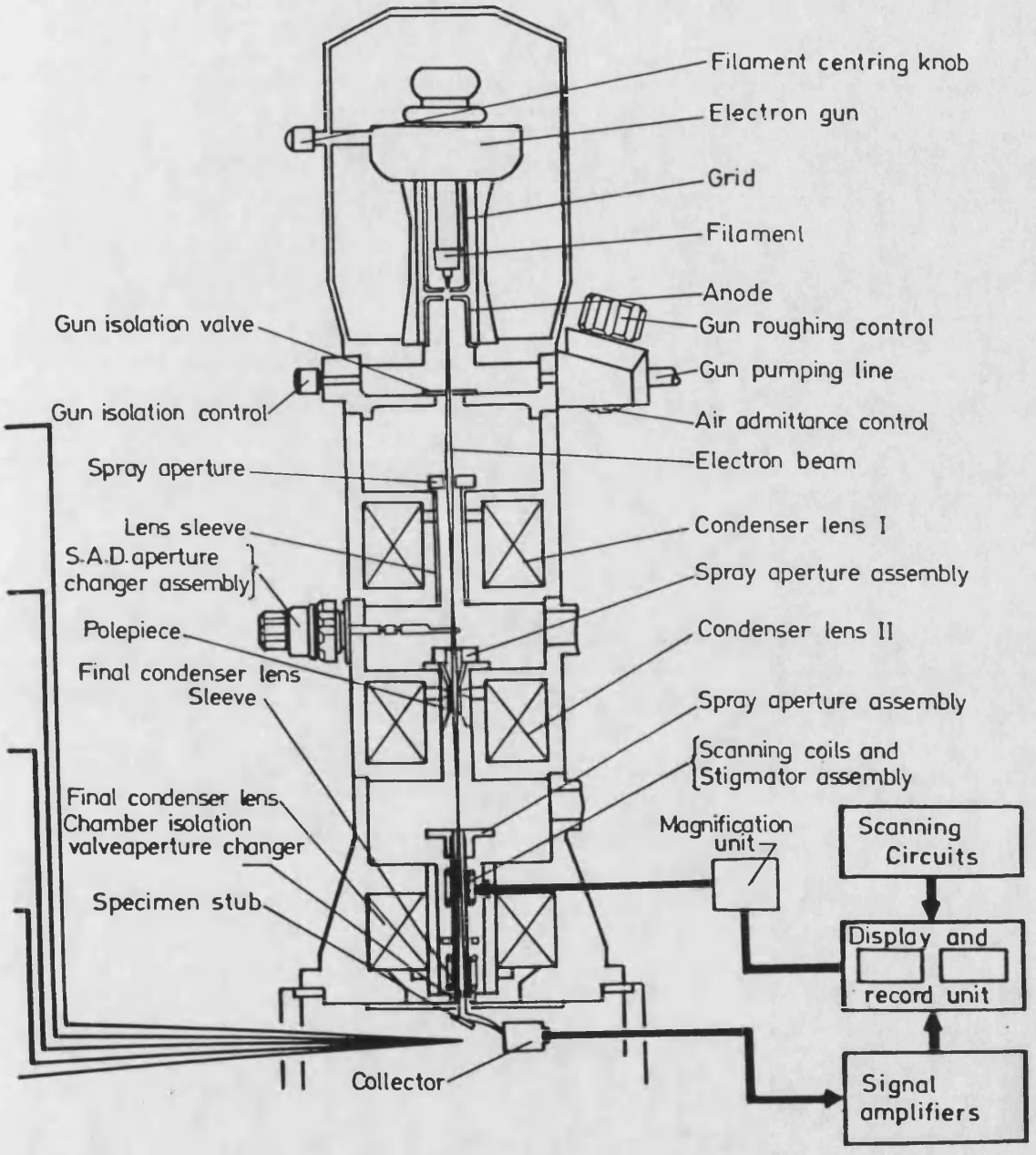

FIG. A : A SCHEMATIC DIAGRAM OF SCANNING ELECTRON MICROSCOPE.

to improve the angle of resolution in electron channeling patterns.

A deflection coil system in front of the last lens scans the electron probe in a raster across the specimen and in synchronism with the electron beam of a seperate cathode-ray tube. The intensity of the electron beam is modulated by one of the signals recorded to form an image. The magnification can be increased simply by decreasing the scan-coil current in keeping the image size of 10 x 10 cm^2.

Further beam-deflection modes involve rocking of the electron beam when the electron probe is at rest and the angle of incidence is raster-scanned to form electron channelling patterns for crystal analysis; periodic change of the angle of incidence for recording stereo images at T.V frequencies; and periodic blanking or chopping of the electron beam upto frequencies in the region specific for the stroboscopic modes and time-resolved signals.

As the electron probe aperture is small- of the order - of a few tens of milliradians - with the result that the depth of the focus is much larger than in optical microscopy. Specimens with large variations in depth can be sharply imaged even at the lowest magnification of 20-50 times.

Another advantage of SEM is the wide variety of electron specimen interactions that can be used to form an image and to furnish qualitative and quantitative informations. The large depth of focus, the excellent contrast and the straight-forward preparation of solid specimens are the reasons for the considerable success and the wide spread use of the scanning electron microscopy in the imaging of surfaces over the recent

times. However, it should be kept in mind that the imaging of surface topography by platinum shadowed carbon replicas in a transmission electron microscope (TEM) is superior by some orders of magnitude in resolution.

1. Lowenstam, H.A. and Weiner, S. "On Biomineralization", University Press, Oxford, 1989, p.1.

2. Lowenstam, H.A., Geol. Soc. Am. Bull., 73 (1962) 435.

3. Blakemore, R., Science, 190 (1975) 377.

4. Frankel, R.B., Blakemore, R.P. and Wolfe, R.S., Science, 203 (1979) 1355.

5. Gould, J.L., Kirschvink, J.L. and Deffeyes, K.S., Science, 201 (1978) 1026.

6. Walcott, C., Gould, J.L. and Kirschvink, J.L., Science, 205 (1979) 1027.

7. Parker, S.B., D. Phil thesis, Oxford University, 1983.

8. Mann, S., Parker, S.B., Ross, M.D., Skarnulis, A.S. and Williams, R.J.P., Proc. R. Soc., Lond., B218 (1983) 415-424.

9. Tayler, G., J. Zool (Lond), 158 (1969) 395-412.

10. Solomon, S.E., and Baird, T., J. Exp. Mar: Biol. Ecol., 22 (1976) 145-6.

11. Mutvel, H., Zool. Scripta, 7 (1978) 287-296.

12. Hall, A. and Taylor, J.D., Mineral. Mag., 38 (1971) 521.

13. Carlstrom, D., Biol. Bull. (Woods Hole) 125 (1963) 441.

14. Palmork, K.H., Taylor, M.E.V. and Coates, R, Acta Chem. Scand., 17 (1963) 1457.

15. Phemister, D.B., Aronsohnand, H.G., Pepinski, R., Ann. Surg., 109 (1939) 161.

16. Epprecht, W., Rosemund, H. and Schinz, H.R., Fortschr. Geb. Roentgenstr. Nuklearmed, 79 (1953) 1.

17. Lagergren, C., Acta Chir. Scand., 124 (1962) 320.

18. Sutor, D.J. and Wooley, S.E., Science, 159 (1968) 1113.

19. Lowenstam, H.A. and Abbot, D.P., Science, 100 (1975) 363.

20. Watabe, N., J. Crystal Growth, 24 (1974) 116-122.

21. Lowenstam, H.A., Science, 211 (1981) 1126-27.

22. Gibson, R.J., Am. Min., 59 (1974) 1177-1182.

23. Been, J.M., Bills, P.M. and Lewis, D., Gut, 18 (1977) 836-842.

24. Mann, S., Nature, 332 (1988) 119-124.

25. Westbroek, P., de Jong, E.W., Vander Wal, P., Borman, A.H., de Vrind, J.P.M., Kok, D., de Bruijn, W.C. and Parker, S.B., Phil. Trans. R. Soc., Lond., B304 (1984) 345-444.

26. Markel, K., Roser, U., Mackenstedt, U. and Klosterman, M., Zoomorphology, 106 (1986) 232-43.

27. Watabe, N., Calc. Tissue Res., 1 (1967) 114-121.

28. Mann, S. and Sparks, N.H.C., Suzanne, C.B., Larcombe, M.C. and Frankel, R.B., J. Chem. Soc. Faraday Trans I., 85 (9) (1989) 3033-44.

29. Whitlock, H.P., New York State Mus. Mem., 13 (1910) 5.

30. Palache, C., unpublished contrib. No. 249, Dept. Mineral. Petrogr. Harvard Uni., p.27, (1943).

31. Palache, C., Berman, H. and Frondel, C., "The System of Mineralogy" (Eds) James Dwight Dana and Edward Salisbury Dana, Wiley, New York, 1951, p. 1124.

32. Runnegar, B., Mem. Ass. Australas. Palaeontols I, (1983) 121-144.

33. Watabe, N., Prog. Crystal Growth Characteristics, Pergamon Press, Great Britain, 4 (1981) 99-147.

34. Mann, S., Struct. and bond., 54 (1983) 125-174.

35. Ledger, P.W. and Frank, S., Cell Tissue Res., 192 (1978) 249-266.

36. Lowenstam, H.A., Traub, W. and Weiner, S., Paleobiology, 10 (1984) 268-279.

37 Wilbur, K.M., Am. Zool., 24 (1984) 839-45.

38. Simkiss, K., "Biomineralization in lower plants and animals", B.S.C. Leadbeater and R. Riding (Eds.), Clarendon Press, Oxford, 1986, 19-37.

39. Boskey, A.L., "Cell mediated calcification and matrix vesicles" S.Y. Ali (Ed.), Elsevier, Amsterdam, 1986, 175-9

40. Weiner, S., in "Organisation of extracellularly mineralized tissues: a comparative study of biological crystal growth", CRC Crit. Rev.

Biochem., 20 (1986) 365-408.

41. Le Gros Clark, W.E., "The tissue of the body", Oxford University Press, Oxford, 1945.

42. Berman, A., Addadi, L. and Weiner, S., Nature (Lond), 331 (1987) 546-548.

43. Weiner, S., Biochem., 22 (1983) 4139-44.

44. Hare, P.E. and Abelson, P.H., Carnegie Institution of Washington Year Book, 64 (1965) 223-231.

45. Price, T.J., Thayar, G.W., Lacroix, M.W. and Montgomery, G.P., Proc. Nat. Shellfish Assoc., 65 (1976) 26-31.

46. Weiner, S., J. Exp. Zool., 234 (1985) 7-15.

47. Swift, D.M., Sikes, C.S. and Wheeler, A.P., J. Exp. Zool., 240 (1986) 65-73.

48. Wheeler, A.P., Blackwedder, P.L. and Wilber, K.M., Biol. Bull., 148 (1975) 472-82.

49. Currey, J.D. and Taylor, J.D., J. Zool. (Lond), 173 (1974) 395-406.

50. Holland, P.W.H., Harper, S.J., McVey, J.H. and Hogan, B.L.M., J. Cell. Biol., 105 (1987) 473-82.

51. Silverman, H., Sibley, L.D. and Steffens, W.J., J. Exp. Zool., 241 (1988) 224-231.

52. Weiner, S., Traub, W. and Lowenstam, H.A. in "Biomineralization and biological metal accumulation", P. Westbroek, E.W. de Jong (Eds.), Dordrecht, Holland, D. Reidel, publishers, 1983, 205-224.

53. Weiner, S. and Traub, W., Phil. Trans. R. Soc. (Lond), 304B (1984) 425-434.

54. Meenaksi, V.R., Hare, P.E. and Wilbur, K.M., Comp. Biochem. physiol., 40B (1971) 1037-43.

55. Crenshaw, M.A. in "Skeletal growth of aquatic organisms", D.C. Rhodes, R.A. Lutz (Eds.), Plenum Press, New York, 1980, 115-132.

56. Gregoire, C. in "Chemical Zoology", M. Florkin, B. Sheer, (Eds), Academic press, New York, 1972, Vol.7, pp. 45-102.

57. Goffinet, G., Jeuniaux, C., Cashiers de Biologie Marine 20 (1979) 341-349.

58. Wilbur, K.M., Collinvaux, L.H. and Watabe, L., Phycologia, 8, (1969) 27-35.

59. Nakahara, H. and Bevelander, G., J. Phycol. (Japan), 26 (1978) 9-12.

60. Borowitzka, M.A. Int. rev. cytol. 74 (1982) 127-160.

61. Mann, S., Sparks, N.H.C. S., Proc. Roy. Soc. B, 234 (1988) 441-453.

62. Eanes, E.D., Hailer, A.W. and Heywood, B.R., Calcif. Tiss. Inst., 43 (1988) 226.

63. Weiner, S., Phil. Trans. R. Soc., B304 (1984) 425-34.

64. Nakahara, H., in "Biomineralization and biological metal accumulation", P. Westbroek and E.W. de Jong (Eds.), Reidel, Amsterdam, 1983, 225-230.

65. Smith, J.W., Nature, 219 (1968) 157-158.

66. Miller, A., Phil. Trans. R. Soc., B304 (1984) 455-77.

67. Fraser, R.D.B., Macrae, T.P., Miller, A. and Suzuki, E., J. Molec. Biol., 167 (1983) 497-521.

68. Katz, E.P. and Li, S., J. Molec. Biol., 73 (1973) 351-69.

69. Glimcher, M.J., Hodge, A.J. and Schmidt, F.O., Proc. Natn. Acad. Sci., U.S.A., 43 (1957) 860-67.

70. Degens, E.T., Spencer, D.W. and Parker, R.H., Comp. Biochem. Physiol., 20 (1967) 553-79.

71. Hare, P.E., Science, 139 (1963) 216-17.

72. Weiner,S., Am. Zool., 24 (1984) 945-51.

73. Weiner, S. and Traub, W., FEBS Lett., 101 (1980) 311-316.

74. Weiner, S., Talmon, Y. and Traub, W., Int. J. Biol. Macromolecules, 5 (1983) 325-328.

75. Greenfield, E.M., Wilson, D.C. and Crenshaw, M.A., Am. Zool., 24 (1984) 1925-35.

76. Sykes, C.S. and Wheeler, A.P., in "Biomineralization and biological metal accumulation", P. Westbroek and E.W. de Jong (Eds.), Reidel, Amsterdam, 1983, 285-289.

77. Lee, S.L., Veis, A. and Glonek, T., Biochem., 16 (1977) 2971-79.
78. Crenshaw, M.A. and Ristedt, H., Biomineralization, 8 (1975) 1-8.

79. Lee, S.L., Glonek, T. and Glimcher, M.J., Calcif. Tissue Int., 35 (1983) 815-18.

80. Glimcher, M.J., in "The chemistry and biology of mineralised connective tissues", A. Veis (Ed.), Elsevier, New York, 1981, 617-75.

81. Kretsinger, R.K. and Nelson, D.J., Coordination Chem. Rev., 18 (1976) 29-124.

82. Goddard, E.D., in "Advances in colloid and Interface Science", Vol.4, 1974, p.45-78.

83. Addadi, L., Moradian, J., Shay, E., Maroudas, N.G. and Weiner, S., Proc. Natn. Acad. Sci., U.S.A., 84 (1987) 2732-2736.

84. Nawrot, C.F., Campbell, D.J., Schroeder, J.K. and Van Valkenburg, H., Biochemistry, 15 (1976) 3445-49.

85. Termine, J.D., Eanes, E.D. and Conn, K.M., Calcif. Tissue Int., 31 (1980) 247-51.

86. Wheeler, A.P., George, J.W. and Evans, C.A., Science, 212 (1981) 1397-98.

87. Wilbur, K.M. and Bernhardt, A.M., Biol. Bull., 166 (1984) 251-59.

88. Termine, J.D., Kleinman, H.K., Whitson, S.W., Conn, K.M., McGarvey, M.L. and Martin, G.R., Cell, 26 (1981) 99-105.

89. Watabe, N. and Wilbur, K.M., J. Biophys. Biochem. cytol., 9 (1961) 761-772.

90. Greenfield, E.W., Wilson, D.C. and Crenshaw, M.A., Am. Zool., 24 (1985) 925-932.

91. Addadi, L. and Weiner, S., Proc. Natl. Acad. Sci., U.S.A., 82 (1985) 4110-4114.

92. Addadi, L., Berkovitch-Yellin, Z., Domb, N., Gati, E., Lahav, M. and Leiserowitz, L., Angew. Chem. Int. Ed. Engl., 24 (1985) 466-85.

93. Addadi, L., Berkovitch-Yellin, Z., Domb, N., Gati, E., Lahav, M. and Leiserowitz, L., Nature, 296 (1982) 21-27.

94. Landau, E.M., Popovitz-Biro, R., Levanon, M., Leiserowitz, L.,

Lahav, M. and Sagiv, J., Molec. cryst. Liq. cryst., 134 (1986) 323-335.

95. Landau, E.M., Girayerwolf, S., Levanon, M., Leiserowitz, L., Lahav, M. and Sagiv, J., J. Am. Chem. Soc., 111 (1989) 1436.

96. Landau, E.M., Levahon, M., Leiserowitz, L., Lahav, M. and Sagiv, J., Nature, 318 (1985) 353-356.

97. Gaines, G.L., Jr., "Insoluble Monolayers at Liquid-gas interfaces", Wiley-Interscience, New York, 1966.

98. Pockels, A., Nature, 43 (1891) 437-439.

99. Blodgett, K.B., J. Am. Chem. Soc., 57 (1935) 1007-1022.

100. Blodgett, K.B., Phys. Rev., 55 (1939) 391-404.

101. Langmuir, I., Proc. R. Soc., Lond., A170 (1939) 1-239.

102. Adam, N.K., in "The Physics and Chemistry of Surfaces", 3rd ed., Oxford University Press, London, 1941.

103. Trurnit, H.J., Fortschr. Chem. Org. Naturst., 4 (1945) 347-476.

104. Kuhn, H., Mobius, D. and Bucher, H., in "Physical Methods for Chemistry", A. Weissbergerand B.W. Rossiter (Eds.), Vol. 1, Part IIIB, Wiley-Interscience, New York, 1972, pp. 577-701.

105. Adamson, A.W., in "The Physical Chemistry of Surfaces", 3rd ed., Wiley-Interscience, New York, 1976.

106. Gershfeld, N.L., Annu. Rev. Phys. Chem., 27 (1976) 349-368.

107. Goddard, E.D., in "Monolayers", Advances in Chemistry Series, E.D. Goddard (Ed.), Vol. 144, American Chemical Society, Washington, D.C, 1975.

108. Blank, M., in "Progress in Surface and Membrane Science", D.A. Cadenhead and J.F. Danielli (Eds.), Vol. 13, Academic Press, New York, 1979, pp. 87-139.

109. Cadenhead, D.A., in "Recent Progress in Surface Science", J.F. Danielli, A.C. Riddiford and M.D. Rosenberg (Eds.), Vol. 3, Academic Press, New York, 1970, 169-192.

110. Bergerou, J.A., Gaines, G.L.,Jr., and Bellamy, W.P., J. Colloid Interface Sci., 25 (1967) 97-106.

111. Aghion, J., Broyde, S.B. and Brody, S.S., Biochemistry, 8 (1969) 3120-3126.

112. Malcolm, B.R., Prog. Surf. Sci. Membr. Struct., 7 (1973) 183-229.

113. Rosoff, M., in "Physical Methods in Macromolecular Chemistry", B. Carroll (Ed.), Marcel Dekker, New York, 1969, pp. 1-107.

114. Gaines, G.L., Jr., in "MTP International Review of Science, Vol. 7, Surface Chemistry and Colloids", M. Kerker (Ed.), Butterworths, London, 1972, pp. 1-24.

115. Baret, J.F., Hasmonay, H., Firpo, J.L., Dupin, J.J. and Duplyrat, M., Chem. Phys. Lipids, 30 (1982) 177-187.

116. Adam, N.K. and Jessop, G., Proc. R. Soc. Lond., A110 (1926) 423.

117. Langmuir, I., J. Am. Chem. Soc., 39 (1917) 1848.

118. Miller, A., Proc. R. Soc., Lond., A114 (1927) 542.

119. Albrecht, O., Gruler, H. and Sackman, E., J. Phys. (Orsay, France), 39 (1978) 301-313.

120. Sackman, E., Ber. Bunsenges. Phys. Chem., 82 (1978) 891-909.

121. Davies, J.T. and Rideal, E.K., in "Interfacial Phenomena", Academic press, New York, 1963.

122. Goddard, E.D., Croat. Chem. Acta., 42 (1970) 143-150.

123. Fourt, L. and Harkins, W.D., 15th Colloid symposium held at Cambridge, Masachusetts, USA, 1938.

124. Jarvis, N.L., J. Phys. Chem., 69(1965) 1789-97.

125. Sanders, J.V. and Spink, J.A., Nature, 175 (1955) 644-645.

126. Rosano, H.L. and Lamer, V.K., J. Phys. Chem., 60 (1956) 348-352.

127. Blank, M., J. Phys. Chem.,66 (1962) 1911-1919.

128. Goddard, E.D. and Ackilli, J.A., J. Colloid. Sci., 18 (1963) 755-764.

129. Ellis, J.W. and Pauley, J.L., J. Colloid. Sci., 19 (1964) 755-764.

130. Deamer, D.W., Meek, D.W. and Cornwell, D.G., J. Lipid Res., 8 (1967) 255-263.

131. Gun, J., Iscovici, R. and Sagiv, J., J. Colloid & Interface Sci., 101 (1984) 201-213.

132. Dote, J.L. and Mowery, R.W., J. Phys. Chem., 92 (1988) 1571-75.

133. Bagg, J., Abramson, M.B., Fichman, M., Haber, M.D. and Gregor, H.P., J. Am. Chem. Soc., 86 (1964) 2759-2763.

134. Kuchhal, Y.K., Katti, S.S. and Biswas, A.B., J. Colloid. & Interface Sci., 29 (1969) 521-535.

135. Stickland, F.G.W., J. Colloid. & Interface Sci., 40 (1972) 142-153.

136. Neuman, R.D., J. Colloid & Interface Sci., 53 (1975) 161-171.

137. Neuman, R.D., J. Colloid & Interface Sci., 56 (1976) 505-510.

138. Smith, R.D. and Berg, J.C., J. Colloid & Interface, 74 (1980) 273-286.

139. Motomura, K., Terazono, T., Matuo, H. and matuura, R., J. Colloid & Interface Sci., 57 (1976) 52-57.

140. Barnes, G.T., J. Collod & Interface Sci., 65 (1978) 566-577.

141. Snik, A.F.M., Crone, A.H.M., Joos, P. and Kruger, A.J., J. Colloid & Interface Sci., 70 (1979) 147-148.

142. Xu, S., Miyano, K. and Abraham, B.M., J. Colloid & Interface Sci., 89 (1982) 581-583.

143. Nevoti, L. and Croce, P., Revue Phys. Appl., 15 (1980) 761.

144. Rice, S.A., Nature, 316 (1985) 108.

145. Bosio, L. Benatter, J.J. and Rieutord, F., Revue Phys. Appl., 22 (1987) 775-778.

146. Richardson, R.M. and Roser, S.J., Liquid Crystals, 2 (1987) 778.-794

147. Watanabe, M., Kosaka, Y., Oguchi, K., Sanui, K. and Ogata, N., Macromolecules, 21 (1988) 2997-3003.

148. Laschewsky, A., Ringsdorf, H. and Schmidt, G., Polymer, 29 (1988) 448-456.

149. Bohanon, T.M., Lin, B., Shih, M.C., Ice, G.E. and Dutta, P., (Paper communicated).

150. Dutta, P., Peng., J.B., Lin, B., Ketterson, J.B. and Prakash, M., Phys. Review Lett., 58 (1987) 2228-2231.

151. Mohwald, H., Angew. Chem., Int. Ed. Engl., 27 (1988) 728-734.

152. Wolf, S.G., Landau, E.M., Lahav, M. and Leiserowitz, L., Thin solid Films, 159 (1988) 21-49.

153. Kajaer, K. and Als-Nielsen, J., Thin Solid Films, 159 (1988) 17-28.

154. Barton, S.W., Thomas, B.N., Flom, E.B., Rice, S.A., Lin, B., Pong, J.B., Ketterson, J.B. and Dutta, P., J. Chem. Phys., 159 (1988) 395-407.

155. Petty, M.C., in "Polymer surfaces and Interfaces", (Eds.) W.J. Feast and H.S. Munro, John Wiley & Sons, 1987, pp.163-185.

156. Baker, S., Proc. Symp. future electronic devices, bioelectronic and molecular electronic devices, Tokyo, Nov. 1985.

157. Schiebold, E., Math.- Phys. KL. Sachs. Akad. Wiss., 36 (1919) 67-213.

158. Wyckoff, R.W.G., AM. J. Sci. 4th Ser., 50 (1920) 317-360.

159. Lippmann, F., in "sedimentary carbonate minerals", (Eds.) W. Engelhardt, T.T. Hahn and A.R. Roy, Springler-Verlag, New York, 1973, pp. 6-9 and 53-71.

160. Reeder, R.J., in "Crystal chemistry of rhombohedral carbonates" Rew. Miner. 11 (1983) 1-47

161. Turnbull, A.G., Geochem. Cosmochem. Acta., 37 (1973) 1593.

162. Stumm, W. and Morgan, J.L., in "Aquatic chemistry", John Wiley Interscience, 1981.

163. Reddy, M.M. and Nancollas, G.H., J. Colloid & Interface Sci., 37 (1971) 166.

164. Nancollas, G.H. and Reddy, M.M., J. Colloid & Interface Sci., 37 (1971) 824.

165. Kitano, Y., Bull. Chem. Soc. Japan, 35 (1962) 1973-1980.

166. Friedman, G.M., Amiel, A.J and Schneiderman, N., J. Sedimentary Petrology, 44 (1974) 816.

167. Watabe, N., J. Crystal Growth, 24 (1974) 116.

168. Reddy, M.M. and Nancollas, G.H., J. Crystal Growth, 38 (1978) 166-168.

169. House, W.A., J. Chem. Soc., Faraday Trans. I, 77 (1981) 341-59.

170. Lippmann, F., Estudios Geol., 38 (1982) 199-208.

171. Florke, W. and Florke, O.W., Neues. Jb. Mineral Mh., 196 (1961) 179-181.

172. Turnbull, A.G., Geochim. Cosmochim. Acta, 37 (1973) 1593-1601.

173. Koutsoukos, P.G. and Kotoyannis, C.G., J. Chem. Soc., Faraday Trans. I, 80 (1984) 1181-1192.

174. House, W.A., J. Colloid & Interface Sci., 119 (1987) 505-511.

175. Compton, R.G. and Daly, P.J., J. Colloid & Interface Sci., 115 (1987) 493-498.

176. Ogino, T., Toshio, S. and Kiyoshi, S., Geochim. et Cosmochim. Acta., 51 (1987) 2757-2767.

177. Dalas, E., Kallitsis, J. and Koutsoukos, P.G., J. Crystal Growth, 89 (1988) 287-294.

178. Sikes, C.S. and Wheeler, A.P., in "Chemical aspects of regulation of mineralization", (Eds.) C.S. Sikes and A.P. Wheeler, University of Alabama Publications, Mobile, Alabama, 1988.

179. Khayat, A. A., Garside J., (unpublished data)

180. Kitano, Y., Bull. Chem. Soc. Japan. 32 (1960) .

181. Worms, D. and Weiner, S., J. Exp. Zool. 237 (1986) 11-20.

182. Betts, J.J. and Pethica, B.A., Trans. Faraday Soc., 52 (1956) 1581-1589

183. Reference (149) referred again.

184. Grayer-Wolf, S., Leiserowitz, L., Lahav, M., Deutsch, M., Kajar, K. and Als-Nielsen, J., Nature, 328 (1987) 63-66.

185. Grayer-Wolf, S., Landau, E.M., Lahav, M. and Leiserowitz, L., Thin Solid Films, 159 (1988) 29-41.

186. Havinga, E., Rec. Trav. Chim., 71 (1952) 72.

187. Kitano, Y., Bull. Chem. Soc. Japan. 35 (1962) 1973-1980.

188. Kitano, Y. and Hood, D.W., Geochimica et Cosmochimica Acta, 29 (1965) 29-41.

189. Reddy, M.M. and Nancollas., J. Crystal Growth., 35 (1976) 33-38.

190. Ostwald, W., Z. Phys. Chem., 22 (1897) 289-330.

191. Cardew, P.T. and Davey, R.J., North Western Branch Symposium on "Tailoring of crystal growth" held at Manchester on 20th Oct., 1982. (Back reference: Young, S. W and Burke, W.J., J. Am. Chem. Soc., 28 (1906) 315.

192. Lieser., Tieke, B. and Wegner, G., Thin Solid Films., 68 (1980) 77-90.

193. Hoffman, E.J., Boyd, G.E. and Ralston, A.W., J. Am. Chem. Soc., 64 (1942) 498.

194. Porter, E.F., J. Chem. Soc., 59 (1937) 1883-1888.

195. Sears, D.F. and Schulman, J.H., J. Phys. Chem., 68 (1964) 3529.

196. Mann, S., Heywood, B.R., Rajam, S. and Walker, J.B.A., Advanced Materials-2, 5 (1990) 257-261.

197. Ries, H.E. Jr., Matsumoto, M., Uyeda, N. and Sutto, E., J. Colloid and Interface Sci., 57 (2) (1976) 396-398

198. Cadenhead, D.A. and Philips, M.C., J. Colloid and Interface Sci., 24 (1967) 491-499.

199. Shaw, O.D. and Schulman, J.H., J. Lipid research, 8 (1967) 215-226.

200. Gershfield, N.L. and Pagano, R.E., The J. Phys. Chem., 76 (9) (1972) 1244-1249.

201. Birdi, K.S. in Lipid and bioploymer monolayers at liquid interfaces., Plenum publishing corporation, New York, (1990) 65-80.

202. Didymus, J.M., University of Bath, personal communication.

203. Pethica, B.A., Trans. Faraday Soc., 51 (1955) 1402.

204. Billings, G.K. and Ragland, P.C., Chem. Geol., 3 (1968) 135-153.

205. Kitano, Y. and Hood, D.W., Geochim. Cosmochim. Acta., 29 1966 29-41.

206. Land, L.S. and Hoops, G.K., J. Sediment. Petrol., 43 (1973) 614-617.

207. Pilkey, O.H and Harris, R.C., Limnol. Oceanogr., 11 (1976) 381-385.

208. White, A.F., Chem. Geol., 23 (1978) 65-72.

209. Okumura, M. and Kitano, Y., Geochim. Cosmochim. Acta., 50 (1986) 49-58.

210. Robinovitch, W., Robertson, R.F. and Mason, S.G., J. Colloid Sci., 13 (1958) 600.

211. Hoffman, E.J., Boyd, G.E. and Ralston, A.W., J. Am. Chem. Soc., 64 (1942) 498.

212. Gaines, G.L. Jr., Unpublished results.

213. Ducloux, J., Dupuis, T. and Laouina, A., Catena, An interdisciplinary J. Soil Sci.- Hydrology - Geomorphology., 14 (1987) 553-559.

214. ASTM - Crystallographic data book.

215. Roser, S.J., and Deards, P., University of Bath, Personnel communications.

216. Ishikava, M., and Ichikuni, M., Chemical geology, 42 (1984) 137-146.

217. Onuma, N.. Masuda, F., Hirano, M. and Wada, K., Geochem. J.,13 (1979) 187.

218. Mann, S., New Scientist, 1707 10-3-1990, 42-47.